**Data-driven Frameworks for Hybrid Analysis of Structures
Under Seismic Loading**

by

Fardad Mokhtari Dizaji

A thesis submitted in partial fulfillment of the requirements for the degree of

Master of Science

in

Structural Engineering

Department of Civil and Environmental Engineering
University of Alberta

Abstract

Numerical simulation and hybrid simulation are extensively used in earthquake engineering to evaluate the seismic response of structures under seismic loading. Despite the advances in computing power and the development of efficient integration algorithms in the past, numerical simulation techniques suffer from a high computational cost and the uncertainty associated with the definition of constitutive material models, boundary conditions, and mesh density, in particular in highly nonlinear, large or complex structures. On the other hand, the results of hybrid simulation can become biased when only one or limited number of potential critical components, seismic fuses, are physically tested due to laboratory or cost constraints.

The recent progress in machine learning algorithms and applications in engineering has motivated novel and innovative simulation techniques achieved by leveraging data in various fields of engineering including seismic engineering where complexities arising from the stochastic nature of the phenomenon can be tackled by making use of available experimental and numerical data towards the development of more reliable simulation models and dynamic analysis frameworks. Furthermore, to better exploit the potential of data-driven models, such models can efficiently be incorporated into the physics-based and experimental techniques, leading to improved seismic response assessment methods. This M.Sc. thesis proposes two new hybrid analysis frameworks by integrating emerging data-driven techniques into the conventional structural response assessment techniques, namely numerical simulation and hybrid testing, to perform the nonlinear structural analysis under seismic loading. The first framework, referred to as the hybrid data-driven and physics-based simulation (HyDPS) technique,

combines the well-understood components of the structure modeled numerically with the critical components of the structure, e.g., seismic fuses, simulated using the proposed data-driven PI-SINDy model. The data-driven model is developed for steel buckling-restrained braces based on experimental data to mathematically estimate the underlying relationship between displacement history and restoring force.

The second framework incorporates the data-driven model into the conventional seismic hybrid simulation framework where the experimental test data of one of the critical components (physical twin), e.g., steel buckling-restrained brace, produced during hybrid simulation can be used in real-time to predict the nonlinear cyclic response of the other critical components of the system (digital twins) that are not physically tested. This framework features a novel multi-element seismic hybrid simulation technique achieved by recursively updating the force-deformation response of the digital twin.

The performance of the proposed data-driven hybrid analysis frameworks is verified using past experimental test data and nonlinear response history analyses performed under representative earthquake ground motion accelerations. The results reveal that integrating data-driven techniques into conventional seismic analysis methods, namely numerical simulation and hybrid simulation, yields a more efficient seismic simulation tool that can be used to examine the seismic response of structural systems.

Preface

This thesis is an original work by Fardad Mokhtari Dizaji. An excerpt of Chapter 3 has been accepted as Mokhtari, F. and Imanpour, A., (2022). "Data-Driven Substructuring Technique for Pseudo-Dynamic Hybrid Simulation of Steel Braced Frames" to be published in the proceeding of the 10th *STESSA Behaviour of steel structures in seismic areas conference*. Also, an excerpt of Chapter 4 has been submitted as Mokhtari, F. and Imanpour, A., (2022). "A Recursive Model Updating Algorithm for Multi-element Hybrid Simulation of Structures" to the 14th *International Conference on Computational Structures Technology*.

Chapter 3 under the title "Hybrid Data-driven and Physics-based Simulation Framework for Seismic Analysis of Structural Systems" will be submitted to the *ASCE Journal of Engineering Mechanics*. Chapter 4 under the title "A Digital Twin-based Framework for Multi-element Seismic Hybrid Simulation of Structures" will be submitted to the *Journal of Mechanical Systems and Signal Processing*.

Fardad Mokhtari Dizaji was responsible for developing the methodology, collecting data, performing computations, analysing the results, and drafting the manuscripts. Ali Imanpour supervised the findings of this work, provided critical feedback, and reviewed the manuscripts.

Acknowledgements

Words fall short of expressing my gratitude to my unique friends at the University of Alberta: Alireza Memarian, Eshagh Derakhshan, Hossein Farboodi, Mahdi Mokhtari, Mahyar Mehranfar, Mehrdad palizi, Reza Mousapour, Vahab Esmaeili, and Yousef Salehi for all the informative research discussions and happy moments we shared together. Thank you for being that one person I can always count on.

Last but not least, I wish to express my heartfelt gratitude to my parents and brother for their abiding love and constant encouragement to engage in scientific curiosity, without whom I could not have embarked upon this journey.

Table of Contents

List of Tables

List of Figures

Abbreviations

2DLFM: 2D Low-fidelity Model.

3DHFM: 3D High-fidelity Model.

AIC: Akaike Information Criterion.

ANN: Artificial Neural Network.

BRB: Buckling-restrained brace.

BRBF: Buckling-restrained braced Frame.

BW: Bouc-Wen.

CBF: Concentrically Braced Frame.

CHS: Conventional Hybrid Simulation.

CNN: Convolutional Neural Network.

DMHS: Digital Twin-based Multi-element Hybrid Simulation.

DOF: Degree-of-freedom.

EOM: Equation of Motion.

FE: Finite Element.

GDHS: Geographically-distributed Hybrid Simulation.

GMP: Giuffrè-Menegotto-Pinto.

HS: Hybrid Simulation.

HyDPS: Hybrid Data-driven and Physics-based Simulation.

LS-SVM: Least-squares Support-vector Machine.

LSTM NN: Long Short-term Memory Neural Network.

MDOF: Multi Degree-of-freedom.

MeHS: Multi-element Hybrid Simulation.

ML: Machine Learning.

MRF: Moment Resisting Frame.

NRMSE: Normalized Root Mean Squared Error.

PI: Prandtl-Ishlinskii.

PINN: Physics-informed Neural Network.

PPE: Peak Point Error.

PsDHS: Pseudo-dynamic Hybrid Simulation.

RLS: Recursive Least Squares.

RMU: Recursive Model Updating.

RNN: Recurrent Neural Network.

RTHS: Real-time Hybrid Simulation.

SDOF: Single Degree-of-freedom.

SFRS: Seismic Force Resisting System.

SINDy: Sparse Identification of Nonlinear Dynamics.

Chapter 1

Introduction

1.1 Background

The failure of "Sleipner A", which was a combined offshore accommodation, production, and processing platform located in the Norwegian sector of the North Sea, on 23 August 1991 is known for one of the most catastrophic structural failures with a total economic loss of 700 million USD. The cause of this failure was in part a flaw in the structural analysis software used for the structural design of this platform [1, 2]. The list of computer-caused catastrophes, which are defined as the disasters attributed to malfunctioning analysis programs, does not end here [3], which suggests the need for improved and reliable structural response assessment techniques to achieve resilient structures under extreme loading conditions, including those caused by natural hazards.

In earthquake engineering, there are generally four main response assessment approaches: 1) numerical simulation, 2) experimental testing, 3) hybrid simulation, which is a combination of numerical simulation and experimental testing techniques [4], 4) data-driven simulation. The three fundamental techniques, as well as the hybrid simulation, are briefly explained in the following.

Numerical simulation enabled the engineering communities and researchers to efficiently perform the response evaluation and structural design of a wide range of complex structural systems. It has been possible to implement various powerful computational methods to

analyze the structures subjected to various extreme loading, including those with dynamic effects such as wind, earthquake, or tornado. The Finite Element (FE) analysis, developed by Clough [5] in the 1960s, offered a powerful tool for computer modelling of engineering structures. FE method has been extensively applied in engineering and science to solve various problems in different areas [6] including solid mechanics, structural dynamics, computational fluid dynamics (CFD), electromagnetism, biomechanics, heat transfer, and even finance [7]. In spite of the advances in computing processing power (e.g. parallel computing and high-performance computing clusters), simulation of large complex structural systems under random dynamic loads, e.g., ground motion excitation, still consumes a great deal of time and, in some cases, may lead to inaccurate or unreliable results. Additionally, assumptions such as mass, damping, constitutive model parameters, and mesh density associated with the FE model can add to the uncertainty of the results.

As an alternative to numerical simulation, experimental testing offers a more reliable but less efficient solution towards the structural response assessment. Quasi-static cyclic and shake table tests are the two major experimental testing methods that have widely been used in seismic engineering to study the performance of structural systems when subjected to seismic loads, validate and calibrate their responses under earthquake loads in order to achieve a better understanding of the physical phenomena controlling their response, develop design guidelines for improved seismic performance or develop new resilient seismic force-resisting systems. In quasi-static cyclic testing, a predefined history of loads, displacements, or a combination of both is applied to a structural component or subassembly to examine the effects of various parameters such as material properties, geometry, loads, boundary conditions, or bracing conditions. The quasi-static testing method is well suited when determining the static hysteretic behaviour of the component, but the imposed demand in the quasi-static testing method does not necessarily represent the actual seismic-induced demand of the structure. Moreover, this method fails to account for dynamic and rate-dependent effects. Shake table tests can more realistically represent seismic loading conditions on structures and their

components, taking into account damping characteristics, inertial forces as well as material and geometric nonlinearities. However, physical limitations of available shake tables, including payloads, overturning moment and specimen sizes, often lead to testing of reduced-scale models, which raises questions on the reliability of test results and often makes shake table testing an uneconomical and complex structural testing approach [8].

Hybrid simulation is a mixed numerical simulation - physical testing method, which was first introduced by Koichi Takanashi et al. [9] as a sub-structuring technique in the early 1970s to achieve the trade-off between the reliability of test results and the complexity of large-scale testing. The underlying idea of hybrid simulation is to divide the structure into two computationally-parallel substructures. The well-understood parts of the structure are simulated numerically using a finite element analysis program while the critical component or components expected to respond in the inelastic range or experience instability, e.g., seismic fuses, are tested physically in the laboratory. The displacements of inter-facial nodes are computed by numerically solving the governing equation of motion in each time step and are applied to the physical specimen. Restoring forces of the specimen are then measured and fed back to the numerical model for the subsequent analysis increment [10]. There exist two main HS techniques in earthquake engineering, real-time hybrid simulation (RTHS) and pseudo-dynamic hybrid simulation (PsDHS). Compared to the other two seismic testing techniques, hybrid simulation offers a versatile and economically-viable solution for full-scale testing of structural members or subassemblies. Over the last decades, hybrid simulation has significantly advanced in terms of accuracy, stability and reliability [11–16] including the development of numerical integration techniques [17], delay compensation approaches [13], force-based control methods [18], and geographically distributed hybrid simulation techniques [19]. These improvements placed hybrid simulation as one of the reliable response evaluation techniques used widely by research communities worldwide [20–28]. Some sources of error, such as actuator tracking errors and controller tuning, calibration errors of the instrumentation, noise generated in the measurement system, inaccurate force measurements,

3

displacement errors due to flexibility of test frames or reaction walls, and analog-to-digital converters, still need improvement [28–31].

Data-driven simulation techniques have been the focus of intensive research efforts in recent years. A wealth of experimental test data is generated from laboratory testing of full-scale structural components and assemblies as a result of advanced testing equipment, control systems, new structural testing facilities, modern instrumentation and sensors. The available data can be leveraged by the emerging Artificial Intelligence (AI) techniques towards a more accurate and efficient structural response prediction, which would offer a viable and more efficient alternative to traditional finite element-based simulations, in particular, taking into account the challenges associated with numerical methods as described earlier. In recent years, various data-driven simulation approaches [32–37] have been used for the assessment of the dynamic response of structural systems, which allows to synergically use past experimental test data to estimate the behaviour of structures, in particular, when responding to extreme loading conditions.

1.2   Problem Statement

The key features of the structural response assessment techniques (numerical simulation, experimental testing and hybrid simulation, and data-driven simulation) are shown in Fig. 1.1, which include 1) generalization ability, e.g., development of multiple frames with various geometries and material properties, 2) development efficiency, e.g., financial or computational costs associated with modelling or equipment, and 3) reliability of results, e.g., dependency of the results to modelling assumptions. It should be noted that the weight of each feature in this figure is given relative to the other features and among the methods to the best of the author's knowledge. As shown in Fig. 1.1a, numerical simulation can offer the best technique when it comes to generalization ability as multiple frames with different geometries and properties can efficiently be made and analysed. However, since a large number of modelling assumptions must be made during simulation and model development, the reliability

4

of this technique can become skeptical, in particular, when a complex geometry or uncommon material is involved. On the other hand, experimental testing techniques, as shown in Fig. 1.1b, are most beneficial when the reliability of the results are of paramount importance. Inevitably, this comes at the cost of financial constraints and equipment limitations, which makes this method the least favourable technique in terms of development efficiency. The data-driven simulation technique, as shown in Fig. 1.1c, can represent the most efficient technique with regards to simplicity of model development as it only requires basic and straightforward modelling assumptions using a surrogate model that maps the inputs of the structural system, e.g., ground motion acceleration time series, to structural response, e.g., displacements. Data-driven techniques, however, cannot be easily generalized as opposed to numerical simulation techniques because the input-output mathematical model is only created based on a specific dataset collected from the structure, e.g., data obtained from sensors mounted on bridges or from a prototype structural component, e.g., experimental specimen. Therefore, a new dataset would be needed to train the data-driven model for the new structural system or component with distinct properties.
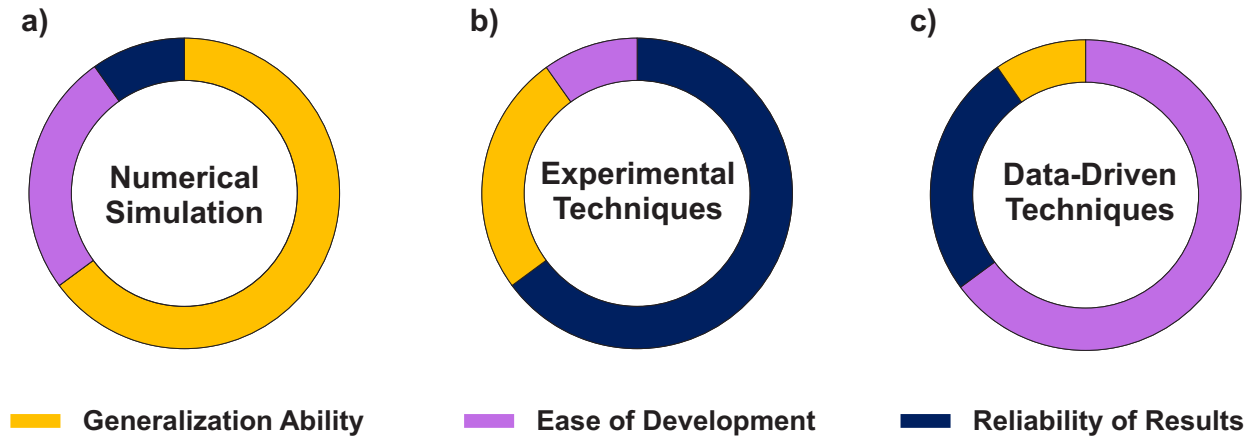
Figure 1.1: Comparison of the three main structural response assessment techniques, experimental techniques include both conventional experimental techniques (e.g., quasi-static cyclic and shake table tests) and hybrid simulation.

Motivated by the underlying idea of seismic hybrid simulation that combines two main structural response assessment techniques for an improved and more efficient method, this

thesis explores the potentials of incorporating data-driven models into the well-established physics-based numerical and experimental techniques, leading to improved seismic response assessment methods. Therefore, the following research gaps are identified in the literature.

The *first gap*, is the need for the development of a new response assessment framework that integrates the data-driven and physics-based numerical techniques as shown in Fig. 1.2 for the assessment of the dynamic response of structures with the focus on the estimation of the hysteretic response of the structural components experiencing nonlinear response, i.e., critical components, using data-driven models. This platform should balance generalization and ease of model development while demonstrating sufficient reliability.
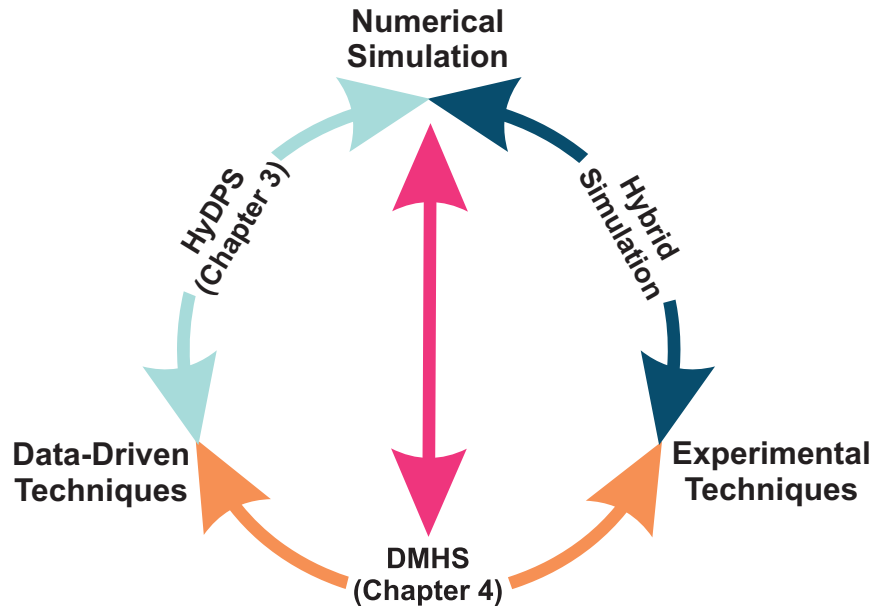
Figure 1.2: Emergence of new structural response assessment techniques by combining conventional response assessment methods: 1) hybrid simulation combining numerical simulation and experimental technique; 2) proposed hybrid data-driven and physics-based simulation (HyDPS) combining numerical simulation and data-driven technique; and 3) proposed digital-twin based multi-element hybrid simulation (DMHS) combining experimental, numerical simulation and data-driven simulation techniques.

Seismic hybrid simulation results may become biased when only one or a limited number of potential critical components are physically tested due to laboratory or financial constraints. Therefore, the *second gap* is the need to develop a multi-element hybrid simulation framework

integrating numerical, data-driven, and experimental testing techniques as shown in Fig. 1.2 to examine the seismic response of structural systems under seismic loading. This technique should overcome potential bias in hybrid simulation results for structures having more than one critical component, e.g., seismic fuses in multi-story structures or bridges, increasing the reliability of hybrid simulation results.

1.3   Research Objectives

The general objective of this M.Sc. thesis is to develop new frameworks by integrating emerging data-driven techniques into the conventional structural response assessment techniques, namely numerical simulation and experimental testing, to perform the structural seismic structural analysis 1) when sufficient hysteresis experimental data featuring the force-deformation (or moment-rotation) response of the critical component of the structure is available to train a data-driven model and use the model combined with the numerical model of the well-understood parts of the structure to study the seismic response of structures; 2) when the response of the critical component cannot be reproduced using available past data, e.g., there is lack of high quality training data, and there are multiple critical components in the structure; a data-driven model is implemented in a conventional hybrid simulation framework and trained recursively using the real-time data collected during hybrid simulation in which only one critical element is modelled physically in the laboratory and the response of other critical components are predicted by the data-driven models. To achieve the general objective of this research, the following specific objectives are defined:

1. develop a data-driven model for predicting the nonlinear hysteretic response of structural components using a machine learning algorithm (Chapters 3 and 4),

2. establish a platform - Hybrid Data-driven and Physics-based Simulation (HyDPS) framework - to effectively combine the i) data-driven model of Specific Objective 1 simulating the hysteretic response of critical components with the ii) numerical model

constructed to simulate the rest of the frame (Chapter 3),

3. develop a machine learning-based framework – Data-driven Multi-element Hybrid Simulation (DMHS) – that combines i) the data-driven model of Specific Objective 1 used to simulate the critical components of the structure not experimentally tested, ii) the experimental specimen physically modelling one of the critical components of the structure providing the real-time training data to the data-driven model, and iii) the numerical model simulating the well-understood parts of the structure (Chapter 4).

1.4   Research Methodology

The objectives of this research are achieved in three phases as described below:

Phase 1: A new data-driven method referred to as PI-SINDy is developed to simulate the hysteretic response of structural elements experiencing nonlinear response under dynamic loading. This new hysteresis model combines Prandt-Ishlinskii [38] hysteresis model with the Sparse Identification of Nonlinear Dynamics (SINDy) algorithm [39]. The proposed data-driven model is validated using the hysteresis data obtained from full-scale experimental tests and numerical simulation results. This data-driven model was the basis for establishing the structural response assessment techniques in Phases 2 and 3.

Phase 2: A hybrid data-driven and physics-based simulation (HyDPS) framework is proposed by integrating the numerical model of the well-understood components of the structure simulated using the physics-based modelling approach and the data-driven model of the critical components of the structure expected to respond in the inelastic range of the material. The proposed hybrid technique is developed for the seismic response evaluation of structural systems under dynamic loading such as earthquakes. This technique is analogous to the pseudo-dynamic hybrid simulation technique proposed by Hakuno et al. [10] to combine numerical modelling with experimental testing techniques to evaluate the seismic performance of structures. The displacements at each DOF at the interface of the data-driven and physics-

based components are calculated by solving the dynamic equation of motion (EOM) and are sent to the data-driven model. The restoring force prediction of the data-driven model will then be fed back to the physics-based model for solving the EOM during the next time step.

Phase 3: A new seismic hybrid simulation technique, digital twin-based multi-element hybrid simulation (DMHS), is proposed for the seismic analysis of structural systems with multiple critical elements, which benefits from an adaptive data-driven model (digital twin) that predicts the hysteretic response of similar critical elements. This is achieved using the recursive least-squares (RLS) algorithm powered by the Prandtl-Ishlinskii (PI) model. The developed algorithm functions in two subsequent steps: 1) the sparse identification of nonlinear dynamics (SINDy) algorithm is utilized to obtain a computationally-efficient PI model in the initial (passive) training phase. This phase is triggered before hybrid simulation to estimate the response of the digital twin during the initial time steps of the analysis; 2) the new incoming (experimental test) data as obtained from the physical specimen is fed into the RLS algorithm to progressively improve the prediction of digital twin's hysteretic response, particularly the hardening behaviour affected by the real-time dynamic loading protocol. This phase, referred to as the recursive model updating (RMU), is activated during the hybrid simulation test.

1.5   Organization

This M.Sc. thesis is organized in five chapters:

Chapter 1 provides background information, problem statement, research objectives, and research methodology.

Chapter 2 presents a survey of past literature on the methods used for hysteretic response simulation of structural elements, and machine learning algorithms used in predicting structural response.

Chapter 3 proposes, demonstrates, and verifies the HyDPS framework and the PI-SINDy data-driven model. This chapter under the title "Hybrid Data-driven and Physics-based

Simulation Framework for Seismic Analysis of Structural Systems" will be submitted to the *ASCE Journal of Engineering Mechanics*.

Chapter 4 is devoted to the development of the proposed DMHS framework for seismic hybrid simulation of structural systems followed by demonstration and validation of the framework using 2D low-fidelity and 3D high-fidelity nonlinear response history analyses. This chapter under the title "A Digital Twin-based Framework for Multi-element Seismic Hybrid Simulation of Structures" will be submitted to the *Journal of Mechanical Systems and Signal Processing*.

Chapter 5 presents the summary, scientific contributions, conclusions, limitations of the study, and recommendations for future studies.

The mathematical formulation of the PI-SINDy data-driven model is described in both Sections 3.4 and 4.3.2 of this thesis to help reader easily follow the steps associated with the development of each chapter while aiming for a standalone chapter. However, examples and applications specific to each chapter are provided to describe the PI-SINDy model in these two sections.

Chapter 2

Literature Review

2.1   Introduction

This chapter presents past studies concerning hysteretic response simulation of structural components and machine learning (ML) algorithms used in seismic engineering. The parameter and operator-based models as conventional hysteretic response simulation techniques are first reviewed, followed by the summary on the applications of ML algorithms in system-level and component-level structural response assessment, performance evaluation of structures, and seismic hybrid simulation.

2.2   Conventional Hysteresis Simulation Techniques

The etymological meaning of hysteresis is "deficiency" or "lagging behind". In engineering technical terms, a system is called hysteretic when the state of the system is dependent on its history. Hysteresis has manifested itself in many fields, including physics, chemistry, mechanics, biology, and economics [38]. Ewing [40] coined the term "hysteresis" for the first time in 1881 in a study where he observed that there was a lagging effect between the thermoelectric quality of the stretched wire and the associated tensile stress [41].

Hysteresis appears in mechanical and structural systems as a physical mechanism for materials to dissipate energy and provide restoring forces to deformations [42]. The restoring force behaviour of these systems can not be defined explicitly as a function of the instanta-

neous deformation, instead it involves a complex dependency on the history of deformation. The modeling of the restoring force behaviour of structural systems subjected to random vibrations has been an active research area in the past decades [42]. The challenge associated with simulating the restoring force behaviour is mainly attributed to the nonlinearity and hysteretic behaviour of structural components.

Various models have been proposed to describe the hysteretic behaviour of the structural systems experienced forces beyond the elastic limit [43–45]. The detailed modeling of hysteretic structural systems using the laws of classical mechanics is considered troublesome as such models will lose their practicality in computationally intensive engineering tasks such as the analysis of scholastically excited systems, nonlinear response history analysis, structural optimization, inverse identification, and control. As a more viable solution for simulating hysteretic behaviour of structures, alternative mathematical models, referred to as phenomenological models, have been proposed in the past. A phenomenological hysteresis model attempts to express the mathematical relationship between the restoring force and deformation such that it remains consistent with fundamental theory and empirical observations rather than being directly driven from mechanical principles.

Within the context of this research, two conventional types of phenomenological hysteresis models are introduced in the following.

2.2.1 Parameter-based Models

Parameter-based models require several parameters in their mathematical formulation to describe the properties of hysteresis loops. The main benefit of such models is that they can be used directly in the differential equations that govern the dynamics of a structural system (i.e. equation of motion) while assigning values to the parameters that describe the hysteretic behaviour of the system. However, there are two drawbacks that can be recognized, 1) the parameter calibration is considered arduous because it typically requires numerous simulations with trial and errors, in particular, when the effect of the combination of parameters

is highly nonlinear, and it is not possible to easily determine how a parameter affects the overall hysteresis shape. 2) there is no universal model that can be used for various hysteretic behaviours because each parameter-based model has its own specific characteristics [46].

Various parameter-based models were developed in the past for different applications, for example, Ramberg-Osgood [47, 48] and Giuffrè-Menegotto-Pinto (GMP) [49] are widely used for modelling steel hysteresis under cyclic loading, Bouc-Wen (BW) model [50, 51] for simulating seismic isolation systems, and Steel4 [52, 53] for modelling buckling restrained brace (BRB). The GMP and BW models are described in more detail.

Giuffrè-Menegotto-Pinto Model

Giuffrè-Menegotto-Pinto (GMP) model was first proposed by Giuffrè [49, 54] and since then has been widely used in simulating the hysteretic behaviour of steel components under cyclic loading [55]. This model is fundamentally formulated using the nonlinear stress-strain relationship proposed by Goldberg and Richard [56] to take the Bauschinger effect [57] into account as observed in steel coupons test. The model was further extended by Menegotto and Pinto [54] and later by Filippou et al. [58] to include the isotropic hardening effects. Subsequently, it became a widely used hysteretic model in the literature [59–61] since the stress-strain response of structural steel was more accurately predicted using this model in comparison with other models such as the bilinear and Ramberg-Osgood models [47].

The hysteretic relationship in the GMP model is formed using curvilinear transitions between two asymptotes, one with slope E_0 and the one with slope $E_1 = bE_0$ where b is the strain hardening ratio. A cyclic curvature parameter controls the curvature of the transition between two asymptotes, which reproduces the Bauschinger effect. Four optional parameters are incorporated in the model to capture the isotropic hardening in compression and tension, i.e., two parameters for each compression and tension [58].

Bouc-Wen Model

Bouc-Wen (BW) hysteresis model [50, 62] encompasses seven parameters and is based on first-order differential equations. The effect of the parameters in this model is complex, and the properties in the hysteresis shape are not individually attributed to a separate parameter [63]. The BW model is especially promoted for its suitability in identification problems, where given a set of experimental data points, a curve that follows the experimental data with the least amount of error is to be produced by evaluating the model parameters [41, 64, 65].

The BW model was further improved by Baber and Noori [66] to include the pinching behaviour. This improved model is highly nonlinear and consists of nine control parameters, including stiffness and strength degradation parameters.

The mathematical formulation of the BW model is given in chapter 3.

2.2.2 Operator-based Models

In operator-based models, the input signal, e.g., deformation history in structural engineering applications, is first inputted to multiple operators, called hysterons, and the output of each of them is then linearly superimposed by means of a density function to create the hysteresis curve. The density function should be approximated in the identification phase to find the hysteretic relationship from experimental test data. The key difference between each model in the operator-based model category is that they incorporate a different operator to create the hysteresis shape. For instance, Preisach [67, 68], Prandtl-Ishlinskii (PI) [69, 70], and the Krasnoselskii–Pokrovskii (KP) [71, 72] models take advantage of using the relay, stop, and KP operators, respectively, in their model architecture. The simulation accuracy of operator-based models can be enhanced by increasing the number of superposed elementary operators, but this may cause more computational burden and sometimes result in over-fitting [38].

The key benefit of the operator-based models is that they can transform the input signals to a higher dimensional space in order to reformulate the hysteretic response, i.e., output signal, in a one-to-one mapping problem, which is favourable for most ML algorithms. Furthermore,

these models are integration-free offering a more efficient hysteretic estimation with minimum numerical convergence issues compared to models based on differential equations, e.g., the BW model.

2.3   Machine Learning in Seismic Engineering

Machine learning (ML), a sub-field of artificial intelligence (AI), focuses on developing algorithms that can learn to predict or make decisions by leveraging data. The application of ML methods has overhauled a wide variety of disciplines in recent years, leading to a wide range of advanced tools and technologies [73]. The core goal in ML is to build an efficient mathematical model to accurately perform the tasks that involve prediction or classification based on unseen data, known as testing data, after having experienced sufficient known data, referred to as training data. In the mathematical model, each training data should be represented by an array of attributes called the feature vector, which defines the data and a different array containing the model's required outputs, known as a label.

There exist four ML techniques: 1) supervised, 2) unsupervised, 3) semi-supervised, and 4) reinforcement learning. Fig. 2.1 illustrates the categories and subcategories of ML algorithms described in the following.

supervised learning algorithms [74] deal with the problems where a set of input variables are to be mapped to one or more outputs. A supervised learning algorithm is considered as pattern recognition or classification when the output is categorical and regression when the output is a numerical range. *Unsupervised learning* algorithms [74] are, however, used to find the underlying relationship and get insights from a large unlabeled dataset. Unsupervised learning aims to analyse the training data to explain how it can be structured or clustered. *Semi-supervised learning* algorithms [75] sit somewhere between supervised (with fully labelled training data) and unsupervised (without labelled training data) learning where a model needs to be trained on training data with a combination of a small number of labelled data and a large number of unlabeled data. The fourth type of ML algorithms, *Reinforce-*

ment Learning (RL) algorithms [76], are an emerging area of ML that are concerned with how an intelligent system, referred to as "agent" in the context of RL, interacts with the environment so as to maximize its cumulative reward. The agent receives a positive reward if it takes a suitable action and will be penalized if an undesirable action is taken. RL differs from supervised learning in the sense that labelled data is not available beforehand, and the agent is bound to learn from its own experience when interacting with the environment. It should be noted that the application of RL is outside the scope of this thesis.
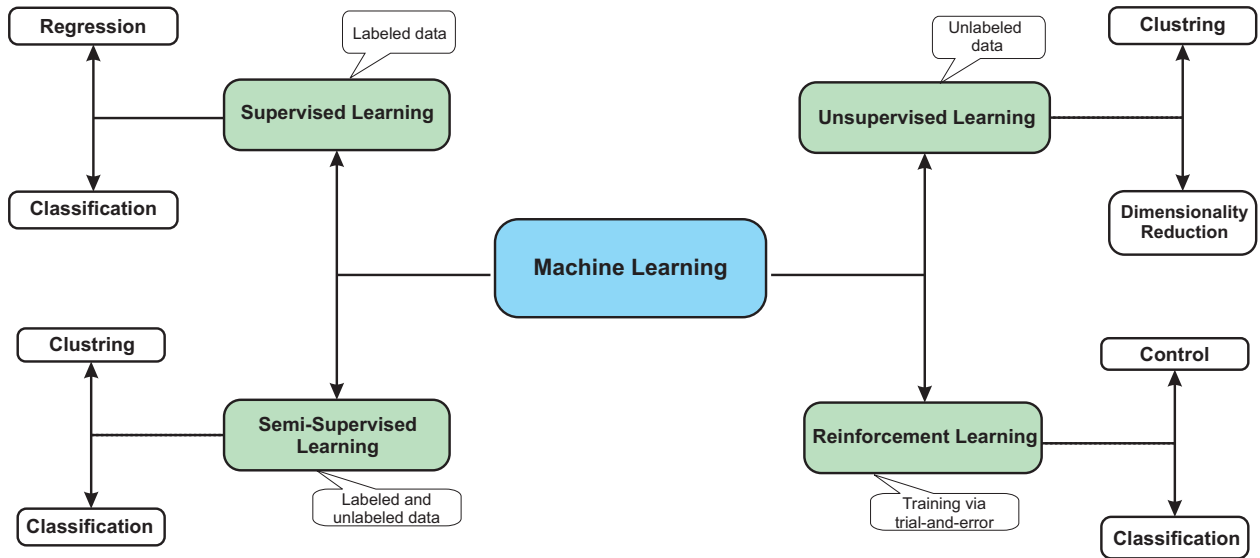
Figure 2.1: ML algorithms

Machine Learning-based methodologies for structural design and performance assessment have been around since the late 1980s when Adeli and Yeh [77] developed and applied a methodology based on ML to solve a beam design problem. Following this pioneering study, a series of studies involving neural networks were applied to structural design problems [78–80]. Among them, Vanluchene and Sun [81] used back-propagation neural networks to design a reinforced concrete beam and analyse a simply-supported plate.

In the early days of applying ML algorithms to structural engineering problems, relatively simple problems with small datasets were addressed. However, owing to the significant growth in computing power and resurgence of AI over the past two decades, more advanced

tools are now being developed and used to harness the new data streams in order to solve highly nonlinear problems seen in applied structural and earthquake engineering. Relevant recent applications of ML techniques in structural design and performance assessment are summarized in the following.

2.3.1 Structural Response and Seismic Performance Assessment

Since computer simulations became available, the nonlinear response history analysis has been used by structural engineers and researchers as a powerful tool to assess the response of structures under extreme loading conditions such as earthquake, blast, fire, tornados. ML algorithms have been implemented in the past to build the so-called data-driven models (also referred to as surrogate models or metamodels in the literature) that act as a black-box mathematical representation of the relationship between inputs, e.g., material and geometric properties or loading, and outputs, e.g., structural response or performance quantities. Such models are especially useful for computationally intensive applications such as seismic fragility analysis, structural optimization, and control, because of saving time and computational efforts by reducing the number of physics-based simulations and numerical integration schemes needed to complete the simulation [82].

A summary of the past studies that implemented different ML algorithms to estimate structural response and/or performance metrics, including the type of case study structure, research domain, and the type of the machine learning algorithm used, are given chronologically in Table 2.1. In this table, different structural systems such as masonry buildings, reinforced concrete (RC) frames, steel moment-resisting frames (MRFs), trusses, and steel bridges were used as the case study to showcase the performance of the respective machine learning algorithm.

Referring to Table 2.1, ML algorithms were employed in most of the listed studies [34, 83–85] towards the development of a model responsible for estimating the structural demand parameters including peak inter-storey drift ratio, and peak floor acceleration; in some other

instances [32, 33, 35–37], the full structural response history under seismic ground motion was predicted. In the latter, more advanced ML algorithms, including Deep Convolutional Neural Networks (Deep CNN) [37], Deep Long Short-Term Memory Neural Networks (Deep LSTM) [35], were often implemented. In relatively older studies [85–87], simpler algorithms based on the Response Surface Methodology (RSM) were used that enabled fast and efficient computation but lacked enough accuracy for highly nonlinear problems. In recent years, the concept of physics-informed (also known as physics-guided or physics-induced) machine learning [88] has found its way into structural and seismic response assessment problems as a promising alternative to old ML-based methods when limited data is available [36, 37]. Finally, several studies listed in Table 2.1 [84–87, 89–95] enjoyed ML algorithms in the collapse assessment and fragility analysis.

2.3.2 Data-driven Models for Response Assessment of Structural Components

The availability of larger datasets created ample opportunity to create more complex constitutive models, compared to phenomenological models, using ML algorithms to accurately estimate the nonlinear hysteretic response of structural components. Some of the most recent studies concerning the implementation of ML algorithms for the simulation of the hysteretic response of structural components are summarized here.

Data-driven models [82] have attracted the attention of research communities in recent years to develop a universal mathematical form that can identify different hysteretic shapes expected in structural and mechanical systems, which is a challenging task for parameter-based models.

Neural Networks [98] as one of the most prominent ML algorithms, have widely been used for function approximation, classification, pattern recognition, and data processing. Owing to the simple architecture of Neural Networks, they lack internal memory to simulate the hysteretic response. Yun et al. [99] proposed a particular class of Neural Networks,

called Recurrent Neural Networks (RNNs), to simulate the cyclic behaviour of materials by incorporating the past state of the system into the input layer. Similarly, Joghataie and Dizaji [100, 101] utilized RNNs to simulate the nonlinear dynamic response of concrete gravity dams. The main drawback of RNNs for hysteresis simulation is that they are prone to error accumulation because the input values are dependent on previous outputs.

Machine learning algorithms have also been used to predict specific structural response parameters instead of simulating the complete hysteretic response. For example, the component-level structural parameters such as nonlinear deformation capacity of reinforced concrete columns [102], punching shear strength of reinforced concrete slabs [103], reinforced concrete beam-column shear strengths [104], and reinforced concrete columns' backbone curve parameterss [105] were predicted using Locally Weighted Least Square Support Vector Machine (SVM) regression, sequential piecewise linear regression and artificial neural network, Multivariate Adaptive Regression Splines (MARS), and Least Square SVM regression algorithms, respectively. Note that these algorithms are considered supervised ML algorithms. The studies listed here used the material and geometric properties of the structural component in addition to applied loads as the input parameters. The number of experimental test specimens from which training and testing data were obtained, ranged from 160 [102] to 516 [104].

2.3.3 Seismic Hybrid Simulation

Machine learning algorithms have recently been implemented in the seismic hybrid simulation [4, 8] to address the challenges arising from the computational power and equipment limitations. Having a large complex numerical substructure in hybrid simulation can be computationally challenging, particularly in real-time hybrid simulation (RTHS), due to the time-consuming nature of numerical integration in nonlinear problems when using numerical approaches such as the Finite Element Method. Several attempts have been made in recent years by training and implementing a metamodel to estimate the response of a portion of

the structure not being tested in RTHS, i.e., numerical substructure. Since metamodels as passively-trained ML algorithms can predict the response of the portion of the structure not being tested in the laboratory much faster compared to a numerical substructure. Bas and Moustafa [106, 107] studied the performance and accuracy of the RTHS tests when the Deep LSTM algorithm replaced the numerical substructure in the RTHS framework to minimize delays during hybrid simulation. The Deep LSTM algorithm was trained using the results from finite element simulations under earthquake ground motion excitation.

For seismic force-resisting systems (SFRS) that contain more than one critical component, such as multi-storey braced frames, the nonlinear response of the structural system is not localized. Thus, physically testing only a few critical components may not yield reliable results. To overcome this challenge, novel HS methods based on the model updating technique have been taken in recent years. The concept of model updating in HS was first introduced by Yang et al. [108] by exploiting the experimental data exchanged explicitly through the interfacial nodes to implicitly refine the response of the numerical substructure in real time [109]. The model updating technique is expected to yield a more accurate response provided that the constitutional and geometrical characteristics of the numerical and experimental substructures are similar to each other. Kwon et al. [110] proposed a model updating strategy for pseudo-dynamic hybrid simulation (PsDHS) that is achieved by an iterative calibration of weighting factors applied to several imaginary numerical counterparts, which encompassed the potential variation in physical specimen properties. The accuracy of this approach is highly dependent on the properties assumed for alternative numerical counterparts. Over the past decade, the class of Kalman filter-based system identification gained attention in real-time hybrid simulation (RTHS). In this method, Bouc-Wen hysteresis model [62] parameters that best-fit to the experimental substructure are identified through the constrained unscented Kalman filter [111, 112] or unscented Kalman filter algorithm [113–115] and then are used to update the hysteresis parameters of the numerical component in each time step of RTHS [116].

Table 2.1: Summary of machine learning algorithms used for seismic response and performance assessment of structures [82]

Reference	Year	Case Study Structure Type	Research Goal	Machine Learning Algorithm
[86]	2004	Masonry Building	Fragility Analysis	Response Surface
[84]	2011	RC Frame	Fragility Analysis	ANN
[85]	2012	Steel MRF	Fragility Analysis	Linear Regression with Polynomial Basis Function
[87]	2013	Steel Bridge	Fragility Analysis	Response Surface
[89]	2014	Steel MRF	Fragility Analysis	ANN
[32]	2015	Multi-storey Shear Frame	Data-driven Seismic Response Simulation	polynomial chaos NARX
[96]	2015	RC Frame	seismic reliability analysis	Kriging
[90]	2016	Steel MRF	Fragility Analysis	K-Means, Cuckoo algorithm, Takagi-Sugeno-Kang fuzzy model
[91]	2017	RC Infilled Frames	Estimating Aftershock Collapse Vulnerability	LS, PCA, LASSO, Ridge
[92]	2018	RC Frame	Post-earthquake Structural Safety Assessment	Random Forest
[93]	2018	RC Frame	seismic reliability analysis	Support Vector Regression
[94]	2019	Steel MRF	Fragility Analysis	Logistic, LASSO, SVM, Naïve Bayes, DT, RF, KNN, DA, ANN
[97]	2019	Tall RC Frame	Assess the Residual Structural Capacity	LASSO, SVM
[33]	2019	MDOF structural system with negative stiffness device (NSD)	Data-driven Seismic Response Simulation	SINDy
[35]	2019	Steel MRF	Data-driven Seismic Response Simulation	Deep LSTM
[95]	2019	Truss, MRF	seismic reliability analysis	Radial Basis Functions, Genetic Algorithm
[34]	2019	SDOF System	Data-driven Seismic Response Simulation	Deep CNN
[36]	2020	Steel MRF	Data-driven Seismic Response Simulation	Physics-informed Multi-LSTM
[37]	2020	RC Frame	Data-driven Seismic Response Simulation, Fragility Analysis	Physics-guided CNN
[83]	2020	RC Frame	Probabilistic Seismic Response Evaluation, Fragility Analysis	Bayesian Deep Learning

Chapter 3

Hybrid Data-driven and Physics-based Simulation Framework for Seismic Analysis of Structural Systems

3.1 Abstract

This study proposes a new hybrid analysis framework by integrating a data-driven method with a physics-based technique to perform a nonlinear structural analysis under seismic loading. The proposed hybrid data-driven and physics-based simulation (HyDPS) framework offers an efficient approach and is expected to address the challenges associated with computational cost and modelling uncertainties inherent in physics-based seismic analysis using numerical methods. In this framework, the well-understood components of the structure modeled numerically are combined with the critical components of the structure, e.g., seismic fuses, simulated using the data-driven PI-SINDy model proposed as part of the HyDPS framework. The PI-SINDy data-driven model is developed for hysteretic response simulation by incorporating an operator-based hysteresis model, Prandtl-Ishlinskii (PI) model, as the basis functions into the sparse identification of nonlinear dynamics (SINDy) algorithm. The proposed PI-SINDy data-driven model trained using hysteresis data obtained from experimental testing of a buckling-restrained brace and numerically-generated hysteretic data from a single degree-of-freedom system, is shown to accurately and efficiently predict the inelastic hysteretic response of structural components. Furthermore, the performance of the

HyDPS framework powered by the PI-SINDy model is verified as compared to two other data-driven models proposed in the past studies using the nonlinear response history analyses performed on a steel buckling-restrained braced frame under a set of earthquake ground motion accelerations.

3.2 Introduction

Numerical methods such as the Finite Element Method (FEM) have widely been used as the primary technique for computational modelling of structural and mechanical systems [117]. Particularly, in structural and earthquake engineering applications, the FEM has been applied to solve a wide range of problems such as the nonlinear dynamic response of structures [118], structural optimization [119], model updating [120], and damage detection [121]. Despite the growth in computational power and the development of efficient algorithms to solve nonlinear problems, detailed finite element simulation of full-scale prototype structural systems or assemblies with realistic nonlinear material properties under extreme loading conditions remains a challenging task. Furthermore, several assumptions made in the course of developing a numerical model, including constitutive model parameters, damping definition, boundary condition definition, element shape function and integration points, mesh density, numerical solution method and parameters, may result in an inaccurate structural response. A potential alternative to detailed finite element simulation is to use low-fidelity numerical models, e.g., fiber-based models [118], to examine the global response of the structure and take advantage of high-fidelity modelling technique to only study the local response of critical components, which heavily influence the global dynamic response of the structure, e.g., connections or yielding elements in steel seismic force-resisting systems.

A wealth of experimental test data is generated from laboratory testing of structural components and assemblies as a result of numerous advanced testing equipment, new structural testing facilities, modern instrumentation and sensors. The available data can be leveraged by the emerging Artificial Intelligence (AI) techniques towards a more accurate and efficient

structural response prediction, which would offer a viable alternative to traditional finite element-based simulations, in particular, taking into account the challenges associated with numerical methods as described earlier. In recent years, various data-driven approaches have been used for the assessment of the dynamic response of structural systems, which allows to synergically use past experimental test data to estimate the performance of structures, in particular, when responding to environmentally induced loads such as earthquake [122], extreme wind events [123], tornadoes [124], landslide [125]. As shown in Fig. 3.1, a fully data-driven model is developed just based on data, e.g., experimental data, that is typically a functional mapping between inputs, i.e., structural demands such as ground motion acceleration data, and outputs, i.e., structural response, using statistical methods and machine learning techniques unlike numerical methods in which experimental data is only used to initialize numerical modelling by calibrating predefined constitutive models or elements. Several machine learning techniques for data-driven simulation of structures were proposed in the past, including response surface methodology [86, 87, 126], Kriging [96, 127], radial basis functions [95, 128], polynomial chaos expansions [32], and support vector machine [93, 129]. More recently, different variations of artificial neural networks (ANNs) have been implemented to map input parameters of a structural system to its output data, which include shallow ANNs [100, 101, 130–132], recurrent neural network (RNN) [99, 133, 134], convolutional neural network (CNN) [34], and long short-term memory (LSTM) network [35]. Shallow ANNs are not capable of learning complex nonlinear structural systems due to their simple architecture. Thus, they can only be implemented in systems with a small number of degrees-of-freedom (DOFs) and relatively simple constitutive behaviour. On the other hand, deep neural networks have been proven to be powerful in learning complex dynamic behaviour of structures that comes at the cost of acquiring rich training data.

To address the issue of data scarcity for training deep neural networks, several recent studies [88, 135, 136] proposed a modified algorithm called physics-informed neural network (PINN) by incorporating physical laws, e.g., equation of motion in a dynamic problem, into

the learning process of deep neural networks to better guide the algorithm in predicting the structural behaviour from rare, sparse, or noisy data. For instance, Zhang et al. [36] incorporated the equation of motion into the loss function of the LSTM network such that not only the error between predicted response and measurements are minimized, but also the equation of motion of the nonlinear structure is concurrently satisfied. In a similar study by Zhang et al. [37] the same concept was used with CNNs and verified through numerical and field sensing measurements.

Input Ground Motion Acceleration

$$\begin{bmatrix} \ddot{u}_g(t_1) \\ \ddot{u}_g(t_2) \\ \ddot{u}_g(t_3) \\ . \\ . \\ . \\ \ddot{u}_g(t_{m-2}) \\ \ddot{u}_g(t_{m-1}) \\ \ddot{u}_g(t_m) \end{bmatrix}$$

Machine Learning Algorithm

Output Displacement Signals

$$\begin{bmatrix} u_1(t_1) & u_2(t_1) & & u_n(t_1) \\ u_1(t_2) & u_2(t_2) & \cdots & u_n(t_2) \\ u_1(t_3) & u_2(t_3) & & u_n(t_3) \\ . & . & & . \\ . & . & \cdots & . \\ . & . & & . \\ u_1(t_{m-2}) & u_2(t_{m-2}) & & u_n(t_{m-2}) \\ u_1(t_{m-1}) & u_2(t_{m-1}) & \cdots & u_n(t_{m-1}) \\ u_1(t_m) & u_2(t_m) & & u_n(t_m) \end{bmatrix}$$

Data Loss:
$$J_D(\boldsymbol{\theta}) = ||\boldsymbol{u}_1 - \hat{\boldsymbol{u}}_1|| + ||\boldsymbol{u}_2 - \hat{\boldsymbol{u}}_2|| + ... + ||\boldsymbol{u}_n - \hat{\boldsymbol{u}}_n||$$

Solution:
$$\boldsymbol{\theta}_{Optimal} = \underset{\boldsymbol{\theta}}{arg\ min}\ J_D(\boldsymbol{\theta})$$
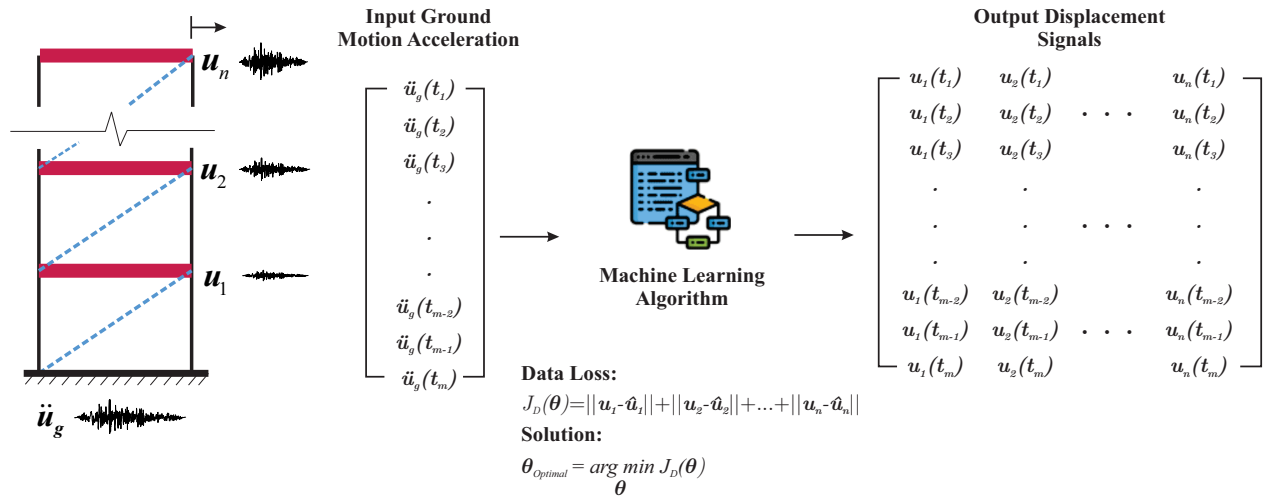
Figure 3.1: Simulation of structural systems using data-driven models.

The prediction of the structural response in the majority of the fully data-driven techniques - with or without incorporation of physics-based equations - is only limited to the same structure, with identical geometry, material properties, and boundary conditions, from which the training data has been collected, raising concerns regarding the ability of such methods to be generalized. The reason is that the input parameters of fully data-driven techniques include only the structural demands such as base excitation time series as shown in Fig. 3.1 and not the geometrical or material properties of the structure. Motivated by the idea of combining data-driven and physics-based techniques as demonstrated in [137–139], this chapter proposes a hybrid data-driven and physics-based simulation (HyDPS) framework by integrating the physics-based numerical model of the well-understood components of the

structure, which are typically accurate enough to reproduce the behaviour of less-complex elements responding in the linear range of the material, and the data-driven model of the critical components of the structure expected to undergo inelastic deformation, which would typically involve high computational costs and sometimes inaccurate or sensitive predictions had numerical techniques been utilized. In principle, the proposed HyDPS framework provides the best of both worlds, 1) more accurate and computationally efficient prediction capability of data-driven techniques used for critical components excluding the need for the calibration of the material constitutive behaviour or adjusting modelling assumptions, 2) robustness of the FEM in predicting the well-understood components of the structure, which eliminates the demand for more data by data-driven algorithms. The second goal of this chapter is to propose a new data-driven model referred to as PI-SINDy for the simulation of the nonlinear hysteretic response of structural elements experiencing nonlinear response under dynamic loading.

The proposed model combines Prandt-Ishlinskii [38] hysteresis model with the Sparse Identification of Nonlinear Dynamics (SINDy) algorithm [39]. This data-driven model combined with FEM is then implemented in the proposed HyDPS platform. The architecture of the proposed HyDPS framework is first presented, followed by the introduction of the PI-SINDy data-driven model. The simulation capability of PI-SINDy is then verified using numerical simulation and experimental test data. The performance of the proposed HyDPS framework is finally examined in comparison with HyDPS developed using two data-driven models proposed in the past, namely LS-SVM and RNN, to validate the overall architecture proposed while illustrating the HyDPS framework in simulating the cyclic nonlinear behaviour of structural components.

3.3 Architecture of the Proposed Simulation Technique

The hybrid data-driven and physics-based simulation technique (HyDPS) consists of substructuring a data-driven model to represent the critical components of the structure, which

are expected to respond in the nonlinear range of material or geometry with complex computation, and a physics-based numerical model to simulate the rest of the structure, which are expected to remain elastic demanding relatively low computational efforts. It is anticipated that HyDPS can reduce the computing time and effort by substructuring the structure. The proposed hybrid technique is developed for the seismic response evaluation of structural systems under dynamic loading such as earthquakes. This technique is analogous to the pseudo-dynamic hybrid simulation technique combining numerical modelling and experimental testing techniques to evaluate the seismic performance of structures [10]. The architecture of the HyDPS framework is shown in Fig. 3.2. The data-driven model (the left box in Fig. 3.2) is powered by a machine learning algorithm that is trained using experimental test data and is capable of predicting the nonlinear dynamic response of the critical components, e.g., seismic fuses in a structural system. The numerical substructure (the right box of Fig. 3.2) consists of the structural elements that remain elastic, e.g., capacity-protected members in a structural system, under earthquake loads and will act in parallel to the data-driven model exchanging data, i.e., restoring force and displacement, at each time step in order to solve the equation of motion (EOM) incrementally.

The equation of motion at time step $n + 1$ is defined as follows:

$$\boldsymbol{M}\ddot{\boldsymbol{U}}_{n+1} + \boldsymbol{C}\dot{\boldsymbol{U}}_{n+1} + \boldsymbol{R}_{n+1} = \boldsymbol{P}_{n+1} \qquad (3.1)$$

in which $\boldsymbol{M}$ and $\boldsymbol{C}$ are the system mass and damping matrices, respectively; R_{n+1} is the restoring force vector; and $\boldsymbol{U}$, $\dot{\boldsymbol{U}}$, and $\ddot{\boldsymbol{U}}$ are the displacement, velocity, and acceleration vectors, respectively. The integration of the EOM (Eq. 3.1) is performed in the physics-based model at each increment of the analysis. Furthermore, the masses and damping, including the ones associated with the data-driven model, are simulated in the physics-based model. By applying the structural decomposition to Eq. 3.1 the following is obtained:

$$\boldsymbol{M}\ddot{\boldsymbol{U}}_{n+1} + \boldsymbol{C}\dot{\boldsymbol{U}}_{n+1} + \boldsymbol{R}_{n+1}^{Phy} + \boldsymbol{R}_{n+1}^{DD} = \boldsymbol{P}_{n+1} \qquad (3.2)$$

27

where DD and Phy superscripts represent the restoring force collected from the data-driven and physics-based models, respectively. The initial stiffness of the data-driven substructure should be determined before the simulation so that the differential equation can be solved in the first time step. The initial stiffness can either be calculated manually or predicted by the data-driven model under a small displacement input as the system is expected to respond in the linear range during the initial step. As shown in Fig. 3.2, the displacements at each DOF at the interface of the data-driven and physics-based components are calculated by solving the EOM and are sent to the data-driven model, $\boldsymbol{R}_{n+1}^{DD}$, which will then be fed back to the physics-based model for solving the EOM during the next time step.
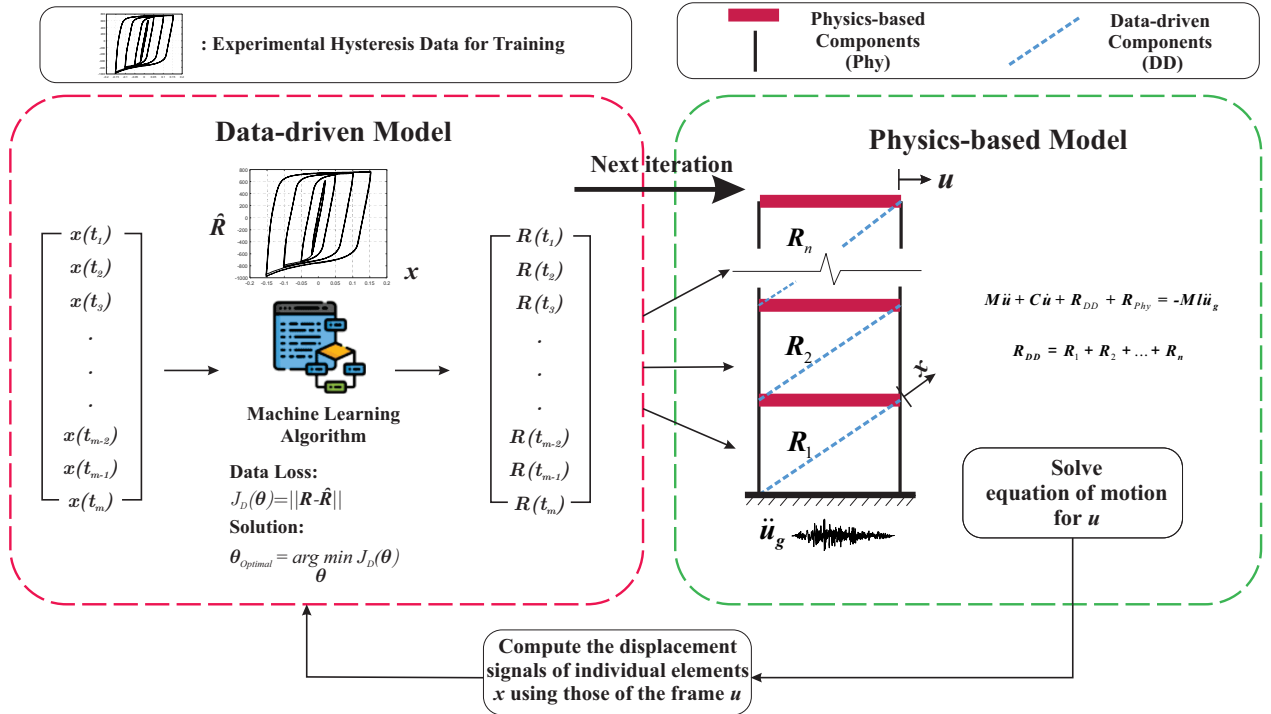
Figure 3.2: Hybrid simulation framework by combining data-driven models and physics-based structural analysis.

Since the data-driven model is the most influential component of HyDPS, special attention is given in this study to the development of a robust algorithm for meta-modelling of the critical component using experimental test data. The PI-SINDy model developed for this purpose is introduced in the next section, followed by the description of two other data-driven

modelling techniques developed in the past for hysteretic structural elements, which will be compared with the proposed PI-SINDy.

3.4 PI-SINDy Data-driven Model for Hysteresis Simulation

The data-driven simulation technique proposed here uses the Sparse Identification of Nonlinear Dynamics (SINDy) algorithm powered by the Prandtl-Ishlinskii (PI) model, which is referred to as the PI-SINDy hysteresis model. The proposed hysteresis model as well as its main components (PI model and SINDy algorithm) are introduced here.

Sparse Identification of Nonlinear Dynamics (SINDy) Algorithm

The Sparse Identification of Nonlinear Dynamics (SINDy) as a model discovery algorithm was recently proposed by Brunton et al. [39]. This model uses the sparse identification algorithm to describe the governing equation of dynamical systems, i.e., the relationship between input variables such as displacements and measured dynamics such as resisting stiffness forces as a function of time. SINDy allows us to define the mathematical relationship, $y = f(x(t))$, between the component's force y and its displacement $x(t)$ using training data that features predefined force-displacement hysteresis, e.g., the hysteretic data obtained from experimental testing of a prototype structural component in the laboratory. For this purpose, a set of potential functions are stacked in a library matrix, $\boldsymbol{\Theta}$:

$$\boldsymbol{\Theta}(\boldsymbol{x}) = \begin{bmatrix} | & | & | & | \\ g_1(\boldsymbol{x}) & g_2(\boldsymbol{x}) & \cdots & g_m(\boldsymbol{x}) \\ | & | & | & | \end{bmatrix}_{n \times m} \tag{3.3}$$

in which $\boldsymbol{x} = [x(t_1), x(t_2), ..., x(t_n)]^T$ is the displacement vector of the training data, $g_i(.), i = 1, 2, ..., m$ are the candidate functions, i.e., basis functions, n and m are the number of measured data points and candidate functions selected to form $\boldsymbol{\Theta}$, respectively. The basis

29

functions should be selected based on the nature of the phenomenon to be predicted by SINDy [39]. A higher number of basis functions involved in the library matrix can help improve discovering the relationship by the algorithm, but with higher computational efforts. Once the library matrix, $\boldsymbol{\Theta}$, is defined, the restoring force vector of the component $\hat{\boldsymbol{y}}$ can be expressed as:

$$\underset{n\times 1}{\hat{\boldsymbol{y}}} = \underset{n\times m}{\boldsymbol{\Theta}} \times \underset{m\times 1}{\boldsymbol{\Xi}} \tag{3.4}$$

in which $\boldsymbol{\Xi} = [\xi_1, \xi_2, ..., \xi_m]^T$ is the coefficient vector that determines which combination of the basis functions should be used to best approximate the nonlinearity involved in the hysteretic behaviour. Sparse regression algorithms such as L_1-regularized regression (LASSO) can then be employed to find the active entries of the $\boldsymbol{\Xi}$ vector. LASSO regression is chosen here due to its ability in setting irrelevant terms to zero, which helps promote sparsity and avoid overfitting [140]. LASSO regression is defined as the following minimization problem:

$$minimize \; \frac{1}{2n}||\boldsymbol{y} - \boldsymbol{\Theta}\boldsymbol{\Xi}||_2^2 + \lambda||\boldsymbol{\Xi}||_1 \tag{3.5}$$

where $\boldsymbol{y}$ is the restoring force vector obtained from training data, $||.||_1$ and $||.||_2$ represent L_1-norm and L_2-norm, respectively. λ denotes the regularization parameter that controls the sparsity of the solution. To achieve an accurate estimation of the model error, the 10-fold cross-validation technique is used in the LASSO regression. $\boldsymbol{\Xi}_{lasso}$ is obtained by solving the LASSO minimization problem, which is then used to describe the relationship $y = f(x(t))$ as follows:

$$\hat{y} = \boldsymbol{\Theta}(x) \times \boldsymbol{\Xi}_{lasso} \tag{3.6}$$

where $\boldsymbol{\Theta}(x)$ is the symbolic function of the displacement x, in contrast to $\boldsymbol{\Theta}(\boldsymbol{x})$ that is the data library matrix of the displacement defined in Eq. 3.3.

Prandtl-Ishlinskii (PI) Model

Given that the efficiency of SINDy highly depends on the basis functions chosen for the library matrix, it is crucial to appropriately select these functions to accurately reproduce the hys-

teretic response of nonlinear systems. In this study, SINDy is paired with the stop operators in Prandtl-Ishlinskii (PI) model [38], which provides SINDy with a hysteretic memory.

The PI model is a phenomenological operator-based hysteretic model defined as the weighted superposition of multiple elastic-perfectly plastic stop operators. The stop operator, which was first introduced for continuum mechanics applications to describe the elastoplastic behaviour of materials [38], is defined as follows:

$$y_r(0) = e_r\left(x(0)\right) \tag{3.7}$$

$$y_r(t) = e_r(x(t) - x(t_i) + y_r(t_i)) \quad for \; t_i < t \le t_{i+1}; \; \; 0 \le i \le N - 1 \tag{3.8}$$

$$e_r(s) = min(r, max(-r, s)) \tag{3.9}$$

in which $y_r(t) = E_r[x(t)]$ is the output of the stop operator for the given input signal $x(t)$, which is defined using a threshold r $(r > 0)$. Within each stop operator, the time domain $[0, T]$ should be discretized into N subintervals, i.e. $0 = t_0 < t_1 < ... < t_N = T$, such that the input signal, $x(t)$, becomes monotonic within each time step $\Delta t = t_{i+1} - t_i$. The PI model is therefore expressed by linearly combining multiple stop operators with different thresholds, i.e., r values:

$$y(t) = \sum_{i=1}^{m} \xi_i E_{r_i}[x(t)] \tag{3.10}$$

where $y(t)$ is the total output signal when the hysteretic system is subjected to an input signal $(x(t))$, e.g., random excitation, $(x(t))$. The PI model parameters including the weights ξ_i and thresholds r_i are adjusted as part of the training process.

The results obtained from a sample numerical simulation to illustrate the role of stop operators in generating hysteretic responses are shown in Fig. 3.3. In this example, an input signal in the form of $x(t) = 5t\sin(2t)$ shown in Fig. 3.3a was first discretized with $\Delta t = 0.02$; the signal was then given as an input to three stop operators with different thresholds ($r_1 = 49.6$, $r_2 = 99.1$, & $r_3 = 148.7$) shown in Fig. 3.3b. Fig. 3.3c shows the output signal of each stop operator. Each stop operator created a hysteretic response as shown in Fig. 3.3d. A

more complex hysteretic response as given in Eq. 3.10 can be generated by linearly combining the output response of each stop operator, $E_{r_i}[x(t)]$, with the corresponding weight, ξ_i. The summation of output signals creating the final hysteretic response is shown in Fig. 3.3e. This illustration example confirmed that a nonlinear hysteretic response, with respect to $x(t)$, can be expressed as the superposition of multiple linear problems with respect to $E_{r_i}[x(t)]$ by taking advantage of stop operators. In other words, stop operators take the initial input signal to a higher dimension in which the nonlinear hysteretic problem can be expressed in the linear form.
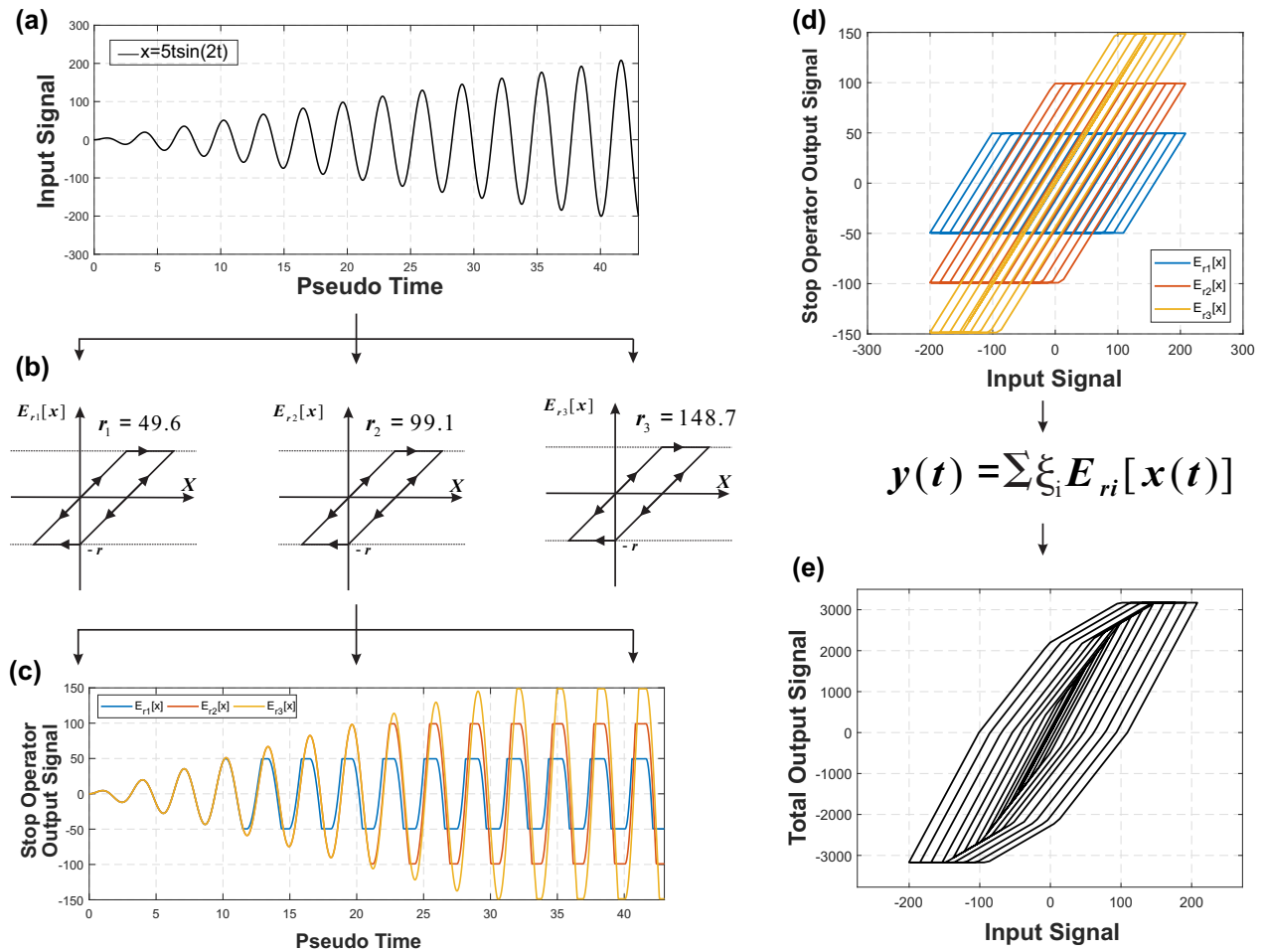
Figure 3.3: Illustration of PI model.

32

3.4.1 PI-SINDy Model

The proposed PI-SINDy model combines the PI model and the SINDy algorithm to simulate the nonlinear hysteretic response of structural components. The stop operators of the proposed model play the role of basis functions of the library matrix (Eq. 3.3), and the Ξ_{lasso} vector contains optimized weights (ξ_i) obtained from LASSO regression (Eq. 3.5). The PI-SINDy data-driven model is therefore defined as follows:

$$
\hat{\boldsymbol{y}}_{n\times 1} = \begin{bmatrix} \vert & \vert & & \vert & \vert & \vert \\ E_{r_1}[\boldsymbol{x}] & E_{r_2}[\boldsymbol{x}] & \cdots & E_{r_m}[\boldsymbol{x}] & \boldsymbol{x} & 1 \\ \vert & \vert & & \vert & \vert & \vert \end{bmatrix}_{n\times(m+2)} \times \underset{(m+2)\times 1}{\Xi_{lasso}} \tag{3.11}
$$

Several potential thresholds r_i are fed to stop operators, which are then used to build the library matrix so that SINDy can determine which combination of thresholds can best describe the hysteretic response of training data. The initial set of thresholds are determined based on the maximum input displacement signal ($|x_{max}|$) as $r_i = \frac{i}{m+1}|x_{max}|$, $i = 1, 2, ..., m$, in which m is obtained using a sensitivity analysis. m should be increased until a good match is seen between the training data and the results obtained from PI-SINDy. It is worth noting that the larger value of m would result in a finer discretization but a computationally expensive optimization.

The parameter λ in Eq. 3.5 is obtained using the Akaike Information Criterion (AIC) [141], which is an estimator for ranking different statistical models based on their accuracy and complexity. Accuracy is defined here as the error between the real measurement available and the estimated value by the model. However, the complexity of the model is represented by the number of parameters used to construct the model. The following equation combines both accuracy and complexity for the SINDy model in the form of the AIC:

$$
AIC = 2K + n\ln\left(\frac{||\boldsymbol{y} - \boldsymbol{\Theta}\boldsymbol{\Xi}||_2^2}{n}\right) \tag{3.12}
$$

in which K is the number of active or non-zero parameters in the $\boldsymbol{\Xi}$ matrix, which penalizes complexity in the model by magnifying the value of AIC while the second term in Eq. 3.12

computes the error. The AIC would return the optimal λ parameter in Eq. 3.5, which corresponds to the point at which the greatest change in slope occurs in the AIC-λ plot, to make a trade-off between accuracy and complexity.

3.5 Alternative Data-driven Models for Hysteresis Simulation

Two alternative data-driven models proposed in the past studies to predict the nonlinear hysteretic behaviour of structural systems are briefly presented here. These models include Lease-Squares Support Vector Machine (LS-SVM) [129], and recurrent Neural Networks (RNN) [99]. These data-driven models will be used in a comparative study later to examine the efficiency of the proposed PI-SINDy data-driven model for the prediction of hysteretic behaviour of structural elements. All data-driven models are implemented in the proposed HyDPS framework.

3.5.1 LS-SVM Data-driven Model

Least-Squares Support Vector Machine (LS-SVM), which was first introduced by Boser et al. [142], is an extension of SVM [143] for solving function estimation problems. This method as a machine learning algorithm was the basis for several data-driven model in the past [129, 144, 145].

Given a training set of N data points, $(\mathbf{z}^k, y_k), k = 1, 2, ..., N$, in which $\mathbf{z}^k$, and y_k are the input and output vectors respectively, LS-SVM first maps the input data into a higher dimensional space, called feature space, and then estimates the output using the following linear regression model:

$$\hat{y}(\mathbf{z}) = \boldsymbol{w}^T.\phi(\mathbf{z}) + b \tag{3.13}$$

in which $\hat{y}$ is the estimated output, $\boldsymbol{w}$ is the weight vector, b is the bias, and $\phi(*)$ is the nonlinear mapping function from the input space to feature space. To estimate a function

using LS-SVM, the respective cost function, $J(w, e)$, should be minimized as given in Eq. 3.14 when subjected to constraints of Eq. 3.15:

$$\min_{\boldsymbol{w},b,\boldsymbol{e}} J(\boldsymbol{w}, \boldsymbol{e}) = \frac{\gamma}{2} \sum_{k=1}^{N} e_k^2 + \frac{1}{2}\|\boldsymbol{w}\|^2 \tag{3.14}$$

$$y_k = \mathbf{w}^{\mathrm{T}}\phi\left(\mathbf{z}^k\right) + b + e_k, \quad k = 1, 2, \ldots, N \tag{3.15}$$

where γ is the regularization factor for balancing the complexity of the model and estimation accuracy, and e_k is the error. Eq. 3.16 is computed using the Lagrange multipliers method [146] as follows:

$$\mathcal{L}(\mathbf{w}, b, \mathbf{e}, \boldsymbol{\alpha}) = J(\mathbf{w}, \mathbf{e}) - \sum_{k=1}^{N} \alpha_k \left(\mathbf{w}^T\phi\left(\mathbf{z}^k\right) + b + e_k - y_k\right) \tag{3.16}$$

where α_ks are the Lagrange multipliers. Using the Karush-Kuhn-Tucker conditions for optimality [147], the partial derivatives of Eq.3.16 are taken to obtain the following:

$$
\begin{aligned}
\frac{\partial \mathcal{L}}{\partial \mathbf{w}} &= 0 \rightarrow \mathbf{w} = \sum_{k=1}^{N} \alpha_k \phi\left(\mathbf{z}^k\right) \\
\frac{\partial \mathcal{L}}{\partial e_k} &= 0 \rightarrow \alpha_k = C e_k \\
\frac{\partial \mathcal{L}}{\partial b} &= 0 \rightarrow \sum_{k=1}^{N} \alpha_k = 0 \\
\frac{\partial \mathcal{L}}{\partial \alpha_k} &= 0 \rightarrow \mathbf{w}^{\mathrm{T}}\boldsymbol{\phi}\left(\mathbf{z}^k\right) + b + e_k - y_k = 0
\end{aligned}
\tag{3.17}
$$

by eliminating e_k and $\boldsymbol{w}$, the parameters $\boldsymbol{\alpha}$ and b are computed using the following system of equations:

$$
\begin{bmatrix} 0 & \mathbf{1}_N^T \\ \mathbf{1}_N & \boldsymbol{\Omega} + \mathbf{I}/\gamma \end{bmatrix}
\begin{bmatrix} b \\ \boldsymbol{\alpha} \end{bmatrix} =
\begin{bmatrix} 0 \\ \mathbf{y} \end{bmatrix}
\tag{3.18}
$$

in which $\boldsymbol{\alpha}^T = [\alpha_1, \alpha_2, ..., \alpha_N]$, $\boldsymbol{y}^T = [y_1, y_2, ..., y_N]$, $\mathbf{1}_N^T = [1, 1, ..., 1]$, and $\boldsymbol{I}$ is the identity matrix of size $N \times N$. Ω is defined according to the Mercer's condition [148] as:

$$\Omega_{kl} = \phi\left(\mathbf{z}^k\right)^T \phi\left(\mathbf{z}^l\right) = K\left(\mathbf{z}^k, \mathbf{z}^l\right), k, l = 1, 2, \ldots, N \tag{3.19}$$

in which $K(*, *)$ represents a predefined kernel function intended to achieve the goal of avoiding explicit definitions of mapping $\phi(*)$. The LS-SVM model can finally be expressed as:

$$\hat{y}(\mathbf{z}) = \sum_{k=1}^{N} \alpha_k K\left(\mathbf{z}, \mathbf{z}^k\right) + b \tag{3.20}$$

where α_ks and b are determined by solving a set of linear equations given in Eq. 3.18.

There are several possibilities for choosing the kernel function. We found that the linear kernel for the technique proposed in this study yields more accurate predictions when compared to radial basis kernel function. The linear kernel takes the following form:

$$K\left(\mathbf{z}, \mathbf{z}^k\right) = \mathbf{z}^T \mathbf{z}^k \tag{3.21}$$
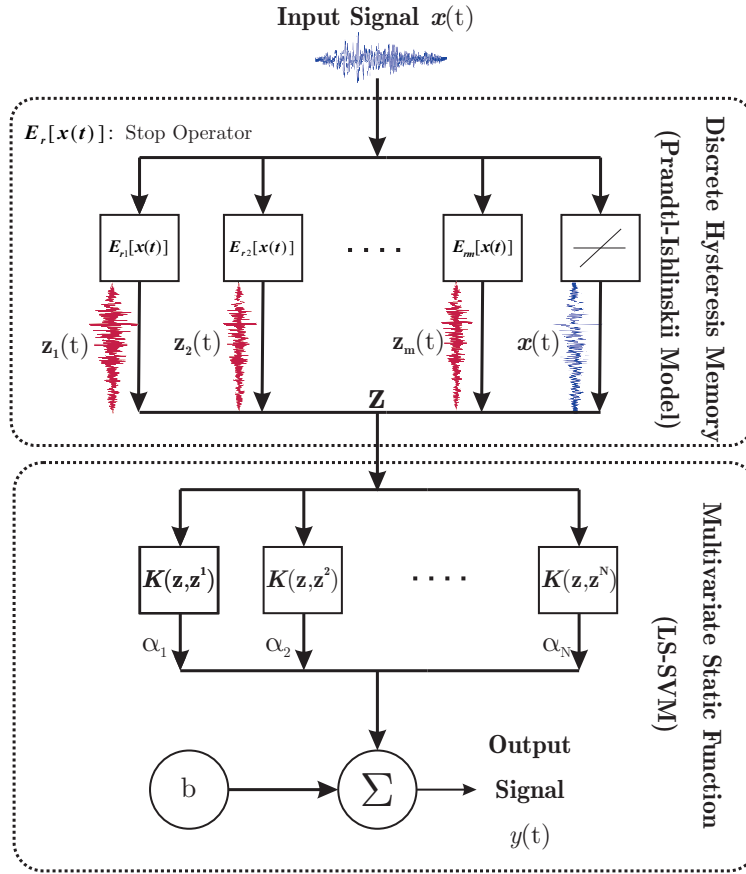
Figure 3.4: LS-SVM data-driven model for hysteresis simulation [129].

The LS-SVM hysteresis data-driven model proposed by [129] uses a series of stop operators, which creates a discrete hysteresis memory in which the LS-SVM algorithm is used for learning the functional mapping from feature space to output space. The model function is shown in Fig. 3.4. In this figure, the discrete hysteresis memory section consists of m stop operators with the thresholds that are assigned based on $r_i = i/(n+1)|x|_{max}, i = 1, 2, ..., n,$

in which $|x|_{max}$ is the maximum of absolute displacement of training hysteresis data. The output of multiple stop operators from the discrete hysteresis memory step is then given to the multivariate static function step as input values. LS-SVM is used in the multivariate static function step to approximate the mapping between the stop operator outputs and the restoring force provided by the training data.

3.5.2 RNN Data-driven Model

Recurrent Neural Networks (RNNs) have been employed in the past to predict the hysteretic behaviour of structural elements [79, 99, 109, 149]. In this study the model proposed by Yun et al. [99] was used. RNN is a variation of ANN in which previous outputs are used as inputs of the current step.

The RNN model is created by assembling multiple layers each comprised of several neurons (i.e., Fig. 3.5c) passing their output as the input to the connected neuron in the next layer. Each vector transformation from layer $r-1$ with d neurons to the immediate next layer r with m neurons can be expressed as:

$$\underbrace{\begin{bmatrix} h_1^{(r)} \\ \vdots \\ \vdots \\ h_m^{(r)} \end{bmatrix}}_{\boldsymbol{h}^{(r)} \in \mathbb{R}^{m \times 1}} = S \left\langle \underbrace{\begin{bmatrix} \dots & \boldsymbol{w}_1^{(r-1)} & \dots \\ \dots & \boldsymbol{w}_2^{(r-1)} & \dots \\ \dots & \vdots & \dots \\ \dots & \boldsymbol{w}_m^{(r-1)} & \dots \end{bmatrix}}_{\boldsymbol{W}^{(r)} \in \mathbb{R}^{m \times d}} \underbrace{\begin{bmatrix} h_1^{(r-1)} \\ h_2^{(r-1)} \\ \vdots \\ h_d^{(r-1)} \end{bmatrix}}_{\boldsymbol{h}^{(r-1)} \in \mathbb{R}^{d \times 1}} + \underbrace{\begin{bmatrix} b_1^{(r-1)} \\ b_2^{(r-1)} \\ \vdots \\ b_m^{(r-1)} \end{bmatrix}}_{\boldsymbol{b}^{(r)} \in \mathbb{R}^{m \times 1}} \right\rangle \tag{3.22}$$

in which $S \langle * \rangle$ is the nonlinear activation function, $h_i^{(r)}$ is the output of ith neuron in layer r. $\boldsymbol{W}^{(r)}$ and $\boldsymbol{b}^{(r)}$ are the weight matrix and bias vector, respectively, that connect layer $r-1$ to layer r and should be optimized in the training phase. Eq. 3.22 can be succinctly written as:

$$\boldsymbol{h}^{(r)} = S \left\langle \boldsymbol{W}^{(r)} \boldsymbol{h}^{(r-1)} + \boldsymbol{b}^{(r)} \right\rangle \tag{3.23}$$

To obtain a deeper fully-connected neural network multiple layers should be stacked next to

each other, which can be expressed as:

$$\boldsymbol{h}^{(1)} = S \left\langle \boldsymbol{W}^{(1)} \boldsymbol{x} + \boldsymbol{b}^{(1)} \right\rangle$$
$$\boldsymbol{h}^{(2)} = S \left\langle \boldsymbol{W}^{(2)} \boldsymbol{h}^{(1)} + \boldsymbol{b}^{(2)} \right\rangle \qquad (3.24)$$
$$\vdots$$
$$\boldsymbol{y}(\boldsymbol{x}) = S \left\langle \boldsymbol{W}^{(p)} \boldsymbol{h}^{(p-1)} + \boldsymbol{b}^{(p)} \right\rangle$$

in which $\boldsymbol{x}$ and $\boldsymbol{y}$ are the inputs and outputs of the neural network, respectively, and p is the number of layers in the neural network architecture.

Yun et al [99] proposed the application of five variables to achieve the single-valuedness between input and output as shown in Fig. 3.5a to facilitate the learning capability of RNN and to efficiently convert one-to-many mapping to a one-to-one mapping problem owing to several potential force outputs (e.g., loading and unloading cycles) for a given displacement input. In this figure, ϵ_n and σ_n denote strain and stress at the nth time step. In addition to stress and strain of the previous step two additional internal variables shown in Fig. 3.5b are used as the model inputs:

$$\psi_n = \sigma_{n-1} \epsilon_{n-1} \qquad (3.25)$$

$$\eta_n = \sigma_{n-1} \left(\epsilon_n - \epsilon_{n-1} \right) \qquad (3.26)$$

in which the subscript n denotes the nth data point in the hysteresis curve. The internal variable Ψ_n represents an energy quantity based on the previous state equilibrium path, while the internal variable η_n indicates the load step in the direction of equilibrium path. Therefore, the hysteresis learning capability in the RNN model is achieved by introducing $\boldsymbol{x} = [\epsilon_n, \sigma_n, \sigma_{n-1}, \Psi_n, \eta_n]^T$ as the recurrent inputs which depend on the output of the RNN in previous prediction step, i.e., $y = \sigma_{n-1}$.
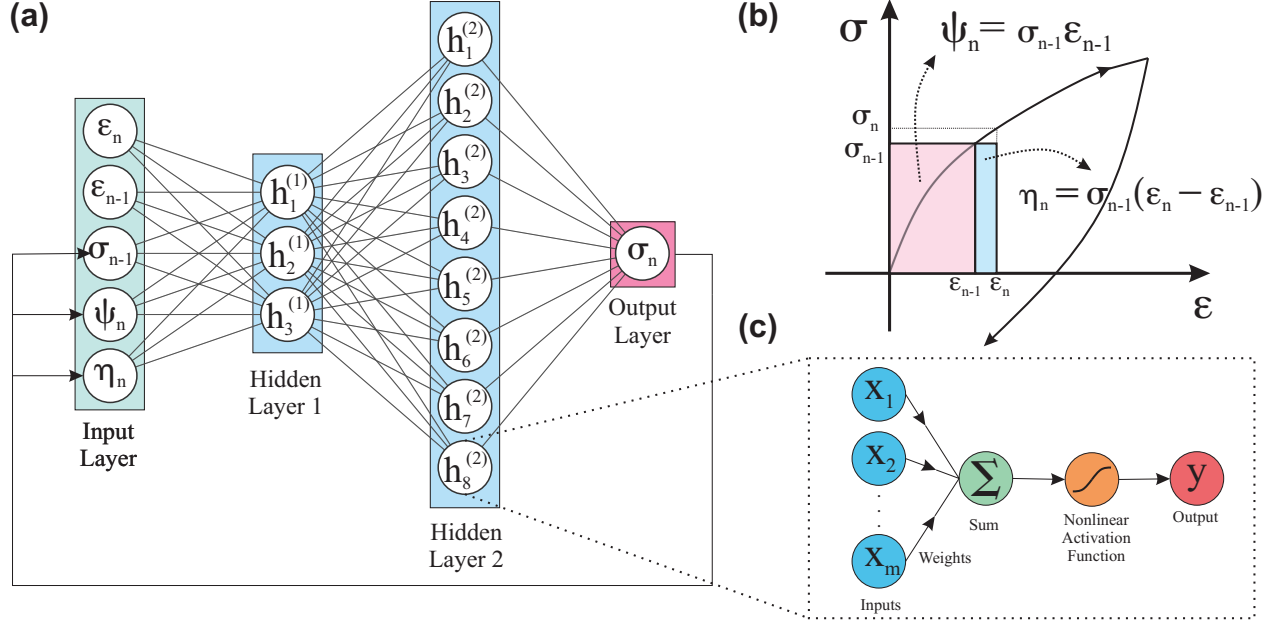
Figure 3.5: RNN-based model for hysteresis simulation [99]; a) architecture of the RNN, $h_i^{(j)}$ represents the ith neuron in the jth hidden layer, b) definition of two internal parameters, ψ and η, used in the RNN, c) architecture of a single neuron.

3.6 Verification of the Data-driven PI-SINDy Model

The PI-SINDy data-driven model was verified in two steps. In the first step, the test data obtained from experimental testing of steel buckling-restrained braces experiencing nonlinear cyclic response was used to assess the performance of PI-SINDy model in predicting the hysteretic response of structural elements in real-life conditions. In the second step, various hysteresis shapes anticipated in energy-dissipating structural elements under seismic loading were then used to numerically verify PI-SINDy.

3.6.1 Model Performance Metrics

The performance of the trained data-driven model was evaluated using both the training and testing datasets to measure how well the proposed model can predict the cyclic nonlinear responses such as displacement, drift ratio and restoring force as compared to their respective reference values. In this study, two performance metrics including 1) Normalized Root-Mean-

Square-Error (NRMSE) given in Eq. 3.27, and 2) Peak Point Error (PPE) given in Eq. 3.28 were used to evaluate the performance of the PI-SINDy model:

$$NRMSE = \frac{\sqrt{\sum_{i=1}^{N}(y_{ref,i} - y_{model,i})^2/N}}{|y_{ref}^{max} - y_{ref}^{min}|} \tag{3.27}$$

$$PPE = \frac{||y_{ref}|^{max} - |y_{model}|^{max}|}{|y_{ref}|^{max}} \tag{3.28}$$

in which N indicates the number of data points, y_{ref} and y_{model} refer to the reference and predicted responses, respectively. NRMSE represents the total error over time history of the data, while PPE only accounts for the error at peak points.

3.6.2 Hysteretic Response Prediction of Steel BRBs

The experimental data obtained from full-scale laboratory testing of all-steel BRB specimens conducted by Dehghani et al. [150] were used to evaluate the performance of PI-SINDy in predicting the hysteretic response of steel BRBs. The BRB specimen was approximately $6021mm$ long between work-points with a yielding segment equal to $3000mm$. The BRB core was made of CSA G40.21-350WT Category 4 steel with the minimum yield strength of $F_y = 350MPa$ and core area of $2858mm^2$. The BRB was subjected to a linearly-increasing cyclic displacement protocol that created maximum positive and negative strains of $\pm3\%$ in the core (Fig. 3.6a). The test data was not filtered nor smoothed out.

The history of axial strain in the BRB core shown in Fig. 3.6a was used to train the PI-SINDy model. The optimal λ parameter in the training phase was chosen using the AIC plot of training shown in Fig. 3.6b. To illustrate the influence of the value of λ on the prediction, two extreme λ values, which are shown with blue ($\lambda = 10^{-5}$) and green ($\lambda = 10^{+3}$) points in the AIC plot (Fig. 3.6b) were also used in training. Figs. 3.6d- 3.6f show the BRB axial stress-axial strain data (solid line) that was used to train PI-SINDy plus the hysteretic response predicted by the proposed data-driven model (dashed line). As shown in Fig. 3.6d, a low λ parameter resulted in over-complex training, which required a large number of stop operators

(51) than those used when an optimal λ resulting in 12 active stop operators was selected for training (Fig. 3.6e). However, a large λ parameter gave rise to an over-sparse solution such that the number of active stop operators (2) was considerably lower than the optimal case (Fig. 3.6f vs. Fig. 3.6e), which created a significantly poor hysteretic response as shown in Fig. 3.6f. Fig. 3.6e represents the trade-off between model complexity and accuracy in PI-SINDy, which indicated that PI-SINDy can efficiently de-noise training experimental data and identify the true relationship between the input and output parameters if an optimal λ is selected using the AIC. To further illustrate the role of the AIC in selecting optimal λ parameter, the trace plot of each weight in the PI-SINDy model associated with a stop operator is shown in Fig. 3.7. As referring to this figure, a more sparse and less complex model is achieved by increasing the λ parameter, meaning that fewer stop operators are achieved.

The PI-SINDy model trained using the cyclic test data was finally used to predict the dynamic response of the BRB specimen tested under the earthquake-induced displacement history shown in Fig. 3.6c with a loading rate similar to that of the earthquake ground motion. The same set of the λ parameters obtained from the AIC plot ($\lambda = 10^{-5}$, 10^1 and 10^3) were used to perform the dynamic analysis. The hysteretic behaviours of the BRB predicted using PI-SINDy was compared to the response measured in the experiment in Figs. 3.6g - 3.6i for $\lambda = 10^{-5}$, 10^1 and 10^3, respectively. The NRMSE computed for $\lambda = 10^{-5}$, 10^1 and 10^3 were 2.23%, 2.13%, and 19.44%, respectively, which shows the influence of the AIC selection on how well experimental data under a random input signal such as the earthquake-induced displacement history can be replicated.

A portion of training error observed in Fig. 3.6e using an optimal λ was associated with the fact that the PI model was essentially developed for a symmetric hysteretic response, while the experimental test data of the BRB used here exhibited an asymmetric response owing to the frictional force developed between the core and BRB casing, i.e., restrainer, when the BRB core undergoes compression and tends to buckle [151–153]. A potential solution for

enriching PI-SINDy to simulate the asymmetric response of structural elements such as the BRB core would be adding two separate compression-only and tension-only springs to the PI model arrangement (Fig. 3.3).
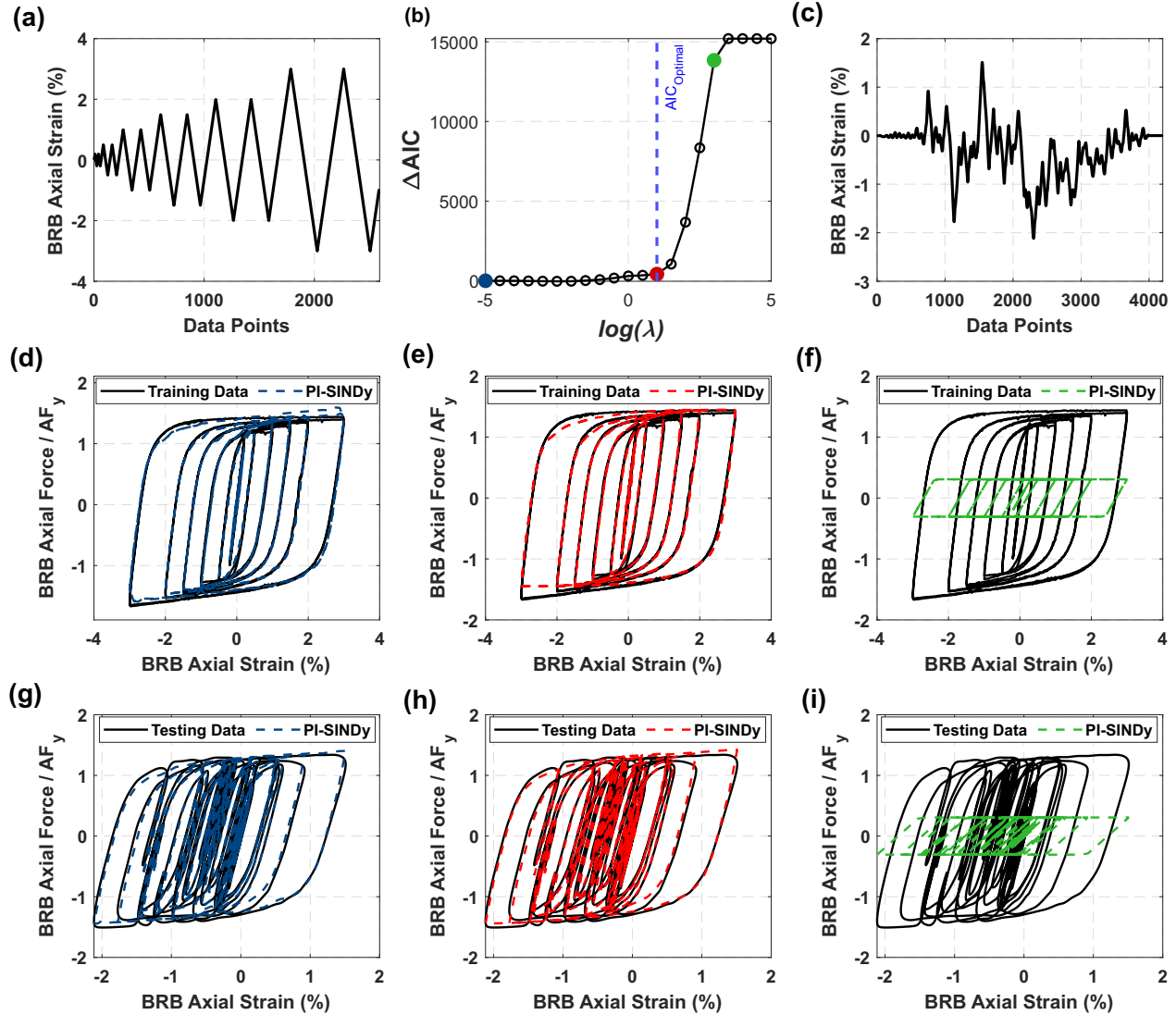
Figure 3.6: PI-SINDy verification: (a) cyclic displacement history used for training, (b) AIC plot (blue, red, and green points correspond to the over-complex, optimal and over-simplified models, respectively), (c) dynamic displacement history used for testing , (d-f) BRB normalized force – normalized deformation responses during training for the over-complex, optimal and over-simplified models, respectively, under the displacement history of (a), (g-i) are the testing results - when the brace is subjected to displacement history shown in graph (c) - for blue, red, and green points, respectively.

The trained data-driven model can be used for simulating the seismic response of buckling-

restrained braced frames (BRBFs) by reproducing the nonlinear cyclic response of BRBs as long as the cross-sectional area and yield strength of the BRB core are identical to those of the PI-SINDy training data. However, in a well-designed multi-storey BRBFs, the geometrical properties of BRBs vary over the stories. This can be addressed by using normalized force (i.e., stress) and normalized axial deformation (i.e., strain) data of the BRB core to train the PI-SINDy model instead of the force-displacement data to eliminate the influence of the cross-sectional area and length of the brace on training. The output signal predicted by the PI-SINDy model trained using the stress-strain data should then be multiplied by the cross-sectional area of the respective BRB at each storey to determine the respective restoring force.
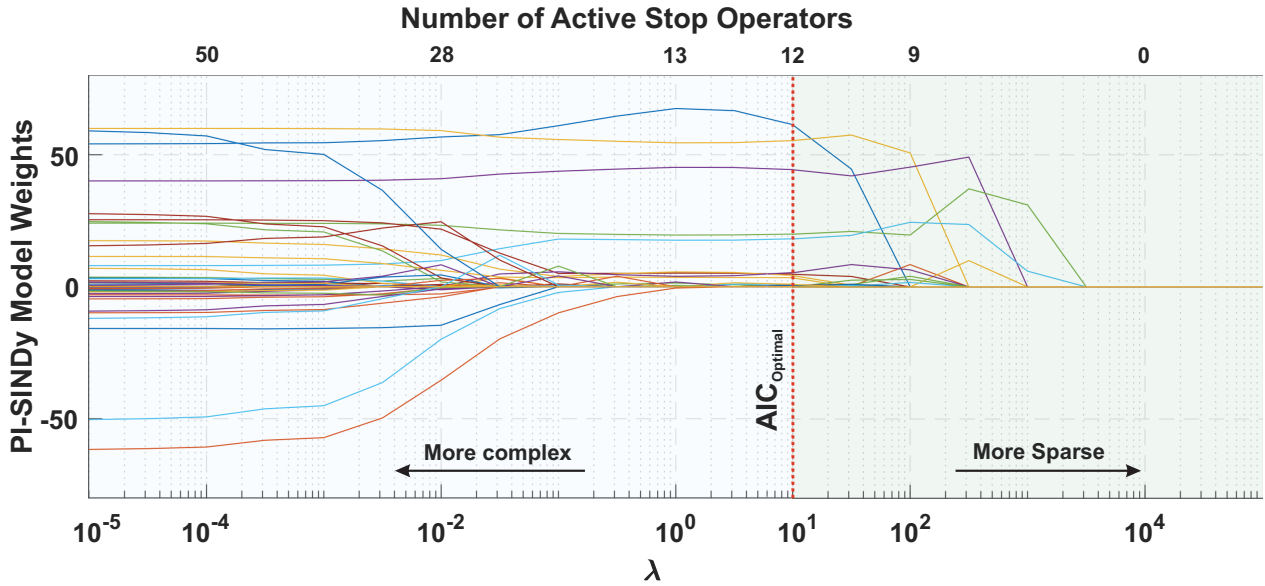
Figure 3.7: Trace plot of the PI-SINDy weights (for 51 stop operators) in a logarithmic scale (each curve shows the variation of the weight associated with a stop operator for the respective λ parameter).

3.6.3 Response Prediction of Hysteretic Single Degree-of-Freedom Systems

The application of the PI-SINDy model in predicting the hysteretic behaviours with various shapes and hardening properties expected in seismic force-resisting system components, e.g.,

buckling-restrained brace (BRB) core, eccentrically braced frame (EBF) link beams, and moment-resisting frame (MRF) beams are assessed using a series of dynamic analyses conducted using the reference model defined as a mass-damper-spring single-degree-of-freedom (SDOF) system with the spring made of the Bouc-Wen (BW) hysteresis model [50, 62] as shown in Fig. 3.8, and the PI-SINDy model that simulates the hysteretic behaviour of the spring.
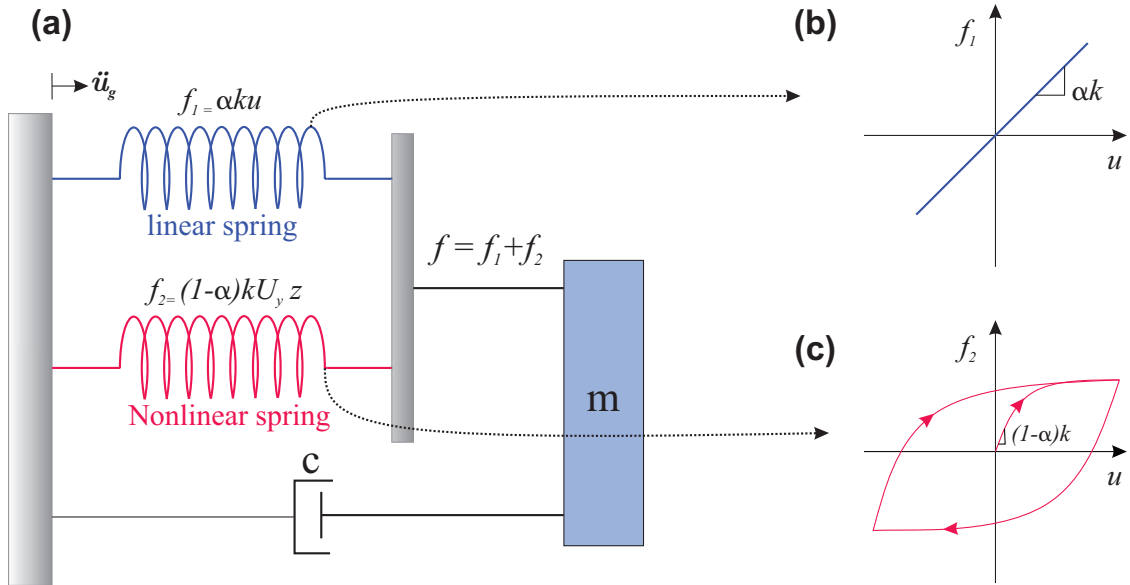
Figure 3.8: Bouc-Wen hysteresis model.

To solve the SDOF system subjected to a base excitation, the equation of motion of the system should be solved numerically:

$$m\ddot{u} + c\dot{u} + f(u,t) = -m\ddot{u}_g \tag{3.29}$$

where m is the mass, c is viscous damping, u is displacement, $\dot{u}$ is velocity, $\ddot{u}$ is acceleration, $\ddot{u}_g$ is the ground acceleration, and $f(u,t)$ is the nonlinear hysteretic restoring force, which is produced using the BW hysteresis model:

$$f(u,t) = \alpha k u + (1-\alpha)kU_y z \tag{3.30}$$

where k is the elastic stiffness prior to yielding, α is the ratio of post-yield to elastic stiffness,

and z is the hysteretic deformation obtained by solving the following differential equation:

$$\dot{z} = \frac{1}{U_y} \left[A\dot{u} - \beta |\dot{u}| |z|^{n-1} z - \gamma \dot{u} |z|^n \right] \tag{3.31}$$

in which n, Uy, β, γ, and A control the shape of the hysteresis loop.

To determine the displacement response of the SDOF system under the ground acceleration, Eqs. 3.29 to 3.31 should be reformulated in the state space format and then solved simultaneously. The Runge-Kutta numerical integration scheme was used to solve the equation of motion of the inelastic SDOF system.

To generate the hysteretic behaviours with various shapes and hardening properties, a suite of 20 various BW material model parameters, each representing a distinct nonlinear hysteretic response, were randomly generated as given in Table 3.1. Fig. 3.9 shows the hysteretic relationship of each set of parameters obtained using the numerical model of the SDOF subjected to a monotonically-increasing cyclic displacement history. These force-displacement datasets were used to train the PI-SINDy model. The spring in the SDOF system was then replaced with the trained data-driven model. The SDOF system was subjected to the horizontal excitation generated by the 1978 Tabas, Iran-Dayhook earthquake acceleration record. The s of the displacement history of the SDOF system were computed against that obtained using the reference model under the same acceleration record. Fig. 3.10 compares the training and testing phases of all 20 hysteretic shapes considered here. The average error of predicted responses was 1.97%, which is slightly higher than that of the dataset used to train the model (0.87%), which reveals the capability of the proposed data-driven hysteretic model in predicting the nonlinear cyclic response of structural components. The results of the prediction also confirmed that training becomes more challenging when a highly nonlinear or polynomial hardening material response is expected, resulting in higher errors in the testing phase. For example, models 2, 12, 14, and 20 that involve more complex hysteretic shapes compared to others featured higher errors in training phase, 1.23%, 1.14%, 1.56%, 0.84%, and in testing phase, 4.30%, 2.93%, 5.70%, 3.48%, respectively (Fig. 3.10). The correlation

coefficient between testing and training errors among all 20 models is 0.71 suggesting that less training error most often gives rise to a more accurate prediction by PI-SINDy when it is tested with an unseen displacement history.

Table 3.1: Bouc-Wen material models for PI-SINDy verification.

Model ID	k	m	ξ	A_0	α	n	β	γ
1	54069	671.1	0.02	1	0.041	3.451	0.439	0.751
2	54069	671.1	0.02	1	0.045	0.661	0.382	0.255
3	54069	671.1	0.02	1	0.006	4.321	0.766	0.506
4	54069	671.1	0.02	1	0.046	4.703	0.795	0.699
5	54069	671.1	0.02	1	0.032	3.554	0.187	0.891
6	54069	671.1	0.02	1	0.005	3.910	0.490	0.959
7	54069	671.1	0.02	1	0.014	3.844	0.446	0.547
8	54069	671.1	0.02	1	0.027	2.265	0.646	0.139
9	54069	671.1	0.02	1	0.048	3.450	0.709	0.149
10	54069	671.1	0.02	1	0.048	1.270	0.755	0.258
11	54069	671.1	0.02	1	0.008	3.677	0.276	0.841
12	54069	671.1	0.02	1	0.049	0.643	0.680	0.254
13	54069	671.1	0.02	1	0.048	1.746	0.655	0.814
14	54069	671.1	0.02	1	0.024	0.708	0.163	0.244
15	54069	671.1	0.02	1	0.040	0.937	0.119	0.929
16	54069	671.1	0.02	1	0.007	4.206	0.498	0.350
17	54069	671.1	0.02	1	0.021	3.627	0.960	0.197
18	54069	671.1	0.02	1	0.046	1.927	0.340	0.251
19	54069	671.1	0.02	1	0.040	4.776	0.585	0.616
20	54069	671.1	0.02	1	0.048	0.655	0.224	0.473
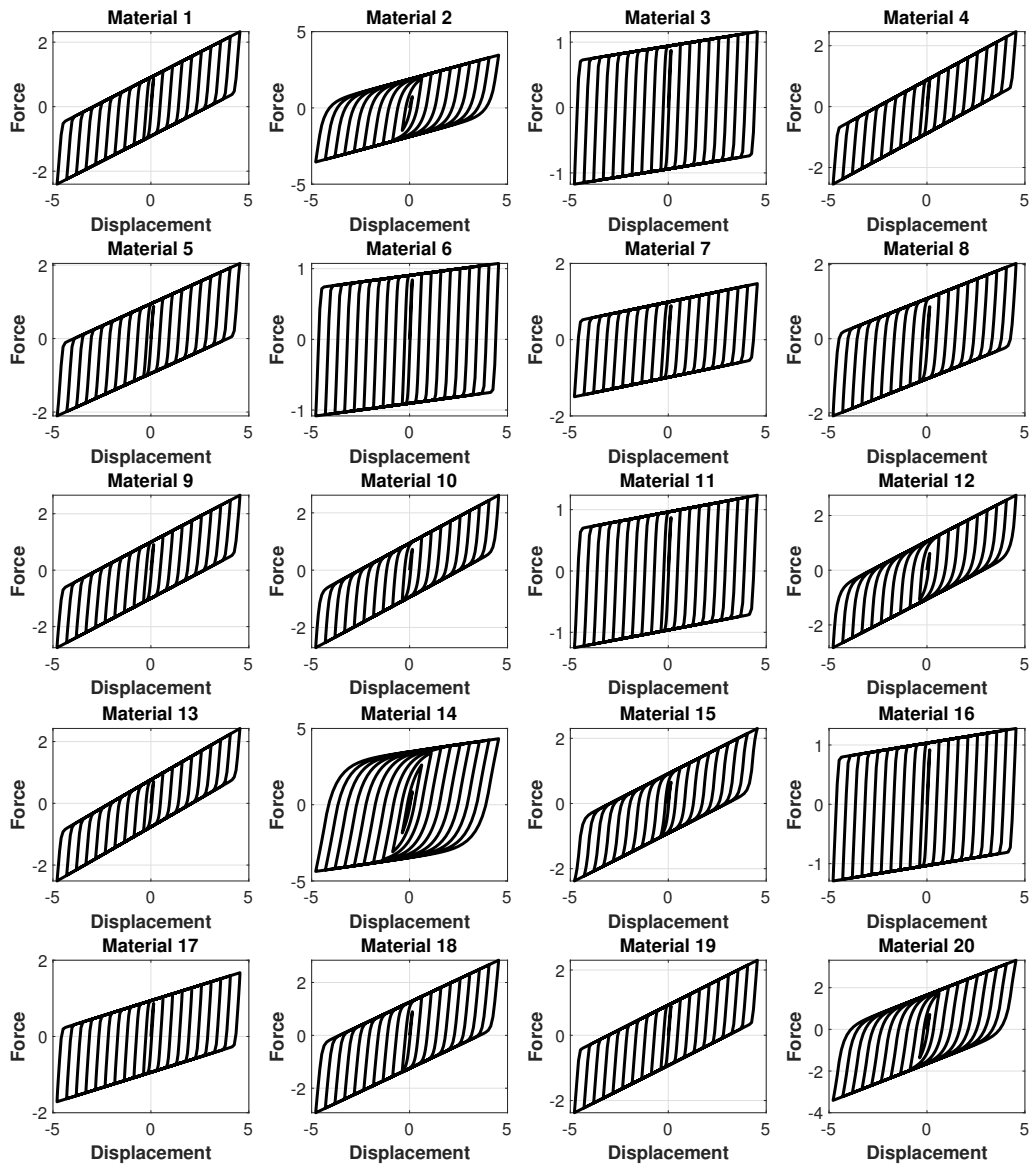
Figure 3.9: Randomly-generated hysteretic responses of a SDOF system under a linearly-increasing cyclic displacement history.

The hysteretic response and the history of the SDOF force for Model 14 are shown in Fig. 3.11. An excellent match was observed between the expected and predicted responses, suggesting that the PI-SINDy model can adapt and learn different hysteresis shapes as long

as the component undergoing plastic deformations does not experience instability or fracture, which are typically not expected in the majority of steel seismic fuses in well-designed structural systems. To extend the application of the model for simulating instabilities expected in bracing members of steel concentrically braced frames or, strength degradation expected in the majority of steel seismic fuses, e.g., when subjected to collapse level ground shaking or the seismic fuses part of existing structures not compiling with the current seismic design provisions, a modified stop operator, called deteriorating stop operator proposed by [132], can be implemented in PI-SINDy.

The results obtained from the dynamic analysis of the SDOF confirmed that the PI-SINDy model could predict the hysteretic response of a nonlinear dynamical system under a random vibration such as earthquake acceleration with an average NRMSE of 2% calculated from all 20 models. This further confirms the power of the PI-SINDy in predicting the nonlinear cyclic behaviour of seismic fuses without the need for rich data (e.g., white noise), which is favorable in seismic engineering applications where the user often has access to a great deal of cyclic loading data.

3.7 Verification of the HyDPS Framework

3.7.1 Verification Methodology and Assumptions

The application of the HyDPS framework in performing seismic hybrid analysis of structural systems was assessed in this section. The PI-SINDy data-driven model was implemented in a Two-Dimensional (2-D) BRBF to predict the hysteretic response of its BRB when the frame is subjected to a ground motion acceleration. The HyDPS framework was used to perform the simulation where the nonlinear hysteretic response of the BRB was reproduced using PI-SINDy and a numerical simulation technique, i.e., physics-based solution, was exploited to simulate the behaviour of well-understood elements of the BRBF, including the beam and columns. The seismic response obtained from this hybrid model was then compared
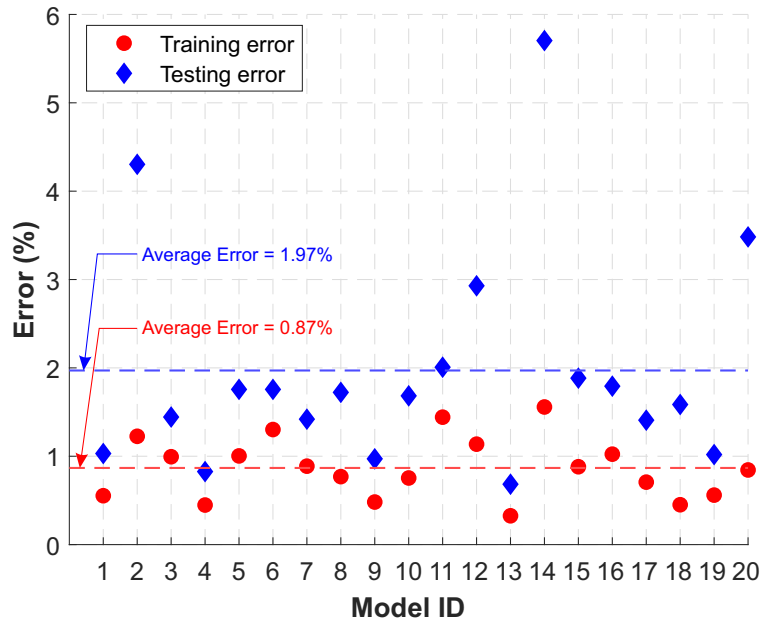
Figure 3.10: PI-SINDy model errors for a SDOF system.
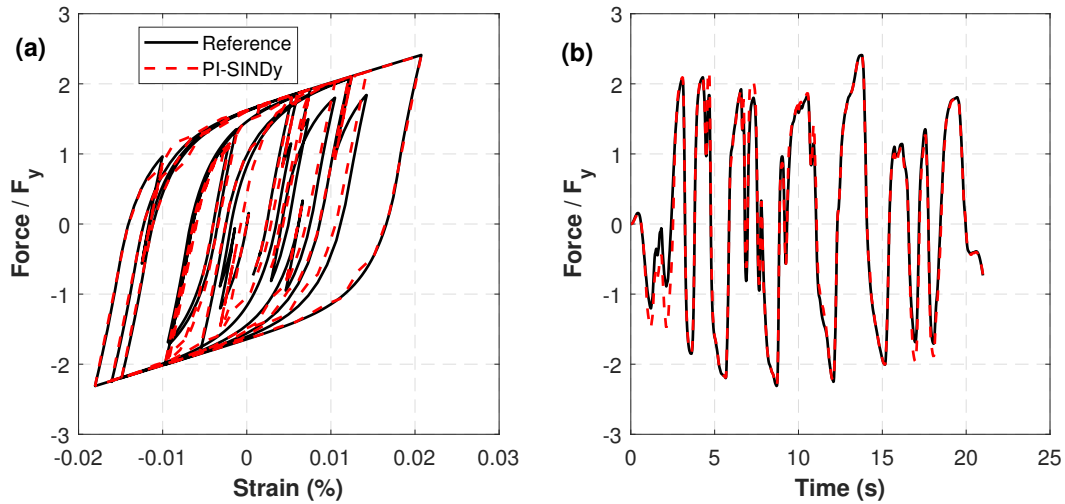
Figure 3.11: PI-SINDy prediction versus reference SDOF system for hysteresis model 14: (a) stress-strain response, (b) normalized restoring force

to the one predicted using full numerical model, pure numerical model hereafter, and those predicted by HyDPS using previously proposed LS-SVM and RNN data-driven models.

The BRBF selected for the verification of HyDPS is shown in Fig. 3.12. The selected frame is located in Vancouver, British Columbia, Canada, on Site Class C. Gravity and

49

seismic loading was performed in accordance with the 2015 National Building Code (NBC) of Canada [154]. The seismic weight of the structure was assumed as $2000kN$, which was shared equally between the two columns and assigned to the top end of each column. The fundamental period of vibration of the frame was $0.49s$. The ductility- and overstrength-related force modification factors R_d and R_o are 4.0 and 1.2, respectively. The importance and higher mode factors are $I_E = 1.0$ and $M_v = 1.0$, respectively. The structural design of the selected BRBF was performed in accordance with the 2019 Canadian steel design standard, CSA S16 [155]. Additional details regarding the design of steel BRBFs can be found in [156].
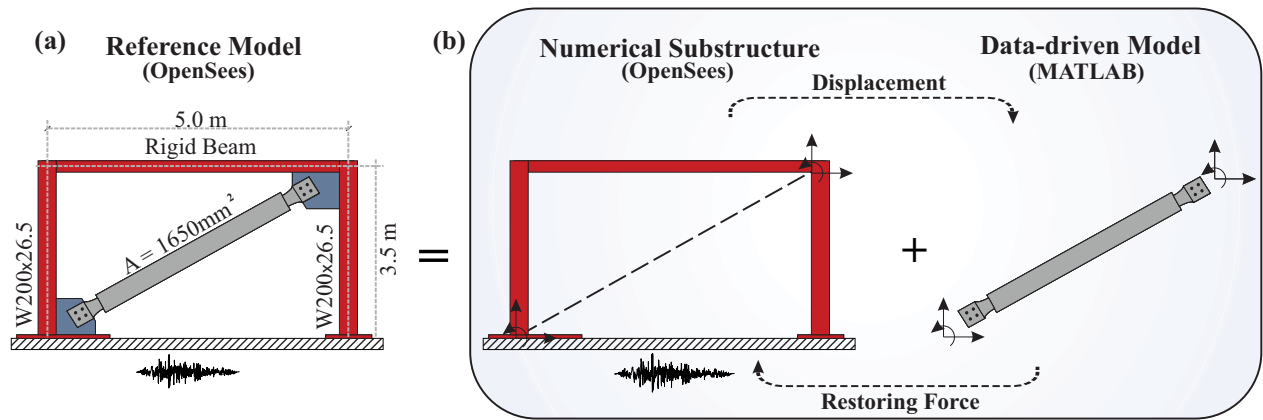
Figure 3.12: Prototype buckling-restrained braced frame: a) pure numerical model (reference model); and b) hybrid (HyDPS) model.

The pure numerical model of the BRBF was developed in the OpenSees program [157]. The beam and columns were modeled using elastic beam-column elements. The Giuffré-Menegotto-Pinto material model [58] assigned to a nonlinear truss element was used to numerically simulate the BRB in the pure numerical model. For simplicity, the influence of frictional forces developed between the BRB core and BRB restrainer, e.g., grout, when the BRB undergoes compression was neglected in the model, resulting in a symmetric cyclic response in tension and compression. The beams and columns expected to develop no or negligible inelastic deformations were modeled using elastic beam-column elements in both pure numerical and HyDPS techniques. Young's modulus $E = 200GPa$ was used in the definition of the steel material. At the column bases, all translational DOFs plus the ro-

tation about the longitudinal axis of the column were restrained to simulate a pinned base condition. The translation at the top end of columns was restrained out-of-plane to account for the lateral out-of-plane support provided by perpendicular framing systems. The top end of the columns was constrained in the horizontal direction to simulate in-plane rigidity of the roof diaphragm. A lumped mass of $102kNs^2/m$ was assigned to the top end of each column to reproduce the seismic weight of the BRBF. To simulate classical viscous damping, the Rayleigh damping method with mass proportional damping corresponding to a critical damping ratio of 2% was specified in the first vibration mode of the structure. The equation of motion was solved using the Generalized-Alpha [158] integration algorithm.

3.7.2 Nonlinear Response History Analysis

The nonlinear Response History analysis was used to verify the proposed HyDPS framework involving PI-SINDy as compared to the other two data-driven models, i.e., LS-SVM and RNN.

The pure numerical model shown in Fig. 3.12a acted as the reference model to verify the HyDPS involving the PI-SINDy data-driven model. In the HyDPS, the BRB was replaced with the PI-SINDy model as shown in Fig. 3.12b. A similar model was created with each LS-SVM and RNN data-driven model used for comparison purposes. All three data-driven models were developed in MATLAB [159] and were linked to the numerical model representing the rest of the frame (Fig. 3.12b) by means of the UT-SIM framework [160–163], which acted as a middle-ware to establish communication between the data-driven and numerical models.

The training data for the PI-SINDy model was generated using a cyclic nonlinear static (pushover) analysis performed on an identical BRB isolated from the frame under a symmetrical reversed-cyclic displacement protocol (Fig. 3.13a). The PI-SINDy model was then trained as described earlier. The result of the training is shown in Fig. 3.13b. A total number of 50 stop operators were selected and used to define the thresholds of the PI model based on the maximum input displacement signal $(|x_{max}|)$ as $r_i = \frac{i}{51}|x_{max}|$, $i = 1, 2, ..., 50$. The

stop operators were finally stacked in the data library matrix. An optimal value of $\lambda = 0.1$ was chosen for the PI-SINDy model using the AIC.

For the data-driven model created using the LS-SVM method, the 10-fold cross-validation method was chosen for training to improve the generalization ability of LS-SVM by tuning the hyper-parameter γ. Hyper-parameter optimization was then performed in two phases: 1) coupled simulated annealing (CSA) [164] searches for an approximate solution of the hyper-parameter, and 2) Nelder-Mead simplex algorithm [165] to improve the accuracy of tuning the hyper-parameter. The LS-SVM function estimation was performed using the LS-SVMlab-version 1.8 [147].
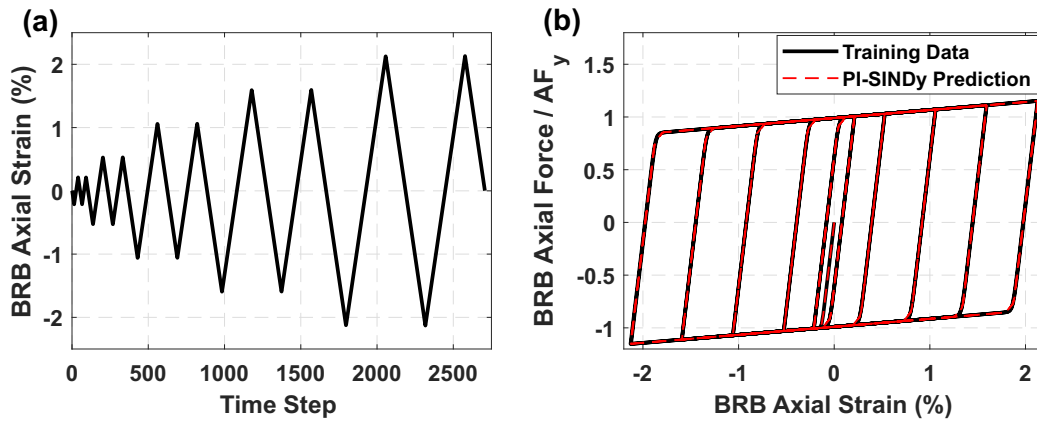
Figure 3.13: PI-SINDy training: (a) displacement protocol, (b) BRB training data generated by a pushover analysis and PI-SINDy prediction.

The architecture of the hidden layers in the data-driven model developed using the RNN technique was identical to the one presented by Sharghi et al. [137]. The Sigmoid activation function was employed in the hidden layers, and Bayesian regularization backpropagation [166] was implemented for training the RNN.

To perform dynamic analyses, a suite of 12 ground motion accelerations (Table 3.2) comprised of four shallow crustal, four deep subduction in-slab, and four deep subduction interface (representing Cascadia subduction zone) records were selected and scaled to match on average the National Building Code (NBC) of Canada [154] uniform hazard spectra for the building location. The selected events represent the main sources of seismic hazard in

Table 3.2: Summary of parameters of ground motion records.

Hazard Type	ID	Ground Motion Name	Magnitude (M_w)	Depth (km)	Year	Recorded Station
Crustal	1	Tabas, Iran	7.35	10.0	1978	Dayhook
	2	San Fernando	6.61	8.4	1971	Castaic-Old Ridge Route
	3	Montenegro, SFRY	7.1	10.0	1979	Herceg Novi-O.S.D. Paviviv
	4	Kobe, Japan	6.9	17.6	1995	Tadoka
In-slab	5	Geivo, Japan	6.8	51.0	2001	1421a
	6	Miyagi, Japan	7.1	66.0	2011	IWT026
	7	Miyagi, Japan	7.1	66.0	2011	MYG016
	8	Miyagi, Japan	7.1	66.0	2011	IWTH24
Interface	9	Southern Peru	8.4	25.7	2001	POCO
	10	Pisco, Peru	8.0	39.0	2007	UNICA
	11	Maule, Chile	8.8	35.0	2010	LACHb
	12	Iquique, Chile	8.4	20.1	2014	PB09

the U.S. and the west coast of Canada. The ground motion acceleration was applied in the horizontal direction at the base of the frame. At each analysis time step, the displacement command produced by OpenSees was sent to MATLAB to predict the restoring force. The predicted force vector in interfacial DOFs was then fed back to OpenSees to complete the numerical integration of the equation of motion at that time step.

The nonlinear response history analysis was performed under the ensemble of selected records using the pure numerical model and HyDPS models. The results obtained under the 2014 Iquique, Chile - PB09 earthquake acceleration (Fig. 3.14a) were presented in Figs. 3.14b and 3.14c for the reference BRBF model and the hybrid models developed using PI-SINDy, LS-SVM, and RNN data-driven BRBs. The storey drift shown in Fig. 3.14b was computed by dividing the, i.e., roof displacement by the storey height. The NRMSE of the storey drift ratio for the data-driven BRBFs developed using PI-SINDy, LSSVM, and RNN was 1.04%, 1.06%, and 11.29%, respectively. As shown in Figs. 3.14b and 3.14c, the storey drift history predicted by both PI-SINDy and LS-SVM approaches matches well that obtained from the reference model. However, the ANN model showed a poor prediction of the BRBF drift

response. The history of the errors calculated between the anticipated and predicted drift ratios from the reference model and each of the data-driven models are shown in Fig. 3.14c. As shown, the error of the RNN method in predicting the BRB restoring force and the frame's lateral displacement is considerably higher than the other two data-driven models, PI-SINDy and LS-SVM. This can be attributed to the fact that some of the parameters associated with the RNN method shown in Fig. 3.5, σ_{n-1}, ψ_n, and η_n, depend on the output in the previous step, which leads to a significant error accumulation while LS-SVM and PI-SINDy models are independent of feedback from the previous output step. Another shortcoming of RNN in predicting the BRB seismic response could be associated with the need to find the number of hidden layers and the number of neurons in the corresponding hidden layers. A sensitivity analysis can address this shortcoming, which may negatively impact the computation time during training. In contrast, the PI-SINDy and LS-SVM methods are automated enough to find the optimal model architecture. For instance, λ parameter in PI-SINDy is automatically chosen by the algorithm through the AIC described earlier. The third reason for the appreciable error observed for the RNN model (Fig. 3.14c) is that RNNs are prone to stick in a local minimum during the weight optimization process compared to other algorithms used here [167], which negatively affects the training of the RNN-based model.

The normalized force-normalized axial deformation response of the BRBs predicted using the PI-SINDy, LS-SVM, and RNN models are shown in Figs. 3.15a– 3.15c, respectively. Overall, a very good match was observed between the anticipated and predicted hysteretic responses when the proposed PI-SINDy and LS-SVM were used to simulate the cyclic inelastic behaviour of the BRB under seismic loading. The NRMSE of the restoring force was equal to 0.80% and 0.86% for these two approaches, respectively. However, the RNN method yielded a less accurate prediction (restoring force NRMSE= 1.57%) as compared to PI-SINDy and LS-SVM models. The BRB hysteresis response reaffirms the previous findings of the accuracy of the PI-SINDy and LS-SVM methods over the RNN approach. Similar results were obtained

for the BRBF studied under the other 11 ground motion records. Fig. 3.16 gives the NRMSE and PPE of the storey drift measured under each nonlinear response history analysis. The average value of the drift NRMSE for crustal, in-slab, and interface earthquakes were 2.55%, 1.27%, and 2.14%, respectively, which reveals that the performance of the PI-SINDy model is reduced under in-slab earthquakes. This may be attributed to the long duration and different frequency content of in-slab records, which may cause higher errors, in particular, near the end of the analysis where large residual drifts were accumulated in the frame.

Algorithm 1 PI-SINDy Algorithm [168]

Require: (i) Experimental deformation history ($\boldsymbol{x} = [x(t_1), x(t_2), ..., x(t_n)]^T$)
    (ii) Experimental restoring force ($\boldsymbol{y} = [y(t_1), y(t_2), ..., y(t_n)]^T$)
    Calculate thresholds $r_i = \frac{i}{m+1}|x_{max}|, \quad i = 1, 2, ..., m$

1: **for** $i = 1\ to\ m$ **do**
2:    Calculate $E_{r_i}[\boldsymbol{X}]$: Eqs. 3.7, 3.8, 3.9
       $\boldsymbol{\Theta}(:, i) = E_{r_i}[\boldsymbol{x}]$: Eq. 3.11
3: **end for**
    LASSO regression: $minimize\ \frac{1}{2n}||\boldsymbol{y} - \boldsymbol{\Theta}\boldsymbol{\Xi}||_2^2 + \lambda||\boldsymbol{\Xi}||_1 \rightarrow find\ \boldsymbol{\Xi}_{lasso}$ in Eq. 3.11

The complete set of nonlinear response history analysis results for all 12 ground motions is given in Appendix A.

3.7.3   Effect of Structural Dynamic Properties

The influence of dynamic properties of the structure on the performance of the HyDPS framework equipped with PI-SINDy model was investigated in this section. This evaluation is meant to provide insight into the application of the proposed hybrid analysis technique in taller multi-storey structures or nonbuilding structures with relatively large mass or small lateral stiffness. In addition to the prototype BRBF (Section 3.7) with a fundamental period of $T = T_0 = 0.49s$, two new BRBFs having longer fundamental periods, 1) BRBF with $T = 2T_0 = 0.98s$ and 2) BRBF with $T = 4T_0 = 1.97s$, representing taller structures were modelled as described in Section 3.7.1. The new BRBFs were created by increasing the seismic weight of the original BRBF. However, they cannot account for higher mode effects

expected in multi-storey buildings with the same fundamental period because the BRBF used in this study represents a single-degree-of-freedom system.
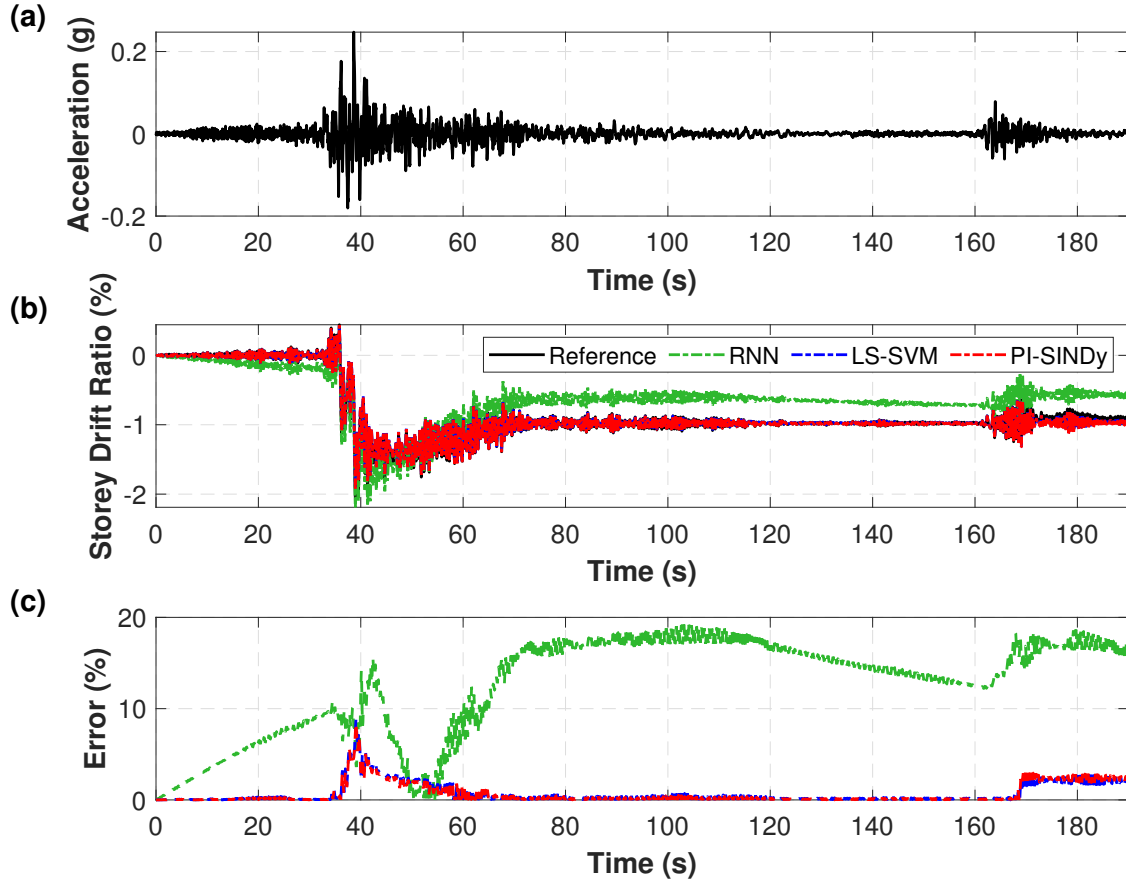
Figure 3.14: (a) 2014 Iquique, Chile - PB09 earthquake acceleration, (b) storey drift ratio of the prototype frame under the 2014 Iquique, Chile - PB09 earthquake, (c) Point-to-point error of the storey drift ratio.

The new BRBFs were subjected to the same 12 ground motions (Table 3.2). The NRMSEs of the storey drift and BRB restoring force are given in Figs. 3.17a and 3.17b, respectively. The errors were calculated using the difference between each parameter (drift ratio or BRB restoring force) from the reference model and that was predicted using the HyDPS model. The mean value of the NRMSE for the drift ratios of BRBFs with fundamental periods of T_0, $2T_0$, and $4T_0$ were 2.57%, 4.63%, and 4.33%, respectively. The same pattern of errors

was observed for the mean values of the NRMSEs of BRB restoring forces, 0.77%, 1.00% and 0.90%, for the BRBFs with fundamental periods of T_0, $2T_0$, and $4T_0$, respectively.
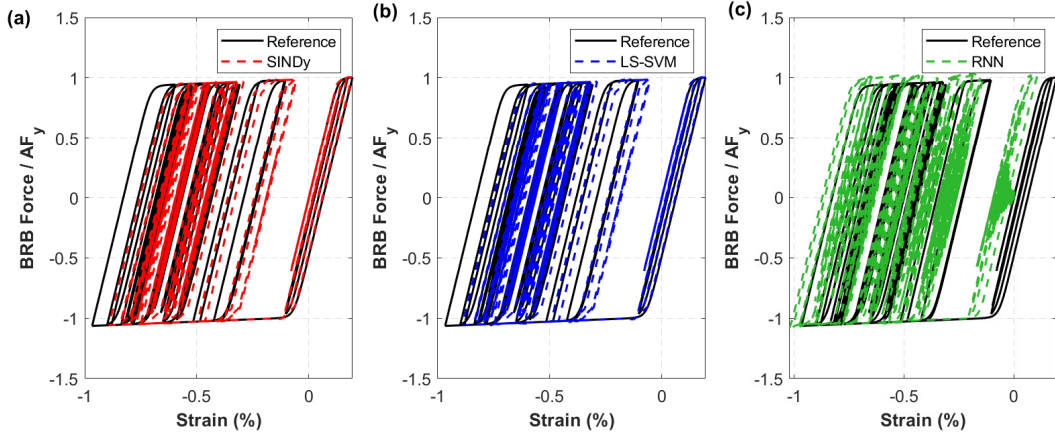
Figure 3.15: Hysteretic responses of the BRB obtained from the HyDPS framework using (a) PI-SINDy, (b) LS-SVM, (c) RNN.
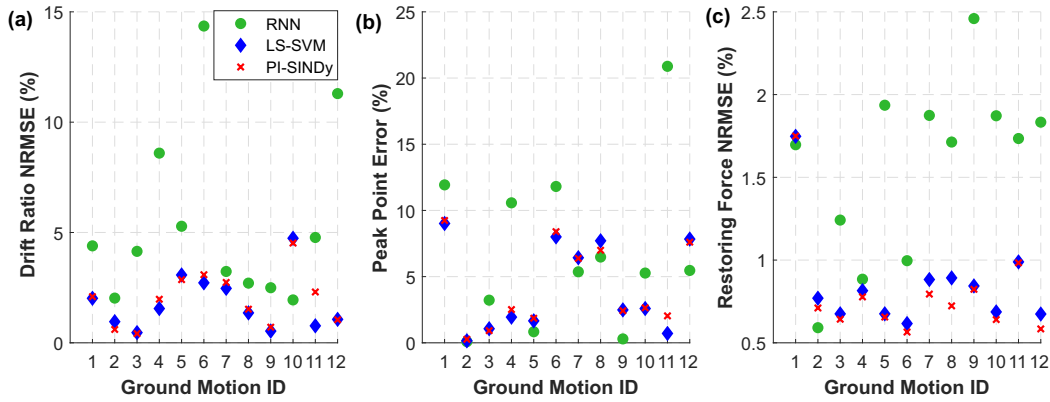
Figure 3.16: (a) NRMSE of storey drift ratio, (b) drift Peak point error, and (c) NRMSE of the BRB restoring force, from dynamic analyses.

Although the mean values of the errors slightly increased for the frames with longer period likely because of higher variability of spectral accelerations of scaled ground motions in the moderate period range, e.g., $1 - 2s$, and dominating frequency of in-slab and subduction events, the predicted displacement and force responses were not affected significantly. The time histories of the storey drift ratios and BRB hysteretic responses for the three BRBFs under the 2001 Geivo, Japan - 1421a earthquake are shown Fig. 3.18 and Fig. 3.19, respectively,

57

as compared to the responses obtained from the reference frames. Referring to Fig. 3.18, the accuracy of the prediction of the displacements for the $T = 1s$ BRBF was reduced during the last 20 seconds of the analysis that can be attributed to the accumulation of error. No significant change was observed in the prediction of the BRB hysteresis responses between the studied frames in Fig. 3.19.

The complete set of nonlinear response history analysis results for all 12 ground motions is given in Appendix B.
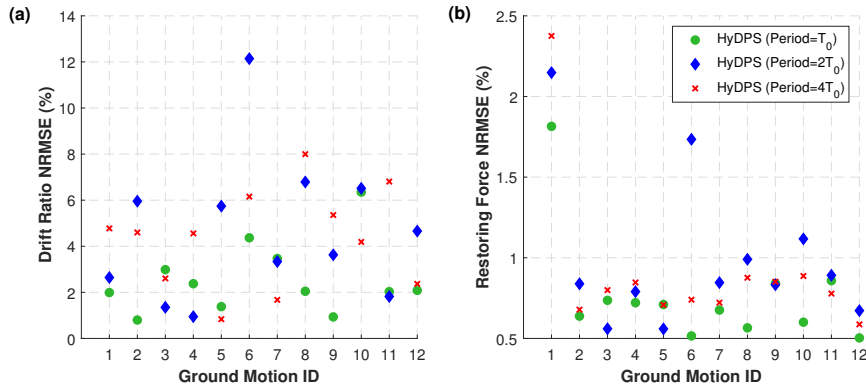
Figure 3.17: (a) Storey drift ratio, and (b) BRB restoring force NRMSEs for BRBFs with different fundamental periods

3.8   Discussion and Future Development

The results of the verification study revealed that the PI-SINDy and LS-SVM data-driven models offer almost the same accuracy in predicting the BRB hysteretic response, which can be attributed to the principles of these two data-driven models. Both models are operator-based models and enjoy Prandtl-Ishlinksii's hysteresis model to construct the discrete hysteresis memory.

In addition to improved prediction accuracy when comparing the performance of the PI-SINDy to that of RNN, the irrelevant stop operators in the library matrix are entirely removed in PI-SINDy, whereas a small value is typically assigned in LS-SVM to the corresponding

weights, which may become sensitive to noise, especially when the HyDPS simulation is carried out under a ground motion acceleration with high-frequency content.
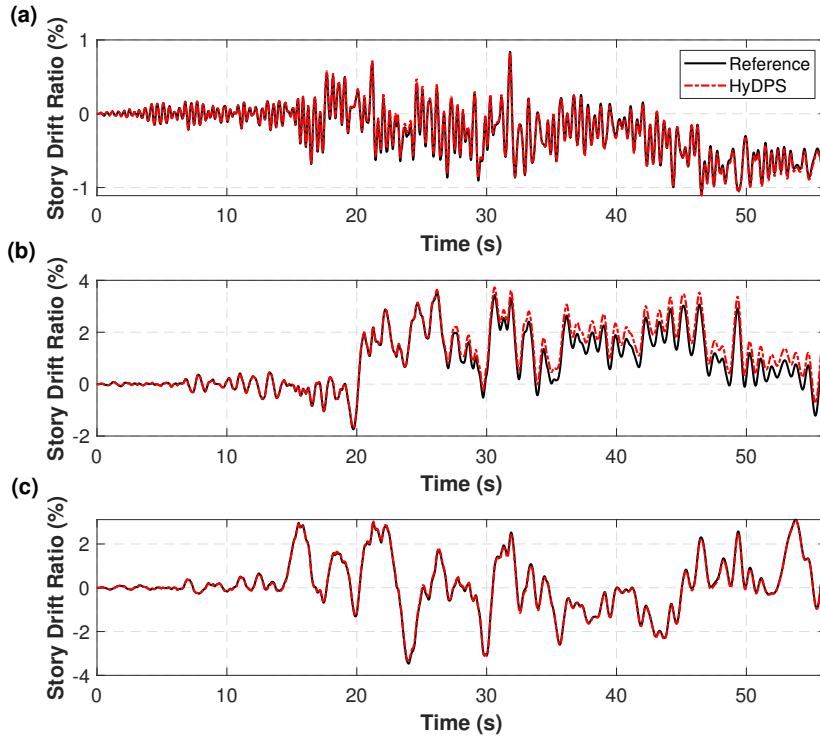
Figure 3.18: Time history of BRBF storey drift ratio under the 2001 Geivo, Japan - 1421a earthquake, (a) BRBF with $T_0 = 0.49s$ (NRMSE=1.38%), (b) BRBF with $2T_0 = 0.98s$ (NRMSE=5.74%), and (c) BRBF with $4T_0 = 1.97s$ (NRMSE=0.84%).
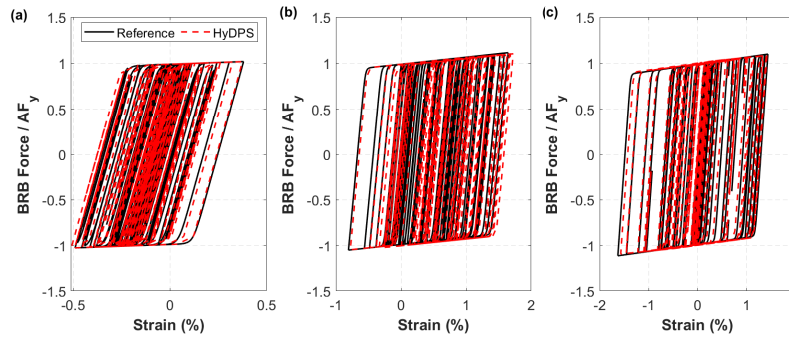
Figure 3.19: BRB hysteretic response under the 2001 Geivo, Japan - 1421a earthquake, (a) BRBF with $T_0 = 0.49s$ (NRMSE=0.71%), (b) BRBF with $2T_0 = 0.98s$ (NRMSE=0.56%), and (c) BRBF with $4T_0 = 1.97s$ (NRMSE=0.71%).

The proposed HyDPS framework can be considered as a robust method for seismic response evaluation of structural systems and can offer a powerful alternative to pure numerical simulation, commonly used by researchers and engineers for seismic response assessment of structures. This stems from the fact that the physics of the problem, e.g., EOM, equilibrium, and compatibility equations, are all satisfied in the physics-based model with high computational efficiency, while the data-driven model predicts the restoring force of highly-nonlinear members only based on input hysteresis data with significantly less computational efforts compared to the pure numerical model. Another key factor that contributes to the power and efficiency of the HyDPS framework is that the convergence in this technique is achieved faster than pure numerical models because the HyDPS framework does not require multiple iterations to solve the nonlinear problem, rather the response is predicted by a trained machine learning algorithm in a single step.

The HyDPS framework can offer increased reliability and computational efficiency in comparison to pure numerical simulation provided that high-quality, reliable, and clean experimental data is available to train the data-driven model. When such experimental data is not available, numerical data generated from corroborating FE simulations can be used to train the data-driven model and perform the analysis using the HyDPS, which, would decrease the computational cost of the simulation, but may compromise the accuracy of simulation. However, limited prediction errors could be traded for high computational efficiency offered by HyDPS when studying the structural response under a wide range of excitations, such as Incremental Dynamic Analysis (IDA), optimization problems, parametric design, and model updating.

3.9   Summary and Conclusions

this chapter proposed a hybrid simulation technique for the nonlinear analysis of structural systems under dynamic loading such as earthquake. This simulation technique combines the conventional numerical simulation method and the data-driven PI-SINDy model developed

here to achieve higher efficiency by leveraging the wealth of experimental test data obtained from past test programs. In HyDPS, the physics-based features of the structure, including equation of motion, mass, damping, and compatibility equations, are realized in the physics-based model, while the critical components that expect to respond in the inelastic range of the material are simulated using the proposed data-driven model that is trained using available hysteresis data. The data-driven model involves a mathematical representation of the function that relates input parameters of the critical component, e.g., displacement signals, to its output parameters, e.g., restoring forces. The data-driven component of HyDPS, the PI-SINDy model, was developed using a machine learning-based algorithm by combining the PI model as the hysteresis model with the SINDy algorithm used for training. The capability of the PI-SINDy model was evaluated in estimating the underlying relationship between the force and deformation obtained from the laboratory testing of a buckling restrained brace. A nonlinear SDOF system was then selected to assess the PI-SINDy model in reproducing various hysteresis shapes expected in structural components experiencing nonlinear cyclic response. The HyDPS framework was finally verified under earthquake excitations through the dynamic analysis of a prototype BRBF created using the PI-SINDy data-driven BRB and numerical representation of the remaining components of the frame. The accuracy and efficiency of PI-SINDy was compared against two previously-proposed data-driven models, LS-SVM and RNN-based models. The key features of the proposed HyDPS framework and data-driven PI-SINDy model are summarized as follows:

1. In the HyDPS framework, the physics of the problem, including equation of motion and compatibility equations, is satisfied in the physics-based numerical model, while the data-driven component of this framework only reproduces the nonlinear cyclic response of the critical element of the structure.

2. The HyDPS framework achieved a trade-off between the reliability of results by minimizing the assumptions needed for constitutive modelling of critical components of the

structure and the size of the training data set.

3. Numerical convergence is easily achieved when performing a dynamic analysis because an explicit input-output surrogate function is created for the critical component, which significantly reduces the number of nonlinear equations to be solved by the numerical solution scheme.

4. The full response of the structure at all DOFs of the structure can be retrieved using the HyDPS framework as opposed to fully data-driven models where the structural responses can only be predicted for the components from which the data for training was previously collected.

5. The PI-SINDy data-driven model trained using the experimental data of a specific critical component, e.g., BRB in a BRBF, can be used to predict the response of various frame architectures, e.g., multi-storey BRBFs.

6. The computational efforts of the HyDPS Framework are appreciably less compared to pure numerical models, commonly used for the response evaluation of structural systems, because of using direct input-output mapping function for the critical element instead of phenomenological or detailed finite element models. This becomes more beneficial when multiple nonlinear components are used in various locations of the structure, making HyDPS favorable for structural response evaluation involving numerous analyses such as nonlinear response history analysis, incremental dynamic analysis, and structural optimization.

7. In the PI-SINDy, the columns in the library matrix that have the least contribution are removed, whereas a small value is typically assigned in LS-SVM to the corresponding weights, which may become sensitive to noise, especially when the HyDPS simulation is carried out under a ground motion acceleration with high-frequency content.

The effectiveness of the HyDPS framework is highly dependent on the performance of the data-driven model, and further studies should be devoted in the future to develop other reliable machine learning algorithms to simulate complex hysteretic behaviours expected in structural elements involving instability, elements experiencing stiffness and strength degradations or pinching behaviour.

Chapter 4

A Digital Twin-based Framework for Multi-element Seismic Hybrid Simulation of Structures

4.1 Abstract

This chapter proposes a digital twin-based multi-element hybrid simulation (DMHS) framework to predict the nonlinear cyclic response of the structural components (digital twin), e.g., seismic fuses, that are not physically tested due to laboratory limitations by leveraging the experimental test data collected from the physical test specimen (physical twin) during hybrid simulation. This data-based simulation approach can address biased results in hybrid simulation of structures that consist of multiple critical components while improving the efficiency of the seismic hybrid simulation. The digital twin is trained in two phases: 1) initial (passive) training phase using the past experimental test data before the hybrid simulation starts, and 2) recursive model updating phase using the real-time data produced by the physical specimen during hybrid simulation. The passive training is achieved using the Prandtl-Ishlinskii (PI) hysteresis model combined with the sparse identification technique, while the recursive least-squares algorithm is used in the second phase as the model updating scheme. The application of the proposed DMHS is demonstrated, and its simulation accuracy is assessed through virtual hybrid simulation of a two-storey steel buckling-restrained braced frame, which consists of a digital twin (second-storey brace) and a virtual experimen-

tal specimen (first-storey brace) integrated into the numerical model of the structure that is subjected to a set of earthquake ground motion accelerations. The results obtained from the verification study serve to verify the proposed architecture of the DMHS framework and evaluate the accuracy and efficiency of this technique in simulating the nonlinear seismic response of structural systems.

4.2 Introduction

Hybrid simulation (HS) offers a versatile and efficient solution to evaluate the behaviour of structures subjected to earthquake loading, quantify the parameters affecting their seismic response, produce data for developing and improving numerical modelling techniques, assess and enhance design guidelines for structural systems. HS was first introduced by Hakuno et al. in 1969 [10] and then formally implemented by Takanashi et al. [9]. Two main HS techniques are typically used in seismic engineering, real-time hybrid simulation (RTHS) and pseudo-dynamic hybrid simulation (PsDHS).

The underlying idea of conventional hybrid simulation (CHS) is to divide the structure into two computationally parallel substructures, the well-understood parts that are simulated numerically using the finite element method and the critical component or components expected to respond in the inelastic range, e.g., seismic fuses, that are tested physically in the laboratory (Fig. 4.1a). The displacements of inter-facial nodes will be computed by solving the governing equation of motion in each time step and be applied to the physical specimen. Restoring forces of the specimen will then be measured and fed back to the numerical model for the subsequent analysis increment [8].

Unlike conventional experimental testing techniques such as quasi-static cyclic testing, pseudo-dynamic testing and shake table testing, HS offers a remarkable trade-off between the reliability of test results and complexity of testing. For instance, the imposed demand in quasi-static testing method does not necessarily represent the actual demand resulting from the seismic response of the structure; shake table tests often involve a great amount of cost

65

associated with test specimen construction and table operation or are only applicable in a scaled-down version of the prototype structure to accommodate the capacity of the available shake table, which raises questions about the reliability of test results [8].

Despite the advantages that CHS can offer over other seismic testing techniques, the results of CHS may become biased when only one or a limited number of potential critical components are physically tested due to laboratory or cost limitations. For instance, the seismic response of multi-storey structures, which typically include multiple seismic fuses or highly nonlinear elements, may not be well-represented using CHS as physical testing of all critical elements, even reduced-scale, is almost beyond the capabilities of the current and perhaps near-future structural testing facilities. Therefore, the majority of hybrid simulations performed in past studies, involve only one or a few physical specimens representing critical components of the structure, while the rest of the structure, including some of the similar highly nonlinear critical elements, are modelled numerically [20–25, 27, 169, 170]. For instance, Imanpour et al. [28], physically tested one of the two critical columns of a two-tiered steel concentrically braced frame in which both columns would have buckled had they physically tested in the laboratory, which would then result in a different response or even column stability behaviour. Limited research studies, however, addressed this challenge in the past. As an alternative, geographically-distributed (multi-site) hybrid simulation (GDHS) technique, as shown in Fig. 4.1b can be used to overcome the limitation of CHS. In GDHS, more than one experimental specimen is tested simultaneously in multiple sites under the demands generated by a single numerical analysis. The specimens are often located in different testing facilities and are linked through the Internet [19]. Despite its advantages in testing more than one critical element, the major challenge associated with the GDHS technique is the communication time delays because of the need for data transfer over long distances [171]. Multi-element hybrid simulation (MeHS) is another alternative in which more than one critical element is physically tested, as shown in Fig. 4.1c, resulting in a reliable but equipment-demanding technique. For example, up to 10 uniaxial steel braces were

concurrently tested using a MeHS platform developed by Mojiri et al. [172–174].

A novel HS method based on the model updating technique has been developed in recent years to address the limitation associated with conventional hybrid simulation (CHS), i.e., the need for MeHS. The concept of model updating in HS was first introduced by Yang et al. [108] by exploiting the experimental data exchanged explicitly through the inter-facial nodes to implicitly refine the response of the numerical substructure in real time [109]. The model updating technique is expected to yield a more accurate response provided that the material and geometrical characteristics of the numerical and experimental substructures are similar to each other. Kwon et al. [110] proposed a model updating strategy for PsDHS that is achieved by the iterative calibration of weighting factors applied to several imaginary numerical counterparts, which encompassed the potential variation in physical specimen properties. The accuracy of this approach is highly dependent on the properties assumed for alternative numerical counterparts. Over the past decade, the class of Kalman filter-based system identification gained attention in RTHS. In this method, Bouc-Wen hysteresis model [62] parameters that best-fit to the experimental substructure are identified through the constrained unscented Kalman filter [111, 112] or unscented Kalman filter algorithm [113–115] and then are used to update the hysteresis parameters of the numerical component in each time step of RTHS [116].

Recent technological advances in Artificial Intelligence (AI) and Digital Twins [175] have revolutionized research and development in infrastructure, aerospace, and automobile industries [176]. Digital twin stands for a high-level computer-generated replica of a physical system that uses data gathered from sensors and/or a computational model to mirror the behaviour of its real physical counterpart [177, 178]. In principle, digital twins can either be developed based on a physics-based modelling technique, data-driven technique or a combination of both [179]. The term physics-based modelling is referred to a model created using fundamental principles such as the law of conservation of energy and material constitutive models. However, in the data-driven paradigm, the digital twin is solely created

using the input-output measurements and mathematical structures capable of learning the embedded pattern and behaviour of the system from data. Although the physics-based modelling approach is usually robust, the utilization of a data-driven approach can offer a more efficient approach if the uncertainty or nonlinearity involved in the system is high. Various machine-learning algorithms have been developed in recent years for the purpose of data-driven modelling of nonlinear dynamical systems, including response surface methodology (RSM) [180], Gaussian process predictors or Kriging [181], radial basis functions [182], polynomial chaos expansions [32], support vector regression [129, 183], and deep neural networks [34–37, 184]. One of the challenges associated with these methods is that they often require a large dataset to be appropriately trained, which may increase the time required to complete the seismic analysis because of the long learning process, limiting its applications in seismic HS, in particular, RTHS where the numerical integration is performed in real-time to solve the structural response. Therefore, the ability of the digital twin for rapid, efficient, and yet accurate identification of the physical twin, i.e., the physical component, should be enhanced by incorporating the physics-based equations into the prediction algorithm. The supplementary information added by the physics-based equations makes the machine learning algorithm faster, more accurate and generalizable.

This chapter introduces a new digital twin-based multi-element hybrid simulation (DMHS) framework for seismic hybrid simulation of structures using a machine learning algorithm that benefits from an adaptive digital twin. The role of the digital twin in the proposed technique is to predict in real-time the nonlinear dynamic response of the critical elements not physically tested and feed the predicted response to the numerical substructure during HS. Training of the digital twin is achieved by using the recursive least-squares (RLS) algorithm powered by the Prandtl-Ishlinskii (PI) hysteresis model. The digital twin is trained in two successive phases: 1) initial (passive) training phase, which is triggered before HS starts to estimate the response of digital twin, involves the sparse identification of nonlinear dynamics (SINDy) algorithm [39] to obtain a calibrated PI model with reduced dimensionality which

is favourable for computational efficiency; and 2) recursive model updating (RMU) phase, which is activated during HS, is designed to progressively improve the prediction of digital twin's hysteretic response by feeding the new incoming data collected from the physical twin into the RLS algorithm. The proposed DMHS framework involving initial and RMU training phases is first introduced. The application of the proposed framework in performing seismic hybrid simulation is demonstrated through a prototype two-storey steel Buckling-Restrained Braced Frame (BRBF). Performance of the DMHS framework is then evaluated through low and high-fidelity numerical simulations that are used to verify the proposed architecture of the DMHS framework and examine the accuracy and efficiency of this technique in simulating the nonlinear seismic response of structural systems.

4.3   Digital Twin-based Multi-element Hybrid Simulation Framework

The digital twin-based multi-element hybrid simulation (DMHS) framework is designed by substructuring the structure as 1) physical twin representing one of the critical components of the structure, which is physically tested in the laboratory, 2) digital twin, a data-driven model predicting the hysteretic response of the physical twin, and 3) numerical substructure, which is the computational model simulated the well-understood parts of the structure using the finite element method. The concept of the proposed DMHS as compared to CHS, which involves the structure decomposed into numerical and physical substructures, is illustrated in Fig. 4.1d. The DMHS benefits from real-time data generated during experimental testing of the physical twin and is capable of predicting real-time the underlying relationship between inputs, e.g., displacement, and target response, e.g., restoring force, of other critical elements of the structure, i.e., digital twins, that would have been physically tested in the laboratory had the MeHS been used. The number of digital twins is a function of the number of critical elements in the structure having similar nonlinear and dynamic properties, e.g., two in Fig. Fig. 4.1d, and is identified by the user. The proposed framework is expected to achieve a

more realistic seismic response evaluation compared to CHS as one of the critical elements is expected to be tested, and the responses of the other critical elements are predicted using real-time data obtained from the experiment, while the well-understood components of the structure are numerically modelled. The hysteretic response of the digital twin is created using two sets of data, the first set is the experimental test data obtained from the past quasi-static cyclic tests of physical twin prototypes that is used for initial (passive) training of the digital twin, and the second set involves the real-time experimental test data that is fed recursively to the digital twin in real-time during HS. The digital twin utilizes the PI hysteresis model combined with sparse identification and the recursive least-squares (RLS) algorithm to learn the nonlinear cyclic response of the physical twin and predict in real-time the force-displacement response of the digital twin. This section describes the development of DMHS.

4.3.1   Phase 1: Initial Training

The initial training phase of the real-time prediction of the hysteretic response of the digital twin involves using past experimental test data of the critical component to initialize the parameters involved in the data-driven model, i.e., digital twin. This phase is particularly important because, under random signals such as earthquake ground motion accelerations, the real-time data is very limited at the beginning of HS, plus the real-time data received from the physical twin may not be rich enough for the prediction of nonlinear response as the amplitude of the ground motion acceleration is extremely small, imposing limited actions on the physical twin. Moreover, initial training will help reduce the order of the PI model, accelerating real-time adaptation of the digital twin to the physical twin during HS. The initial training should therefore be completed before HS starts and real-time training is triggered. The components of the proposed initial training phase include the PI hysteresis model, sparse identification of nonlinear dynamic algorithm and Akaike information criterion, which are described in this section.
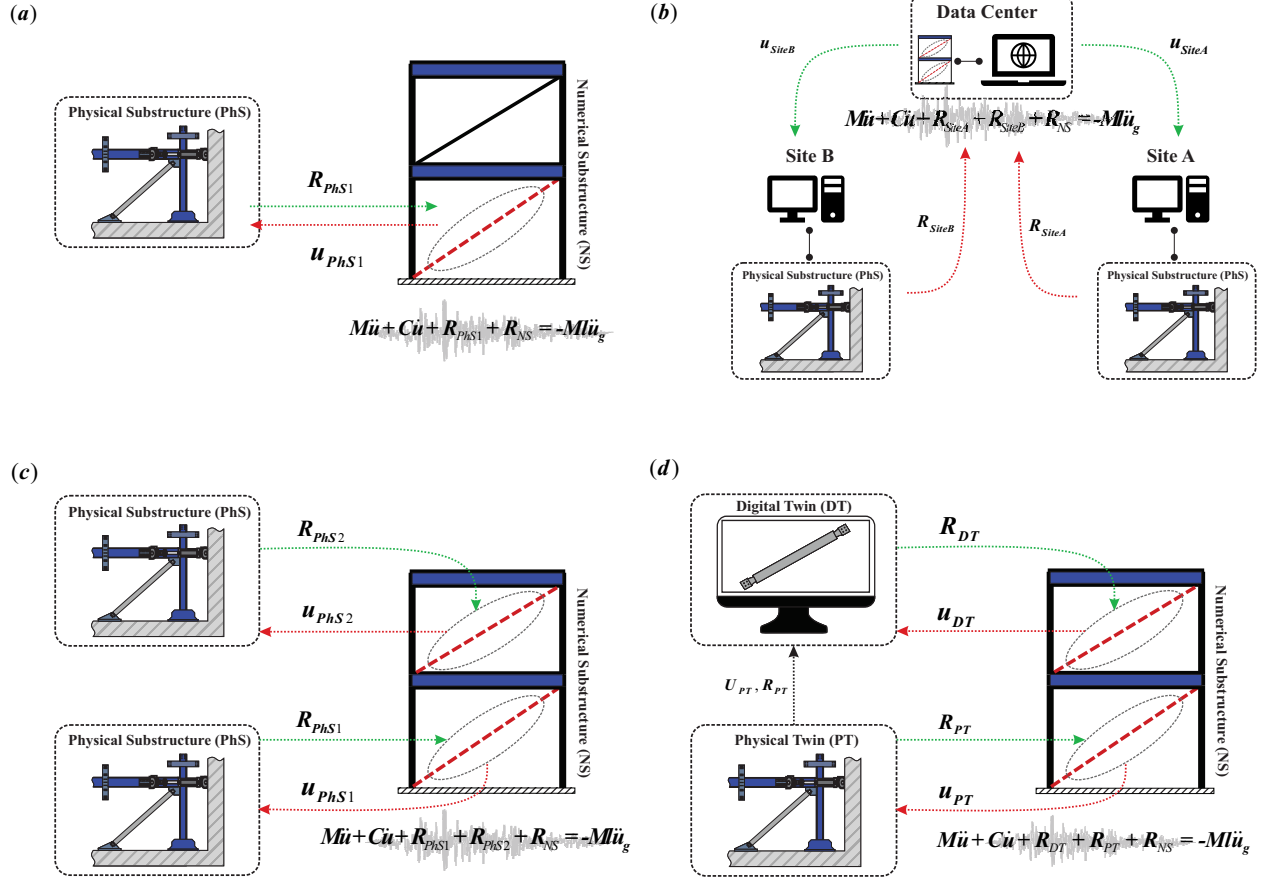
Figure 4.1: Hybrid simulation techniques, (a) Conventional hybrid simulation (CHS), (b) geographically-distributed hybrid simulation (GDHS), (c) multi-element hybrid simulation (MeHS), (d) proposed digital twin-based multi-element hybrid simulation (DMHS) ($\boldsymbol{M}$: mass matrix, $\boldsymbol{C}$: damping matrix, $\boldsymbol{R}$: restoring force matrix, $\boldsymbol{l}$: force distribution matrix, $\boldsymbol{\ddot{u}}_g$: ground acceleration, $\boldsymbol{u}, \boldsymbol{\dot{u}}, \boldsymbol{\ddot{u}}$: displacement, velocity, acceleration vectors, respectively).

Prandtl-Ishlinskii (PI) Hysteresis Model

Various machine learning algorithms, including nonlinear models such as artificial neural networks [130] and deep neural networks [185], and kernel-based models such as least-squares support vector machines (LS-SVM) [186] can learn complex behaviours of nonlinear dynamical systems provided that sufficient data is available. For example, Sharghi et al. [144] used the LS-SVM algorithm to predict the hysteretic response of a Magnetorheological damper subjected to Gaussian white noise, which is rich in frequency content and available for training before attempting to predict the hysteretic force response of the system. However, in

seismic hybrid simulation, data to be used for training is received by the digital twin incrementally and in real-time as the test progresses, limiting the application of such machine learning algorithms in seismic hybrid simulation. To overcome this limitation, a combination of a hysteresis model and a machine learning algorithm is proposed in this chapter to learn the physical twin's behaviour with small seismic input-output datasets. The hysteresis model used here to construct the hysteresis memory of the digital twin is the PI hysteresis model, which serves as the operator-based physical model to enhance the performance of the sparse identification algorithm in the absence of a rich training dataset.
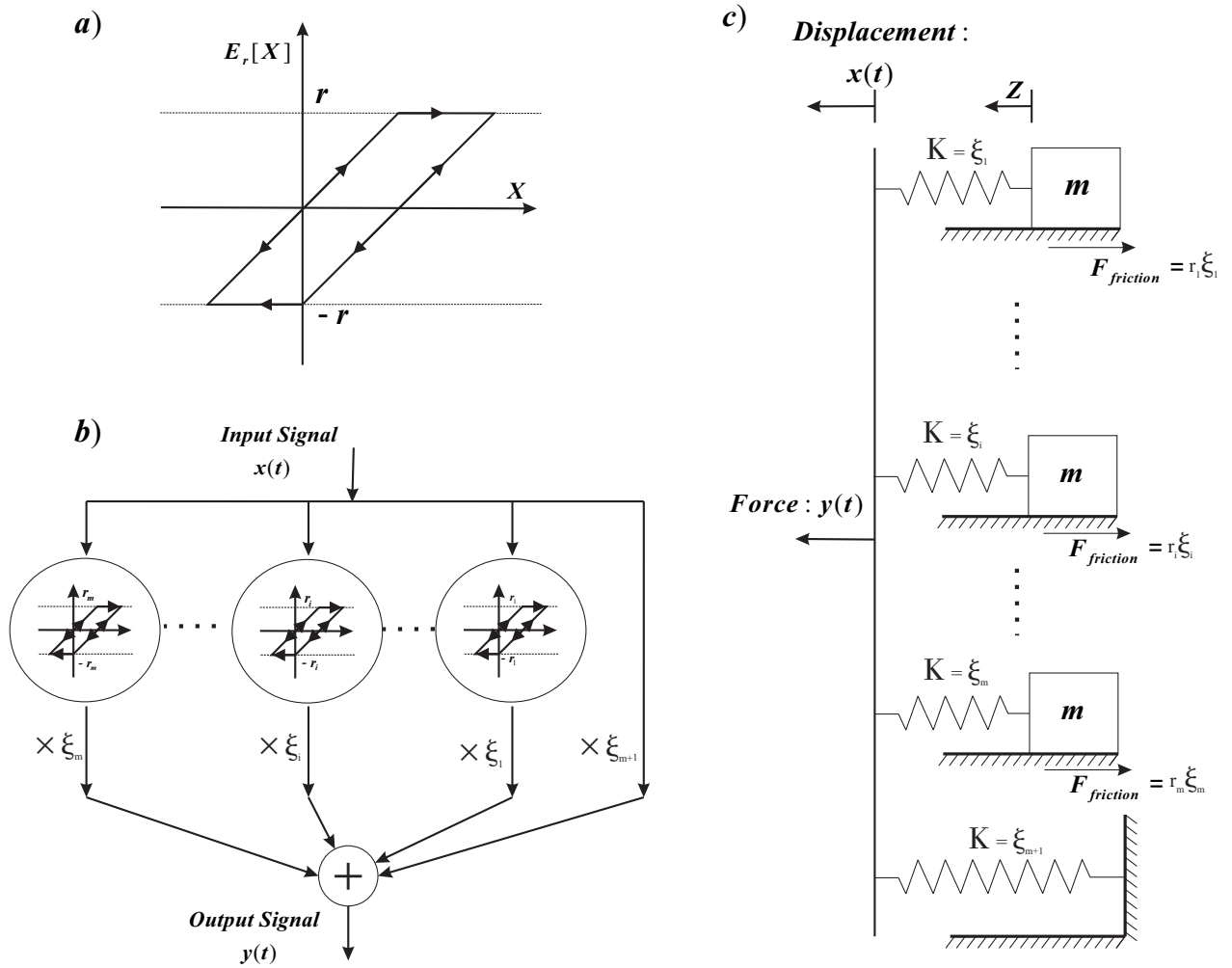
Figure 4.2: PI Model for the simulation of hysteretic response, (a) stop operator, (b) structure of PI Model, (c) equivalent mechanical model.

The PI model can transform the input signal, i.e., deformation history, to a higher dimensional space in order to reformulate the output signal, i.e., restoring force in a one-to-one mapping problem, which is favourable for most machine learning algorithms. The PI model is integration-free as opposed to other common hysteresis models such as the Bouc-Wen model, creating a more efficient model for inverse identification of the parameters.

The PI hysteresis model, as an operator-based phenomenological model, is defined by the weighted superposition of multiple elastic-perfectly plastic stop operators. The concept of stop operators was first introduced to describe the elastoplastic behaviour of materials in continuum mechanics [38]. The stop operator $E_r[.]$ can mathematically be represented by induction as:

$$y_r(t) = E_r[x(t)] \tag{4.1}$$

$$y_r(0) = e_r(x(0)) \tag{4.2}$$

$$y_r(t) = e_r(x(t) - x(t_i) + y_r(t_i)) \quad for \ t_i < t \le t_{i+1}; \ \ 0 \le i \le N-1 \tag{4.3}$$

$$e_r(s) = min(r, max(-r, s)) \tag{4.4}$$

in which, $x(t)$ and $y_r(t) = E_r[x(t)]$ are the input signal and the output signal (i.e., system's response) of a single stop operator, respectively, which are co-related using a threshold r ($r > 0$). The input-output response of a stop operator is shown in Fig. 4.2a. Within each stop operator, the time domain $[0, T]$ needs to be discretized into into N subintervals of $0 = t_0 < t_1 < ... < t_N = T$ such that the input signal, $x(t)$, follows a monotonic path within each time step $[t_i, t_{i+1}]$. In the PI model, the input signal, $x(t)$, and the output signal, $y(t)$, are related to each other using a set of stop operators with different thresholds from zero to infinity:

$$y(t) = \int_0^\infty \Xi(r) E_r[x(t)] dr \tag{4.5}$$

in which, $\Xi(r)$ is the weight function. In order to practically implement the PI model in hysteresis identification, the discrete format of the PI model should be used by linearly

combining multiple stop operators with different thresholds (r values) as defined below:

$$y(t) = \sum_{i=1}^{m} \xi_i E_{r_i}[x(t)] \tag{4.6}$$

where, $y(t)$ is the total output signal at a given time when the hysteretic system is subjected to a random time-dependent input signal $x(t)$. The model parameters, including the weights ξ_i and thresholds r_i, should be selected such that the output signal best fits the training data. In total, $2m$ parameters need to be identified in the training phase. The structure of the PI model is illustrated in Fig. 4.2b. As shown, the input signal is fed to each stop operator individually, and the responses are linearly combined together. In addition to several stop operators, the input signal itself is added to the structure of the PI model as the final input to enhance its performance [129].

The PI model, including its stop operators, can be represented as a mass-spring system with the Coulomb friction force [132] as shown in Fig. 4.2c. In this figure, the last linear spring placed in parallel to the mass-spring systems represents the input signal considered in the structure of the PI model (Fig. 4.2b).

Sparse Identification of Nonlinear Dynamics (SINDy) Algorithm

The Sparse Identification of Nonlinear Dynamics (SINDy) algorithm, which was first introduced by Brunton et al. in 2016 [39] for the purpose of discovering the governing equation of a dynamical system using sparse regression [140, 187] and compressed sensing [188], is used here to estimate the underlying relationship between the input signal, $x(t)$, and the output signal, $y(t) = f(x(t))$, based on the experimental test data used for initial training. To approximate the relationship between input and output signals, multiple candidate functions based on the physical properties of the system are stacked in a library matrix, $\boldsymbol{\Theta}$, as shown

in Fig. 4.3:

$$\boldsymbol{\Theta}(\boldsymbol{X}) = \begin{bmatrix} | & | & | & | \\ g_1(\boldsymbol{X}) & g_2(\boldsymbol{X}) & \cdots & g_m(\boldsymbol{X}) \\ | & | & | & | \end{bmatrix}_{n \times m} \tag{4.7}$$

$$= \begin{bmatrix} g_1(x(t_1)) & g_2(x(t_1)) & \cdots & g_m(x(t_1)) \\ g_1(x(t_2)) & g_2(x(t_2)) & \cdots & g_m(x(t_2)) \\ \vdots & \vdots & \ddots & \vdots \\ g_1(x(t_n)) & g_2(x(t_n)) & \cdots & g_m(x(t_n)) \end{bmatrix}$$

in which, $\boldsymbol{X} = [x(t_1), x(t_2), ..., x(t_n)]^T$ is the input vector of the experimental test data used for initial training, $g_i(.), i = 1, 2, ..., m$ are the candidate functions, n and m are the number of measured data points and candidate functions selected to form the library matrix, respectively. The response function $y(t) = f(x(t))$ can be rewritten using the library matrix defined in Eq. 4.7 (Fig. 4.3):

$$\hat{\boldsymbol{Y}}_{n \times 1} = \boldsymbol{\Theta}_{n \times m} \times \boldsymbol{\Xi}_{m \times 1} \tag{4.8}$$

in which, $\hat{\boldsymbol{Y}}$ is the estimated output vector, and $\boldsymbol{\Xi} = [\xi_1, \xi_2, ..., \xi_m]^T$ is the coefficient vector that can be determined using a sparse regression algorithm such as least absolute shrinkage and selection operator (LASSO) [140] or sparse relaxed regularized regression (SR3) [189]. LASSO regression is capable of efficiently finding the parsimonious solution and effectively removing the irrelevant terms from the library matrix by setting their value to zero. The sparse solution can therefore be obtained using LASSO regression by minimizing the following statement:

$$\hat{\xi}_i = \underset{\xi_i}{argmin} \left\{ \sum_{j=1}^{n} (y(t_j) - \sum_{k=1}^{m} \Theta_{jk}\xi_k)^2 + \lambda \sum_{k=1}^{m} |\xi_k| \right\} \tag{4.9}$$

in which, $\boldsymbol{Y} = [y(t_1), y(t_2), ..., y(t_n)]^T$ is the measured output of the experimental test data used for initial training, $\hat{\boldsymbol{\xi}} = [\hat{\xi}_1, \hat{\xi}_2, ..., \hat{\xi}_m]^T$ is the sparse solution obtained from the LASSO regression that indicates which nonlinearity in the library matrix is active, and λ denotes the regularization parameter that controls the sparsity of solution and overcomes the over-fitting

problems. A more sparse solution would be obtained as a higher value is assigned to λ, which will be optimized using the methodology described later. Thus, the response function $y(t) = f(x(t))$ is approximated as:

$$\hat{y}(t) = \mathbf{\Theta}(x) \times \hat{\mathbf{\Xi}} \tag{4.10}$$

where $\mathbf{\Theta}(x)$ is the symbolic library matrix, as opposed to, $\mathbf{\Theta}(\boldsymbol{X})$, which is the data library matrix defined in Eq. 4.7.

4.3.2 PI-SINDy Model

A new hysteresis simulation model is developed by combing the sparse identification of non-linear dynamics (SINDy) algorithm and the Prandtl-Ishlinskii (PI) hysteresis model to reduce the dimensionality and achieve an efficient data-driven model. The architecture of the PI-SINDy model is shown in Fig. 4.3. The nonlinear candidate functions in the library matrix should be selected to enhance the performance of the SINDy algorithm owing to the fact that its performance is highly dependent on the candidate functions. Stop operators, $E_r[x(t)]$, are used as the candidate functions, $g_i(.)$, to enrich SINDy with a memory to simulate desired hysteretic response.

The thresholds can be assumed as $r_i = i/(m+1)|x|_{max}$, $i = 1, 2, ..., m$, in which $|x|_{max}$ is the maximum amplitude of the input signal. The role of SINDy is, therefore, to determine which candidate functions are needed to best estimate the output signal. As shown in Fig. 4.3, the input signal is fed to each stop operator individually, and SINDy is used to determine the weights of the PI model. If the parameter λ is optimally selected using the method described in the following section, the majority of the terms in the $\mathbf{\Xi}$ matrix will eventually become zero, which will effectively reduce the likelihood of over-fitting and sensitivity of the PI model to noisy experimental data.

The proposed PI-SINDy can be utilized in the disciplines that deal with the hysteresis identification phenomenon. In the current study, the strain and stress data obtained from a

structural component are used as the input $x(t)$ and output $y(t)$ signals, respectively, developing a PI-SINDy algorithm specific for the hysteretic behaviour of structural components.
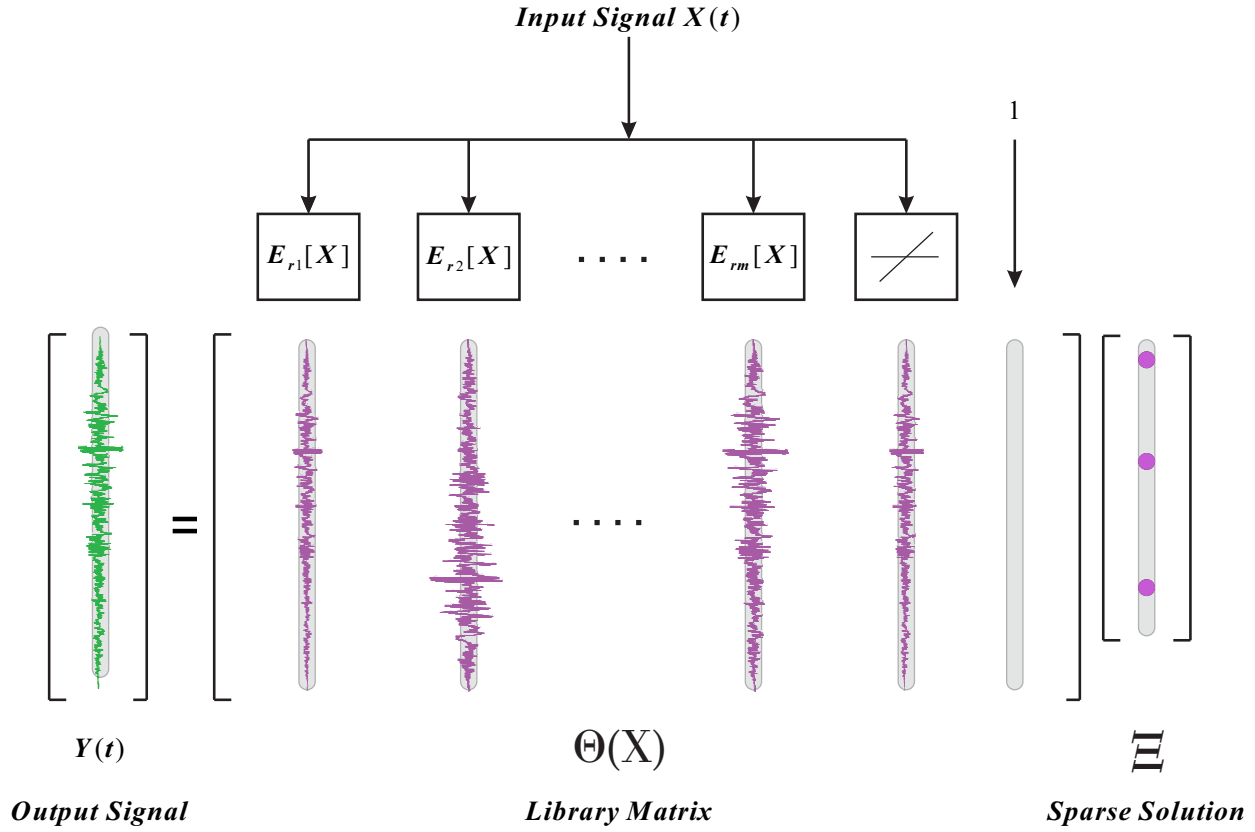
Figure 4.3: Architecture of PI-SINDy model

Akaike Information Criterion (AIC)

The Akaike Information Criterion (AIC) [141] is defined as an estimator for ranking different statistical models based on their accuracy and complexity. The accuracy of the model can be evaluated using the prediction error computed as the difference between the measured values and respective estimated responses by the model. The complexity of the model is associated with the number of parameters used to construct the model. The AIC used in this study to quantify the trade-off between the accuracy of the PI-SINDy prediction and its complexity is defined as:

$$AIC = 2K + n \ln \left(\frac{||\boldsymbol{Y} - \boldsymbol{\Theta\Xi}||_2^2}{n} \right) \tag{4.11}$$

in which, K is the number of active (non-zero) parameters in the $\boldsymbol{\Xi}$ matrix, which penalizes the complex models by magnifying the AIC, while the second term in Eq. 4.11 refers to the model error. The AIC chooses the optimal λ parameter in Eq. 4.9 by tracking the point with the greatest change in the slope of the curve that defines the AIC with respect to λ. To measure the accuracy of the model, i.e., the second term in Eq. 4.11, 10-fold cross-validation technique is used in the LASSO regression.

To illustrate the ability of AIC to automatically select the optimal λ parameter, a sample numerical analysis is performed where an input signal in the form of $x(t) = 5t \sin(t)$ was fed into the PI model with 50 stop operators. 15 λ values ranging from 10^{-4} to 10^3 were assumed as the initial selection. The output signal represented the response of a PI model with eight randomly selected thresholds from the initial 50 stop operators that were contaminated by Gaussian noise ($\mu = 0$ and $\sigma^2 = 2500$, in which μ and σ^2 are the mean and variance of the noise, respectively) to make the identification of the hysteresis more challenging. At each iteration, one λ was chosen from the initial selection list to perform the LASSO regression with 10-fold cross-validation. The results of the sample AIC validation analysis are shown in Fig. 4.4. As illustrated in Figs. 4.4a, 4.4b, and 4.4c, the performance of LASSO regression in identifying the correct eight thresholds was highly dependent on the value of the λ assumed. The optimal model, as shown Fig. 4.4b, corresponds to the point with the greatest change in the slope of the AIC plot as illustrated with a filled red circle in Fig. 4.4d. Note that Fig. 4.4d plots the relative AIC, which is defined as the difference between each AIC value and that of the AIC calculated using the first λ parameter in the selection list. Fig. 4.4e compares the hysteretic response of the noisy reference data and the prediction by the optimal model, suggesting that LASSO regression can effectively identify hysteretic response even in the presence of noise in the input data provided that the AIC is employed in the initial training phase.
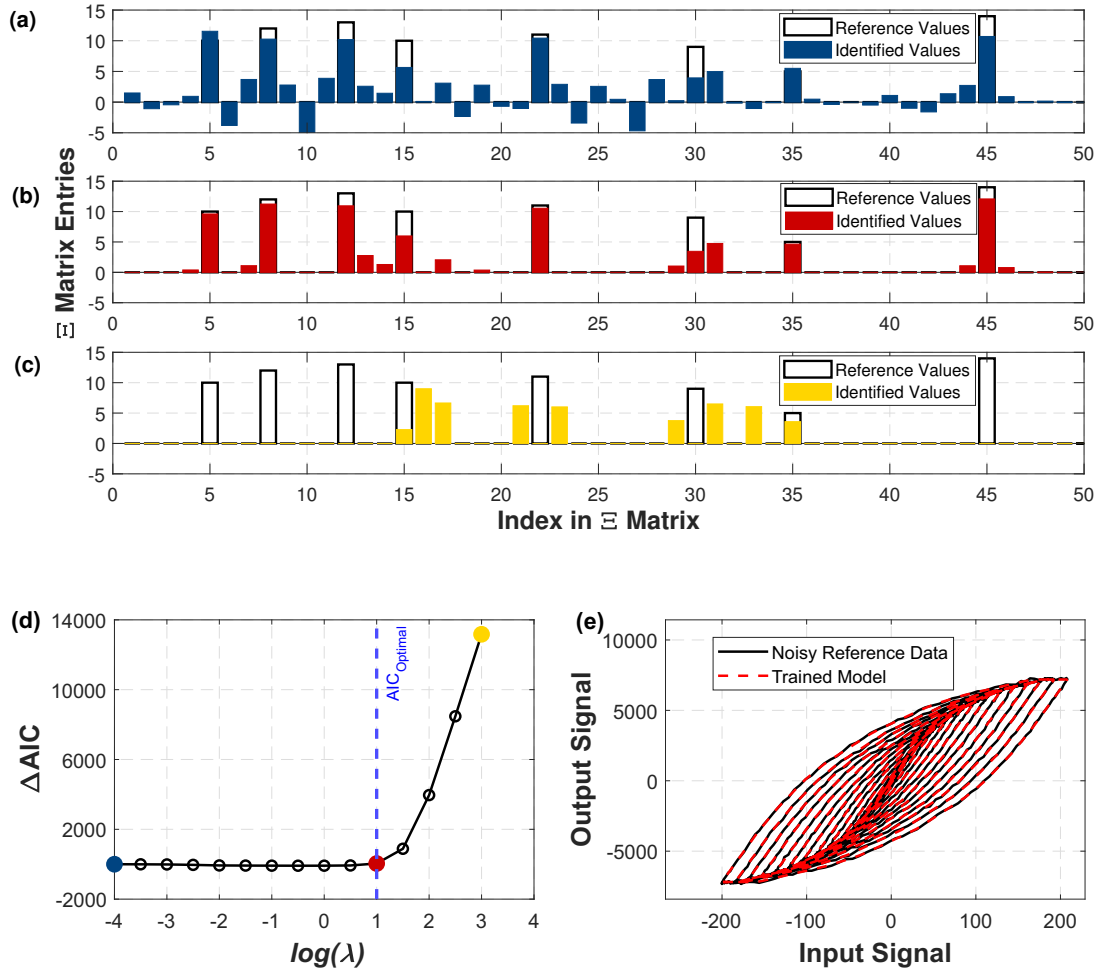
Figure 4.4: Illustration of initial training methodology: (a) Ξ matrix values identified using $\lambda = 10^{-4}$ representing a highly-noisy model; (b) Ξ matrix values Identified using $\lambda = 10$ representing an optimal model in terms of the trade-off between complexity-accuracy;(c) Ξ matrix values identified using $\lambda = 10^3$ representing a highly-sparse model; (d) variation of the AIC amplitude with respect to logarithm of λ; (e) comparison of noisy reference data and the model prediction using $\lambda = 10$ representing an optimally-trained model corresponding to the selected point in (d).

4.3.3   Phase 2: Recursive Model Updating

The digital twin achieved after initial (passive) training is capable of predicting the hysteretic response of the physical twin, however, the accuracy of the prediction would be limited to the available experimental test data fed to the digital twin during initial training. The hysteretic

response of the digital twin, in particular in the nonlinear range of the material, is expected to be affected by the amplitude, frequency and duration of real-time dynamic loading, e.g., earthquake accelerations, as well as the interaction of the physical and digital twins with the rest of the structure. The second phase of training is therefore required to improve the capability of the digital twin in predicting the hysteretic response of its physical counterpart by learning real-time as the hybrid simulation progresses, which produces new experimental dataset that can be made available to digital twin for further training. The adopted algorithm to perform the second phase of the training should be computationally efficient and fast to avoid delays as the hybrid simulation is performed in real-time in the laboratory. To this end, the recursive least-squares (RLS) algorithm is implemented in the second phase of the proposed DMHS framework. The RLS algorithm uses only the new incoming hysteresis data from the physical twin, which is experimentally tested in the laboratory, measured at each time step of the dynamic analysis to refine and enhance the digital twin's prediction in the next time step of the dynamic analysis. For instance, at time step k of the analysis, a set of new measurements comprised of the strain data, x_k, and stress data, y_k, are collected from the physical twin using the sensors installed on the specimen. The RLS algorithm then adjusts the digital twin in time step $k+1$ based on the up-to-date data. The linear recursive estimator is written as [190]:

$$\boldsymbol{y}_k = \boldsymbol{\Theta}(x_k)\boldsymbol{\Xi} + \boldsymbol{\nu}_k \tag{4.12}$$

in which $\boldsymbol{\nu}_k$ is the measurement noise. The RLS algorithm can be used to update the parameters of the digital twin, $\hat{\boldsymbol{\Xi}}$, using:

$$\hat{\boldsymbol{\Xi}}_k = \hat{\boldsymbol{\Xi}}_{k-1} + \boldsymbol{K}_k \left[y_k - \boldsymbol{\Theta}(x_k)\hat{\boldsymbol{\Xi}}_{k-1} \right] \tag{4.13}$$

Referring to Eq. 4.13, the estimated parameters of the previous step, $\hat{\boldsymbol{\Xi}}_{k-1}$, are updated by a corrective term based on the difference between the measured stress, y_k, and the anticipated value of the stress, $\boldsymbol{\Theta}(x_k)\hat{\boldsymbol{\Xi}}_{k-1}$. The correction term is weighted by a gain matrix called, $\boldsymbol{K}_k$,

which can be obtained so that the sum of the variances of estimation errors in step k, $\boldsymbol{J}_k$, is minimized. The objective function for minimization, $\boldsymbol{J}_k$, is therefore defined as:

$$\begin{aligned}
\boldsymbol{J}_k &= \mathbb{E}\left[(\Xi_1 - \hat{\Xi}_1)^2\right] + ... + \mathbb{E}\left[(\Xi_m - \hat{\Xi}_m)^2\right] \\
&= Trace(\boldsymbol{P_k})
\end{aligned} \tag{4.14}$$

where $\boldsymbol{P_k}$ is the estimation-error's covariance matrix and is defined in a recursive form:

$$\boldsymbol{P}_k = (\boldsymbol{I} - \boldsymbol{K}_k\boldsymbol{\Theta}(x_k))\boldsymbol{P}_{k-1}(\boldsymbol{I} - \boldsymbol{K}_k\boldsymbol{\Theta}(x_k))^T + \boldsymbol{K}_k\boldsymbol{R}_k\boldsymbol{K}_k^T \tag{4.15}$$

where $\boldsymbol{R_k}$ is the covariance of the measurement noise, which is taken as a white noise with the variance of 1. $\boldsymbol{K}_k$ can be obtained analytically by minimizing $\boldsymbol{J}_k$ defined in Eq. 4.14:

$$\frac{\partial \boldsymbol{J}_k}{\partial \boldsymbol{K}_k} = 0 \rightarrow \boldsymbol{K}_k = \boldsymbol{P}_{k-1}\boldsymbol{\Theta}(x_k)^T(\boldsymbol{\Theta}(x_k)\boldsymbol{P}_{k-1}\boldsymbol{\Theta}(x_k)^T + \boldsymbol{R}_k)^{-1} \tag{4.16}$$

Three steps associated with the RLS algorithm used to update the initial parameters of the digital twin are summarized as follows:

1. Initialize the estimator:

$$\hat{\Xi}_0 = \mathbb{E}\left[\Xi\right] \tag{4.17}$$

$$\boldsymbol{P}_0 = \mathbb{E}\left[(\Xi - \hat{\Xi}_0)(\Xi - \hat{\Xi}_0)^T\right] \tag{4.18}$$

The initial parameters, $\hat{\Xi}_0$, are set to those obtained from initial training in Section 4.3.1, and the covariance matrix of the initial parameters is assumed as $10^4 \boldsymbol{I}_{m \times m}$ in which $\boldsymbol{I}$ is the identity matrix, and m is the number of stop operators remained active after the initial training phase. The initial parameter covariance matrix reflects the degree of uncertainty in the estimation of the initial parameters. When the covariance of the initial parameters is high, less weight is placed on the initial parameter values and more on the data obtained during the second phase.

2. Set up the model for the digital twin using Eq. 4.12

3. Update the estimate of $\hat{\Xi}$ using Eqs. 4.13, 4.15, and 4.16

The architecture of the DMHS framework is summarized in Fig. 4.5. In this figure, the left box shows the initial training phase that starts with feeding the initial training data, e.g., static cyclic test data, to the PI-SINDy algorithm. A set of candidate λs is then introduced to the algorithm to select the optimal λ using the AIC. Next, the initial data is randomly split into training and validation sets for the purpose of cross-validation. The training will be performed on the training data, and the error is assessed using the validation set. The average error among the permuted sets of training data, as the result of cross-validation, is calculated and used towards determining the AIC. Upon finding the optimal λ and the corresponding $\hat{\Xi}$ matrix using the LASSO regression, the initial training is completed. In the second phase, which is shown in the right box of Fig. 4.5, the entries of the $\hat{\Xi}$ matrix are recursively updated using the RLS algorithm until hybrid simulation reaches the final time step of the dynamic analysis.

4.4 Verification of the DMHS Framework

The DMHS framework proposed in this study is demonstrated and verified through two virtual hybrid simulations (VHS) in which two numerical models are coupled, one represents the computational model of the structure, and the second one plays the role of the experimental substructure. The first VHS involves a simulation using a low-fidelity numerical model (Fig. 4.6a), which offers a computationally efficient method allowing the demonstration and evaluation of various aspects of the framework with a low computational burden. The second VHS uses a high-fidelity simulation (Fig. 4.6b) to assess the capability of the proposed framework when the data involving detailed local and global responses is used to train the digital twin. These verifications were conducted using the PsDHS method. It is significant to be noted that the DMHS framework proposed here is potentially applicable to RTHS.
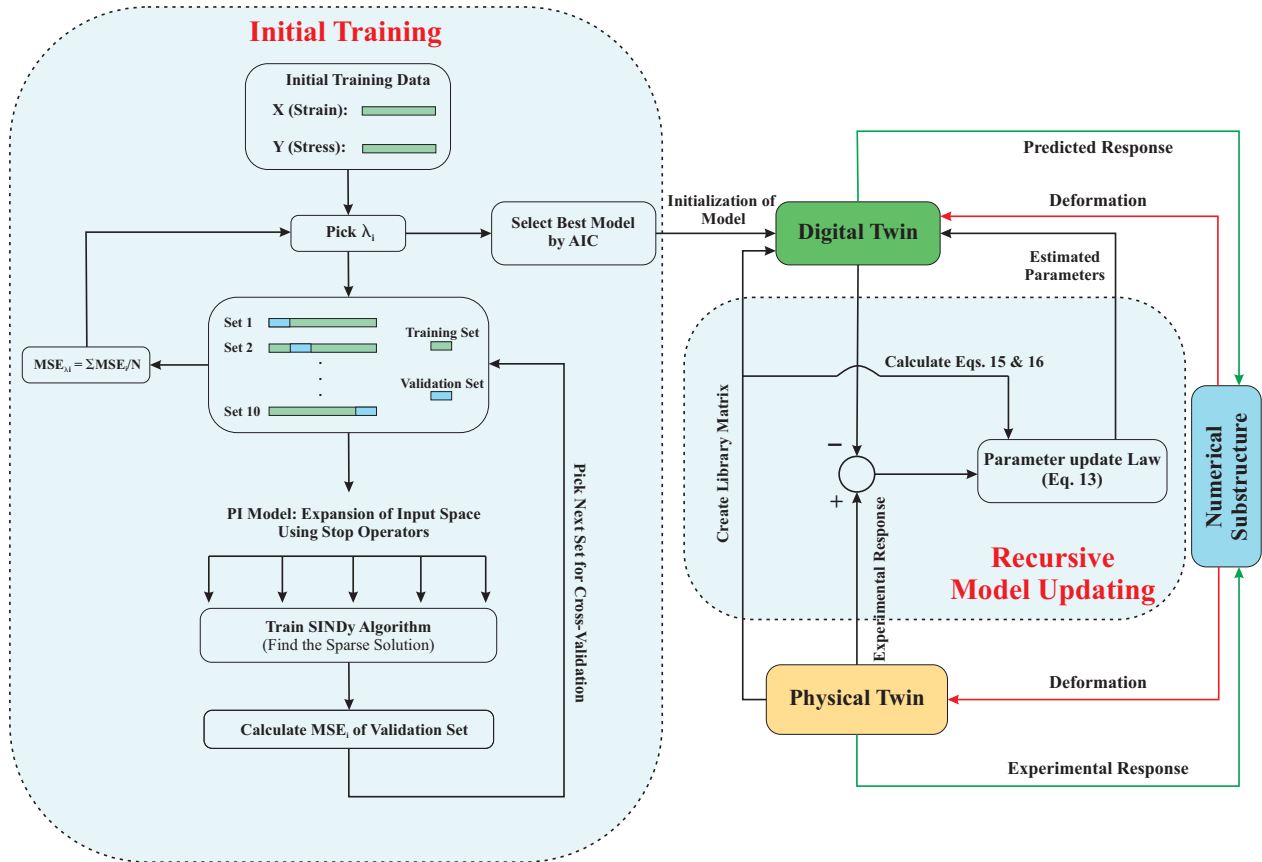
Figure 4.5: Architecture of the digital twin-based multi-element hybrid simulation framework.

4.4.1 Virtual Hybrid Simulation Procedure

The virtual hybrid simulation involved two parallel programs, i.e., a Master program and one or more Slave programs, coupled to analyse a prototype structure under dynamic loading. The master program consisted in the numerical substructure where less critical elements of the structure were reproduced in the OpenSees program [157], and the equation of motion was solved at each time step, whereas the slave programs included the virtual and digital twins, which were connected to the Master program to exchange force, displacement, or velocity signals at the interface degrees-of-freedom (DOFs) of the virtual and digital twins to the numerical substructures. The virtual twin, which plays the role of physical twin in VHS, was constructed in the ABAQUS program] [191], whereas the digital twin was programmed in MATLAB [159]. The UT-SIM framework [160–162] was used in this study

as the middleware to connect the slave programs to the master program using TCP/IP communication protocol in UT-SIM. In order to establish a seamless communication between the Master and Slave programs, super-elements defined in the Master program in the place of removed elements were connected to adapter elements in the slave programs to impose displacement commands [192].

4.4.2 Prototype Frames

A prototype structural system consisting of a two-storey BRBF shown in Fig. 4.6 was selected to verify the proposed DMHS framework. The frame consists of Ductile (Type D) BRBF and is located in Vancouver, British Columbia, Canada, on site Class C. Gravity and seismic loading was calculated in accordance with the 2015 National Building Code (NBC) of Canada [154]. The seismic weights of the first and second stories were assumed as $2000kN$, and $1500kN$, respectively, which were divided equally between the two columns and lumped at the top end of each column at each storey. Different seismic weights assigned to adjacent stories were expected to produce distinct displacement demands at each storey under earthquake ground motion accelerations, triggering uneven hysteretic behaviours for the physical and digital twins. Such a response would demonstrate the capability of the digital twin in approximating nonlinear cyclic response based on the data obtained from a physical twin that has dissimilar cross-sectional properties and distinct hysteretic response. For the prototype frame, the ductility- and overstrength-related force modification factors R_d and R_o are 4.0 and 1.2, respectively. The importance factor of the structure and the factor to account for higher mode effects are $I_E = 1.0$ and $M_v = 1.0$, respectively. The structural design of the selected BRBF was performed in accordance with the 2019 edition of the Canadian steel design standard CSA S16 [155]. Detailed information regarding the design of steel BRBFs can be found in [156].

To perform the dynamic analysis under seismic excitations using the VHS, a suite of 12 ground motion acceleration records comprised of four shallow crustal, four deep subduction

in-slab and four deep subduction interface, which are the main sources of seismic hazard in Southwest British Columbia, were selected and scaled to match on average the code-specified uniform hazard spectra for the building location. Additional information on the selection and scaling of earthquake ground motions can be found in [193].
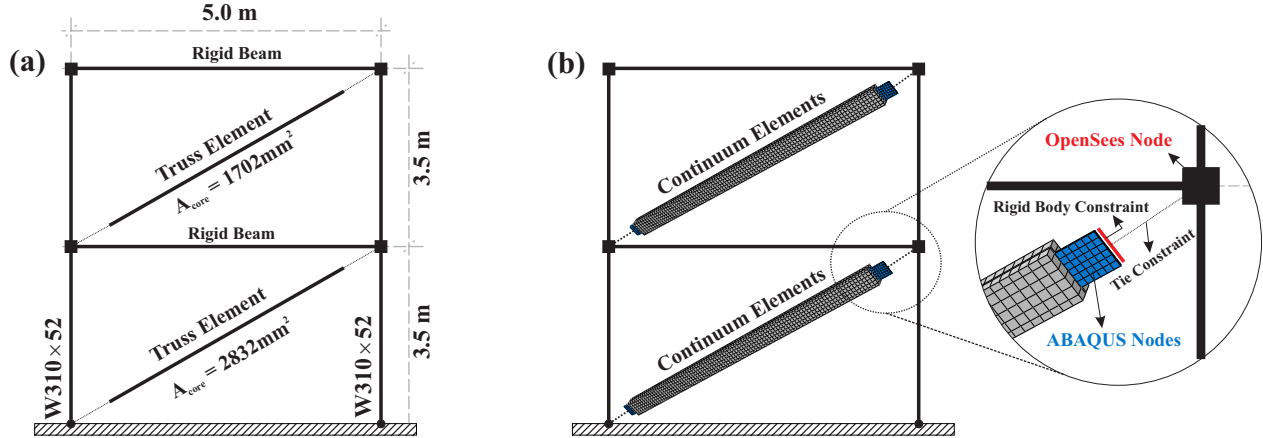
Figure 4.6: Prototype frame, (a) 2D low-fidelity model, (b) 3D high-fidelity model, the geometrical properties and the sections of this frame are identical to the 2D low-fidelity model.

The modelling approaches used to simulate the prototype frame are shown in Fig. 4.7. The reference model (Fig. 4.7a) represented VHS with two virtual twins both simulated in ABAQUS and coupled through the UT-SIM framework to the rest of the frame constructed in OpenSees. This model encompassed an ideal configuration for hybrid simulation because of accurately simulating both critical elements, which is analogous to physical testing of both critical elements in the laboratory, i.e., MeHS. Fig. 4.7b shows the DMHS model, which consisted of the first-storey BRB (virtual twin) simulated in ABAQUS, the second-storey BRB (digital twin) simulated in MATLAB, and the rest of the frame (numerical substructure) modelled in OpenSees.

The communication between the Master program, i.e., OpenSees, and Slave programs, i.e., ABAQUS in the reference model (Fig. 4.7a), ABAQUS and MATLAB in the DMHS model (Fig. 4.7b), was established using UT-SIM. An additional data communication, outside of the UT-SIM platform, was established for the RMU training phase through sending the

hysteresis data obtained from the virtual twin to the digital twin by reading/writing the data from/into a text file. In addition to the simulations shown in Fig. 4.7, a correlative model was created to investigate the effect of the RMU training phase proposed to update the prediction capability of the digital twin as more hysteresis data fed back to the digital twin from the physical twin during VHS. This model was identical to the DMHS model shown in Fig. 4.7b except that there was the real-time communication of data between virtual and physical twins was intentionally prevented. In other words, the digital twin prediction was solely based on the initial training.
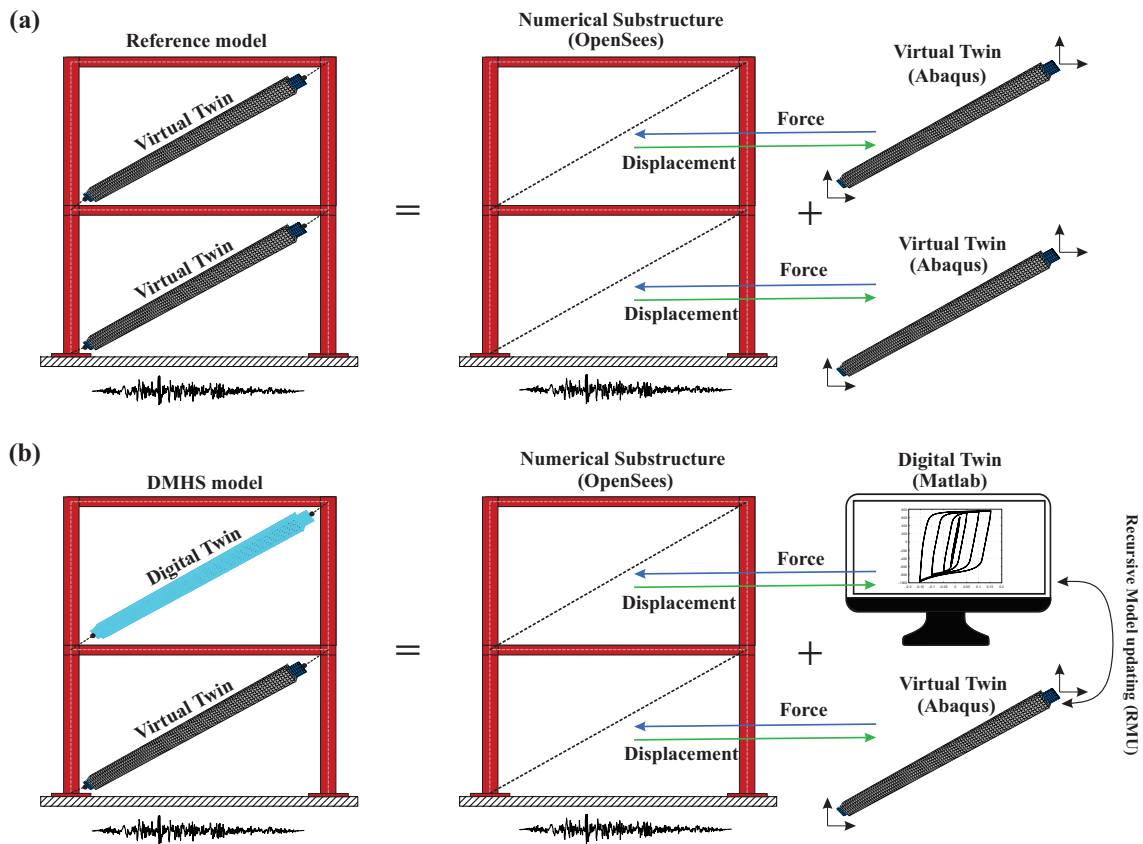
Figure 4.7: Prototype frames for dynamic analysis workflows, (a) reference model, (b) digital twin based multi-element hybrid simulation (the workflows are illustrated for 3D high-fidelity model here).

The simulation techniques employed for the numerical substructure, digital and virtual twins are described below.

Numerical Substructure

The structural components that are expected to remain elastic with no or very limited inelastic response, such as beams and columns, constituted the numerical substructure of VHS and are modelled in OpenSees. These components were constructed using elastic beamcolumn elements. The modelling assumptions used to construct beams and columns are not expected to affect the verification results here. In other words, the digital twin prediction was solely based on the initial training.

Young's modulus $E = 200GPa$ was used for columns and beams. At the bottom of the columns, all translational DOFs and the rotation about the longitudinal axis of the column were restrained to simulate a pinned base condition. The out-of-plane translation was restrained at the top end of columns at each storey to simulate the lateral support provided by the perpendicular framing system or floor slab. A tie constraint in the horizontal direction was used between column ends at each storey to simulate in-plane rigidity provided by the floor or roof diaphragm. Gravity loads were applied as concentrated loads at the top end of columns. Two lumped masses, each equal to 102 and 77 kNs^2/m were assigned at the top end of each column in the floor and roof levels, respectively. P-Delta effects were ignored in the analysis. Mass proportional damping corresponding to 5% of critical in the first structure lateral vibration mode was specified following the Rayleigh damping method [160]. The UT-SIM super-element replaced the braces in the OpenSees model to facilitate data communication between OpenSees and MATLAB/ABAQUS, e.g., sending and receiving displacement and force commands. The initial stiffness of the brace was calculated based on the elastic stiffness of the BRB core to initiate the dynamic analysis. The Generalized-Alpha (AlphaOSGeneralized) integration algorithm [194] was used to solve the equation of motion. For the virtual and digital twins, it was not computationally feasible to obtain the tangent stiffness at every step. The initial stiffness of each time step was therefore used to solve the numerical problem at every iteration [162].

Virtual Twin

The virtual twin representing the BRB was developed in ABAQUS using two modelling techniques: 1) two-dimensional low-fidelity model (2DLFM) consisting of truss elements as shown in Fig. 4.6a and 2) three-dimensional high-fidelity model (3DHFM) consisting of solid elements as shown in Fig. 4.6b.

In 2DLFM, Giuffré-Menegotto-Pinto material model [58] assigned to a nonlinear truss element was used to numerically simulate the BRB. In 3DHFM, the Voce-Chaboce multiaxial plasticity material model [195, 196] with combined isotropic-kinematic hardening parameters was used to define the cyclic nonlinear response of the core [197]. The grout was modelled using an elastic material with Young's modulus $E = 21 \ GPa$. The interaction between the steel core and grout casing was modelled using finite sliding and was assigned normal and tangential behaviours. The normal behaviour was simulated using an exponential softened pressure-overclosure relationship. The tangential behaviour was constructed using a penalty friction algorithm, assuming a friction coefficient of 0.1 for steel core plate and grout casing. In exponential softened contact problems, the pressure starts when two surfaces are closer than a certain threshold, C_o, and increases exponentially as they approach each other. C_o and the contact pressure at no clearance state, P_o, were assumed 1 mm and 5 MPa, respectively, as proposed by [198]. The modelling technique used to create the interaction between steel and concrete enabled the 3DHFM to explicitly reproduce the asymmetric response of the BRB expected due to additional forces generated by frictional forces at the interface of steel core and grout when the BRB is in compression [151–153]. Moreover, it was expected that this technique could minimize potential convergence issues in VHS as ABAQUS and OpenSees run in parallel, solving a highly nonlinear problem. The end nodes of the BRB in the ABAQUS model were tied together using a rigid body constraint, creating a pinned end condition. The pin connection was then tied using UT-SIM to the corresponding node in OpenSees (Fig. 4.7b).

Improved Digital Twin for Asymmetric Response Prediction

The PI model developed for the prediction of the hysteretic response was improved to re-produce the asymmetric behaviour of the BRB as expected in the 3DHFM reference model. This improvement involved the addition of two springs, tension-only and compression-only, to the PI model shown in Fig. 4.2c. These new springs replaced the linear spring without an attached mass shown in Fig. 4.2c. The improved PI model can then be expressed as:

$$y(t) = \xi^+ x(t) \left(\frac{1 + \text{sgn}(x)}{2} \right) + \xi^- x(t) \left(\frac{1 - \text{sgn}(x)}{2} \right) + \sum_{i=1}^{m} \xi_i E_{r_i}[x(t)] \qquad (4.19)$$

$$\text{sgn}\, x := \begin{cases} -1 & \text{if } x < 0 \\ 0 & \text{if } x = 0 \\ 1 & \text{if } x > 0 \end{cases} \qquad (4.20)$$

in which ξ^+ and ξ^- refer to the stiffness components of the compression-only and tension-only springs, respectively. The improved PI model was used in the verification of the proposed framework using the 3DHFM, while the verification using the 2DLFM employed the original PI model, which ignores the asymmetric response of the virtual twin. The limitation of the 2DLFM is not expected to affect the demonstration and verification of the DMHS framework.

Given that the geometrical properties of the critical elements, e.g., BRBs in BRBFs, typically vary between the stories in a well-designed multi-storey structure, the stress-strain data of the BRB, representing normalized input signals, obtained from the virtual twin was used to train the digital twin instead of the force-displacement data as the force and displacement amplitudes are affected by the cross-sectional area and the length of the brace, respectively. Once the relationship between the stress and strain was predicted by the digital twin, the restoring force was computed by multiplying the stress value by the cross-sectional area of the respective BRB core in the storey involving a digital twin.

4.4.3 Low-fidelity Virtual Twin Verification

The results of the initial training phase using the 2DLFM are presented in Fig. 4.8. The cyclic nonlinear static (pushover) analysis was first performed on an isolated BRB, which is identical to that of the digital twin in Fig. 4.7a, in the ABAQUS program to generate fictitious test data for initial training. From the initial 100 stop operators, the AIC found that the λ value associated with only 28 stop operators is sufficient to properly approximate the nonlinear hysteretic behaviour of the BRB (Fig. 4.8a). As shown in Fig. 4.8b, the hysteretic response predicted by the trained model well matched the reference data. The trained Ξ_{LASSO} matrix was then intentionally corrupted by adding Gaussian noise to its entries to further verify the capability of DMHS in discovering the true hysteretic response in lieu of sophisticated initial training data. The corrupt digital twin created based on this hysteresis input as shown in Fig. 4.8b was then used to initialize the digital twin in VHS.
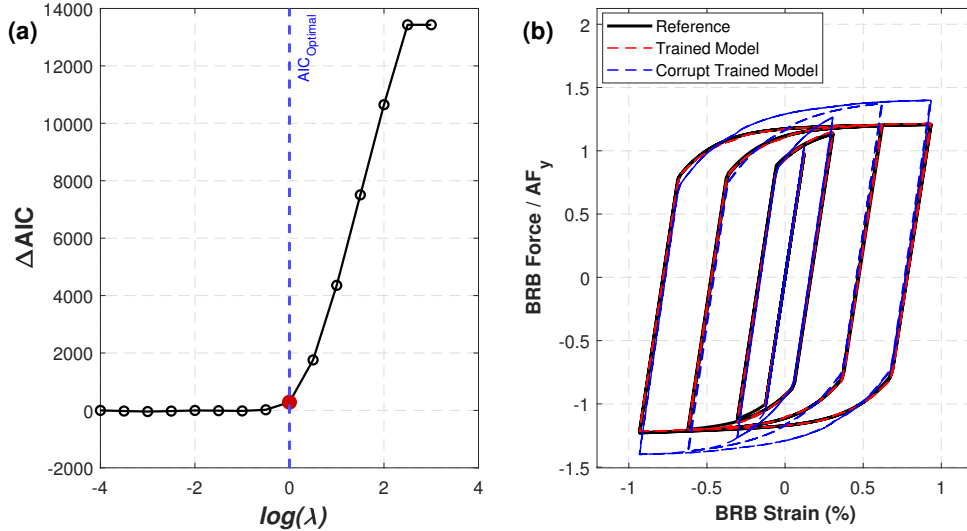
Figure 4.8: DMHS initial training using low-fidelity simulation, (a) AIC plot, (b) comparison of the reference, trained, and corrupt trained hysteretic responses

Two sets of VHSs were performed under the selected suite of ground motion accelerations using the frames shown in Fig.4.7a and Fig.4.7b, referred to as reference model and DMHS model, respectively. The storey drift ratios and BRB hysteretic responses were then obtained

and used to verify the suitability of the digital twin to replicate the nonlinear cyclic behaviour of the BRB. The normalized root-mean square-error (NRMSE) as given in Eq. 4.21 was used to calculate the error between the storey drift ratios of the reference and DMHS models:

$$NRMSE = \frac{\sqrt{\sum_{i=1}^{N}(y_{ref,i} - y_{model,i})^2/N}}{|y_{ref,max} - y_{ref,min}|} \tag{4.21}$$

The NRMSE values for DMHS along with the statistics of errors are given in Table 4.1 for the prototype BRBF studied here. On average, the NRMSE of the relative displacements in the first and second stories were 2.11% and 2.53%, respectively. This suggests that the proposed DMHS can appropriately estimate the underlying relationship between the force and deformation of the digital twin, i.e., BRB. The average NRMSE were obtained as 1.64%, 3.37%, and 1.96% for crustal, in-slab, and interface records, respectively. This shows that the prediction performance of DMHS is reduced under in-slab earthquakes, which may be attributed to their long duration or frequency content. To improve the accuracy of the prediction when pulse-type ground motions are used or ratcheting response is expected, the force-displacement response obtained under an asymmetric cyclic displacement protocol can be used as initial training data.

Seismic Source	Event	Year	Station	DMHS		DMHS without RMU	
				Storey 1 Displacement NRMSE(%)	Storey 2 Displacement NRMSE(%)	Storey 1 Displacement NRMSE(%)	Storey 2 Displacement NRMSE(%)
Crustal	Tabas, Iran	1978	Dayhook	0.5	0.56	1.29	1.5
	San Fernando, US	1971	Castaic - Old Ridge Route	2.02	2.36	10.86	12.24
	Montenegro, Yugoslavia	1979	Herceg Novi - O.S.D Paviviv	1.63	1.9	2.95	3.43
	Kobe, Japan	1995	Tadoka	1.93	2.16	4.88	5.58
In-slab	Geivo, Japan	2001	1421a	2.02	2.46	7.91	9.74
	Miyagi, Japan	2011	IWT026	1.26	1.73	3.75	4.36
	Miyagi, Japan	2011	MYG016	2.24	2.91	7.53	9.74
	Miyagi, Japan	2011	IWTH24	6.57	7.76	11.87	14.12
Interface	Southern Peru	2001	POCO	0.43	0.57	2.35	2.51
	Pisco, Peru	2007	UNICA	1.08	1.33	6.41	7.30
	Maule, Chile	2010	LACHb (Coleigo Las Americas)	4.45	5.25	10.22	12.10
	Iquique, Chile	2014	PB09	1.16	1.37	5.46	7.47
			Average:	2.11	2.53	6.29	7.51

Table 4.1: Relative displacement error using the low-fidelity modelling technique.

To verify the need for real-time RMU training, a third VHS was performed using the model

that lacks the RMU training phase. To set up this VHS, the hysteresis data collected from the physical twin during the hybrid simulation was not sent to the digital twin, resulting in VHS completed using a digital twin lacking the second phase of training. For DMHS lacking RMU, the NRSME values of the relative displacements measured at each storey are given in Table 4.1. As shown, the NRMSE when DMHS was used is on average three times lower than the errors recorded in DMHS lacking RMU (2.1% vs. 6.3% in Storey 1 and 2.5% vs. 7.5% in Storey 2). This finding indicates the benefit of the framework with RMU in achieving a more accurate hysteresis response prediction. In particular, RMU helps predict complex constitutional properties of the material such as yielding, isotropic and kinematic hardening, which cannot be approximated by digital twin unless sufficient data containing those critical hysteresis properties are provided real-time during hybrid simulation, which is being performed under a specific ground motion acceleration. The reason being that the dependency of the kinematic and cyclic hardening properties of the steel material to the loading protocol [199], which is only realized when the real-time data generated under the ground motion acceleration is fed to the digital twin.

The time history of accelerations for three records, the 1971 San Fernando-Castaic-Old Ridge Route earthquake, the 2001 Geivo, Japan-1421a earthquake and the 2007 Pisco, Peru-UNICA earthquake, representing crustal, in-slab and interface events, respectively, are given in Fig. 4.9. The history of BRBF storey drift ratios, which were computed by dividing the relative lateral displacement of each storey by its respective height, and the stress-strain response of the BRB at both stories are shown in Figs. 4.10-4.12 for the representative ground motion records shown in Fig. 4.9. Referring to Figs. 4.10-4.12, DMHS well predicted the hysteretic response of the BRB, which suggests the digital twin can successfully learn the hysteretic response of virtual twin despite the differences in the displacement history induced in each BRB. The comparison of the drift histories between the reference and DMHS show that despite a very good match at the beginning of the analysis where the majority of large displacement cycles occurred, a discrepancy was observed beyond earthquake peaks and

close to the end of the analysis, which stems from the accumulation of prediction errors as the analysis approaches to the end. The comparison between the results obtained using the analysis associated with the DMHS lacking RMU and the reference model results in Figs. 4.10-4.12 indicate the improvement achieved by RMU in predicting the hysteresis response.
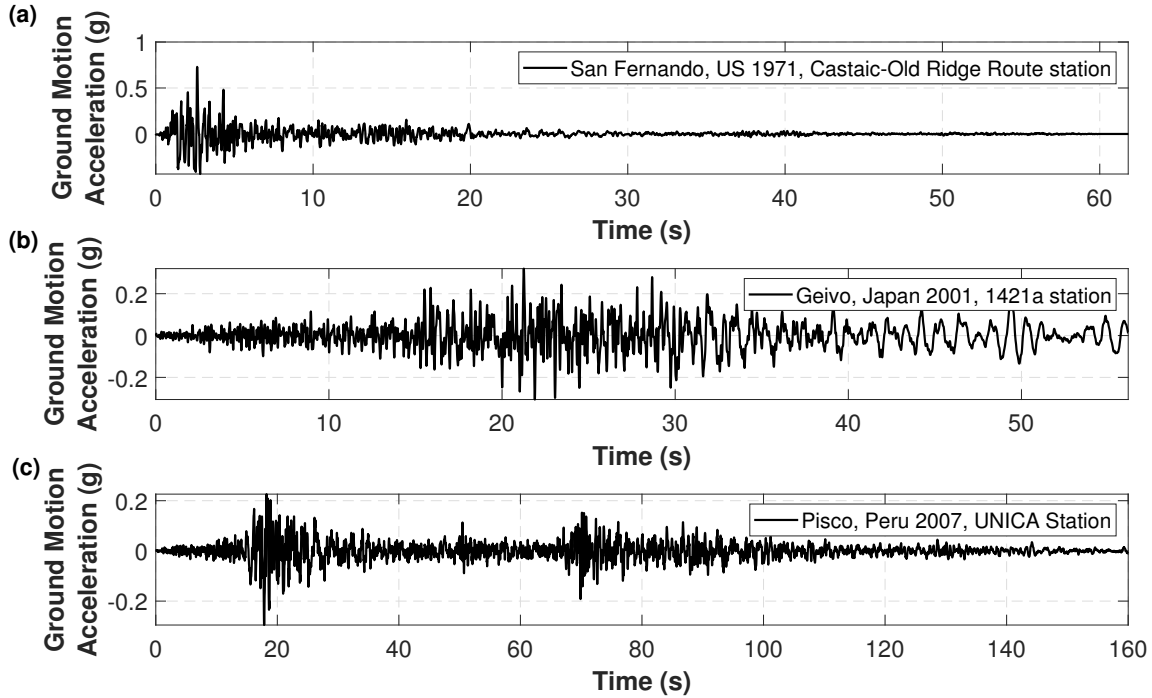
Figure 4.9: Ground motion acceleration examples for three seismic hazard sources, (a) crustal, (b) in-slab, (c) interface

The verification study presented here demonstrated promising results for a BRB digital twin trained using the stress-strain data, which suggests that the proposed framework can reliably be used in multi-storey frames that typically have braces with different cross-sectional areas along the frame height, which often decreases from the bottom to top.

The variation of the first nine entries from the total 28 entries of the Ξ matrix is plotted with respect to ground motion time in Fig. 4.13 for the analysis using DMHS under the 1971 San Fernando-Castaic Old Ridge Route earthquake. Ξ matrix contains the weights of the PI model determined using the SINDy algorithm in the initial training phase and

updated during the RMU phase. Referring to Fig. 4.13, all entries converged as the simulation progresses, despite some fluctuations at the beginning of the simulation, suggesting that the RLS algorithm offers a stable response as long as sufficient hysteresis data is sent to the digital twin. The fluctuations at early stages were attributed to the fact that virtual twin responds almost entirely in the elastic range of the material at the beginning of the excitation, reporting very limited or no data associated with the inelastic response of the virtual twin to the digital twin.

The complete set of nonlinear response history analysis results for all 12 ground motions is given in Appendix C.

4.4.4 High-fidelity Virtual Twin Verification

The second series of the verification of the proposed DTMH framework involved detailed simulation of the first-storey BRB using the finite element method in ABAQUS, while the second-storey BRB was replaced with the improved digital twin to account for the BRB asymmetric force response. The cyclic pushover analysis was first performed on an identical BRB isolated from the BRBF and simulated using a three-dimensional finite element model in ABAQUS. This analysis generated fictitious test data required for the initial training of VHS. From the initial 100 stop operators used in the verification using the 3DHFM, it was found by AIC that the λ value associated with only 20 stop operators was enough to reproduce the nonlinear cyclic behaviour of the BRB (Fig. 4.14a). As shown in Fig. 4.14b, the hysteretic behaviour obtained using the reference model includes the asymmetric response anticipated in steel BRBs. A very similar response, including the additional resistance gained in compression, was predicted using the trained model (Fig. 4.14b). The NRMSE in the initial training hysteretic response, shown in Fig. 4.14b, was 2.94%. The prediction of frictional forces when BRB undergoes compression was realized by adding a penalty factor to the error calculation of the pick reversal point in the last cycle of compression to penalize the LASSO algorithm and add higher weight to capturing the asymmetrical hysteretic response.

94
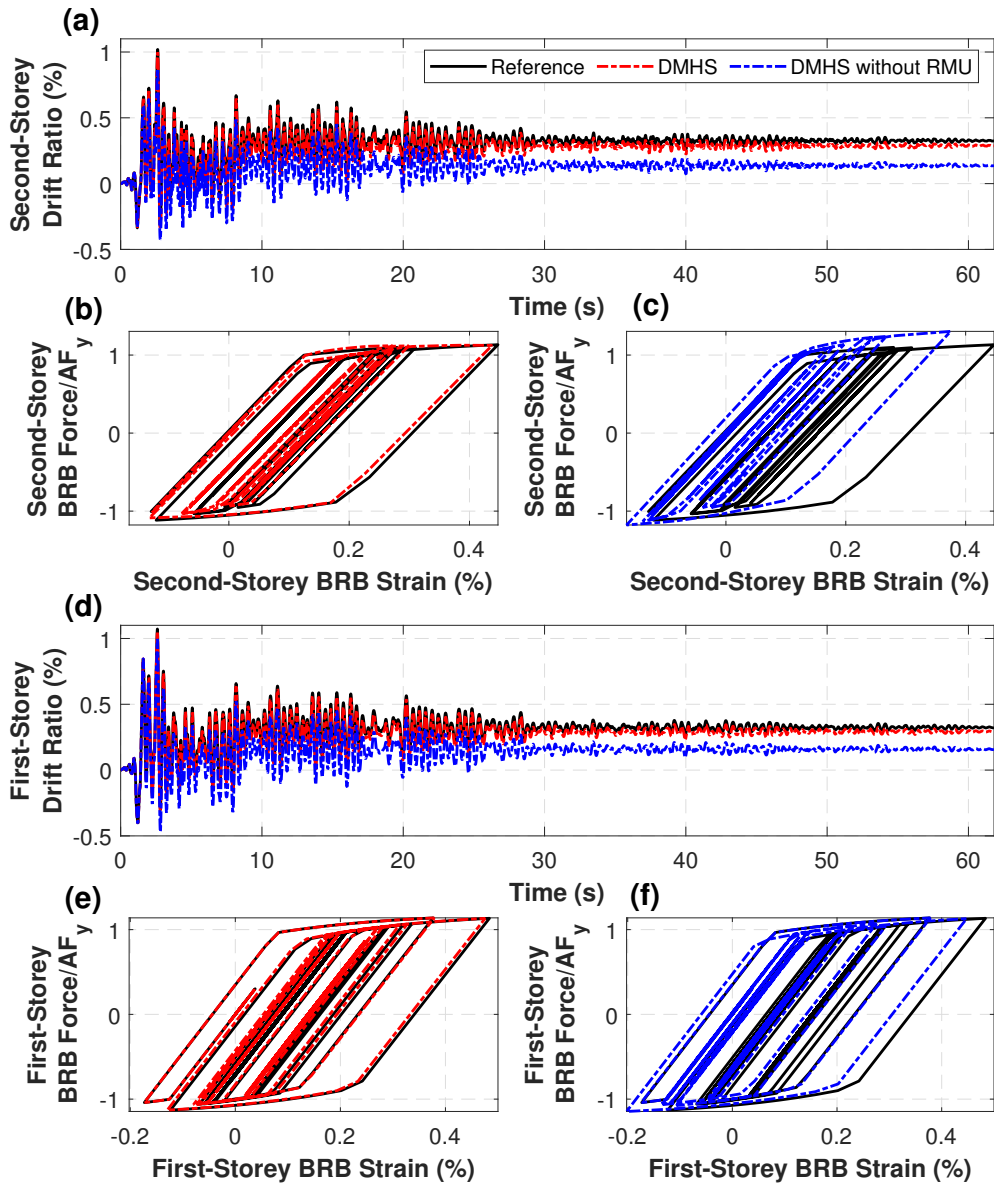
Figure 4.10: Virtual hybrid simulation of the BRBF using 2DLFM under the 1971 San Fernando-Castaic Old Ridge Route earthquake, (a) history of drift ratio in Storey 2, (b) Storey 2 BRB (digital twin) response for DMHS vs. reference, (c) Storey 2 BRB (digital twin) response for DMHS without RMU vs. reference, (d) history of drift ratio in Storey 1, (e) Storey 1 BRB (virtual twin) response for DMHS vs. reference, (f) Storey 1 BRB (virtual twin) response for DMHS without RMU vs. reference.
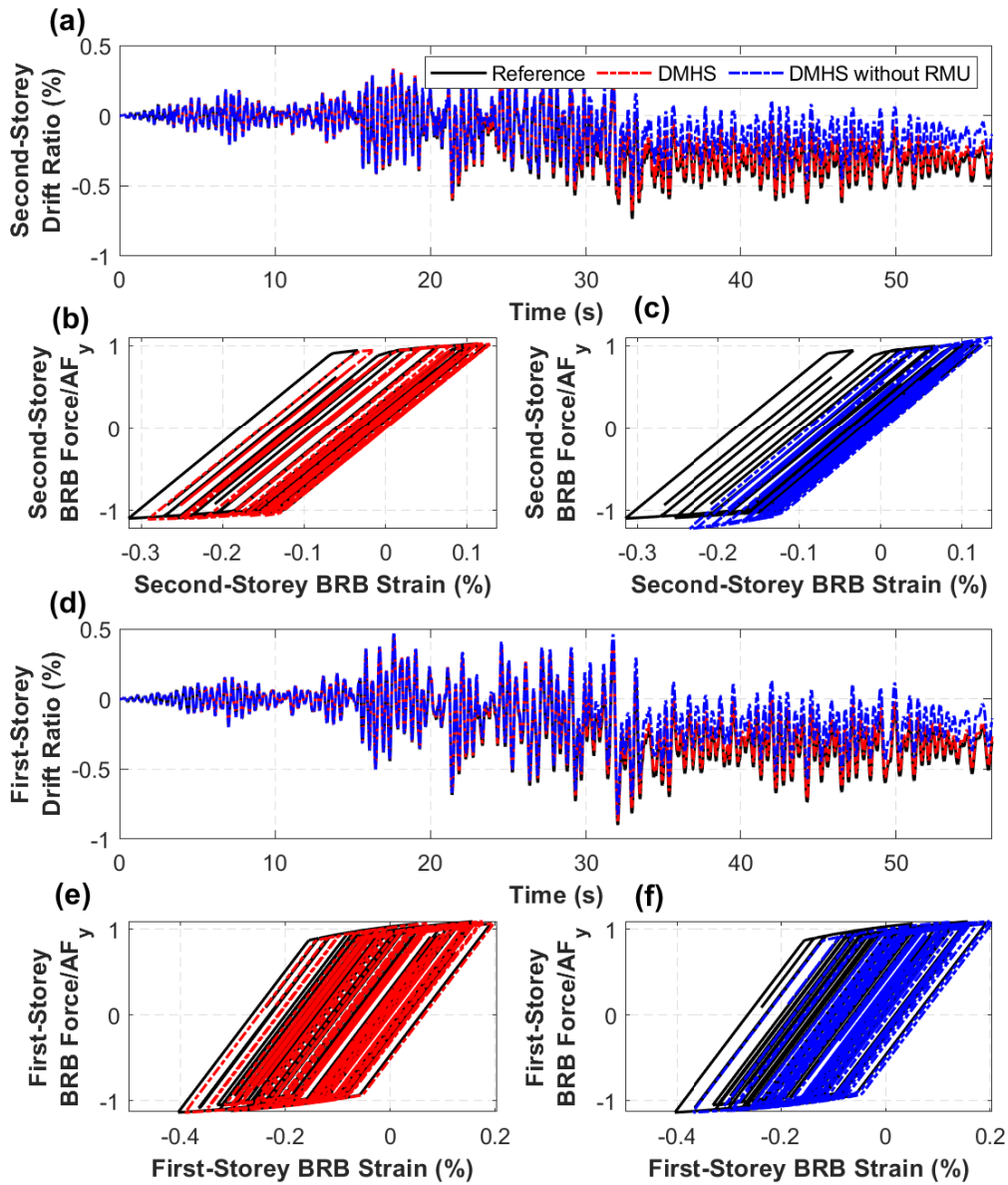
Figure 4.11: Virtual hybrid simulation of the BRBF using 2DLFM under the 2001 Geivo, Japan-1421a earthquake, (a) history of drift ratio in Storey 2, (b) Storey 2 BRB (digital twin) response for DMHS vs. reference, (c) Storey 2 BRB (digital twin) response for DMHS without RMU vs. reference, (d) history of drift ratio in Storey 1, (e) Storey 1 BRB (virtual twin) response for DMHS vs. reference, (f) Storey 1 BRB (virtual twin) response for DMHS without RMU vs. reference.
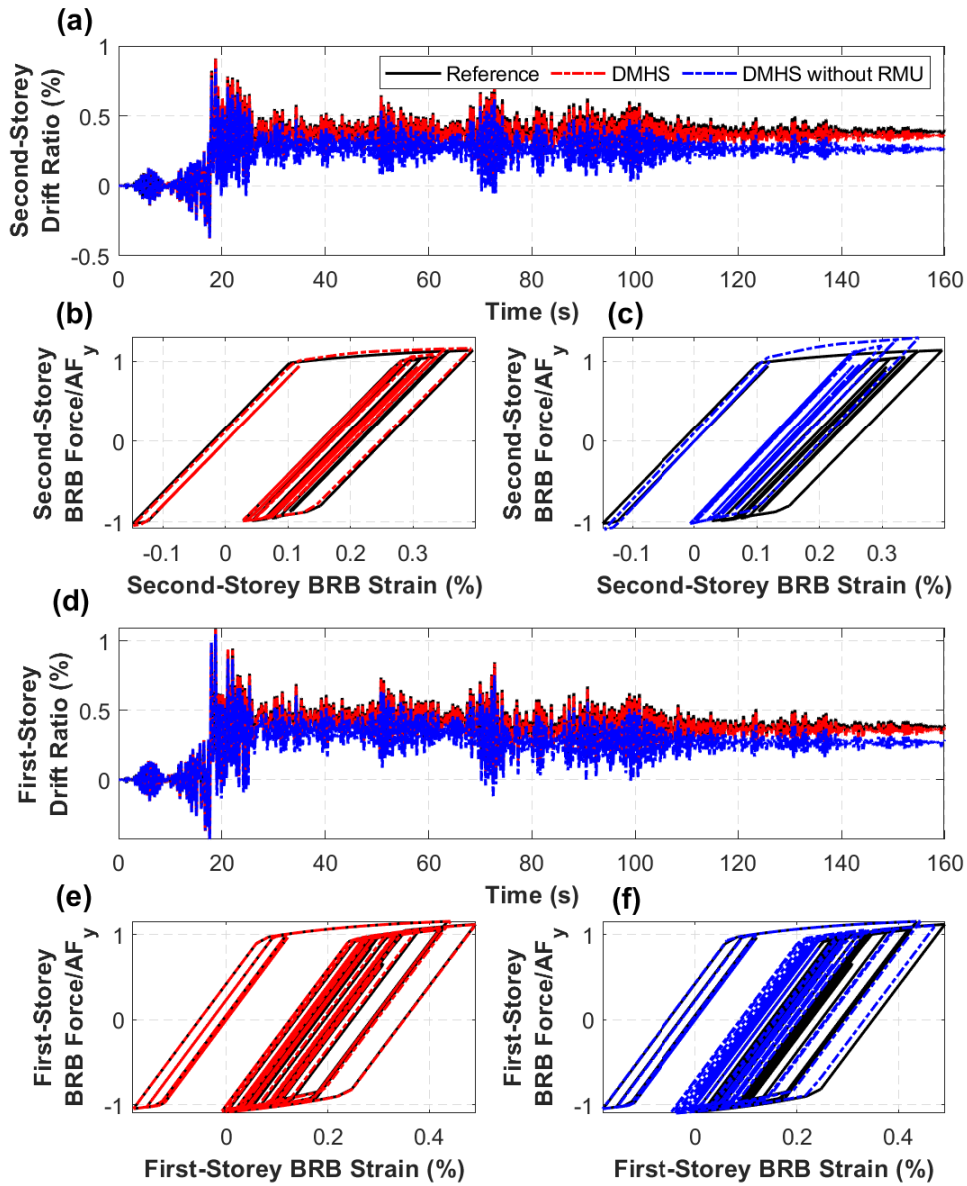
Figure 4.12: Virtual hybrid simulation of the BRBF using 2DLFM under the 2007 Pisco, Peru-UNICA earthquake, (a) history of drift ratio in Storey 2, (b) Storey 2 BRB (digital twin) response for DMHS vs. reference, (c) Storey 2 BRB (digital twin) response for DMHS without RMU vs. reference, (d) history of drift ratio in Storey 1, (e) Storey 1 BRB (virtual twin) response for DMHS vs. reference, (f) Storey 1 BRB (virtual twin) response for DMHS without RMU vs. reference.
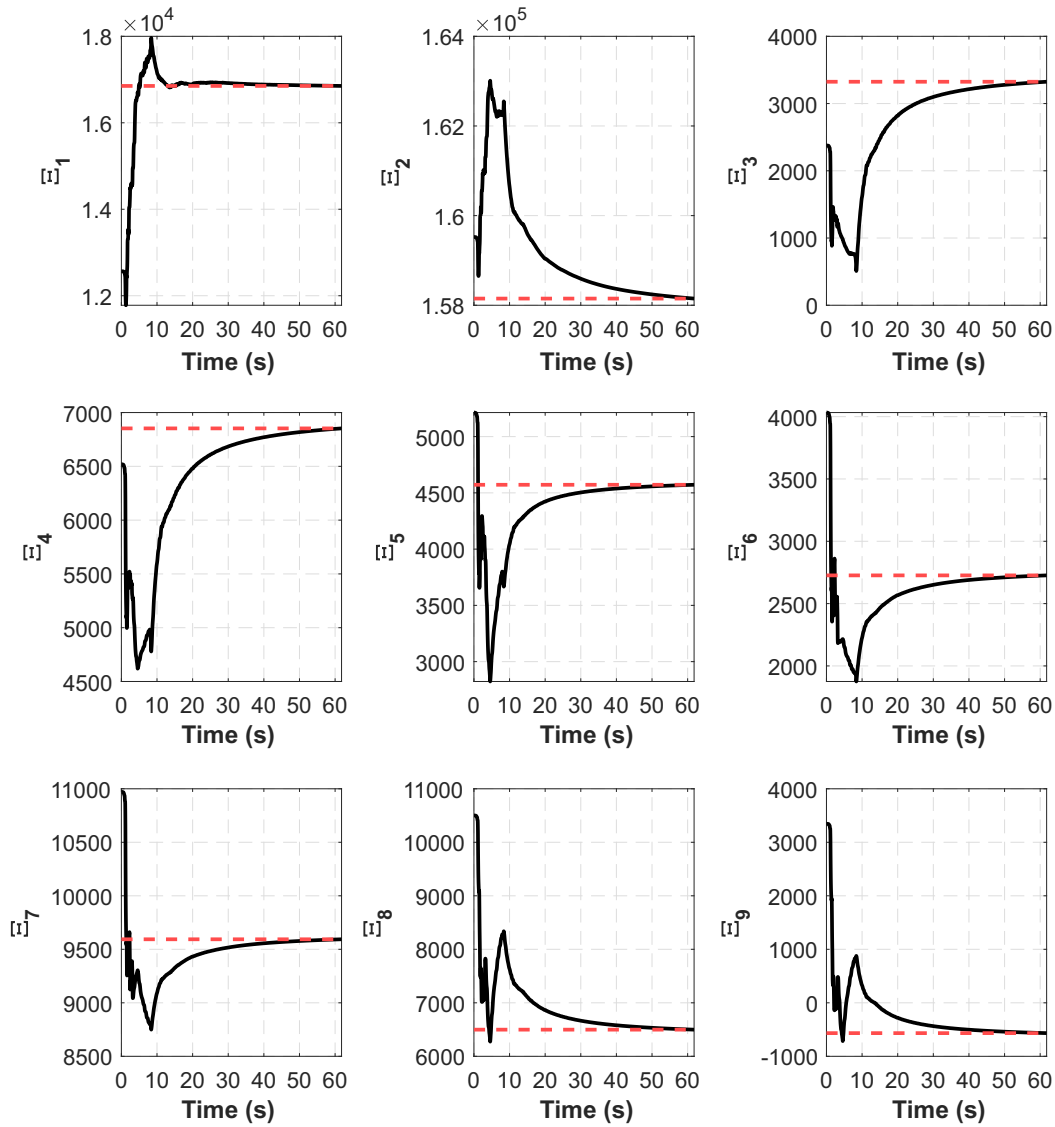
Figure 4.13: Convergence of the first 9 entries of Ξ matrix from DMHS under the 1971 San Fernando - Castaic-Old Ridge Route earthquake.

Otherwise, the LASSO algorithm would minimize the total error associated with all the data points in the hysteresis curve rather than taking into account the importance of peak reversal points in compression, which is critical in simulating frictional forces developed in BRBs under cyclic loading.

Storey drift ratios and BRB hysteretic responses obtained from VHS of the prototype BRBF of Fig. 4.6b under the 1778 Tabas, Iran-Dayhook earthquake (Fig. 4.9a) are shown in Figs. 4.15b-4.15d. A very good match was observed between the storey drifts of the reference model and the DMHS model in both storeys. Referring to the hysteresis curve of the digital twin in Fig. 4.15c, it can be observed that the restoring force response of the digital twin reached 1.03 and 1.20 times the BRB yielding resistance AF_y in tension and compression, respectively, which indicates the successful prediction of the asymmetric response using the improved PI model described in Section 4.4.2. The NRMSE of the first and second storey drift ratios were 1.52% and 2.82%, respectively. The results obtained from high-fidelity simulation confirm the accuracy of the DMHS framework in predicting the cyclic inelastic response of the critical element using the proposed digital twin, although a less-efficient (but more accurate) numerical model was used in initial training and as the virtual twin during VHS.
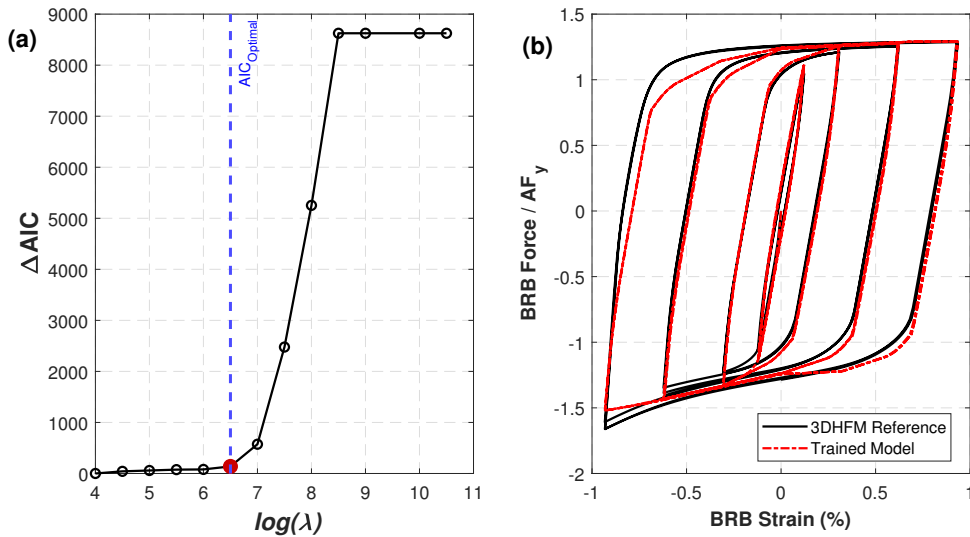
Figure 4.14: DMHS initial training using 3DHFM, (a) AIC plot, (b) comparison of the reference and trained BRB hysteretic responses
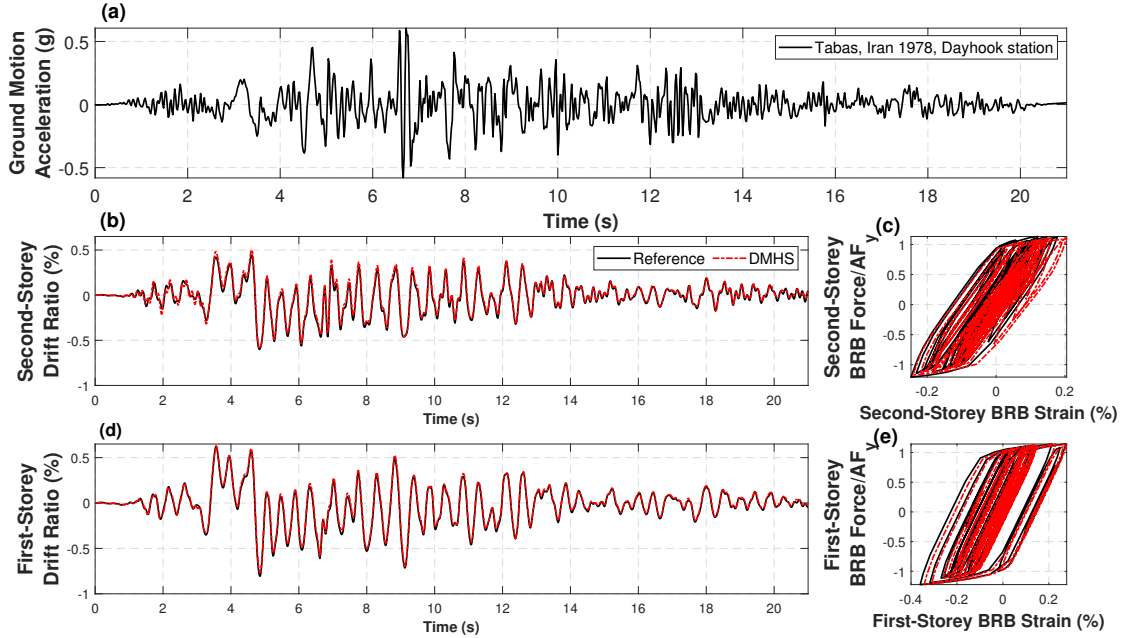
Figure 4.15: Virtual hybrid simulation of the BRBF using 3DHFM under the 1978 Tabas, Iran-Dayhook station earthquake, (a) ground motion acceleration history, (b) history of drift ratio in Storey 2, (c) BRB (digital twin) hysteretic response in Storey 2, (d) history of drift ratio in Storey 1, (e) BRB (virtual twin) hysteretic response in Storey 1.

4.4.5 Computational Cost

The simulations as part of the verification study were carried out on a computer system with 16 GB of RAM and a 2.60 GHz CPU without parallel execution. The computation time required to complete the analysis of the reference model with two 3DHFM virtual twins in ABAQUS was 18.73 hours, while DMHS having a virtual twin created using the 3DHFM in ABAQUS and a digital twin developed in MATLAB was completed in 9.43 hours, which is almost two times faster than the fully-numerical model. It should be mentioned that a major part of the required simulation time is associated with communication delays caused by the VHS platform. The difference in computation times would likely increase considerably had a frame with a larger number of stories been studied. Therefore the proposed DMHS framework represents a computationally-efficient method to perform optimization or structural response evaluations involving numerous dynamic analyses such as nonlinear response history analysis

and incremental dynamic analysis.

4.5   Conclusion

This chapter proposed a novel data-driven method for hybrid simulation of structural systems under earthquake loading. The proposed digital twin-based multi-element hybrid simulation (DMHS) framework was developed by incorporating the PI model as the hysteresis model, SINDy algorithm used for initial training, and RLS algorithm to recursively updating the digital twin, i.e., the digital replica of the physical specimen. The DMHS framework was demonstrated and verified using a series of virtual hybrid simulations performed on a prototype two-storey BRBF under earthquake ground motion accelerations. Two types of virtual twins, representing physical twin in this study, was considered in the simulations 1) 2D low-fidelity virtual twin and 2) 3D high-fidelity virtual twin. In the verification study, the first-storey BRB was modelled using the finite element method as virtual twin, while the response of the second-storey BRB was estimated by the digital twin developed here. The digital twin was initially trained using fictitious test data generated using a cyclic nonlinear static analysis performed numerically on the BRB isolated from the BRBF. RMU was used during the hybrid simulation to improve real-time hysteretic response prediction using the real-time incoming test data collected from the virtual twin. The accuracy and efficiency of the proposed framework were verified in comparison to the results obtained from the pure numerical (reference) model of the frame. The main findings of this study can be summarized as follows:

1. The DMHS framework can alleviate the uncertainties involved in the numerical simulation of the critical elements of structures in conventional hybrid simulation due to laboratory constraints. This method also offers a computationally-efficient and economical alternative to geographically-distributed hybrid simulation or multi-element hybrid simulation when more than one physical twin is essential to achieve the simula-

tion objectives.

2. The verification study confirmed that the DMHS framework is not sensitive to initial training data owing to the power of RMU to estimate with excellent accuracy the underlying relationship between the force and deformation of the digital twin using real-time data collected from the physical twin (specimen).

3. The implementation of the RMU phase is beneficial in the prediction of inelastic cyclic response of structural elements under random excitation such as earthquake loading in a sense that the hysteretic response of the digital twin, in particular in the nonlinear range of the material, is expected to be affected by the amplitude, frequency and duration of real-time dynamic loading, which can not be predicted with confidence before HS, suggesting the superiority of the DMHS framework over common structural simulation techniques based on the calibration of a phenomenological model to experimental test data of a specimen under a predefined loading protocol.

4. The recursive least-squares algorithm used in the recursive model updating showed a stable response as the weight parameters of the PI-SINDy model converged to a stable solution which confirms the robustness of the algorithm.

5. The proposed RMU phase helped the DMHS framework to efficiently refine the response of the digital twin with a small time delay making it potentially suitable for real-time hybrid simulation. The low computational cost of the RMU phase stems from the fact that a recursive algorithm instead of a full-history algorithm is used.

6. The improved digital twin by modifying the PI model proposed was proven to be effective in simulating the asymmetric hysteretic response of structural elements, e.g., BRB, experiencing dissimilar hardening behaviours under load reversal.

Although the proposed data-driven hybrid simulation technique was found to successfully estimate the hysteretic response of structural elements and can be used in the hybrid sim-

ulation of structural systems under earthquake loading, an examination of its limitations is critical. The PI model cannot simulate hysteretic responses with strength and stiffness degradation or hysteretic responses of components experiencing instability such as buckling. To overcome this limitation, the library matrix should be enhanced by the terms capable of learning such responses. Another limitation of the proposed method is that once a term is removed from the library matrix in the initial training phase, it can not be retrieved back during the RMU phase, even if it is deemed to enhance the prediction. This limitation can be mitigated by using the LASSO regression in a recursive format in the RMU phase, which is recommended to be examined in future relevant studies.

This chapter verified the DMHS framework and demonstrated its potential to overcome the limitations of CHS using numerical examples. Small-scale and large-scale experimental test programs are required to further verify the performance of the proposed technique in a real hybrid simulation.

Chapter 5

Conclusions, Recommendations, & Future Work

5.1 Summary

This M.Sc. thesis proposed two hybrid simulation frameworks for nonlinear dynamic analysis of structural systems under seismic loading. The first framework, called hybrid data-driven and physics-based simulation (HyDPS), combines data-driven modelling and conventional numerical simulation methods to achieve more efficiency and accuracy in seismic structural analysis. In this technique, the structure is divided into two substructures; the components expected to remain elastic are modelled using the numerical approach, while the critical components, which may experience yielding or instability, are modelled using the proposed data-driven approach trained by past experimental test data. The data-driven and numerical substructures are coupled by imposing the boundary conditions computed at each analysis time step from the numerical model on the data-driven model and feeding the restoring forces predicted by the data-driven model into the numerical model. HyDPS is particularly useful when sufficient experimental test data is available to train the data-driven model. The proposed HyDPS framework was demonstrated first and its performance was compared against two other data-driven models, namely LS-SVM and RNN proposed in the past studies to estimate the hysteretic response of dynamical systems, which verified the capability of HyDPS framework in simulating the dynamic response of structural systems under seismic

loading.

The second framework, called digital twin-based multi-element hybrid simulation (DMHS), is a variant of seismic hybrid simulation in which, the physical test specimen that represents one of the critical components of the structure (physical twin), the rest of the critical components (digital twins), and the well-understood components of the structure (numerical substructure) are coupled to study the nonlinear behaviour of lateral load-resisting systems under seismic loading. Each analysis time step includes three data exchange steps: 1) the equation of motion is numerically solved, and the calculated displacement are imposed on both physical and digital twins, 2) the displacement and restoring force obtained from the physical twin at each increment are sent to the digital twin for recursively updating the mathematical model incorporated in the digital twin, and 3) the forces predicted by digital twins and the forces measured by the physical twin are sent back to the numerical substructure to perform the numerical integration for the subsequent step. DMHS is proposed to address the biased results associated with the conventional hybrid simulation where there are multiple critical components in the structure, and only one or few of them are physically tested due to the laboratory constraints, and the response of the remaining critical components are reproduced numerically, which poses questions about the reliability of hybrid simulation results. The performance of the proposed hybrid simulation framework was demonstrated and verified using a two-storey BRBF in which the brace of the first storey was simulated using a detailed finite element model, replacing experimental testing in this study, and the brace of the second storey was modelled using the proposed data-driven model, while the rest of the frame, beams and columns, were simulated numerically in the OpenSees program.

5.2   Research Contributions & Conclusions

The academic contributions and conclusions of the data-driven model and frameworks developed in this study can be summarized individually in the following subsections.

5.2.1   PI-SINDy Data-driven Model

The key features of the PI-SINDy data-driven model implemented in both hybrid frameworks proposed here are summarized as follows:

1. The PI-SINDy data-driven model is developed for hysteretic response simulation, which consists of a physics-based hysteresis model, i.e., Prandtl-Ishlinskii (PI) model, integrated as the basis functions into a machine learning algorithm, i.e., sparse identification of nonlinear dynamics (SINDy) algorithm. The LASSO regression algorithm was used in SINDy to optimize the weights of the PI model. Akaike information criterion (AIC) was employed to identify the optimal value of the hyper-parameter (λ) in the LASSO regression.

2. The integration of the PI model into SINDy improved the capability of the algorithm in learning the underlying hysteretic response of the structural component experiencing significant material plasticity and hardening by leveraging limited training data - compared to previously proposed hysteresis prediction algorithms in the past.

3. The AIC incorporated in the PI-SINDy model reduced the likelihood of over-fitting to the training data, offering an excellent trade-off between model complexity and accuracy.

4. The basis functions, i.e., stop operators, which contribute less to the relationship between force and displacement, are removed in PI-SINDy using the LASSO regression, which confirms the robustness of the model in the presence of the experimental noise. This feature makes PI-SINDy superior to similar machine learning techniques used in the past to predict hysteretic response of dynamical systems, including LS-SVM or RNN.

5. The architecture of the PI-SINDy model, i.e., the number of active columns in the library matrix, is determined automatically by SINDy, which makes it suitable for

practical applications. This may not be the case in other algorithms used to reproduce hysteretic response of dynamical systems, for instance, neural networks lack a fixed architecture, and the number of hidden layers and neurons in each layer should be optimized by trial-and-error, which reduces their computational efficiency.

6. The PI-SINDy model is not prone to error accumulation because it is designed to act independently of feedback from past outputs.

7. The PI-SINDy model can efficiently be generalized from training data to testing data.

8. The improved PI model by adding two springs, tension-only and compression-only, to the PI model was proposed to simulate the asymmetric hysteretic response of structural elements, exhibiting different hardening response under reversal loading. The verification study showed the improved model could well predict asymmetric hysteretic response expected in structural components under load reversals such as BRBs experiencing dissimilar hardening behaviours in tension and compression.

5.2.2 HyDPS Framework

The key features of the proposed HyDPS Framework are summarized as follows:

1. The proposed PI-SINDy algorithm developed using PI hysteresis model and SINDy algorithm was implemented in the HyDPS framework to simulate the hysteretic response of structural components under seismic loading such as BRBs in a BRBF.

2. The physics of the problem, including equation of motion and compatibility equations, are satisfied in the physics-based numerical model acting as part of the HyDPS framework.

3. The PI-SINDy, RNN, and LS-SVM data-driven models were independently implemented in HyDPS to predict the response of the critical component of the structure

and coupled with the numerical substructure to perform dynamic analysis under seismic loading.

4. The HyDPS framework reduces the number of modelling assumptions associated with the material and finite element method needed for numerical simulation of the structure.

5. One of the concerns associated with fully data-driven methods, which is addressed by the HyDPS framework, is the need for a comprehensive dataset for the entire components of the structure. The reason being that the HyDPS framework efficiently uses the data to develop the data-driven model only for the critical component and relies on numerical simulation for the well-understood components of the structure.

6. Numerical convergence is easily achieved in the dynamic analysis because an explicit input-output surrogate model is created for the critical component, which significantly reduces the number of nonlinear equations solved by the numerical solution scheme.

7. The full response of the structure at all DOFs can be retrieved using the HyDPS technique as opposed to fully data-driven models where the structural responses can only be predicted for the DOFs for which the training data was previously collected.

8. The PI-SINDy data-driven model trained using the experimental data of a specific critical component, e.g., BRB in a BRBF, can be used to predict the response of various frame architectures, e.g., multi-storey BRBFs. Thus, offering a great deal of flexibility to the user to investigate multiple aspects of the structural system by changing the geometry of the frame.

9. The computational efforts of the HyDPS technique are appreciably less compared to pure numerical models, commonly used for the response assessment of structural systems, because of using a black-box input-output mapping function for the critical element instead of phenomenological or detailed FE models. This becomes more beneficial

when multiple nonlinear components are used in various locations of the structure, making HyDPS favourable for structural response assessments involving numerous analyses such as incremental dynamic analysis (IDA) or structural optimization.

10. Other data-driven models, such as those developed in the past studies can be integrated in the HyDPS framework to perform seismic structural analysis.

5.2.3 DMHS Framework

The key features of the proposed DMHS technique are summarized as follows:

1. The proposed DMHS is a novel data-driven method for hybrid simulation of structural systems under earthquake loading, which is developed by incorporating the PI model as the hysteresis model, SINDy algorithm used for initial training, and recursive least-squares (RLS) algorithm to recursively update the digital twin, i.e., the digital replica of the physical specimen.

2. The DMHS framework can efficiently alleviate the uncertainties involved in conventional hybrid simulation associated with the numerical simulation of the critical elements of structures due to laboratory constraints. This method also offers a computationally-efficient and economical alternative to geographically distributed hybrid simulation when more than one physical twin, i.e., experimental specimen, is needed.

3. The RMU or real-time training implemented in DMHS improves the prediction of the hysteretic response of the digital twin, in particular in the nonlinear range of the material, because the amplitude, frequency and duration of real-time dynamic loading, e.g., earthquake accelerations, are explicitly accounted for in the simulation of the digital twin during hybrid simulation. This confirms the benefit of the DMHS framework over the conventional hybrid simulation technique where the numerically-modelled critical components are often calibrated against experimental test data of similar prototype

specimens under a predefined loading protocol, which lacks taking into consideration the influence of dynamic loading characteristics during hybrid simulation.

4. The hysteresis prediction capability of the DMHS framework is not sensitive to initial training data owing to the power of the RMU phase that approximates with an excellent accuracy the underlying relationship between the force and deformation of the digital twin using real-time data produced by the physical twin.

5. The RLS algorithm used in the recursive model updating showed a stable response as the weight parameters of the PI-SINDy model converged to a stable solution which confirms the robustness of the algorithm.

6. As a hypothesis that needs to be explored in future research, the proposed RMU may be suitable for real-time hybrid simulation of structural systems given its computational efficiency. The low computational cost of the proposed RMU stems from the fact that a recursive algorithm is used instead of a full-history algorithm, and a vectorized mathematical model for hysteresis simulation is proposed using the PI model where all unknown parameters are isolated in the weight matrix. The initial training phase also helps speed up the RMU phase by eliminating unnecessary terms from the PI-SINDy library matrix..

5.3 Limitations & Future Work

1. Although the proposed PI-SINDy model used in both frameworks successfully estimated the hysteretic response of structural elements experiencing material plasticity, it cannot simulate hysteretic shapes associated with strength and stiffness degradation (Fig. 5.1a), pinching (Fig. 5.1b), instability (Fig. 5.1c) or combination of these responses. To solve this limitation, the library matrix should be enhanced by the terms having the ability to learn such responses. One possible solution would be taking advantage of deteriorating stop operator [132], as shown in Fig. 5.2, instead of

the stop operator used in this study. The challenge associated with implementing deteriorating stop operator in the library matrix is the increase in computational cost, which can potentially be solved by using a dimensionality reduction method, such as principle component analysis (PCA) [200] or discrete empirical interpolation method (DEIM) [201], to reduce the dimensionality of the library matrix before performing the optimization.

Training during the RMU phase of the DMHS framework for critical components that are susceptible to instability, pinching or strength degradation such as concentrically braced frame (CBF) braces, may involve a longer process, because such responses are sudden and more complex.
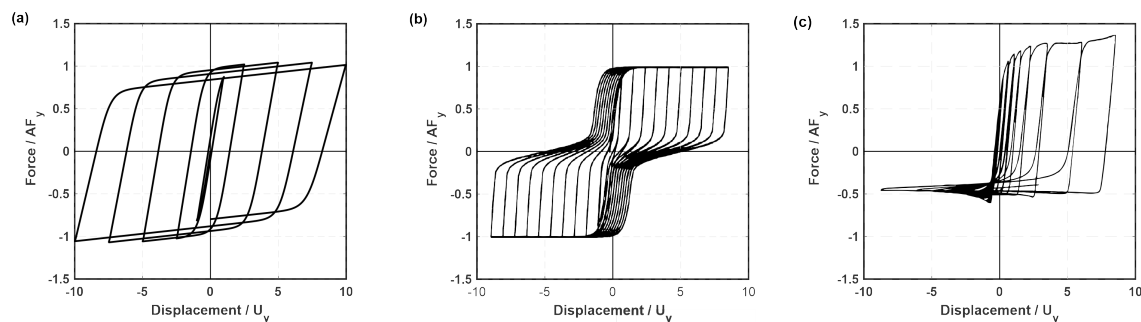

Figure 5.1: Hysteresis behaviours involving, (a) strength degradation, (b) pinching [202], (c) instability [203]

2. The proposed frameworks were only tested using single-degree-of-freedom systems, single-storey and two-storey BRBFs. Further investigations are needed to verify the effectiveness of the proposed frameworks in multi-storey structures consisting of other seismic force-resisting systems.

3. This study verified the capability of the DMHS framework and demonstrated its potential to overcome the limitations of conventional hybrid simulation using numerical examples. The proposed framework should be verified using small-scale and large-scale experimental test programs.
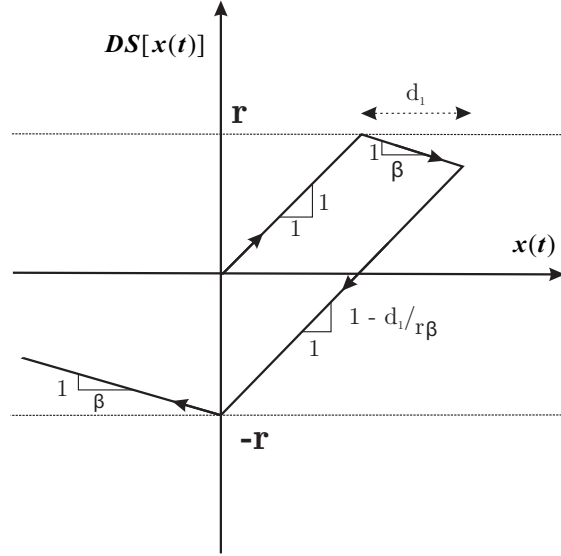
Figure 5.2: Deteriorating stop operator [132]

4. The use of physics-informed machine learning approach [88] could improve the data-efficiency and prediction accuracy of the frameworks. In this approach, an additional term consisting of the physics of the problem (e.g., EOM or force-deformation response of the member obtained from plastic analysis) is added to the cost function of the machine learning algorithm, which is optimized so that not only the error between the training data and the predicted values is minimized but also the physical constraints associated with the problem are taken into account in the optimization.

5. Different data-driven models can be trained using available experimental datasets to estimate the hysteretic response of common seismic fuses, including BRBs, CBF braces, eccentrically braced frame (EBF) link beams, and moment-resisting frame (MRF) beams. These off-the-shelf data-driven models can be implemented in common structural analysis programs as a separate library of elements compared to conventional physics-based elements, e.g., beam elements or concentrated plasticity-based spring elements.

Bibliography

[1] I. Holand, "Sleipner a gbs loss. report 17. main report," 1997.

[2] M. Collins, F. J. Vecchio, R. G. Selby, and P. R. Gupta, "The failure of an offshore platform," *CONCRETE INTERNATIONAL-DETROIT-*, vol. 19, pp. 28–36, 1997.

[3] P. Mellor, "Computer-aided disaster," *Environmental engineering*, vol. 9, pp. 16–30, 1996.

[4] M. Nakashima, "Hybrid simulation: An early history," *Earthquake Engineering & Structural Dynamics*, 2020.

[5] R. W. Clough, "The finite element method in plane stress analysis," in *Proceedings of 2nd ASCE Conference on Electronic Computation, Pittsburgh Pa., Sept. 8 and 9, 1960*, 1960.

[6] S. S. Rao, *The finite element method in engineering.* Butterworth-heinemann, 2017.

[7] R. Geske and K. Shastri, "Valuation by approximation: A comparison of alternative option valuation techniques," *Journal of Financial and Quantitative Analysis*, vol. 20, no. 1, pp. 45–71, 1985.

[8] D. McCrum and M. Williams, "An overview of seismic hybrid testing of engineering structures," *Engineering Structures*, vol. 118, pp. 240–261, 2016.

[9] K Takanashi, K Udagawa, M Seki, T Okada, and H Tanaka, "Nonlinear earthquake response analysis of structures by a computer-actuator on-line system (details of the system).," *Trans. of the Architectural Institute of Japan*, vol. 229, pp. 77–83,190, 1975.

[10] M. Hakuno, M. Shidawara, and T. Hara, "Dynamic destructive test of a cantilever beam, controlled by an analog-computer," *Proceedings of the Japan Society of Civil Engineers*, vol. 1969, no. 171, pp. 1–9, 1969.

[11] M Nakashima, T Kaminoso, M Ishida, and K Ando, "Integration techniques for substructuring pseudodynamic test," in *fourth US National Conference on Earthquake Engineering*, vol. 2.

[12] S. A. Mahin, P.-S. B. Shing, C. R. Thewalt, and R. D. Hanson, "Pseudodynamic test method—current status and future directions," *Journal of Structural Engineering*, vol. 115, no. 8, pp. 2113–2128, 1989.

[13] M. Nakashima and N. Masaoka, "Real-time on-line test for mdof systems," *Earthquake engineering & structural dynamics*, vol. 28, no. 4, pp. 393–420, 1999.

[14] P Pegon and A. Pinto, "Pseudo-dynamic testing with substructuring at the elsa laboratory," *Earthquake engineering & structural dynamics*, vol. 29, no. 7, pp. 905–925, 2000.

[15] T. Horiuchi and T. Konno, "A new method for compensating actuator delay in real–time hybrid experiments," *Philosophical Transactions of the Royal Society of London. Series A: Mathematical, Physical and Engineering Sciences*, vol. 359, no. 1786, pp. 1893–1909, 2001.

[16] M Ahmadizadeh, G Mosqueda, and A. Reinhorn, "Compensation of actuator delay and dynamics for real-time hybrid structural simulation," *Earthquake Engineering & Structural Dynamics*, vol. 37, no. 1, pp. 21–42, 2008.

[17] A. Bonelli and O. S. Bursi, "Predictor-corrector procedures for pseudo-dynamic tests," *Engineering computations*, 2005.

[18] C. K. Shield, C. W. French, and J. Timm, "Development and implementation of the effective force testing method for seismic simulation of large–scale structures," *Philosophical Transactions of the Royal Society of London. Series A: Mathematical, Physical and Engineering Sciences*, vol. 359, no. 1786, pp. 1911–1929, 2001.

[19] S Campbell, "A system for simultaneous pseudodynamic testing of multiple substructures," in *Proc. of 6th US National Conference on Earthquake Engineering, 1998*, 1998.

[20] P. B. Shing, O. S. Bursi, and M. T. Vannan, "Pseudodynamic tests of a concentrically braced frame using substructuring techniques," *Journal of Constructional Steel Research*, vol. 29, no. 1-3, pp. 121–148, 1994.

[21] M. R. Eatherton and J. F. Hajjar, "Hybrid simulation testing of a self-centering rocking steel braced frame system," *Earthquake engineering & structural dynamics*, vol. 43, no. 11, pp. 1725–1742, 2014.

[22] V Kammula, J Erochko, O Kwon, and C Christopoulos, "Performance assessment of the self centering energy dissipative (sced) bracing system using hybrid simulation," in *Proceedings of the 15th world conference on earthquake engineering, Lisbon*, 2012.

[23] M. Obata and Y. Goto, "Development of multidirectional structural testing system applicable to pseudodynamic test," *Journal of Structural Engineering*, vol. 133, no. 5, pp. 638–645, 2007.

[24] J. Dang and T. Aoki, "Bidirectional loading hybrid tests of square cross-sections of steel bridge piers," *Earthquake engineering & structural dynamics*, vol. 42, no. 8, pp. 1111–1130, 2013.

[25] M. Del Carpio Ramos, G. Mosqueda, and M. J. Hashemi, "Large-scale hybrid simulation of a steel moment frame building structure through collapse," *Journal of Structural Engineering*, vol. 142, no. 1, p. 04 015 086, 2016.

[26] M. J. Hashemi, Y. Al-Ogaidi, R. Al-Mahaidi, R. Kalfat, H.-H. Tsang, and J. L. Wilson, "Application of hybrid simulation for collapse assessment of post-earthquake cfrp-repaired rc columns," *Journal of Structural Engineering*, vol. 143, no. 1, p. 04 016 149, 2017.

[27] H. Fatemi, P. Paultre, and C.-P. Lamarche, "Experimental evaluation of inelastic higher-mode effects on the seismic behavior of rc structural walls," *Journal of Structural Engineering*, vol. 146, no. 4, p. 04 020 016, 2020.

[28] A. Imanpour *et al.*, "Development and application of multi-axis hybrid simulation for seismic stability of steel braced frames," *Engineering Structures*, vol. 252, p. 113 646, 2022.

[29] P.-S. B. Shing and S. A. Mahin, "Cumulative experimental errors in pseudodynamic tests," *Earthquake engineering & structural dynamics*, vol. 15, no. 4, pp. 409–424, 1987.

[30] R. Peek and W.-H. Yi, "Error analysis for pseudodynamic test method. i: Analysis," *Journal of engineering mechanics*, vol. 116, no. 7, pp. 1618–1637, 1990.

[31] M. Ahmadizadeh and G. Mosqueda, "Online energy-based error indicator for the assessment of numerical and experimental errors in a hybrid simulation," *Engineering Structures*, vol. 31, no. 9, pp. 1987–1996, 2009.

[32] M. D. Spiridonakos and E. N. Chatzi, "Metamodeling of dynamic nonlinear structural systems through polynomial chaos narx models," *Computers & Structures*, vol. 157, pp. 99–113, 2015.

[33] Z. Lai and S. Nagarajaiah, "Sparse structural system identification method for nonlinear dynamic systems with hysteresis/inelastic behavior," *Mechanical Systems and Signal Processing*, vol. 117, pp. 813–842, 2019.

[34] T. Kim, O.-S. Kwon, and J. Song, "Response prediction of nonlinear hysteretic systems by deep neural networks," *Neural Networks*, vol. 111, pp. 1–10, 2019.

[35] R. Zhang, Z. Chen, S. Chen, J. Zheng, O. Büyüköztürk, and H. Sun, "Deep long short-term memory networks for nonlinear structural seismic response prediction," *Computers & Structures*, vol. 220, pp. 55–68, 2019.

[36] R. Zhang, Y. Liu, and H. Sun, "Physics-informed multi-lstm networks for metamodeling of nonlinear structures," *Computer Methods in Applied Mechanics and Engineering*, vol. 369, p. 113 226, 2020.

[37] R. Zhang, Y. Liu, and H. Sun, "Physics-guided convolutional neural network (phycnn) for data-driven seismic response modeling," *Engineering Structures*, vol. 215, p. 110 704, 2020.

[38] M. Brokate and J. Sprekels, *Hysteresis and phase transitions*. Springer Science & Business Media, 1996, vol. 121.

[39] S. L. Brunton, J. L. Proctor, and J. N. Kutz, "Discovering governing equations from data by sparse identification of nonlinear dynamical systems," *Proceedings of the national academy of sciences*, vol. 113, no. 15, pp. 3932–3937, 2016.

[40] J. A. Ewing, "X. experimental researches in magnetism," *Philosophical Transactions of the Royal Society of London*, no. 176, pp. 523–640, 1885.

[41] M. L. Grimmer, "Analysis of hysteretic systems: Preisach formalism and bouc-wen modeling," Ph.D. dissertation, Rice University, 2017.

[42] R. S. Thyagarajan, *Modeling and analysis of hysteretic structural behavior*. California Institute of Technology, 1990.

[43] Z. P. Bažant and S. Zebich, "Statistical linear regression analysis of prediction models for creep and shrinkage," *Cement and Concrete Research*, vol. 13, no. 6, pp. 869–876, 1983.

[44] D. Hobbs, "The compressive strength of concrete: A statistical approach to failure," *Magazine of Concrete Research*, vol. 24, no. 80, pp. 127–138, 1972.

[45] A Carpinteri, G Ferro, and S Invernizzi, "A truncated statistical model for analyzing the size-effect on tensile strength of concrete structures," *Fracture Mechanics of Concrete Structures (Proc. FRAMCOS-2), AEDIFICATIO Publishers, Freiburg, Germany*, pp. 557–570, 1995.

[46] M Farrokh, F. Dizaji, and M. Dizaji, "Hysteresis identification using extended preisach neural network," *Neural Processing Letters*, pp. 1–25, 2022.

[47] W. Ramberg and W. R. Osgood, "Description of stress-strain curves by three parameters," Tech. Rep., 1943.

[48] P. C. Jennings, "Periodic response of a general yielding structure," *Journal of the Engineering Mechanics Division*, vol. 90, no. 2, pp. 131–166, 1964.

[49] A Giuffrè, "Il comportamento del cemento armato per sollecitazioni cicliche di forte intensità," *Giornale del Genio Civile*, 1970.

[50] R Bouc, "Forced vibrations of mechanical systems with hysteresis," in *Proc. of the Fourth Conference on Nonlinear Oscillations, Prague, 1967*, 1967.

[51] Z. Zhang, X. Tian, and X. Ge, "Dynamic characteristics of the bouc–wen nonlinear isolation system," *Applied Sciences*, vol. 11, no. 13, p. 6106, 2021.

[52] Á. Zsarnóczay and L. G. Vigh, "Steel4–a versatile uniaxial material model for cyclic nonlinear analysis of steel-based elements," *OpenSees Days Portugal 2014-Abstracts*, vol. 11, 2014.

[53] A. Zsarnoczay, "Experimental and numerical investigation of buckling restrained braced frames for eurocode conform design procedure development," 2013.

[54] M. Menegotto, "Method of analysis for cyclically loaded rc plane frames including changes in geometry and non-elastic behavior of elements under combined normal force and bending," in *Proc. of IABSE symposium on resistance and ultimate deformability of structures acted on by well defined repeated loads*, 1973, pp. 15–22.

[55] R Carreño, K. Lotfizadeh, J. Conte, and J. Restrepo, "Material model parameters for the giuffrè-menegotto-pinto uniaxial steel stress-strain model," *Journal of Structural Engineering*, vol. 146, no. 2, p. 04 019 205, 2020.

[56] J. E. Goldberg and R. M. Richard, "Analysis of nonlinear structures," *Journal of the Structural Division*, vol. 89, no. 4, pp. 333–351, 1963.

[57] J Bauschinger, "On the change of the elastic limit and the strength of iron and steel, by drawing out, by heating and cooling, and by repetition of loading (summary)," *Minutes of Proceedings of the Institution of Civil Engineers with Other Selected and Abstracted Papers*, vol. 87, p. 463, 1886.

[58] F. C. Filippou, E. P. Popov, and V. V. Bertero, "Effects of bond deterioration on hysteretic behavior of reinforced concrete joints," 1983.

[59] N. Mitra and L. N. Lowes, "Evaluation, calibration, and verification of a reinforced concrete beam–column joint model," *Journal of Structural Engineering*, vol. 133, no. 1, pp. 105–120, 2007.

[60] C. B. Haselton *et al.*, "An assessment to benchmark the seismic performance of a code-conforming reinforced-concrete moment-frame building," *Pacific Earthquake Engineering Research Center*, no. 2007/1, 2008.

[61] Y. Lu and M. Panagiotou, "Three-dimensional cyclic beam-truss model for nonplanar reinforced concrete walls," *Journal of Structural Engineering*, vol. 140, no. 3, p. 04 013 071, 2014.

[62] Y.-K. Wen, "Method for random vibration of hysteretic systems," *Journal of the engineering mechanics division*, vol. 102, no. 2, pp. 249–263, 1976.

[63] F. Ikhouane, J. E. Hurtado, and J. Rodellar, "Variation of the hysteresis loop with the bouc–wen model parameters," *Nonlinear Dynamics*, vol. 48, no. 4, pp. 361–380, 2007.

[64] M Giuclea, T Sireteanu, and A. Mitu, "Use of genetic algorithms for fitting the bouc-wen model to experimental hysteretic curves," *Rev. Roum. Sci. Techn.–Mec. Appl*, vol. 54, no. 1, pp. 3–10, 2009.

[65] M. Ismail, F. Ikhouane, and J. Rodellar, "The hysteresis bouc-wen model, a survey," *Archives of computational methods in engineering*, vol. 16, no. 2, pp. 161–188, 2009.

[66] T. T. Baber and M. N. Noori, "Random vibration of degrading, pinching systems," *Journal of Engineering Mechanics*, vol. 111, no. 8, pp. 1010–1026, 1985.

[67] F. Preisach, "Über die magnetische nachwirkung," *Zeitschrift für physik*, vol. 94, no. 5, pp. 277–302, 1935.

[68] G. Song, J. Zhao, X. Zhou, and J. A. De Abreu-García, "Tracking control of a piezoceramic actuator with hysteresis compensation using inverse preisach model," *IEEE/ASME transactions on mechatronics*, vol. 10, no. 2, pp. 198–209, 2005.

[69] Z. Li and J. Shan, "Inverse compensation based synchronization control of the piezo-actuated fabry–perot spectrometer," *IEEE Transactions on Industrial Electronics*, vol. 64, no. 11, pp. 8588–8597, 2017.

[70] P. Krejci and K. Kuhnen, "Inverse control of systems with hysteresis and creep," *IEE Proceedings-Control Theory and Applications*, vol. 148, no. 3, pp. 185–192, 2001.

[71] H. T. Banks and A. Kurdila, "Hysteretic control influence operators representing smart material actuators: Identification and approximation," in *Proceedings of 35th IEEE Conference on Decision and Control*, IEEE, vol. 4, 1996, pp. 3711–3716.

[72] M. Zhou, S. He, B. Hu, and Q. Zhang, "Modified kp model for hysteresis of magnetic shape memory alloy actuator," *IETE Technical Review*, vol. 32, no. 1, pp. 29–36, 2015.

[73] P. P. Shinde and S. Shah, "A review of machine learning and deep learning applications," in *2018 Fourth international conference on computing communication control and automation (ICCUBEA)*, IEEE, 2018, pp. 1–6.

[74] T. Hastie, R. Tibshirani, J. H. Friedman, and J. H. Friedman, *The elements of statistical learning: data mining, inference, and prediction*. Springer, 2009, vol. 2.

[75] X. Zhu and A. B. Goldberg, "Introduction to semi-supervised learning," *Synthesis lectures on artificial intelligence and machine learning*, vol. 3, no. 1, pp. 1–130, 2009.

[76] R. S. Sutton and A. G. Barto, *Reinforcement learning: An introduction*. MIT press, 2018.

[77] H. Adeli and C Yeh, "Perceptron learning in engineering design," *Computer-Aided Civil and Infrastructure Engineering*, vol. 4, no. 4, pp. 247–256, 1989.

[78] P Hajela and L Berke, "Neurobiological computational models in structural analysis and design," *Computers & Structures*, vol. 41, no. 4, pp. 657–667, 1991.

[79] J Ghaboussi, J. Garrett Jr, and X. Wu, "Knowledge-based modeling of material behavior with neural networks," *Journal of engineering mechanics*, vol. 117, no. 1, pp. 132–153, 1991.

[80] H.-T. Kang and C. J. Yoon, "Neural network approaches to aid simple truss design problems," *Computer-Aided Civil and Infrastructure Engineering*, vol. 9, no. 3, pp. 211–218, 1994.

[81] R. Vanluchene and R. Sun, "Neural networks in structural engineering," *Computer-Aided Civil and Infrastructure Engineering*, vol. 5, no. 3, pp. 207–215, 1990.

[82] H. Sun, H. V. Burton, and H. Huang, "Machine learning applications for building structural design and performance assessment: State-of-the-art review," *Journal of Building Engineering*, vol. 33, p. 101 816, 2021.

[83] T. Kim, J. Song, and O.-S. Kwon, "Probabilistic evaluation of seismic responses using deep learning method," *Structural Safety*, vol. 84, p. 101 913, 2020.

[84] C. C. Mitropoulou and M. Papadrakakis, "Developing fragility curves based on neural network ida predictions," *Engineering Structures*, vol. 33, no. 12, pp. 3409–3421, 2011.

[85] J. Seo, L. Dueñas-Osorio, J. I. Craig, and B. J. Goodno, "Metamodel-based regional vulnerability estimate of irregular steel moment-frame structures subjected to earthquake events," *Engineering Structures*, vol. 45, pp. 585–597, 2012.

[86] P. Towashiraporn, *Building seismic fragilities using response surface metamodels*. Georgia Institute of Technology, 2004.

[87] J. Seo and D. G. Linzell, "Use of response surface metamodels to generate system level fragilities for existing curved steel bridges," *Engineering Structures*, vol. 52, pp. 642–653, 2013.

[88] G. E. Karniadakis, I. G. Kevrekidis, L. Lu, P. Perdikaris, S. Wang, and L. Yang, "Physics-informed machine learning," *Nature Reviews Physics*, vol. 3, no. 6, pp. 422–440, 2021.

[89] E. Khojastehfar, S. B. Beheshti-Aval, M. R. Zolfaghari, and K. Nasrollahzade, "Collapse fragility curve development using monte carlo simulation and artificial neural network," *Proceedings of the Institution of Mechanical Engineers, Part O: Journal of Risk and Reliability*, vol. 228, no. 3, pp. 301–312, 2014.

[90] F. K. G. Jough and S. Şensoy, "Prediction of seismic collapse risk of steel moment frame mid-rise structures by meta-heuristic algorithms," *Earthquake Engineering and Engineering Vibration*, vol. 15, no. 4, pp. 743–757, 2016.

[91] H. V. Burton, S. Sreekumar, M. Sharma, and H. Sun, "Estimating aftershock collapse vulnerability using mainshock intensity, structural response and physical damage indicators," *Structural Safety*, vol. 68, pp. 85–96, 2017.

[92] Y. Zhang, H. V. Burton, H. Sun, and M. Shokrabadi, "A machine learning framework for assessing post-earthquake structural safety," *Structural safety*, vol. 72, pp. 1–16, 2018.

[93] S. Ghosh, A. Roy, and S. Chakraborty, "Support vector regression based metamodeling for seismic reliability analysis of structures," *Applied Mathematical Modelling*, vol. 64, pp. 584–602, 2018.

[94] J. Kiani, C. Camp, and S. Pezeshk, "On the application of machine learning techniques to derive seismic fragility curves," *Computers & Structures*, vol. 218, pp. 108–122, 2019.

[95] Z. Jing, J. Chen, and X. Li, "Rbf-ga: An adaptive radial basis function metamodeling with genetic algorithm for structural reliability analysis," *Reliability Engineering & System Safety*, vol. 189, pp. 42–57, 2019.

[96] I. Gidaris, A. A. Taflanidis, and G. P. Mavroeidis, "Kriging metamodeling in seismic risk assessment based on stochastic ground motion models," *Earthquake Engineering & Structural Dynamics*, vol. 44, no. 14, pp. 2377–2399, 2015.

[97] Y. Zhang and H. V. Burton, "Pattern recognition approach to assess the residual structural capacity of damaged tall buildings," *Structural safety*, vol. 78, pp. 12–22, 2019.

[98]   J. A. Anderson, *An introduction to neural networks.* MIT press, 1995.

[99]   G. J. Yun, J. Ghaboussi, and A. S. Elnashai, "A new neural network-based model for hysteretic behavior of materials," *International Journal for Numerical Methods in Engineering*, vol. 73, no. 4, pp. 447–469, 2008.

[100] A. Joghataie and M. S. Dizaji, "Nonlinear analysis of concrete gravity dams by neural networks," in *Proceedings of the World Congress on Engineering*, Citeseer, vol. 2, 2009, pp. 1022–7.

[101] A. Joghataie and M. S. Dizaji, "Designing high-precision fast nonlinear dam neuro-modelers and comparison with finite-element analysis," *Journal of Engineering Mechanics*, vol. 139, no. 10, pp. 1311–1324, 2013.

[102] H. Luo and S. G. Paal, "A locally weighted machine learning model for generalized prediction of drift capacity in seismic vulnerability assessments," *Computer-Aided Civil and Infrastructure Engineering*, vol. 34, no. 11, pp. 935–950, 2019.

[103] N.-D. Hoang, "Estimating punching shear capacity of steel fibre reinforced concrete slabs using sequential piecewise multiple linear regression and artificial neural network," *Measurement*, vol. 137, pp. 58–70, 2019.

[104] J.-S. Jeon, A. Shafieezadeh, and R. DesRoches, "Statistical models for shear strength of rc beam-column joints using machine-learning techniques," *Earthquake engineering & structural dynamics*, vol. 43, no. 14, pp. 2075–2095, 2014.

[105] H. Luo and S. G. Paal, "Machine learning-based backbone curve model of reinforced concrete columns subjected to cyclic loading reversals," *Journal of Computing in Civil Engineering*, vol. 32, no. 5, p. 04 018 042, 2018.

[106] E. E. Bas and M. A. Moustafa, "Real-time hybrid simulation with deep learning computational substructures: System validation using linear specimens," *Machine Learning and Knowledge Extraction*, vol. 2, no. 4, pp. 469–489, 2020.

[107] E. E. Bas, M. A. Moustafa, D. Feil-Seifer, and J. Blankenburg, "Using a machine learning approach for computational substructure in real-time hybrid simulation," in *Dynamic Substructures, Volume 4*, Springer, 2021, pp. 163–172.

[108] Y.-S. Yang, K.-C. Tsai, A. S. Elnashai, and T.-J. Hsieh, "An online optimization method for bridge dynamic hybrid simulations," *Simulation Modelling Practice and Theory*, vol. 28, pp. 42–54, 2012.

[109] H. H. Elanwar and A. S. Elnashai, "Framework for online model updating in earthquake hybrid simulations," *Journal of Earthquake Engineering*, vol. 20, no. 1, pp. 80–100, 2016.

[110] O.-S. Kwon and V. Kammula, "Model updating method for substructure pseudo-dynamic hybrid simulation," *Earthquake engineering & structural dynamics*, vol. 42, no. 13, pp. 1971–1984, 2013.

[111] T Wang and B Wu, "Real-time hybrid testing with constrained unscented kalman filter," in *5th International conference on advances in experimental structural engineering*, 2013.

[112] B. Wu and T. Wang, "Model updating with constrained unscented kalman filter for hybrid testing," *Smart Structures and Systems*, vol. 14, no. 6, pp. 1105–1129, 2014.

[113] X. Shao, A. Mueller, and B. A. Mohammed, "Real-time hybrid simulation with online model updating: Methodology and implementation," *Journal of Engineering Mechanics*, vol. 142, no. 2, p. 04 015 074, 2016.

[114] M. J. Hashemi, A. Masroor, and G. Mosqueda, "Implementation of online model updating in hybrid simulation," *Earthquake engineering & structural dynamics*, vol. 43, no. 3, pp. 395–412, 2014.

[115] M. Cheng and T. C. Becker, "Performance of unscented kalman filter for model updating with experimental data," *Earthquake Engineering & Structural Dynamics*, vol. 50, no. 7, pp. 1948–1966, 2021.

[116] G. Ou, S. J. Dyke, and A. Prakash, "Real time hybrid simulation with online model updating: An analysis of accuracy," *Mechanical Systems and Signal Processing*, vol. 84, pp. 223–240, 2017.

[117] O. C. Zienkiewicz, R. L. Taylor, P. Nithiarasu, and J. Zhu, *The finite element method*. McGraw-hill London, 1977, vol. 3.

[118] F. Taucer, E. Spacone, and F. C. Filippou, *A fiber beam-column element for seismic response analysis of reinforced concrete structures*. Earthquake Engineering Research Center, College of Engineering, University . . ., 1991, vol. 91.

[119] N. D. Lagaros, M. Papadrakakis, and G. Kokossalakis, "Structural optimization using evolutionary algorithms," *Computers & structures*, vol. 80, no. 7-8, pp. 571–589, 2002.

[120] P. Ienny, A.-S. Caro-Bretelle, and E. Pagnacco, "Identification from measurements of mechanical fields by finite element model updating strategies: A review," *European Journal of Computational Mechanics/Revue Européenne de Mécanique Numérique*, vol. 18, no. 3-4, pp. 353–376, 2009.

[121] R. Jafarkhani and S. F. Masri, "Finite element model updating using evolutionary strategy for damage detection," *Computer-Aided Civil and Infrastructure Engineering*, vol. 26, no. 3, pp. 207–224, 2011.

[122] Y. Xie, M. Ebad Sichani, J. E. Padgett, and R. DesRoches, "The promise of implementing machine learning in earthquake engineering: A state-of-the-art review," *Earthquake Spectra*, vol. 36, no. 4, pp. 1769–1801, 2020.

[123] A. Kareem, "Emerging frontiers in wind engineering: Computing, stochastics, machine learning and beyond," *Journal of Wind Engineering and Industrial Aerodynamics*, vol. 206, p. 104 320, 2020.

[124] V. Le and L. Caracoglia, "A neural network surrogate model for the performance assessment of a vertical structure subjected to non-stationary, tornadic wind loads," *Computers & Structures*, vol. 231, p. 106 208, 2020.

[125] Z. Fang, Y. Wang, L. Peng, and H. Hong, "Integration of convolutional neural network and conventional machine learning classifiers for landslide susceptibility mapping," *Computers & Geosciences*, vol. 139, p. 104 470, 2020.

[126] A. Cundy, F. M. Hemez, D. J. Inman, and G. Park, "Use of response surface meta-models for damage identification of a simple nonlinear system," in *Key Engineering Materials*, Trans Tech Publ, vol. 245, 2003, pp. 167–174.

[127] G. Abbiati, R. Schöbi, B. Sudret, and B. Stojadinovic, "Structural reliability analysis using deterministic hybrid simulations and adaptive kriging metamodeling," in *16th World Conference on Earthquake Engineering, paper*, 2017.

[128] A. A. Mullur and A. Messac, "Metamodeling using extended radial basis functions: A comparative approach," *Engineering with Computers*, vol. 21, no. 3, pp. 203–217, 2006.

[129] M. Farrokh, "Hysteresis simulation using least-squares support vector machine," *Journal of Engineering Mechanics*, vol. 144, no. 9, p. 04 018 084, 2018.

[130] L. Chuntao and T. Yonghong, "A neural networks model for hysteresis nonlinearity," *Sensors and Actuators A: Physical*, vol. 112, no. 1, pp. 49–54, 2004.

[131] A. Joghataie and M. Farrokh, "Dynamic analysis of nonlinear frames by prandtl neural networks," *Journal of engineering mechanics*, vol. 134, no. 11, pp. 961–969, 2008.

[132] M. Farrokh, M. S. Dizaji, and A. Joghataie, "Modeling hysteretic deteriorating behavior using generalized prandtl neural network," *Journal of Engineering Mechanics*, vol. 141, no. 8, p. 04 015 024, 2015.

[133] A. S. Veeramani, J. H. Crews, and G. D. Buckner, "Hysteretic recurrent neural networks: A tool for modeling hysteretic materials and systems," *Smart Materials and Structures*, vol. 18, no. 7, p. 075 004, 2009.

[134] S. S. Eshkevari, M. Takáč, S. N. Pakzad, and M. Jahani, "Dynnet: Physics-based neural architecture design for nonlinear structural response modeling and prediction," *Engineering Structures*, vol. 229, p. 111 582, 2021.

[135] Z. Lai, C. Mylonas, S. Nagarajaiah, and E. Chatzi, "Structural identification with physics-informed neural ordinary differential equations," *Journal of Sound and Vibration*, vol. 508, p. 116 196, 2021.

[136] E. Haghighat, M. Raissi, A. Moure, H. Gomez, and R. Juanes, "A physics-informed deep learning framework for inversion and surrogate modeling in solid mechanics," *Computer Methods in Applied Mechanics and Engineering*, vol. 379, p. 113 741, 2021.

[137] A. H. Sharghi, R. Karami Mohammadi, and M. Farrokh, "Neuro-hybrid simulation of non-linear frames using prandtl neural networks," *Proceedings of the Institution of Civil Engineers-Structures and Buildings*, pp. 1–18, 2019.

[138] B. Bahmani and W. Sun, "A kd-tree-accelerated hybrid data-driven/model-based approach for poroelasticity problems with multi-fidelity multi-physics data," *Computer Methods in Applied Mechanics and Engineering*, vol. 382, p. 113 868, 2021.

[139] O. Erge and E. van Oort, "Combining physics-based and data-driven modeling in well construction: Hybrid fluid dynamics modeling," *Journal of Natural Gas Science and Engineering*, vol. 97, p. 104 348, 2022.

[140] R. Tibshirani, "Regression shrinkage and selection via the lasso," *Journal of the Royal Statistical Society: Series B (Methodological)*, vol. 58, no. 1, pp. 267–288, 1996.

[141] H. Akaike, "Information theory and an extension of the maximum likelihood principle," in *Selected papers of hirotugu akaike*, Springer, 1998, pp. 199–213.

[142] B. E. Boser, I. M. Guyon, and V. N. Vapnik, "A training algorithm for optimal margin classifiers," pp. 144–152, 1992.

[143] C. Cortes and V. Vapnik, "Support-vector networks," *Machine learning*, vol. 20, no. 3, pp. 273–297, 1995.

[144] A. H. Sharghi, R Karami Mohammadi, and M. Farrokh, "Hybrid simulation of a frame equipped with mr damper by utilizing least square support vector machine," *Journal of Numerical Methods in Civil Engineering*, vol. 2, no. 3, pp. 58–66, 2018.

[145] H.-S. Tang, S.-T. Xue, R. Chen, and T. Sato, "Online weighted ls-svm for hysteretic structural system identification," *Engineering Structures*, vol. 28, no. 12, pp. 1728–1735, 2006.

[146] D. P. Bertsekas, *Constrained optimization and Lagrange multiplier methods.* Academic press, 2014.

[147] J. A. Suykens, T. Van Gestel, J. De Brabanter, B. De Moor, and J. P. Vandewalle, *Least squares support vector machines.* World scientific, 2002.

[148] K. P. Murphy, *Machine learning: a probabilistic perspective.* MIT press, 2012.

[149] G. Yun, J Ghaboussi, and A. S. Elnashai, "Development of neural network based hysteretic models for steel beam-column connections through self-learning simulation," *Journal of Earthquake Engineering*, vol. 11, no. 3, pp. 453–467, 2007.

[150] M. Dehghani and R. Tremblay, "Design and full-scale experimental evaluation of a seismically endurant steel buckling-restrained brace system," *Earthquake Engineering & Structural Dynamics*, vol. 47, no. 1, pp. 105–129, 2017.

[151] C.-M. Uang, M. Nakashima, and K.-C. Tsai, "Research and application of buckling-restrained braced frames," *International Journal of Steel Structures*, vol. 4, no. 4, pp. 301–313, 2004.

[152] R Tremblay, P Bolduc, R Neville, and R DeVall, "Seismic testing and performance of buckling-restrained bracing systems," *Canadian Journal of Civil Engineering*, vol. 33, no. 2, pp. 183–198, 2006.

[153] A.-C. Wu, P.-C. Lin, and K.-C. Tsai, "High-mode buckling responses of buckling-restrained brace core plates," *Earthquake Engineering & Structural Dynamics*, vol. 43, no. 3, pp. 375–393, 2014.

[154] *National building code of canada: 2015*, eng, Jan. 2015. DOI: 10.4224/40002005.

[155] CSA, "Can/csa s16-19: Design of steel structures," *Canadian Standard Association (CSA)*, 2019.

[156] M. Bani and A. Imanpour, "Seismic performance of steel multi-tiered buckling-restrained braced frames in canada," *Behaviour of Steel Structures in Seismic Areas Conference (STESSA 2022)*, 2022.

[157] F. T. McKenna, *Object-oriented finite element programming: frameworks for analysis, algorithms and parallel computing*. University of California, Berkeley, 1997.

[158] J. Chung and G. Hulbert, "A time integration algorithm for structural dynamics with improved numerical dissipation: The generalized-α method," 1993.

[159] *MATLAB version 9.7.0.1216025 (R2019b) Update 1*, The Mathworks, Inc., Natick, Massachusetts, 2019.

[160] P. Mortazavi, X. Huang, O.-S. Kwon, and C. Christopoulos, *Example manual for the university of toronto simulation framework. an open-source framework for integrated multi-platform simulations for structural resilience (second edition)*, Jul. 2017.

[161] P Mortazavi, X Huang, O Kwon, and C Christopoulos, "An overview of the university of toronto simulation (ut-sim) framework and its application to the performance assessment of structures," in *7th International Conference on Advances in Experimental Structural Engineering*, 2017.

[162] X. Huang and O.-S. Kwon, "A generalized numerical/experimental distributed simulation framework," *Journal of Earthquake Engineering*, vol. 24, no. 4, pp. 682–703, 2020.

[163] O.-S. Kwon, "Multi-platform hybrid (experiment-analysis) simulations," in *Dynamic Response of Infrastructure to Environmentally Induced Loads*, Springer, 2017, pp. 37–63.

[164] S. Xavier-de Souza, J. A. Suykens, J. Vandewalle, and D. Bollé, "Coupled simulated annealing," *IEEE Transactions on Systems, Man, and Cybernetics, Part B (Cybernetics)*, vol. 40, no. 2, pp. 320–335, 2009.

[165] J. A. Nelder and R. Mead, "A simplex method for function minimization," *The computer journal*, vol. 7, no. 4, pp. 308–313, 1965.

[166] F. Burden and D. Winkler, "Bayesian regularization of neural networks," *Artificial neural networks*, pp. 23–42, 2008.

[167] M. Gori and A. Tesi, "On the problem of local minima in backpropagation," *IEEE Transactions on Pattern Analysis and Machine Intelligence*, vol. 14, no. 1, pp. 76–86, 1992.

[168] F. Mokhtari and A. Imanpour, "Data-driven substructuring technique for pseudo-dynamic hybrid simulation of steel braced frames," *10th STESSA Behaviour of steel structures in seismic areas conference*, 2022.

[169] M. J. Hashemi, Y. Al-Ogaidi, R. Al-Mahaidi, R. Kalfat, H.-H. Tsang, and J. L. Wilson, "Application of hybrid simulation for collapse assessment of post-earthquake cfrp-repaired rc columns," *Journal of Structural Engineering*, vol. 143, no. 1, p. 04 016 149, 2017. DOI: 10.1061/(ASCE)ST.1943-541X.0001629.

[170] H. N. Mahmoud, A. S. Elnashai, B. F. Spencer Jr, O.-S. Kwon, and D. J. Bennier, "Hybrid simulation for earthquake response of semirigid partial-strength steel frames," *Journal of structural engineering*, vol. 139, no. 7, pp. 1134–1148, 2013.

[171] S. J. Kim, R. Christenson, B. Phillips, and B. Spencer Jr, "Geographically distributed real-time hybrid simulation of mr dampers for seismic hazard mitigation," in *20th Analysis and Computation Specialty Conference*, 2012, pp. 382–393.

[172] S Mojiri, O. Kwon, and C Christopoulos, "Development of 10-element hybrid simulator and its application to seismic performance assessment of structures with hysteretic energy dissipative braces," *6AESE/11ANCRiSST, Champaign, IL*, 2015.

[173] S. Mojiri, P. Mortazavi, O Kwon, and C. Christopoulos, "Multi-element pseudo-dynamic hybrid simulation of concentric braced frames," in *Proceedings of the 7th International Conference on Advances in Experimental Structural Engineering*, 2017.

[174] S. Mojiri, O.-S. Kwon, and C. Christopoulos, "Development of a ten-element hybrid simulation platform and an adjustable yielding brace for performance evaluation of multi-story braced frames subjected to earthquakes," *Earthquake Engineering & Structural Dynamics*, vol. 48, no. 7, pp. 749–771, 2019.

[175] M. Grieves, "Digital twin: Manufacturing excellence through virtual factory replication," *White paper*, vol. 1, pp. 1–7, 2014.

[176] M. Liu, S. Fang, H. Dong, and C. Xu, "Review of digital twin about concepts, technologies, and industrial applications," *Journal of Manufacturing Systems*, vol. 58, pp. 346–361, 2021.

[177] F. Jiang, L. Ma, T. Broyd, and K. Chen, "Digital twin and its implementations in the civil engineering sector," *Automation in Construction*, vol. 130, p. 103 838, 2021.

[178] T. Ritto and F. Rochinha, "Digital twin, physics-based model, and machine learning applied to damage detection in structures," *Mechanical Systems and Signal Processing*, vol. 155, p. 107 614, 2021.

[179] S. Chakraborty and S. Adhikari, "Machine learning based digital twin for dynamical systems with multiple time-scales," *Computers & Structures*, vol. 243, p. 106 410, 2021.

[180] A. I. Khuri and S. Mukhopadhyay, "Response surface methodology," *Wiley Interdisciplinary Reviews: Computational Statistics*, vol. 2, no. 2, pp. 128–149, 2010.

[181] J. P. Kleijnen, "Kriging metamodeling in simulation: A review," *European journal of operational research*, vol. 192, no. 3, pp. 707–716, 2009.

[182] M. F. Hussain, R. R. Barton, and S. B. Joshi, "Metamodeling: Radial basis functions, versus polynomials," *European Journal of Operational Research*, vol. 138, no. 1, pp. 142–154, 2002.

[183] A. Roy, R. Manna, and S. Chakraborty, "Support vector regression based metamodeling for structural reliability analysis," *Probabilistic Engineering Mechanics*, vol. 55, pp. 78–89, 2019.

[184] H. Wang and T. Wu, "Knowledge-enhanced deep learning for wind-induced nonlinear structural dynamic analysis," *Journal of Structural Engineering*, vol. 146, no. 11, p. 04 020 235, 2020.

[185] Y. LeCun, Y. Bengio, and G. Hinton, "Deep learning," *nature*, vol. 521, no. 7553, pp. 436–444, 2015.

[186] J. A. Suykens and J. Vandewalle, "Least squares support vector machine classifiers," *Neural processing letters*, vol. 9, no. 3, pp. 293–300, 1999.

[187] G. James, D. Witten, T. Hastie, and R. Tibshirani, *An introduction to statistical learning*. Springer, 2013, vol. 112.

[188] D. L. Donoho, "Compressed sensing," *IEEE Transactions on information theory*, vol. 52, no. 4, pp. 1289–1306, 2006.

[189] P. Zheng, T. Askham, S. L. Brunton, J. N. Kutz, and A. Y. Aravkin, "A unified framework for sparse relaxed regularized regression: Sr3," *IEEE Access*, vol. 7, pp. 1404–1423, 2018.

[190] D. Simon, *Optimal state estimation: Kalman, H infinity, and nonlinear approaches*. John Wiley & Sons, 2006.

[191] M. Smith, *ABAQUS/Standard User's Manual, Version 6.9*, English. United States: Dassault Systèmes Simulia Corp, 2009.

[192] S. A. M. Andreas H. Schellenberg Yuli Huang, "Structural finite element software coupling using adapter elements," *Computer Modeling in Engineering & Sciences*, vol. 120, no. 3, pp. 719–737, 2019, ISSN: 1526-1506. [Online]. Available: http://www.techscience.com/CMES/v120n3/27512.

[193] A. Ashrafi and A. Imanpour, "Seismic response of steel multi-tiered eccentrically braced frames," *Journal of Constructional Steel Research*, vol. 181, p. 106 600, 2021.

[194] G. M. Hulbert and J. Chung, "Explicit time integration algorithms for structural dynamics with optimal numerical dissipation," *Computer Methods in Applied Mechanics and Engineering*, vol. 137, no. 2, pp. 175–188, 1996.

[195] E. Voce, "The relationship between stress and strain for homogeneous deformations," 1948.

[196] J. Chaboche, K. D. Van, and G Cordier, "Modelization of the strain memory effect on the cyclic hardening of 316 stainless steel," 1979.

[197] Z. Yi and S. Aurel, "Assessment using fea of the influence of detaining parameters on performance of buckling restrained braces," M.S. thesis, POLITEHNICA UNIVERSITY TIMIŞOARA, 2015/2016.

[198] Safaei, Mohsen and De Waele, Wim, "Towards better finite element modelling of elastic recovery in sheet metal forming of advanced high strength steel," eng, in *SUSTAINABLE CONSTRUCTION AND DESIGN*, Van Wittenberghe, Jeroen, Ed., vol. 2, Ghent, Belgium: Ghent University, Laboratory Soete, 2011, 217–227, ISBN: 9789490726010.

[199] M. Dehghani, R. Tremblay, and M. Leclerc, "Fatigue failure of 350wt steel under large-strain seismic loading at room and subfreezing temperatures," *Construction and Building Materials*, vol. 145, pp. 602–618, 2017.

[200] H. Hotelling, "Analysis of a complex of statistical variables into principal components.," *Journal of educational psychology*, vol. 24, no. 6, p. 417, 1933.

[201] S. Chaturantabut and D. C. Sorensen, "Discrete empirical interpolation for nonlinear model reduction," in *Proceedings of the 48h IEEE Conference on Decision and Control (CDC) held jointly with 2009 28th Chinese Control Conference*, IEEE, 2009, pp. 4316–4321.

[202] A. Kottari, A. Charalampakis, and V. Koumousis, "A consistent degrading bouc-wen model," *Engineering Structures*, vol. 60, pp. 235–240, 2014.

[203] Y. Jiang, "Numerical and experimental seismic assessment and retrofit of steel tension-only double angle braced frames designed before the implementation of detailing provisions for ductile seismic response," Ph.D. dissertation, École Polytechnique de Montréal, 2013.

Appendix A: HyDPS Results

This appendix presents the results of the nonlinear response history analyses performed using the hybrid data-driven and physics-based simulations (HyDPSs) as described in Section 3.7.2.
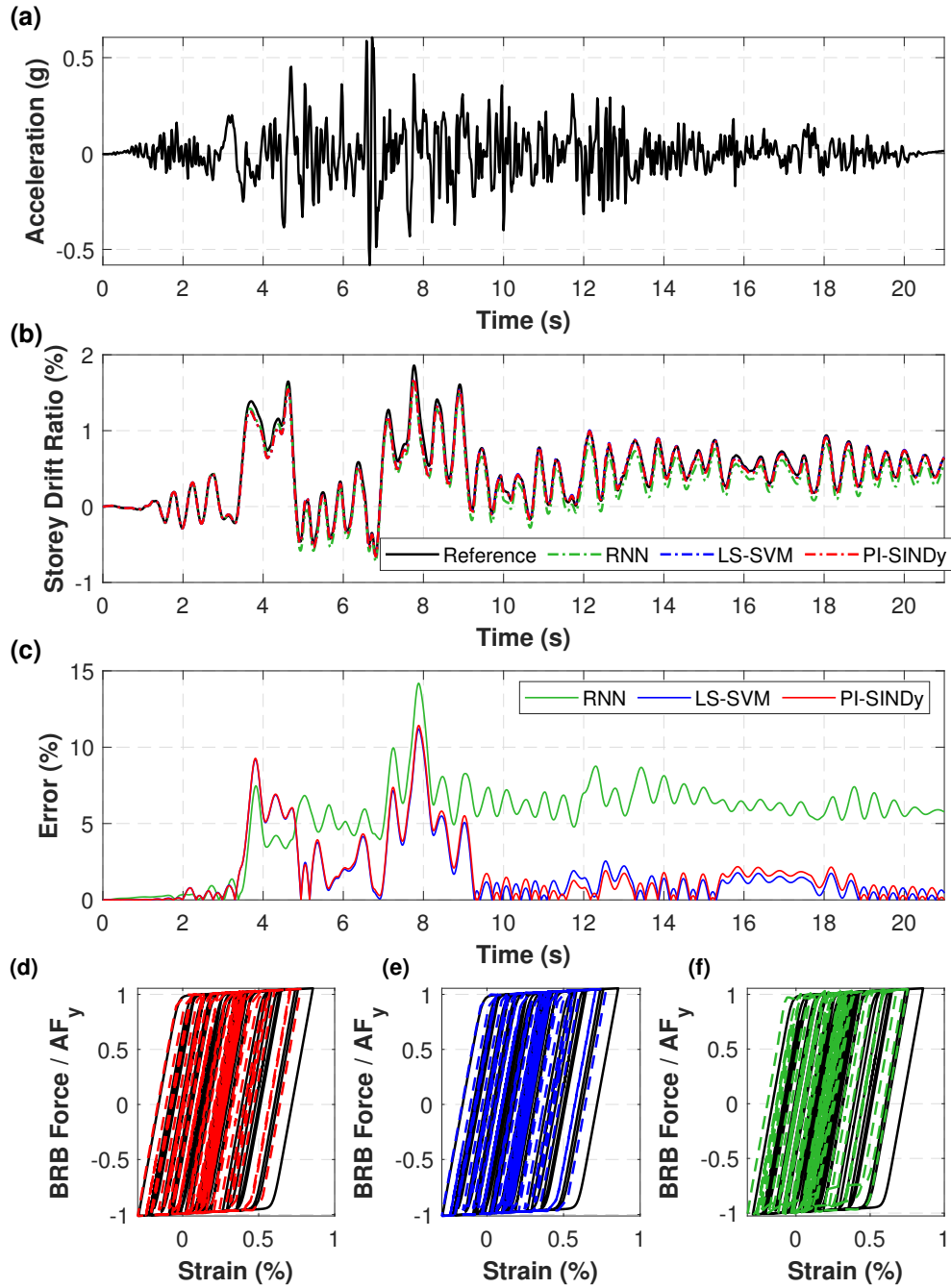
Figure A.1: (a) 1978 Tabas, Iran-Dayhook earthquake acceleration, (b) storey drift ratio of the prototype frame under the 1978 Tabas, Iran-Dayhook, (c) Point-to-point error of the storey drift ratio, hysteretic responses of the BRB obtained from the HyDPS framework using (d) PI-SINDy, (e) LS-SVM, (f) RNN.

129
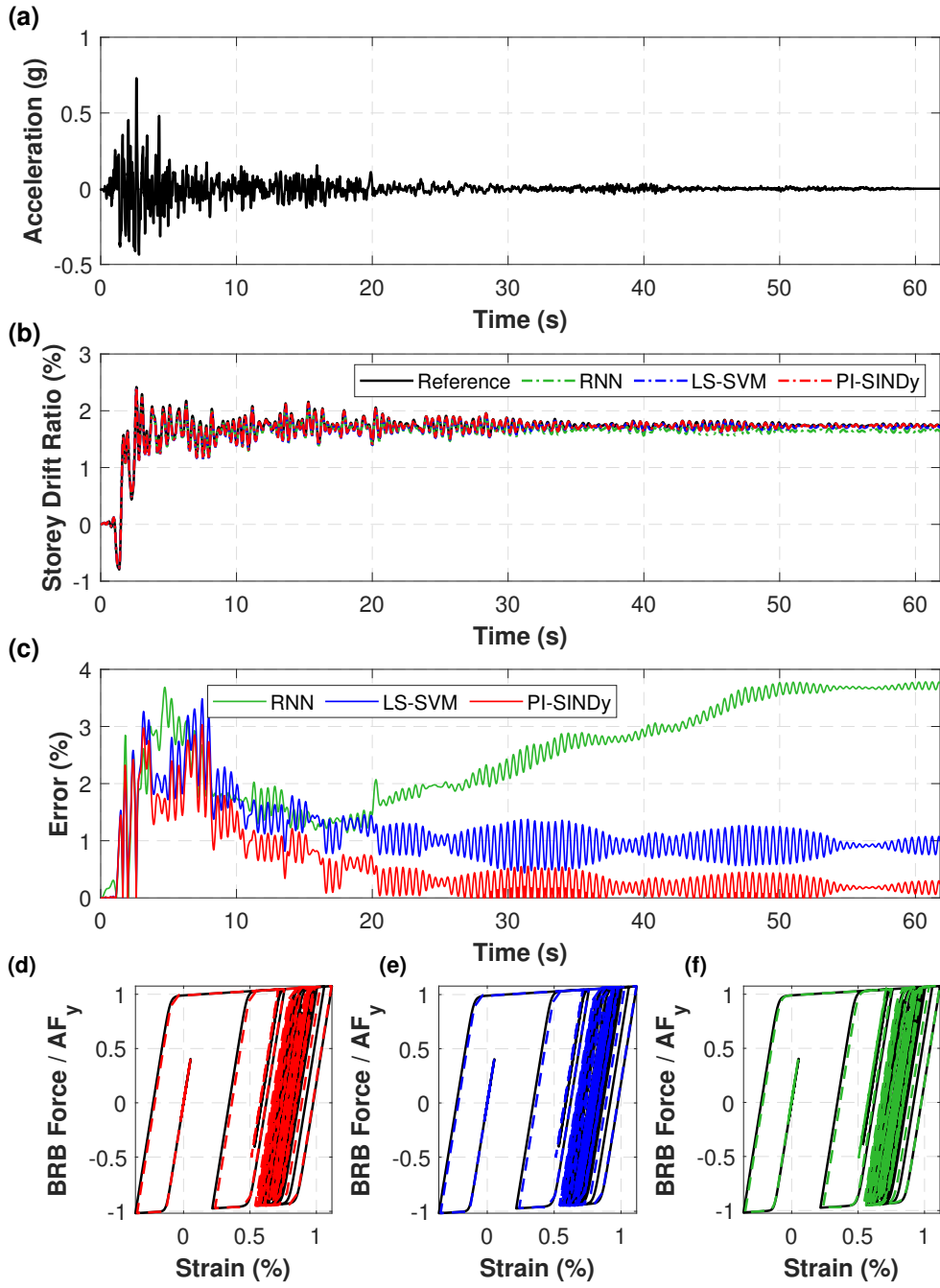
Figure A.2: (a) 1971 San Fernando-Castaic-Old Ridge Route earthquake acceleration, (b) storey drift ratio of the prototype frame under the 1971 San Fernando-Castaic-Old Ridge Route, (c) Point-to-point error of the storey drift ratio, hysteretic responses of the BRB obtained from the HyDPS framework using (d) PI-SINDy, (e) LS-SVM, (f) RNN.
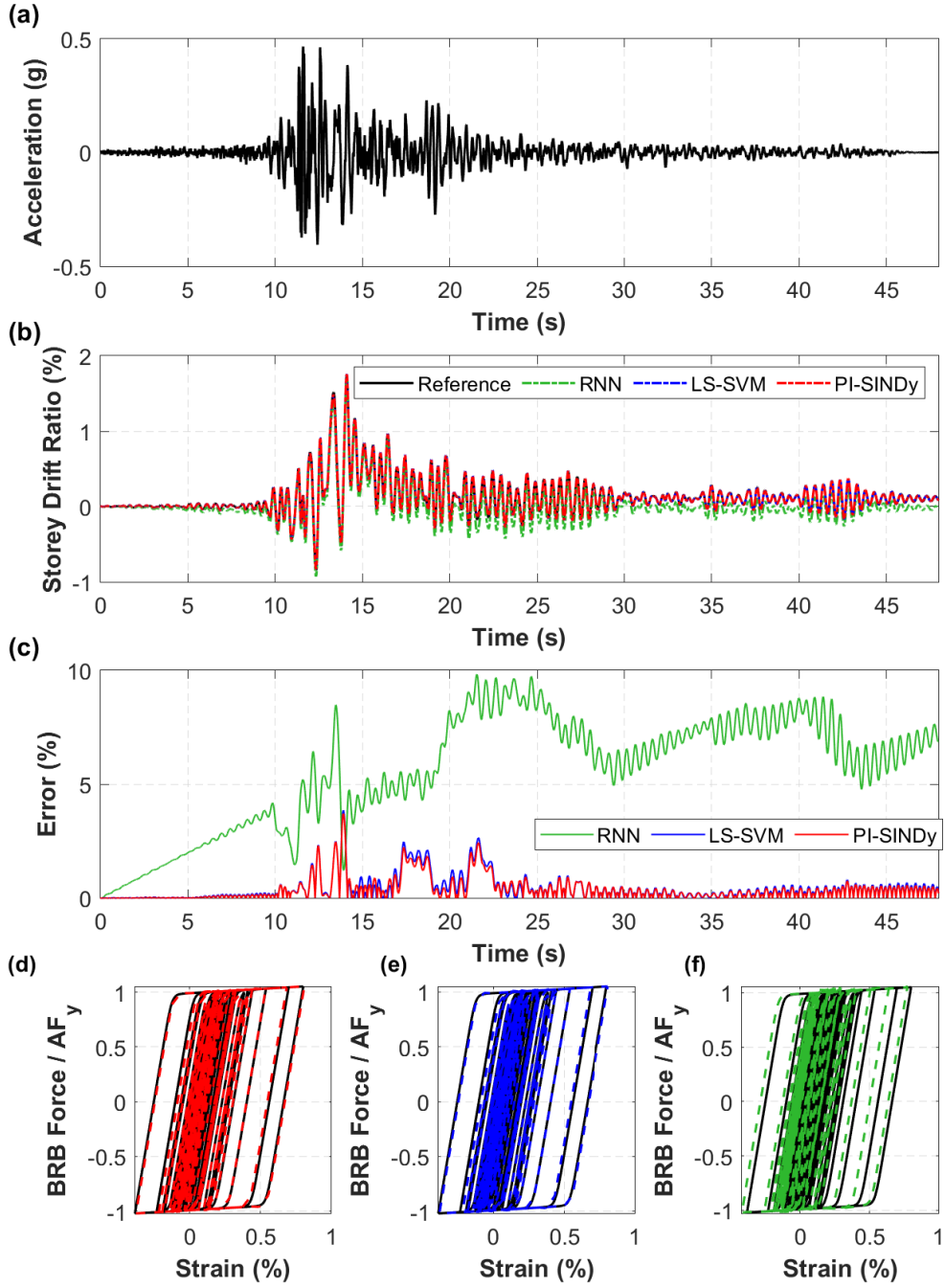
Figure A.3: (a) 1979 Montenegro, SFRY-Herceg Novi-O.S.D. Paviviv earthquake accelera-tion, (b) storey drift ratio of the prototype frame under the 1979 Montenegro, SFRY-Herceg Novi-O.S.D. Paviviv, (c) Point-to-point error of the storey drift ratio, hysteretic responses of the BRB obtained from the HyDPS framework using (d) PI-SINDy, (e) LS-SVM, (f) RNN.
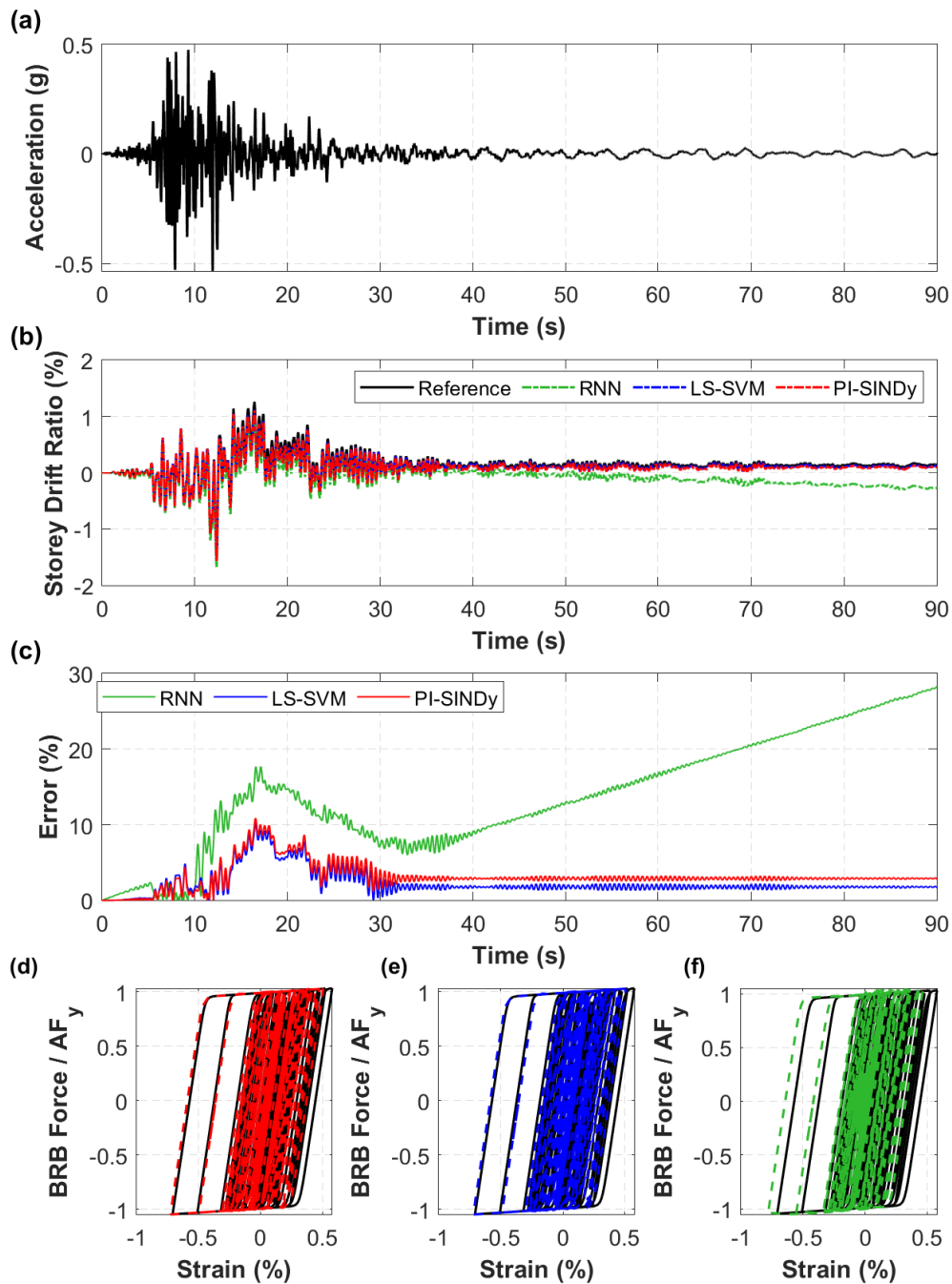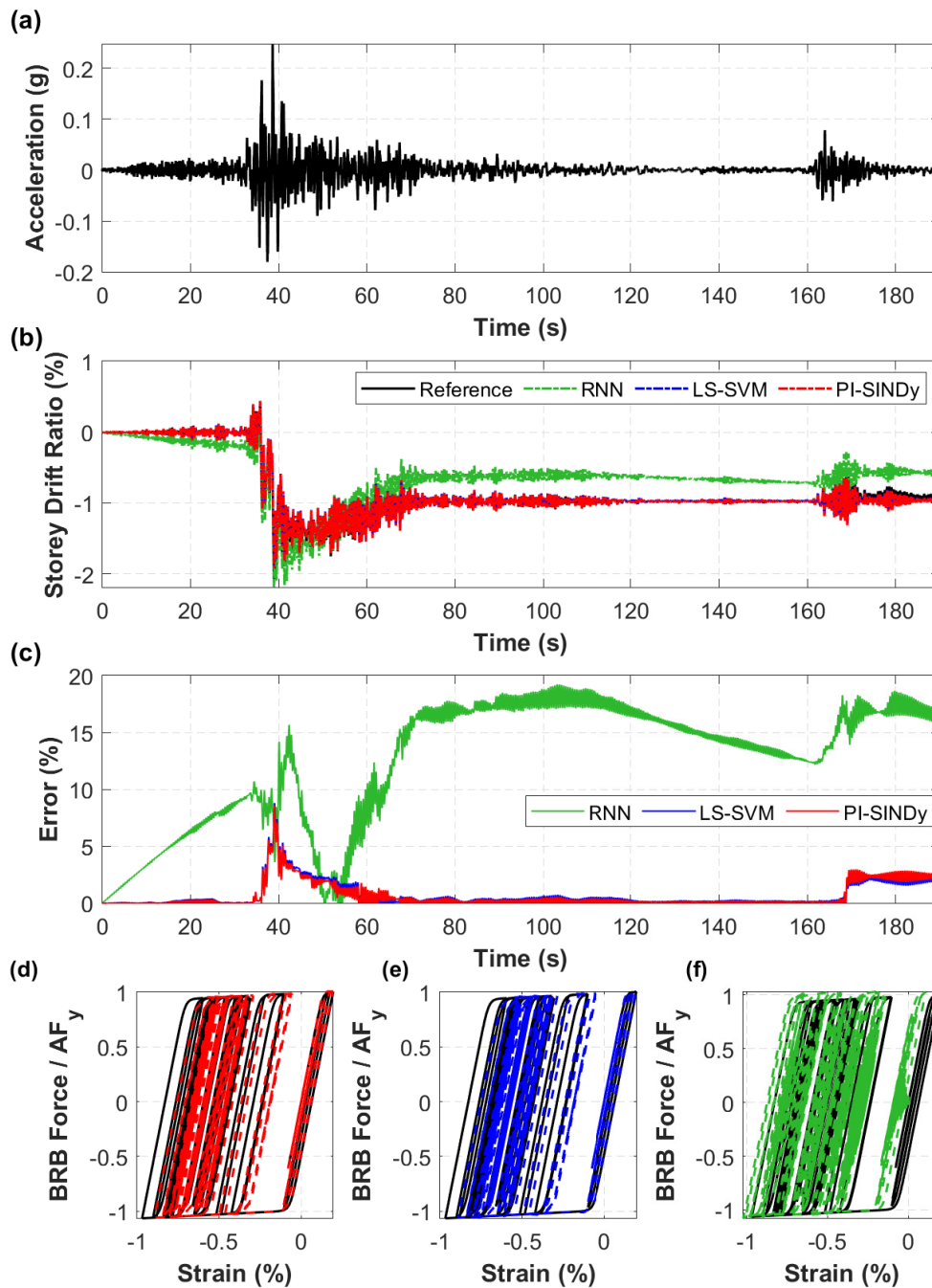
Figure A.4: (a) 1995 Kobe, Japan-Tadoka earthquake acceleration, (b) storey drift ratio of the prototype frame under the 1979 Montenegro, 1995 Kobe, Japan-Tadoka, (c) Point-to-point error of the storey drift ratio, hysteretic responses of the BRB obtained from the HyDPS framework using (d) PI-SINDy, (e) LS-SVM, (f) RNN.
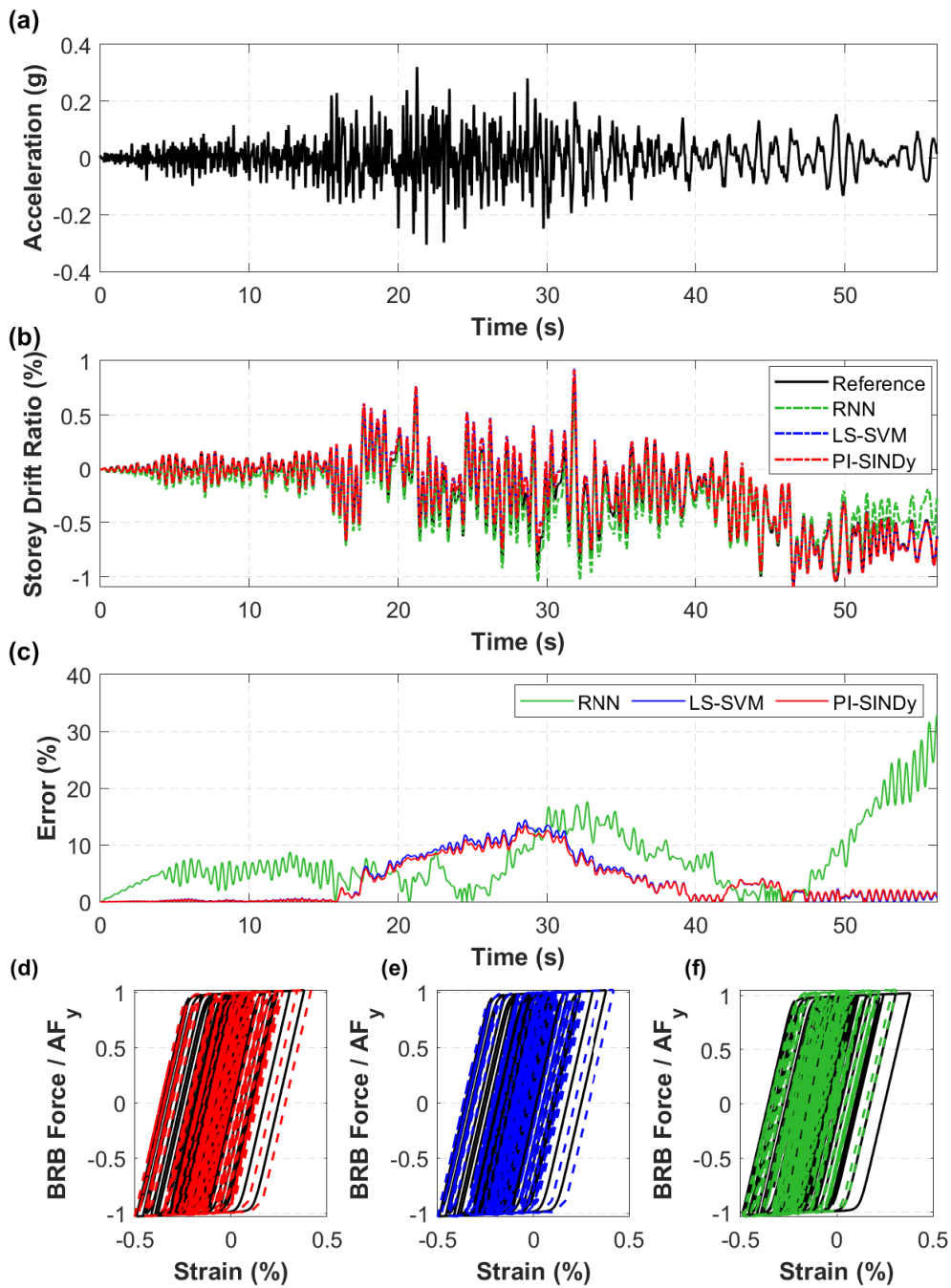
Figure A.5: (a) 2001 Geivo, Japan-1421a earthquake acceleration, (b) storey drift ratio of the prototype frame under the 2001 Geivo, Japan-1421a, (c) Point-to-point error of the storey drift ratio, hysteretic responses of the BRB obtained from the HyDPS framework using (d) PI-SINDy, (e) LS-SVM, (f) RNN.
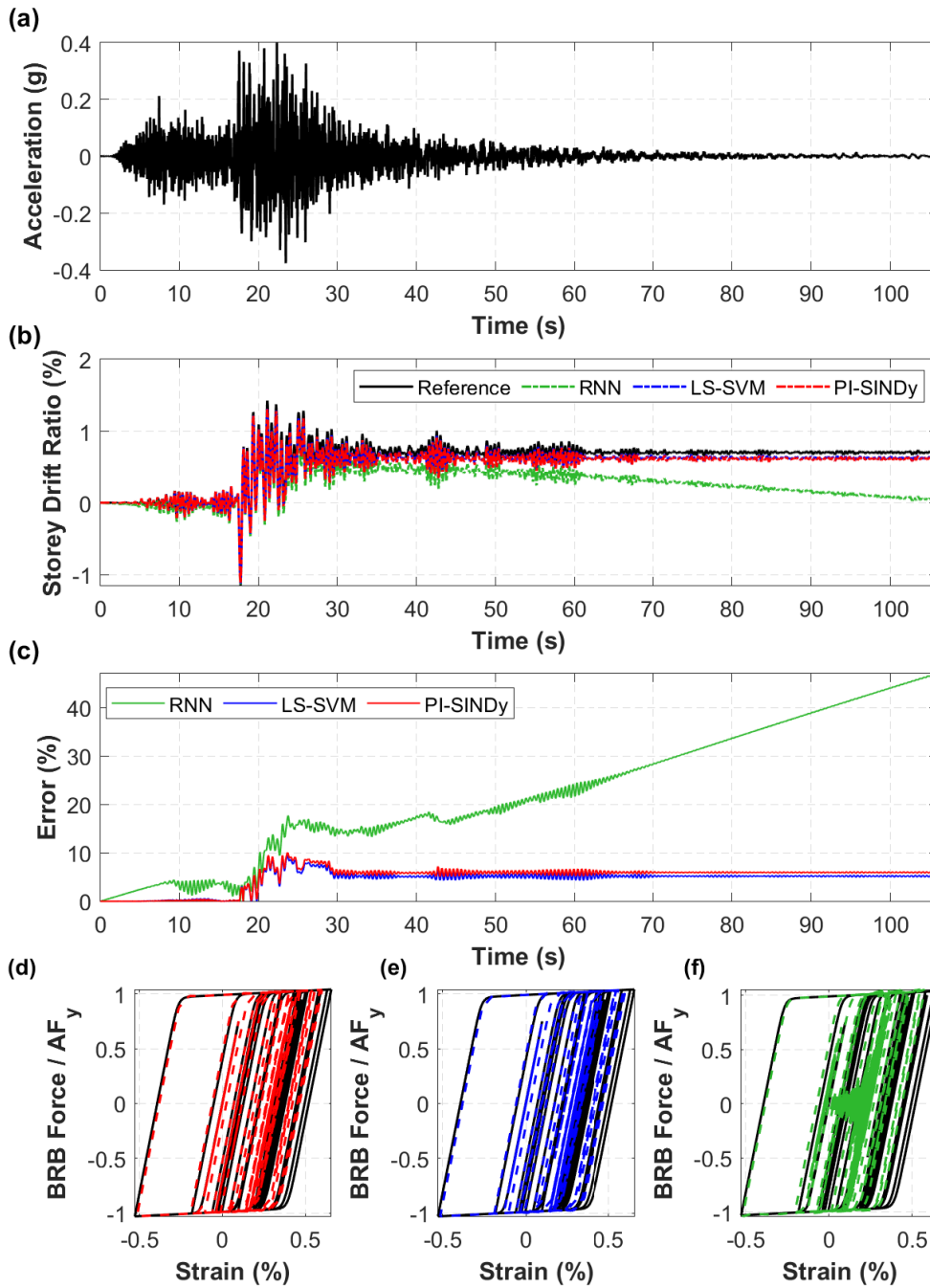
Figure A.6: (a) 2011 Miyagi, Japan-IWT026 earthquake acceleration, (b) storey drift ratio of the prototype frame under the 2011 Miyagi, Japan-IWT026, (c) Point-to-point error of the storey drift ratio, hysteretic responses of the BRB obtained from the HyDPS framework using (d) PI-SINDy, (e) LS-SVM, (f) RNN.

134
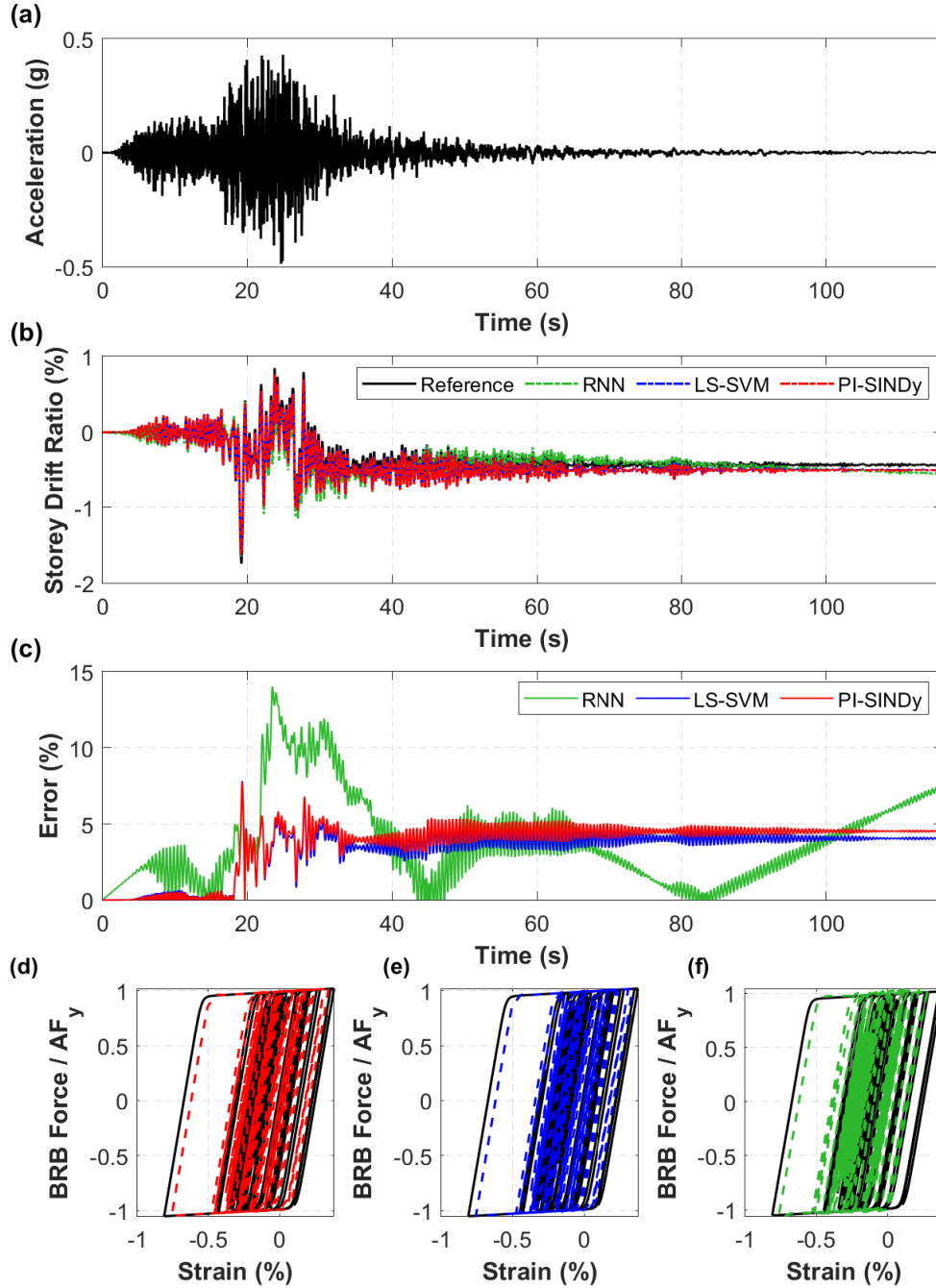
Figure A.7: (a) 2011 Miyagi, Japan-MYG016 earthquake acceleration, (b) storey drift ratio of the prototype frame under the 2011 Miyagi, Japan-MYG016, (c) Point-to-point error of the storey drift ratio, hysteretic responses of the BRB obtained from the HyDPS framework using (d) PI-SINDy, (e) LS-SVM, (f) RNN.
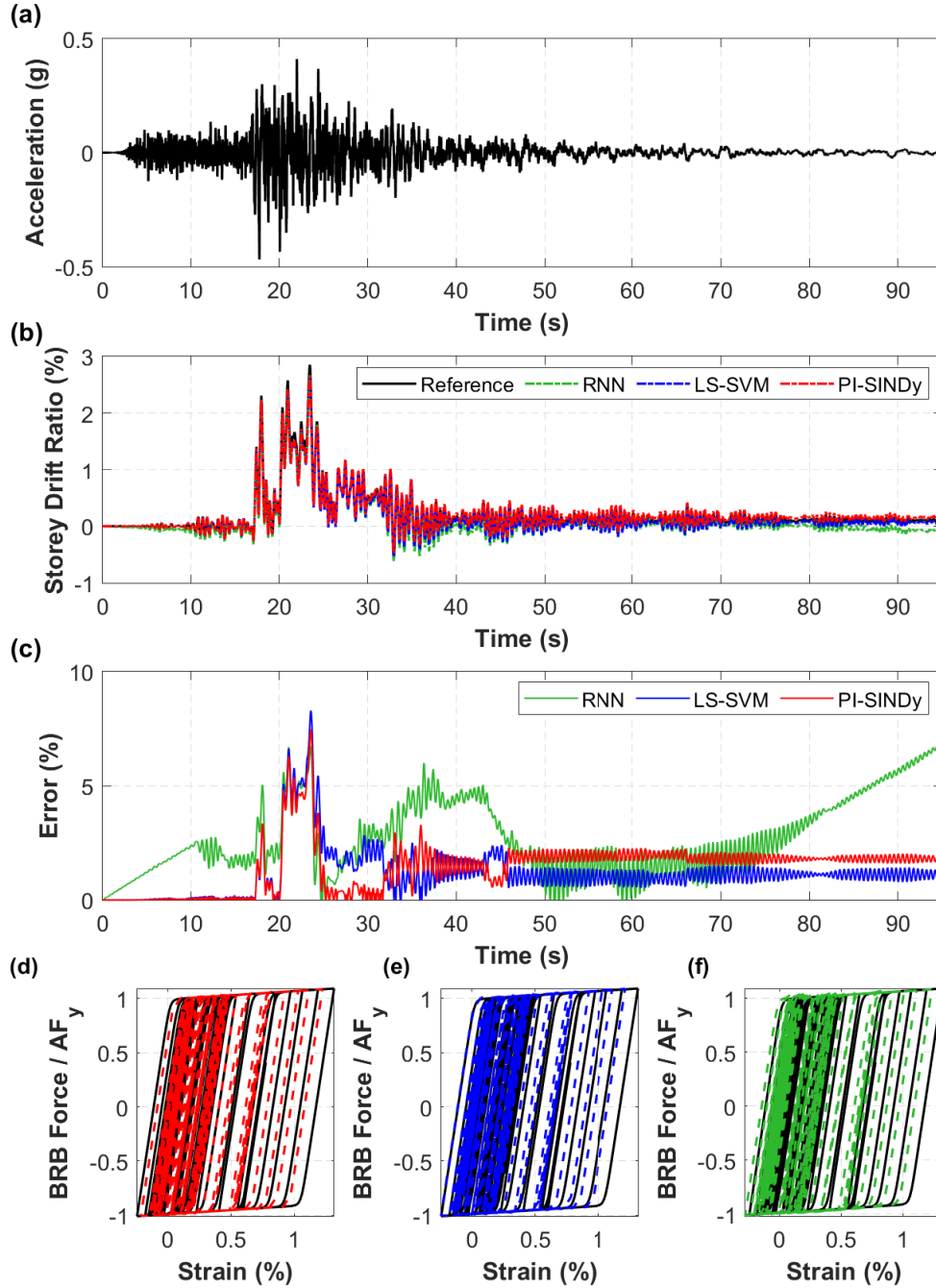
Figure A.8: (a) 2011 Miyagi, Japan-IWTH24 earthquake acceleration, (b) storey drift ratio of the prototype frame under the 2011 Miyagi, Japan-IWTH24, (c) Point-to-point error of the storey drift ratio, hysteretic responses of the BRB obtained from the HyDPS framework using (d) PI-SINDy, (e) LS-SVM, (f) RNN.
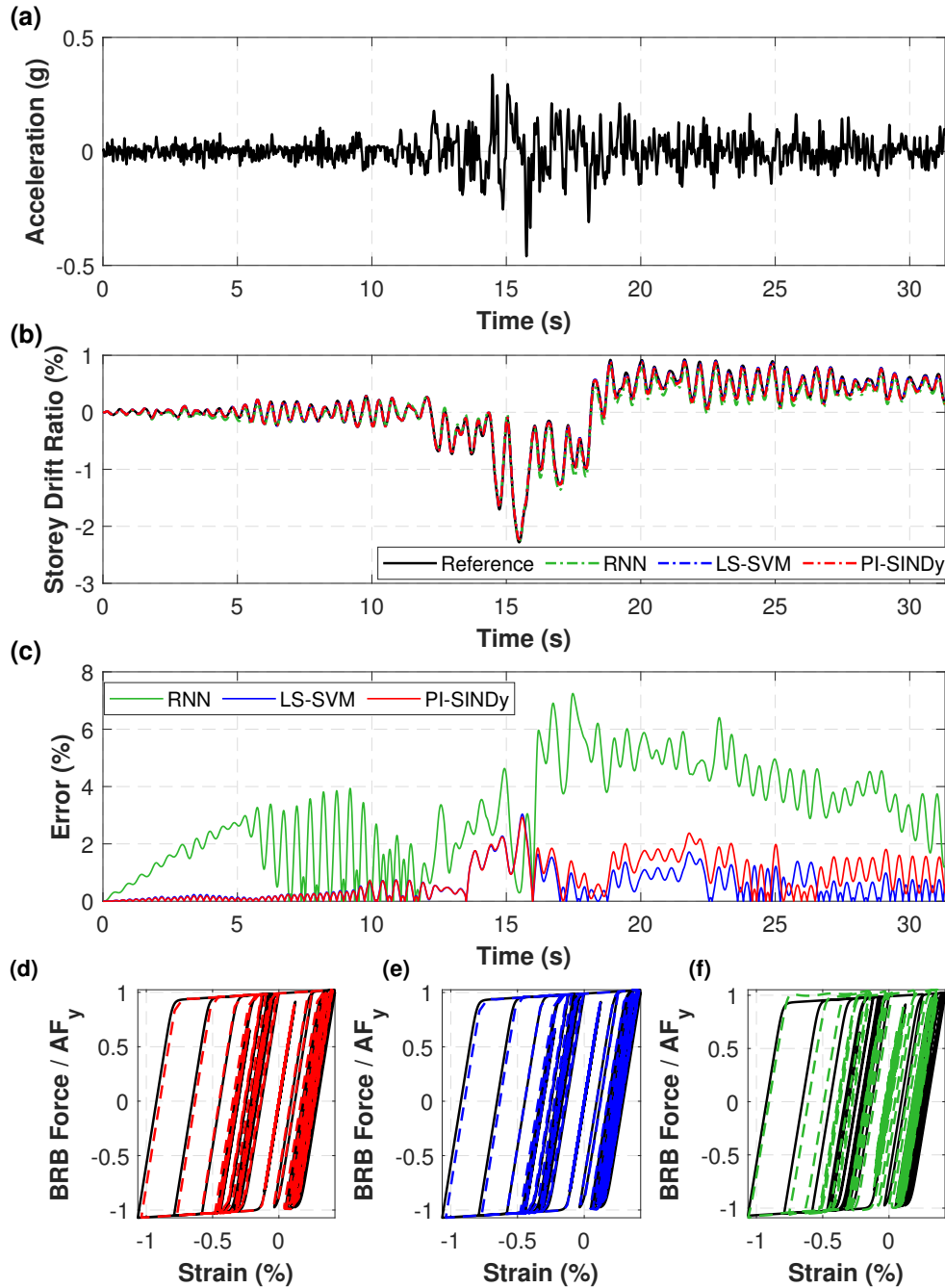
Figure A.9: (a) 2001 Southern Peru-POCO earthquake acceleration, (b) storey drift ratio of the prototype frame under the 2001 Southern Peru-POCO, (c) Point-to-point error of the storey drift ratio, hysteretic responses of the BRB obtained from the HyDPS framework using (d) PI-SINDy, (e) LS-SVM, (f) RNN.
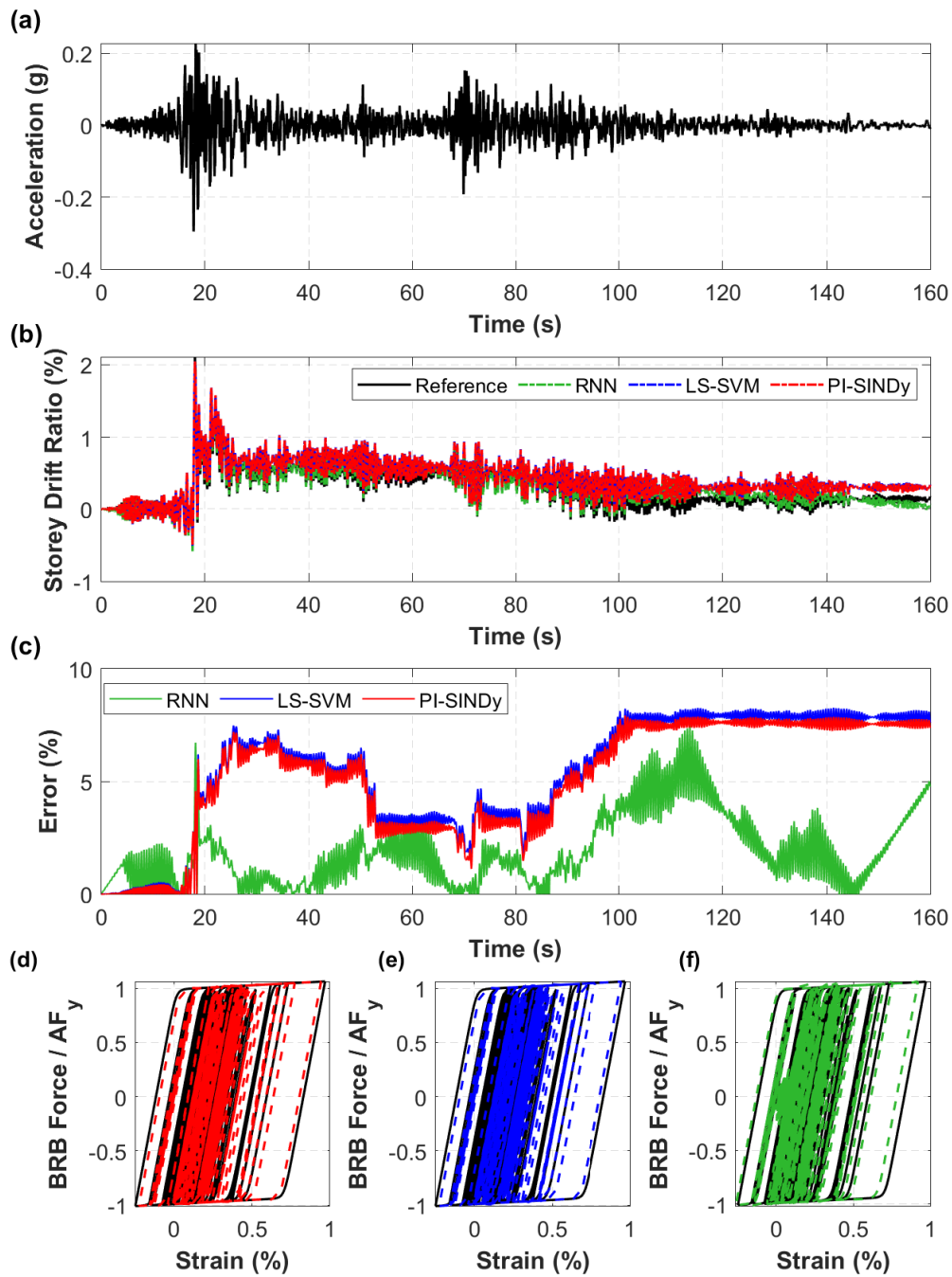
Figure A.10: (a) 2007 Pisco, Peru-UNICA earthquake acceleration, (b) storey drift ratio of the prototype frame under the 2007 Pisco, Peru-UNICA, (c) Point-to-point error of the storey drift ratio, hysteretic responses of the BRB obtained from the HyDPS framework using (d) PI-SINDy, (e) LS-SVM, (f) RNN.
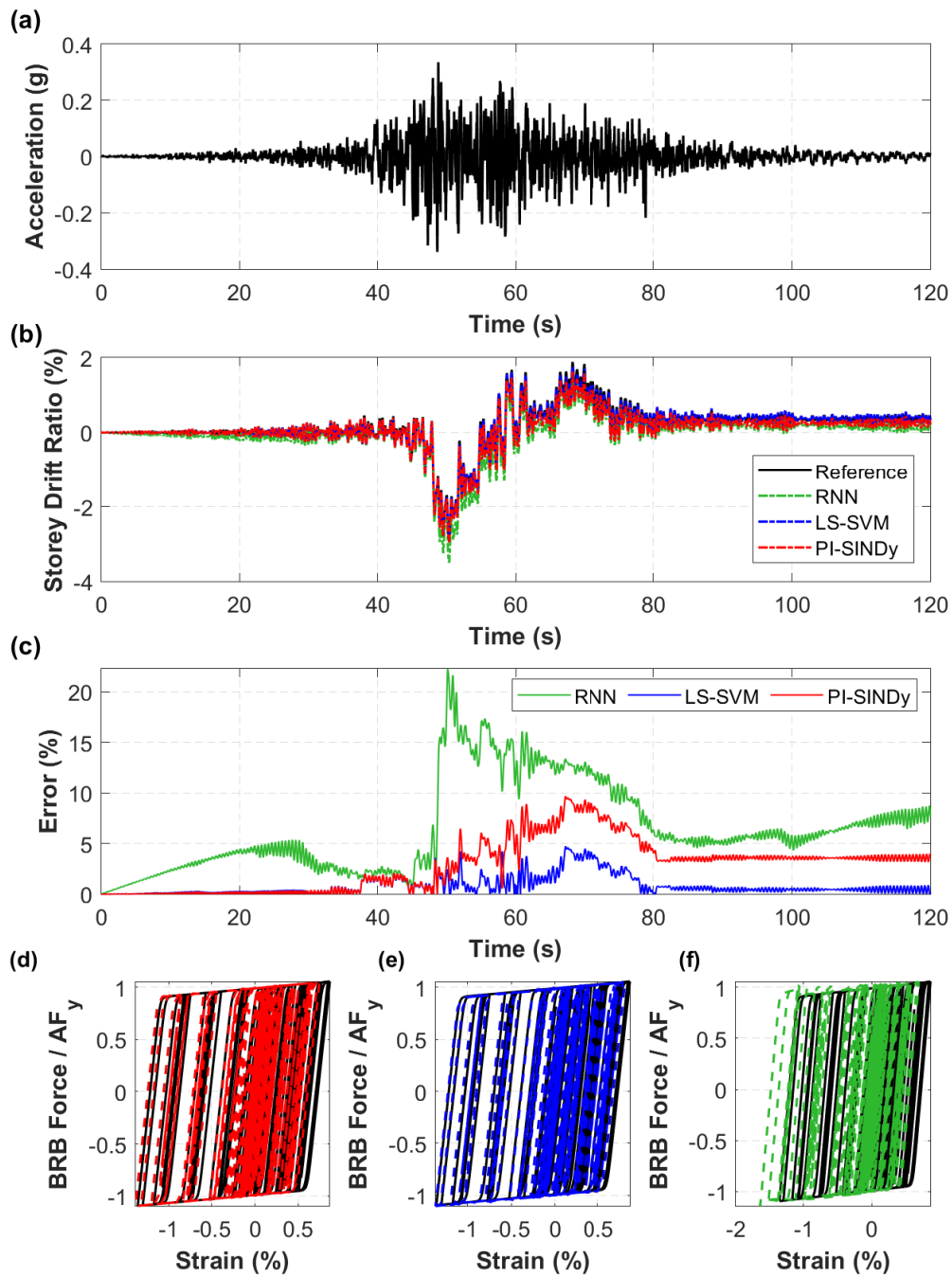
Figure A.11: (a) 2010 Maule, Chile-LACHb earthquake acceleration, (b) storey drift ratio of the prototype frame under the 2010 Maule, Chile-LACHb, (c) Point-to-point error of the storey drift ratio, hysteretic responses of the BRB obtained from the HyDPS framework using (d) PI-SINDy, (e) LS-SVM, (f) RNN.

Figure A.12: (a) 2014 Iquique, Chile-PB09 earthquake acceleration, (b) storey drift ratio of the prototype frame under the 2014 Iquique, Chile-PB09, (c) Point-to-point error of the storey drift ratio, hysteretic responses of the BRB obtained from the HyDPS framework using (d) PI-SINDy, (e) LS-SVM, (f) RNN.

Appendix B: Effect of Structural Dynamic Properties

This appendix presents the results of the nonlinear response history analyses performed using the hybrid data-driven and physics-based simulations (HyDPSs) to investigate the effect of dynamic properties of the structure on the accuracy of HyDPS framework as described in Section 3.7.3.
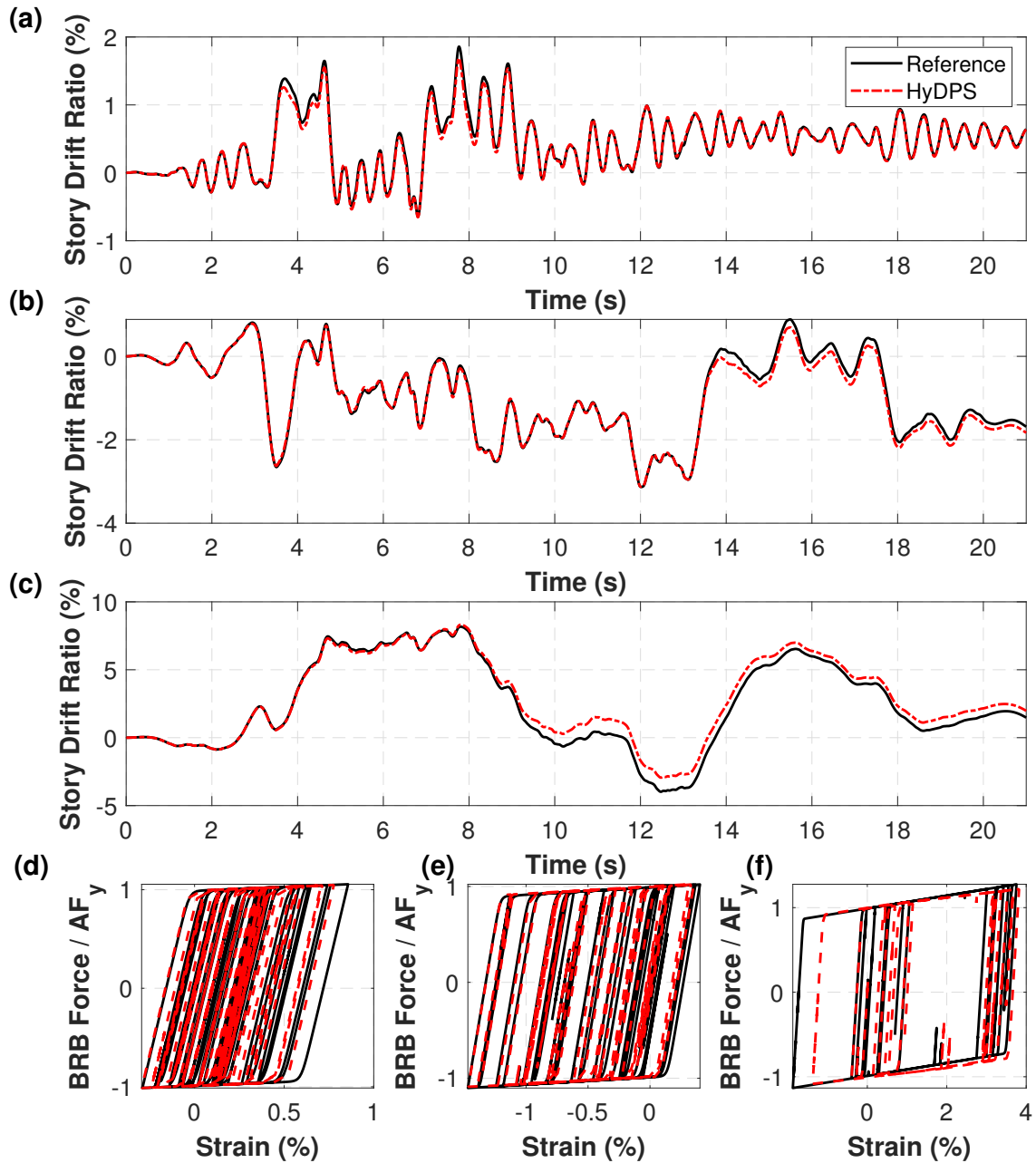
Figure B.1: Time history of BRBF storey drift ratio under the 1978 Tabas, Iran-Dayhook earthquake, (a) BRBF with $T_0 = 0.49s$, (b) BRBF with $2T_0 = 0.98s$, and (c) BRBF with $4T_0 = 1.97s$, and BRB hysteretic response of (d) BRBF with $T_0 = 0.49s$, (e) BRBF with $2T_0 = 0.98s$, and (f) BRBF with $4T_0 = 1.97s$.
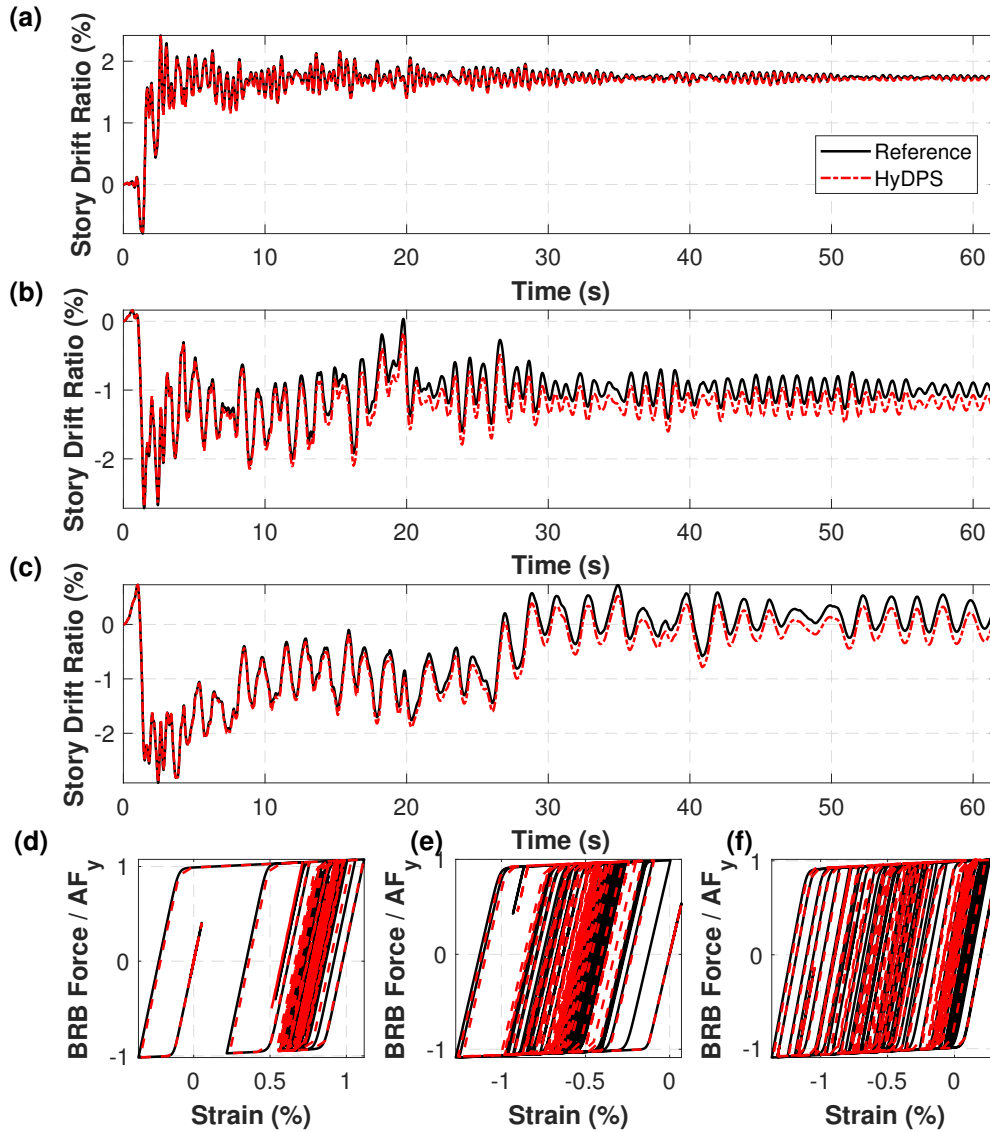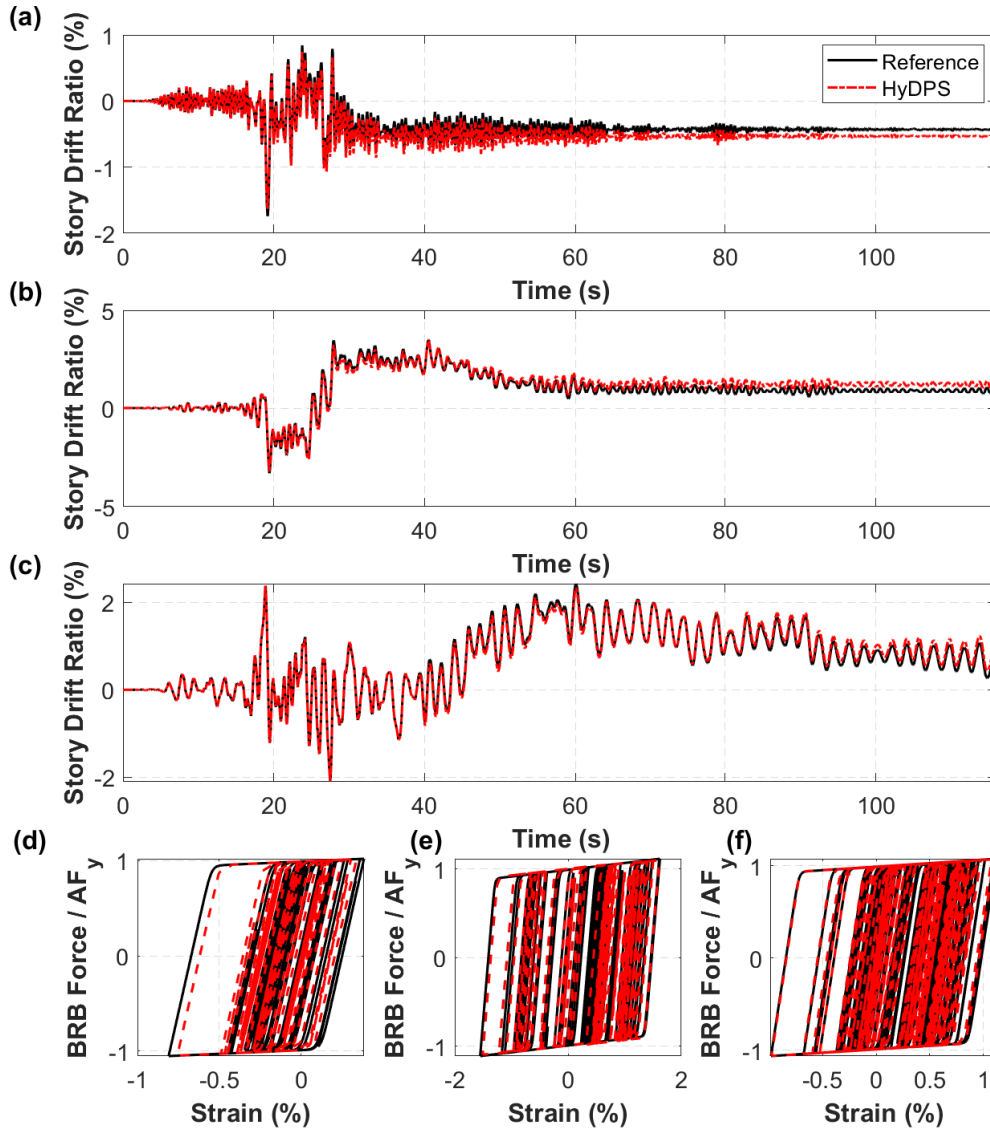
Figure B.2: Time history of BRBF storey drift ratio under the 1971 San Fernando-Castaic-Old Ridge Route earthquake, (a) BRBF with $T_0 = 0.49s$, (b) BRBF with $2T_0 = 0.98s$, and (c) BRBF with $4T_0 = 1.97s$, and BRB hysteretic response of (d) BRBF with $T_0 = 0.49s$, (e) BRBF with $2T_0 = 0.98s$, and (f) BRBF with $4T_0 = 1.97s$.
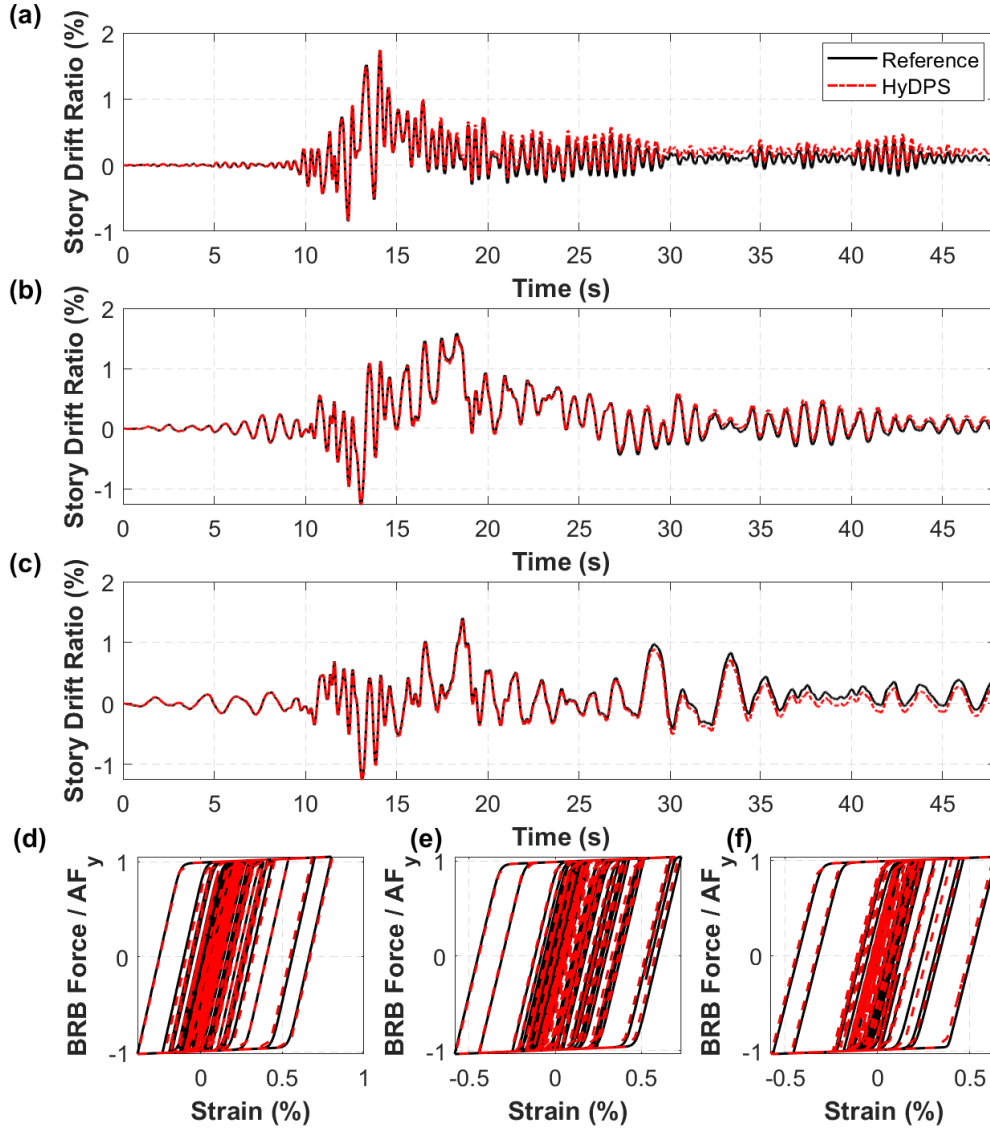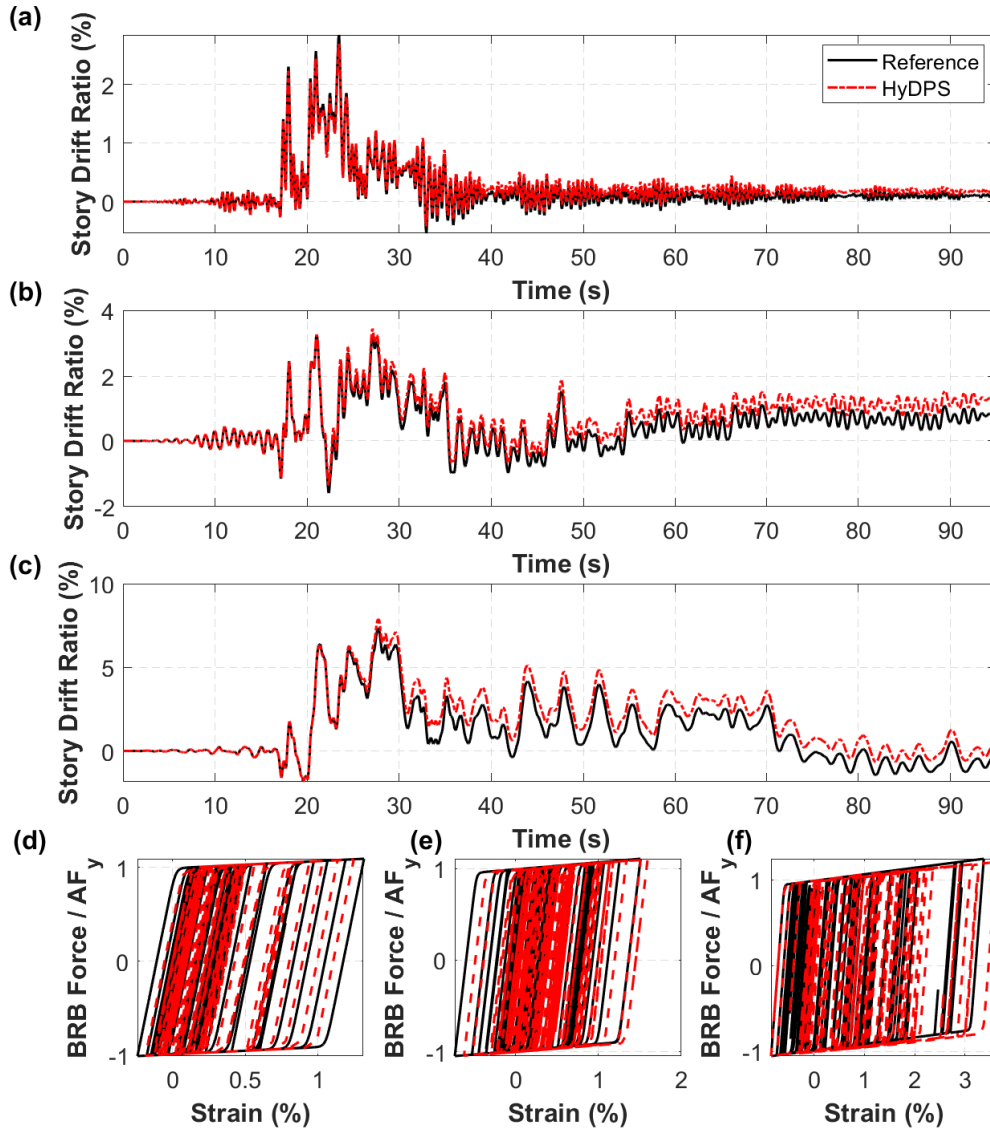
Figure B.3: Time history of BRBF storey drift ratio under the 1979 Montenegro, SFRY-Herceg Novi-O.S.D. Paviviv earthquake, (a) BRBF with $T_0 = 0.49s$, (b) BRBF with $2T_0 = 0.98s$, and (c) BRBF with $4T_0 = 1.97s$, and BRB hysteretic response of (d) BRBF with $T_0 = 0.49s$, (e) BRBF with $2T_0 = 0.98s$, and (f) BRBF with $4T_0 = 1.97s$.
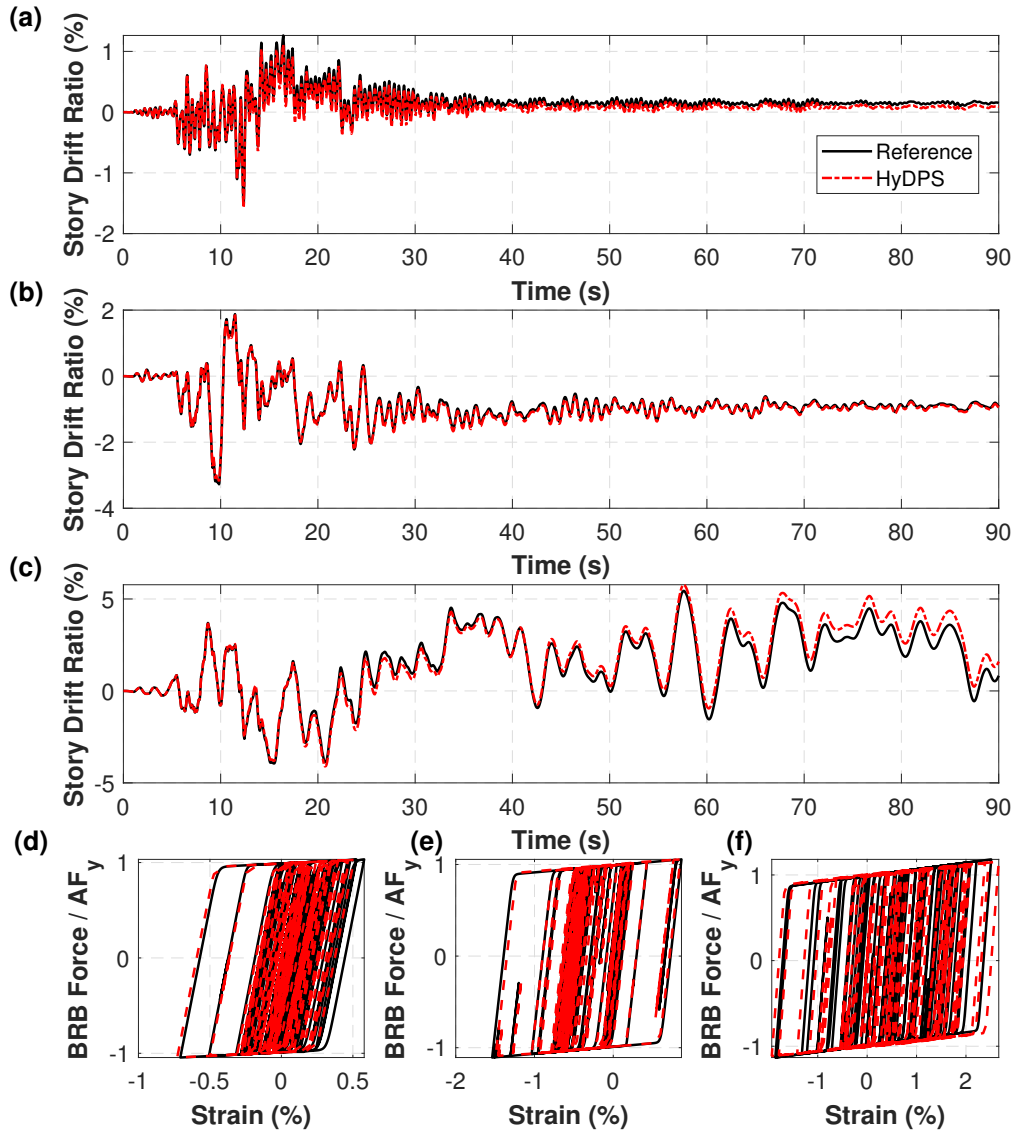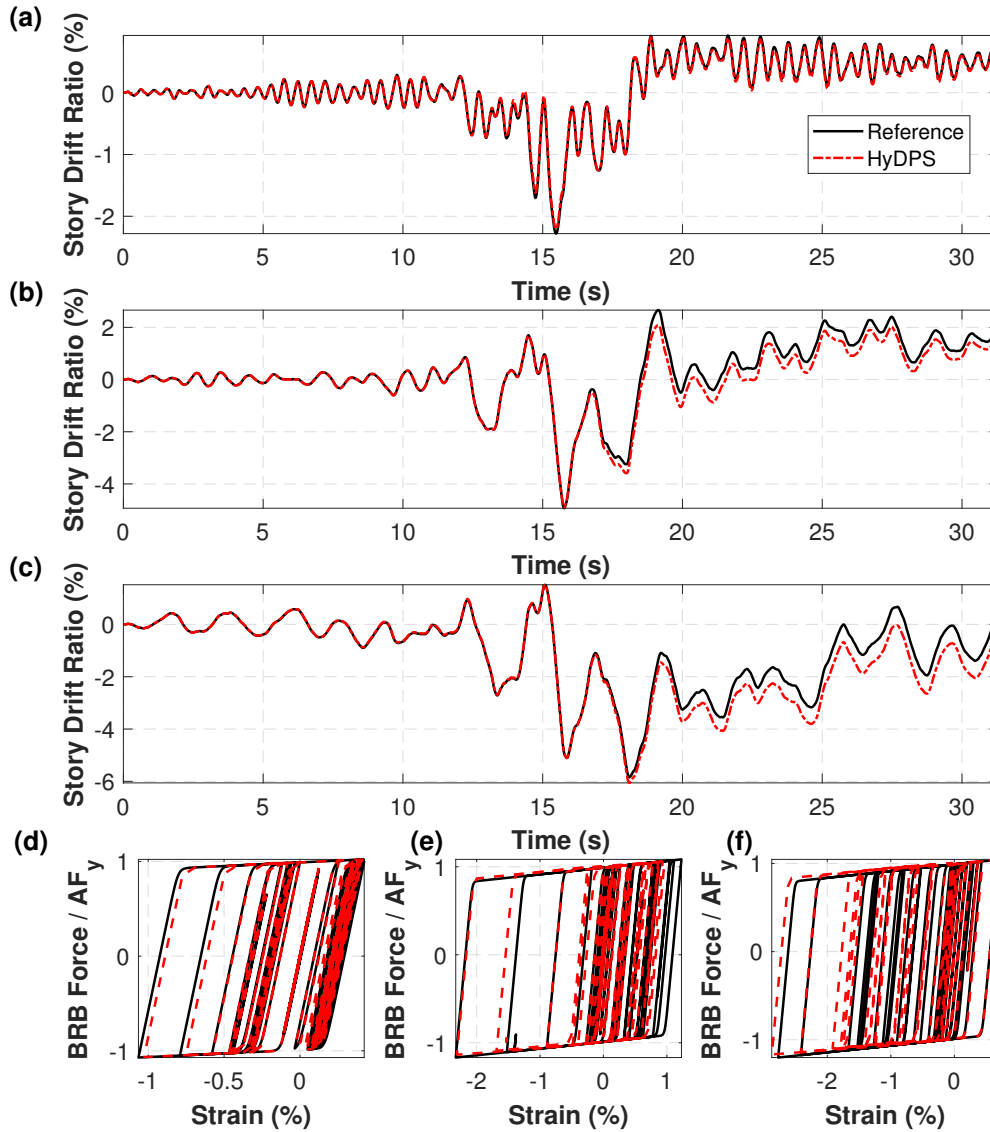
Figure B.4: Time history of BRBF storey drift ratio under the 1995 Kobe, Japan-Tadoka earthquake, (a) BRBF with $T_0 = 0.49s$, (b) BRBF with $2T_0 = 0.98s$, and (c) BRBF with $4T_0 = 1.97s$, and BRB hysteretic response of (d) BRBF with $T_0 = 0.49s$, (e) BRBF with $2T_0 = 0.98s$, and (f) BRBF with $4T_0 = 1.97s$.
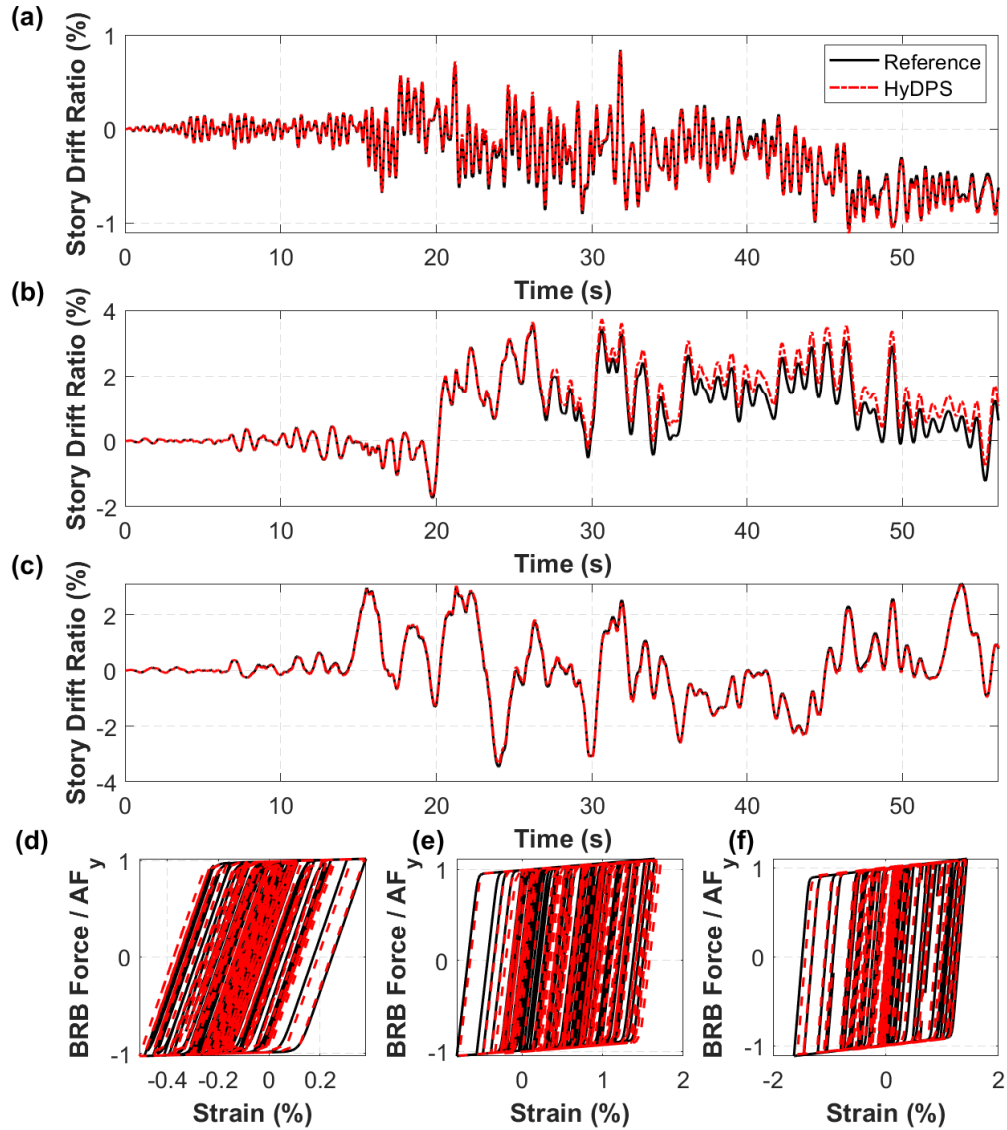
Figure B.5: Time history of BRBF storey drift ratio under the 2001 Geivo, Japan-1421a earthquake, (a) BRBF with $T_0 = 0.49s$, (b) BRBF with $2T_0 = 0.98s$, and (c) BRBF with $4T_0 = 1.97s$, and BRB hysteretic response of (d) BRBF with $T_0 = 0.49s$, (e) BRBF with $2T_0 = 0.98s$, and (f) BRBF with $4T_0 = 1.97s$.
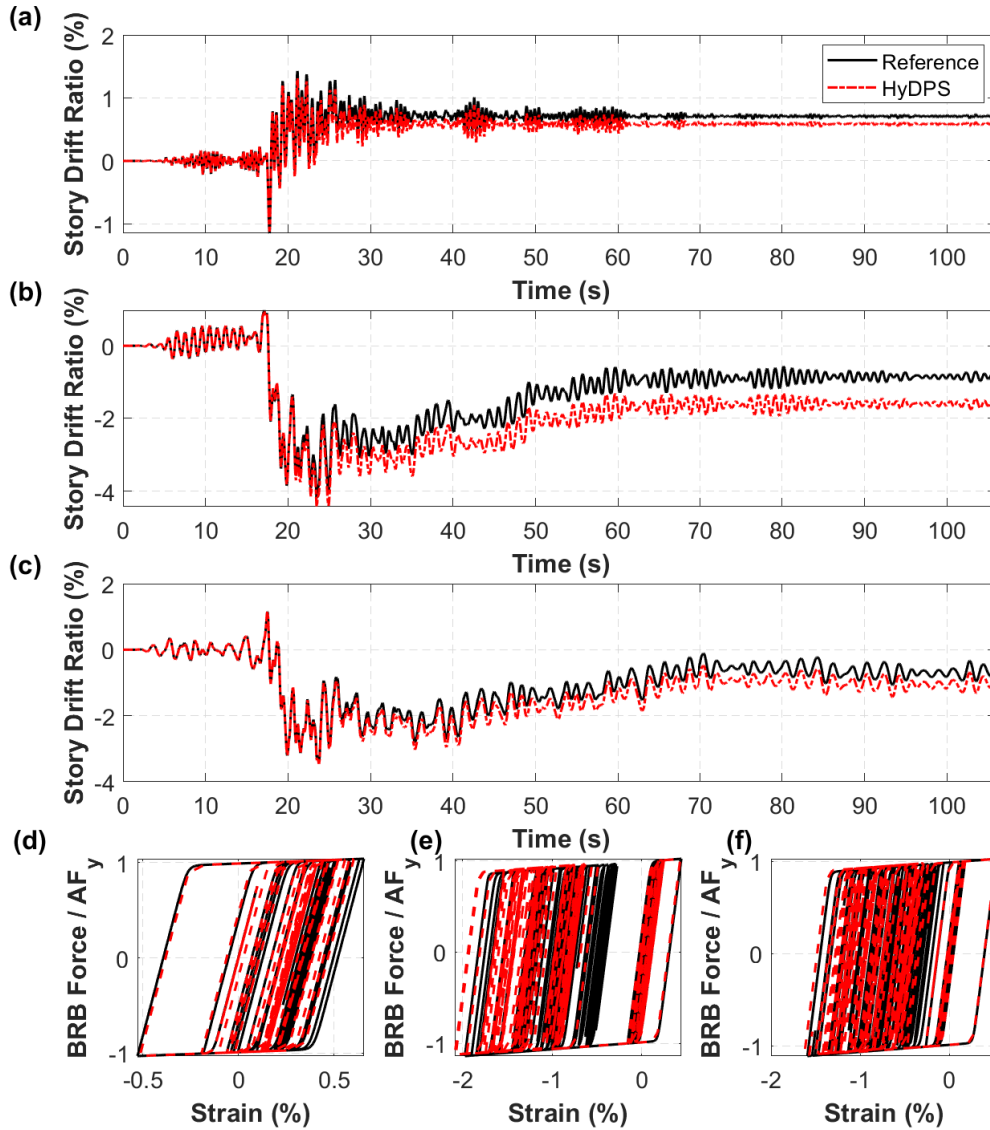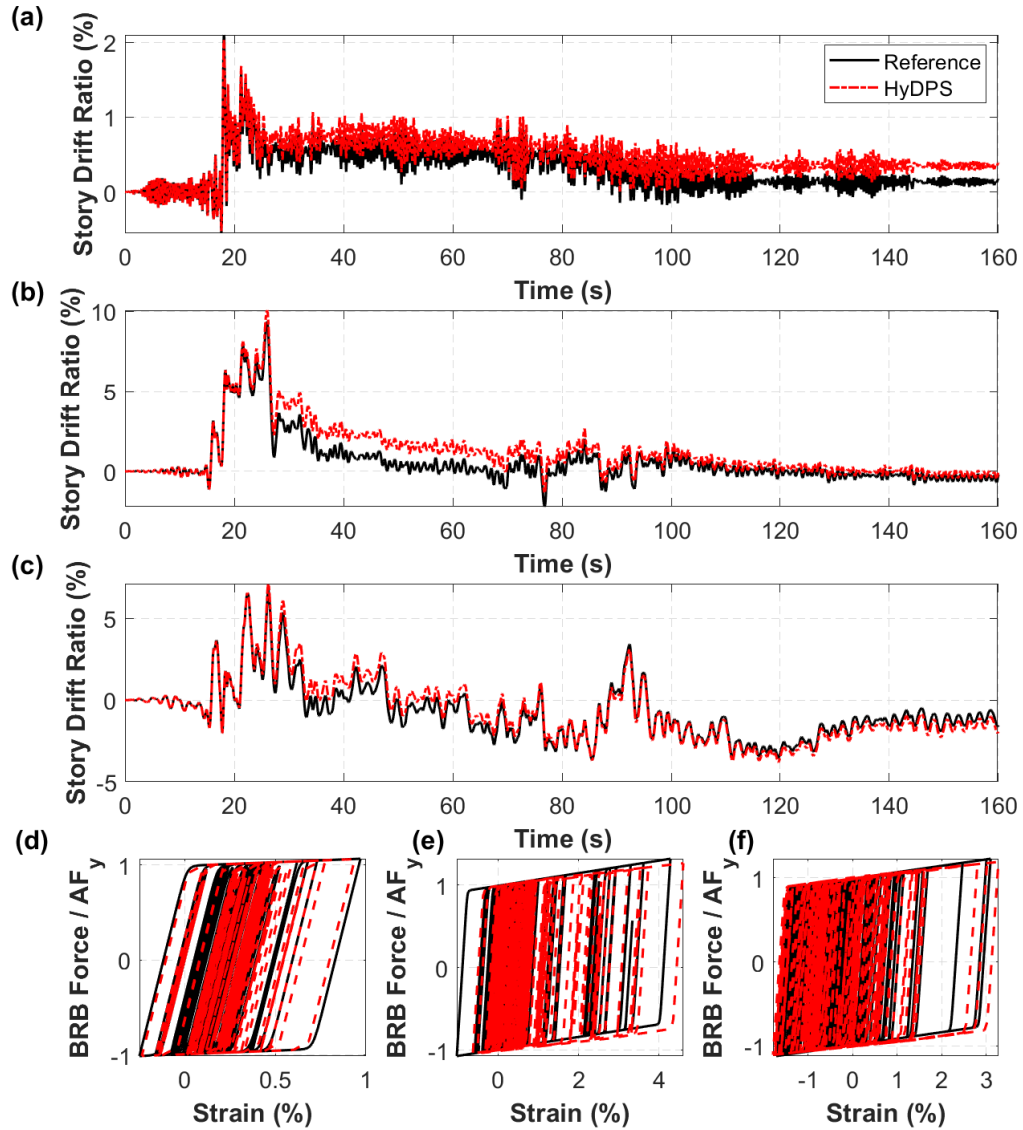
Figure B.6: Time history of BRBF storey drift ratio under the 2011 Miyagi, Japan-IWT026 earthquake, (a) BRBF with $T_0 = 0.49s$, (b) BRBF with $2T_0 = 0.98s$, and (c) BRBF with $4T_0 = 1.97s$, and BRB hysteretic response of (d) BRBF with $T_0 = 0.49s$, (e) BRBF with $2T_0 = 0.98s$, and (f) BRBF with $4T_0 = 1.97s$.
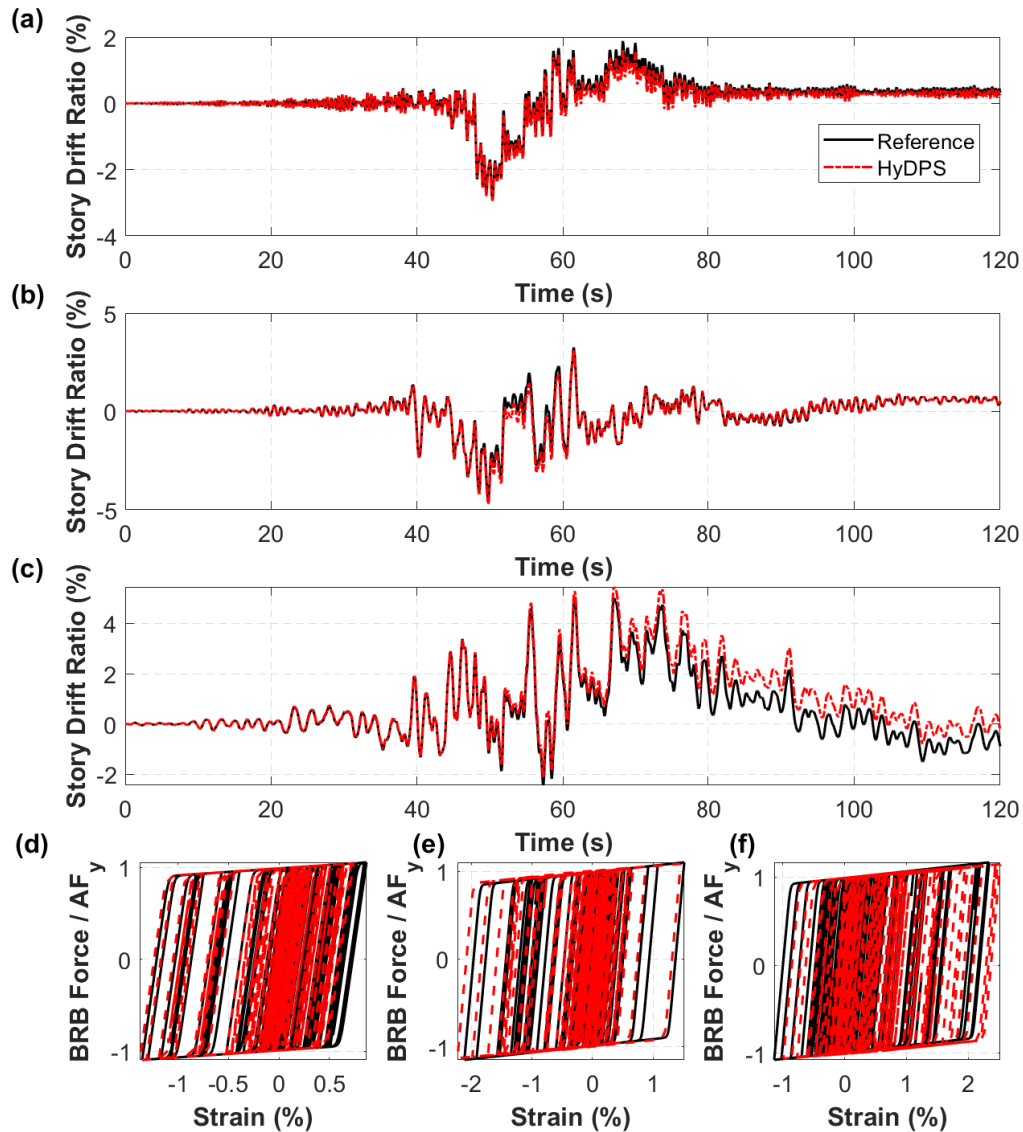
Figure B.7: Time history of BRBF storey drift ratio under the 2011 Miyagi, Japan-MYG016 earthquake, (a) BRBF with $T_0 = 0.49s$, (b) BRBF with $2T_0 = 0.98s$, and (c) BRBF with $4T_0 = 1.97s$, and BRB hysteretic response of (d) BRBF with $T_0 = 0.49s$, (e) BRBF with $2T_0 = 0.98s$, and (f) BRBF with $4T_0 = 1.97s$.

Figure B.8: Time history of BRBF storey drift ratio under the 2011 Miyagi, Japan-IWTH24 earthquake, (a) BRBF with $T_0 = 0.49s$, (b) BRBF with $2T_0 = 0.98s$, and (c) BRBF with $4T_0 = 1.97s$, and BRB hysteretic response of (d) BRBF with $T_0 = 0.49s$, (e) BRBF with $2T_0 = 0.98s$, and (f) BRBF with $4T_0 = 1.97s$.
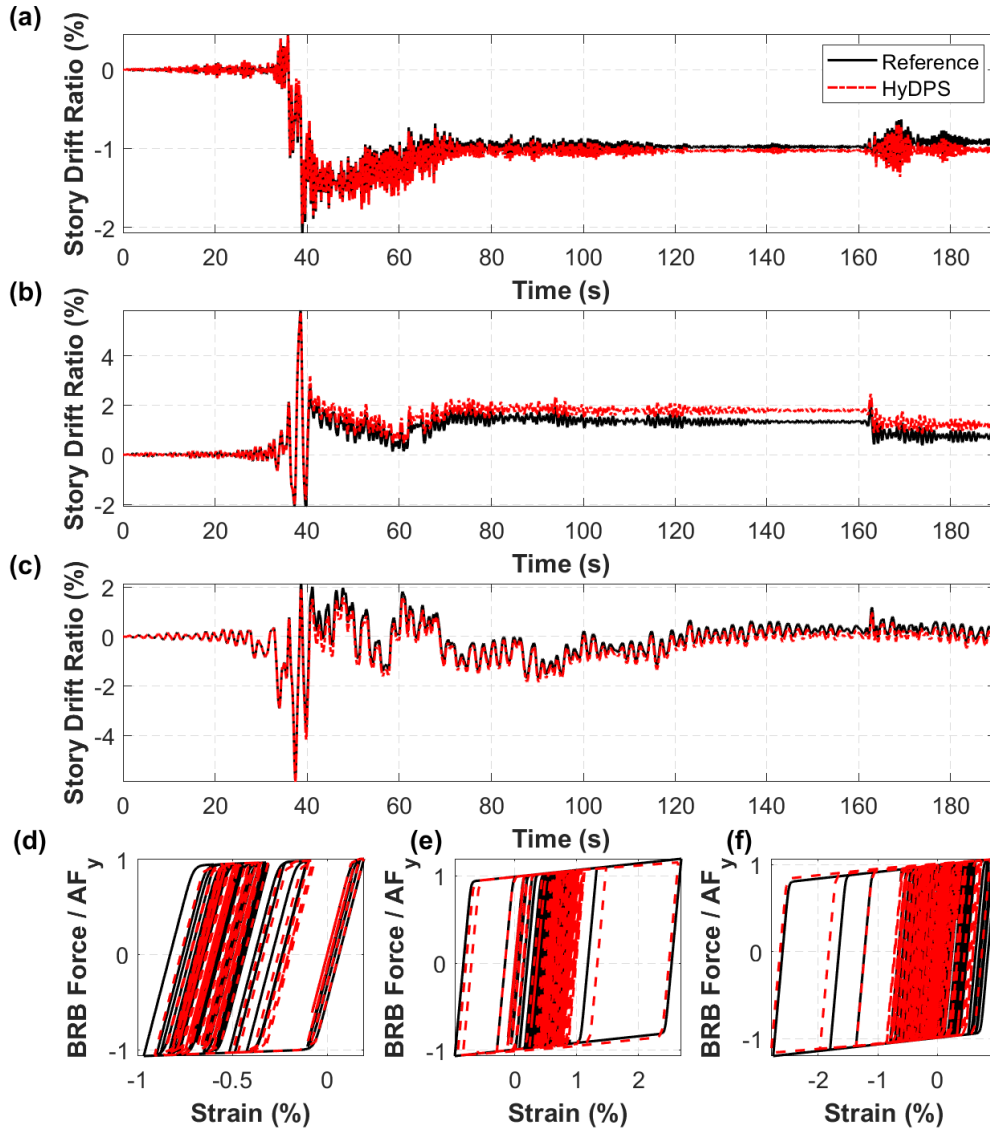
Figure B.9: Time history of BRBF storey drift ratio under the 2001 Southern Peru-POCO earthquake, (a) BRBF with $T_0 = 0.49s$, (b) BRBF with $2T_0 = 0.98s$, and (c) BRBF with $4T_0 = 1.97s$, and BRB hysteretic response of (d) BRBF with $T_0 = 0.49s$, (e) BRBF with $2T_0 = 0.98s$, and (f) BRBF with $4T_0 = 1.97s$.

Figure B.10: Time history of BRBF storey drift ratio under the 2007 Pisco, Peru-UNICA earthquake, (a) BRBF with $T_0 = 0.49s$, (b) BRBF with $2T_0 = 0.98s$, and (c) BRBF with $4T_0 = 1.97s$, and BRB hysteretic response of (d) BRBF with $T_0 = 0.49s$, (e) BRBF with $2T_0 = 0.98s$, and (f) BRBF with $4T_0 = 1.97s$.

151

Figure B.11: Time history of BRBF storey drift ratio under the 2010 Maule, Chile-LACHb earthquake, (a) BRBF with $T_0 = 0.49s$, (b) BRBF with $2T_0 = 0.98s$, and (c) BRBF with $4T_0 = 1.97s$, and BRB hysteretic response of (d) BRBF with $T_0 = 0.49s$, (e) BRBF with $2T_0 = 0.98s$, and (f) BRBF with $4T_0 = 1.97s$.

Figure B.12: Time history of BRBF storey drift ratio under the 2014 Iquique, Chile-PB09 earthquake, (a) BRBF with $T_0 = 0.49s$, (b) BRBF with $2T_0 = 0.98s$, and (c) BRBF with $4T_0 = 1.97s$, and BRB hysteretic response of (d) BRBF with $T_0 = 0.49s$, (e) BRBF with $2T_0 = 0.98s$, and (f) BRBF with $4T_0 = 1.97s$.

Appendix C: DMHS Results

This appendix presents the results of the nonlinear response history analyses performed using the digital twin-based multi-element hybrid simulations (DMHSs) as described in Section 4.4.3.
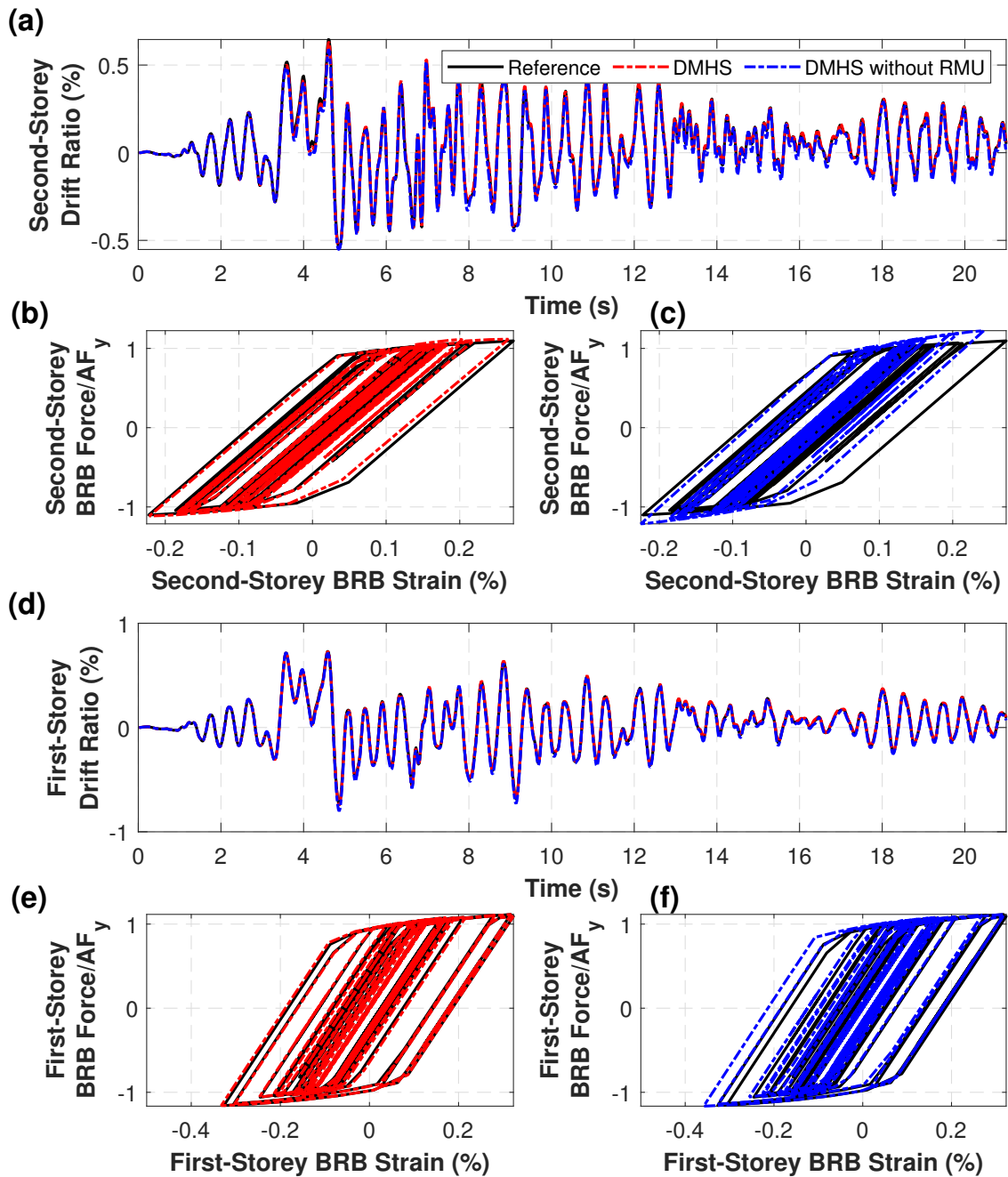
Figure C.1: Virtual hybrid simulation of the BRBF using 2DLFM under the 1978 Tabas, Iran-Dayhook earthquake, (a) history of drift ratio in Storey 2, (b) Storey 2 BRB (digital twin) response for DMHS vs. reference, (c) Storey 2 BR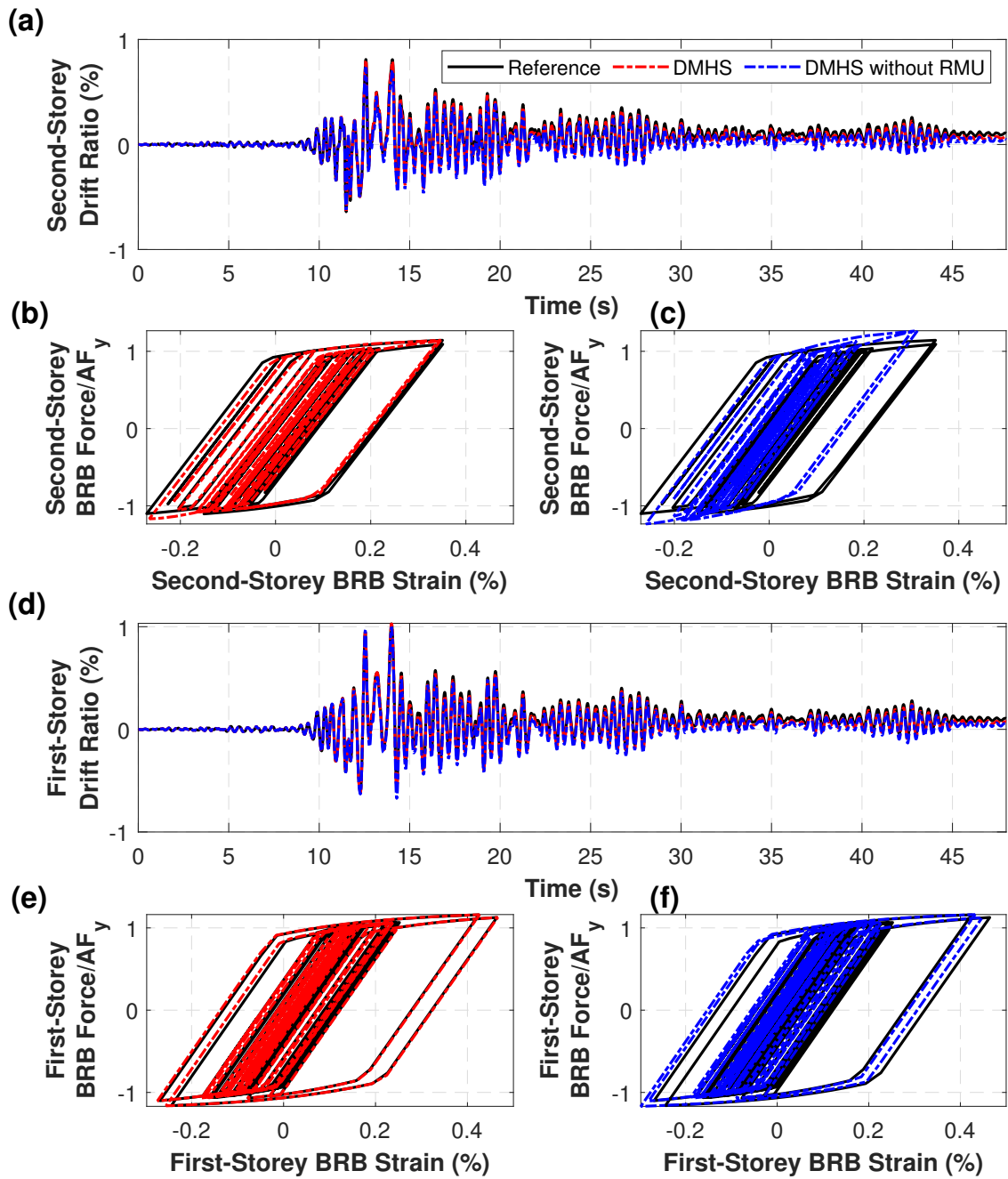B (digital twin) response for DMHS without RMU vs. reference, (d) history of drift ratio in Storey 1, (e) Storey 1 BRB (virtual twin) response for DMHS vs. reference, (f) Storey 1 BRB (virtual twin) response for DMHS without RMU vs. reference.
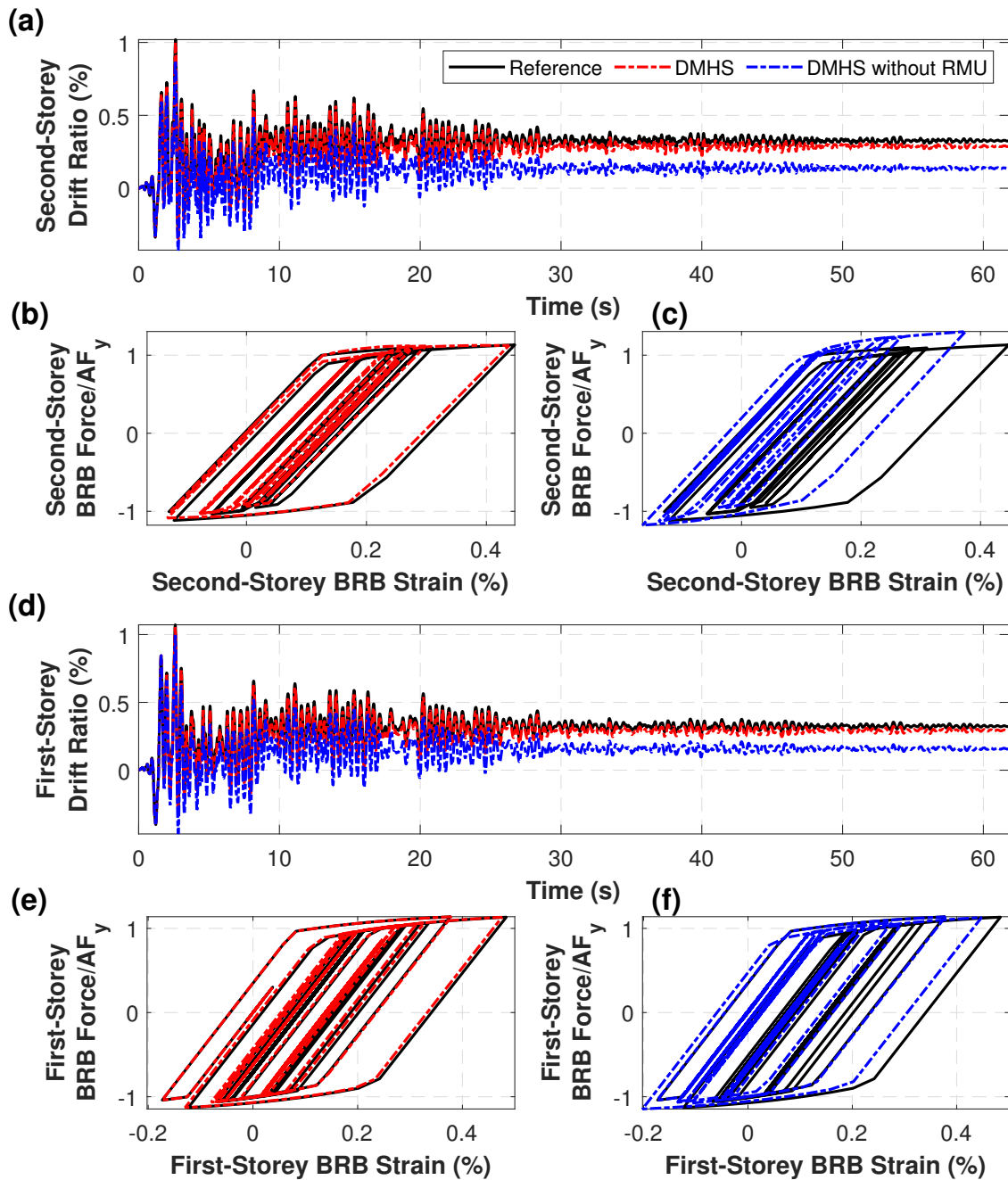
Figure C.2: Virtual hybrid simulation of the BRBF using 2DLFM under the 1971 San Fernando - Castaic-Old Ridge Route earthquake, (a) history of drift ratio in Storey 2, (b) Storey 2 BRB (digital twin) response for DMHS vs. reference, (c) Storey 2 BRB (digital twin) response for DMHS without RMU vs. reference, (d) history of drift ratio in Storey 1, (e) Storey 1 BRB (virtual twin) response for DMHS vs. reference, (f) Storey 1 BRB (virtual twin) response for DMHS without RMU vs. reference.
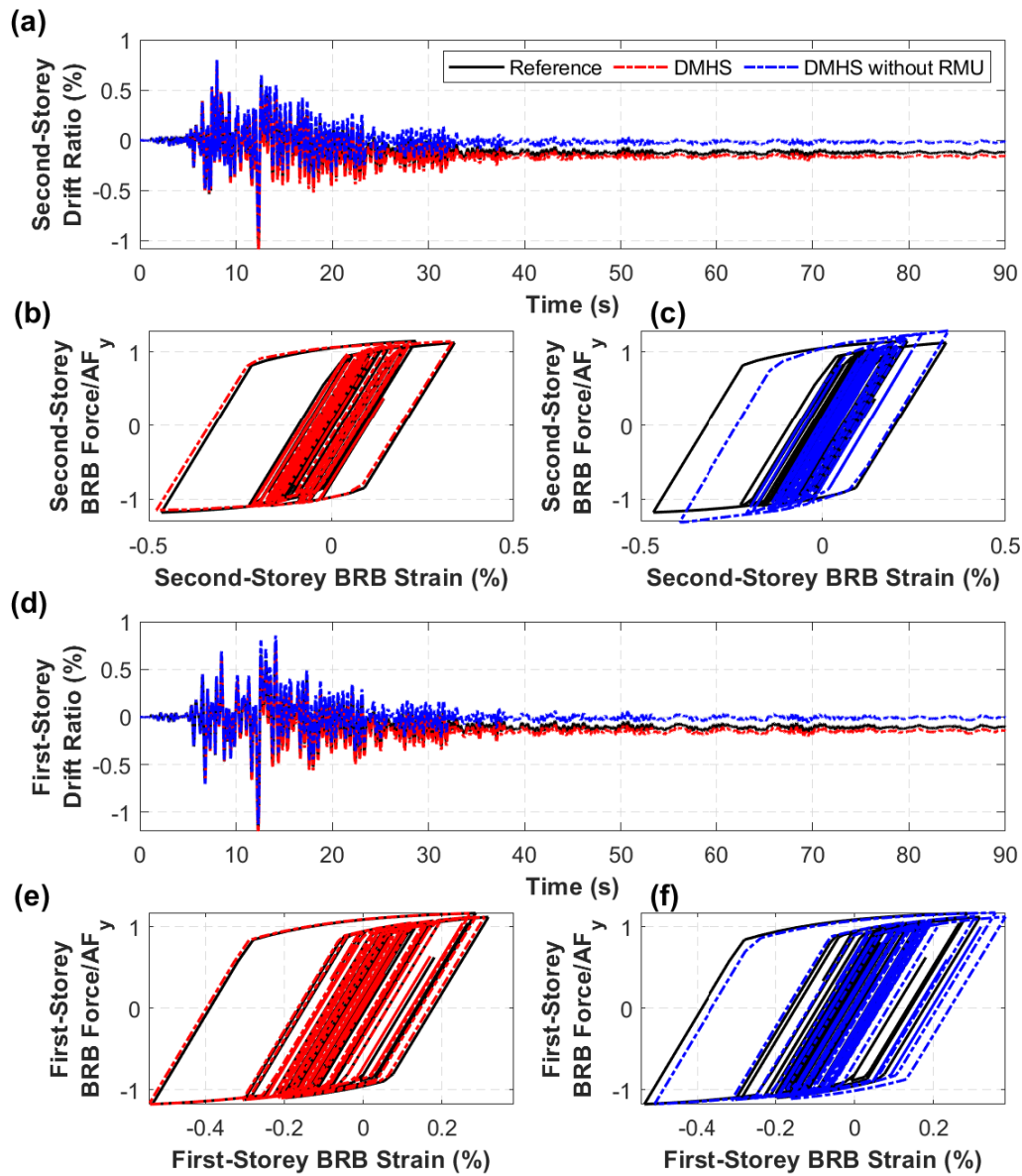
Figure C.3: Virtual hybrid simulation of the BRBF using 2DLFM under the 1979 Montenegro, SFRY-Herceg Novi-O.S.D. Paviviv earthquake, (a) history of drift ratio in Storey 2, (b) Storey 2 BRB (digital twin) response for DMHS vs. reference, (c) Storey 2 BRB (digital twin) response for DMHS without RMU vs. reference, (d) history of drift ratio in Storey 1, (e) Storey 1 BRB (virtual twin) response for DMHS vs. reference, (f) Storey 1 BRB (virtual twin) response for DMHS without RMU vs. reference.
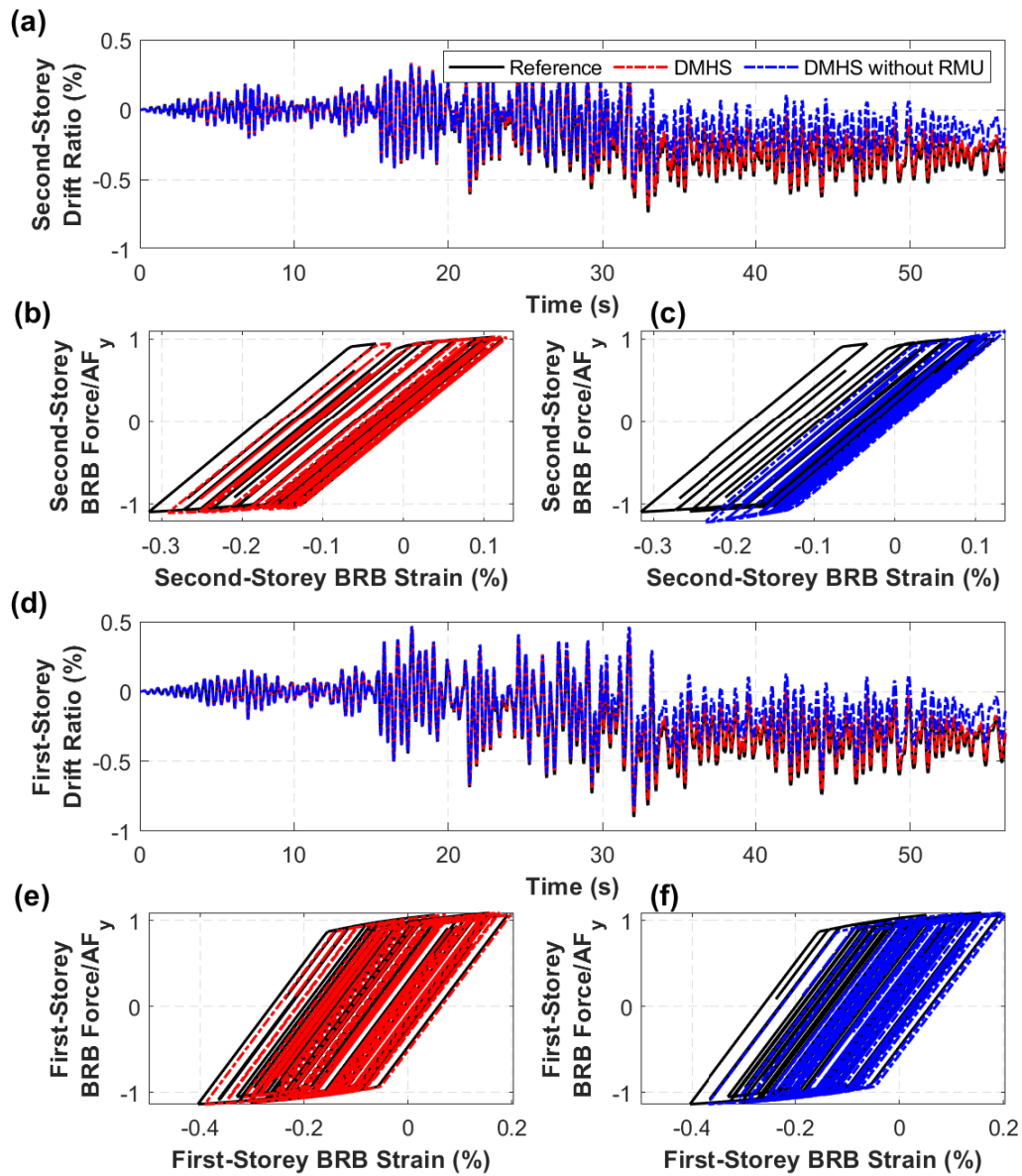
Figure C.4: Virtual hybrid simulation of the BRBF using 2DLFM under the 1995 Kobe, Japan-Tadoka earthquake, (a) history of drift ratio in Storey 2, (b) Storey 2 BRB (digital twin) response for DMHS vs. reference, (c) Storey 2 BRB (digital twin) response for DMHS without RMU vs. reference, (d) history of drift ratio in Storey 1, (e) Storey 1 BRB (virtual twin) response for DMHS vs. reference, (f) Storey 1 BRB (virtual twin) response for DMHS without RMU vs. reference.
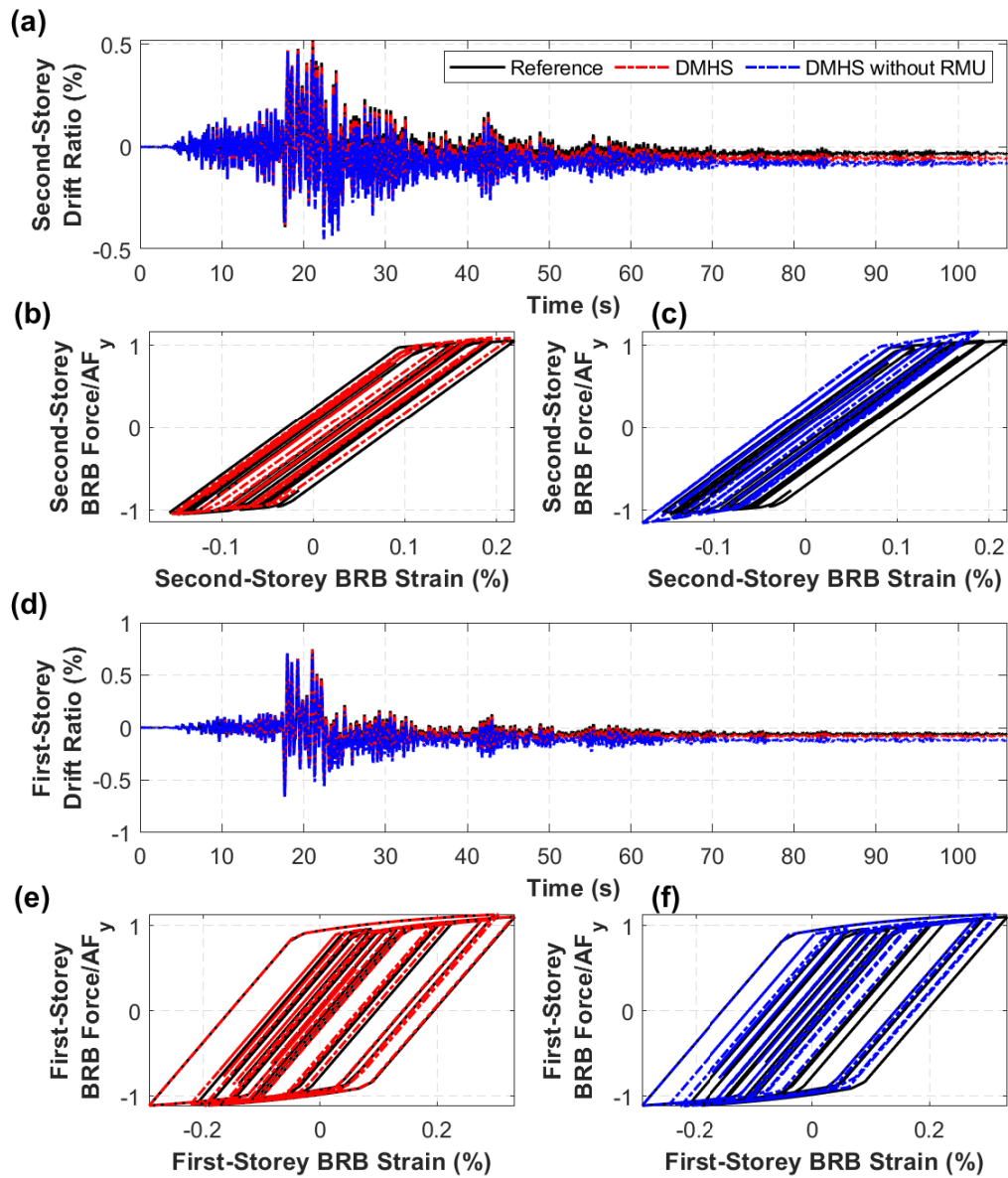
Figure C.5: Virtual hybrid simulation of the BRBF using 2DLFM under the 2001 Geivo, Japan-1421a earthquake, (a) history of drift ratio in Storey 2, (b) Storey 2 BRB (digital twin) response for DMHS vs. reference, (c) Storey 2 BRB (digital twin) response for DMHS without RMU vs. reference, (d) history of drift ratio in Storey 1, (e) Storey 1 BRB (virtual twin) response for DMHS vs. reference, (f) Storey 1 BRB (virtual twin) response for DMHS without RMU vs. reference.
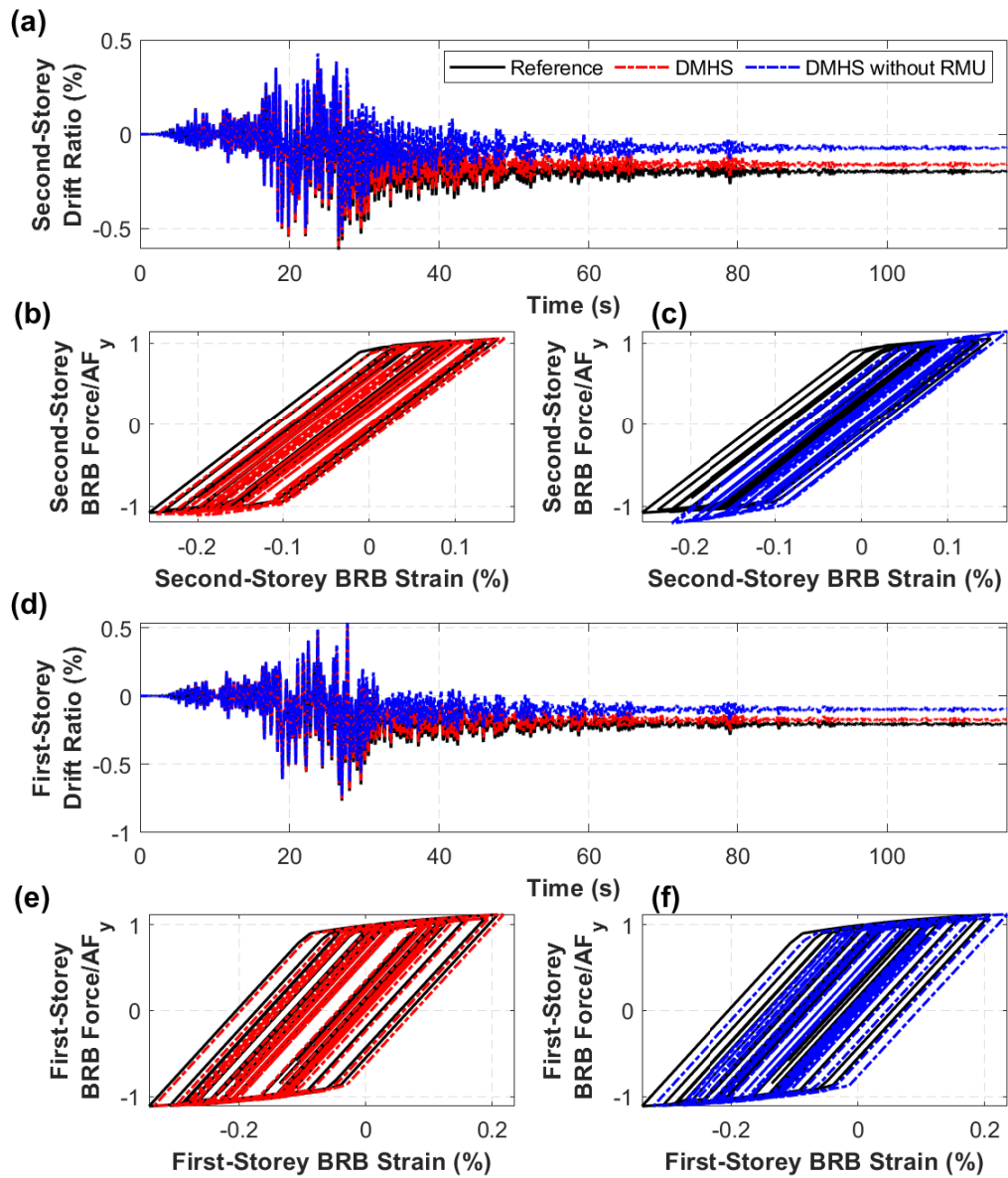
159

Figure C.6: Virtual hybrid simulation of the BRBF using 2DLFM under the 2011 Miyagi, Japan-IWT026 earthquake, (a) history of drift ratio in Storey 2, (b) Storey 2 BRB (digital twin) response for DMHS vs. reference, (c) Storey 2 BRB (digital twin) response for DMHS without RMU vs. reference, (d) history of drift ratio in Storey 1, (e) Storey 1 BRB (virtual twin) response for DMHS vs. reference, (f) Storey 1 BRB (virtual twin) response for DMHS without RMU vs. reference.
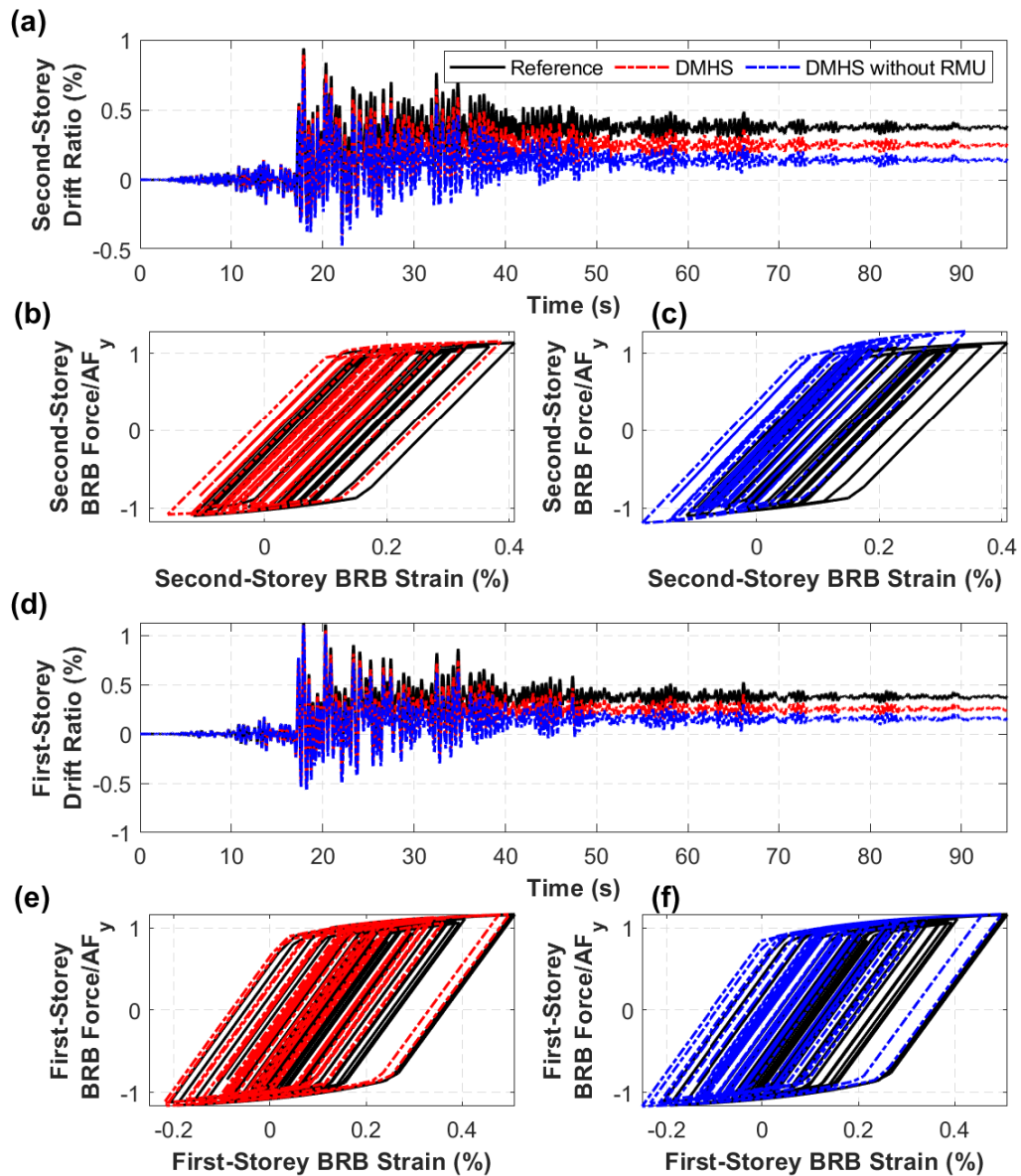
160

Figure C.7: Virtual hybrid simulation of the BRBF using 2DLFM under the 2011 Miyagi, Japan-MYG016 earthquake, (a) history of drift ratio in Storey 2, (b) Storey 2 BRB (digital twin) response for DMHS vs. reference, (c) Storey 2 BRB (digital twin) response for DMHS without RMU vs. reference, (d) history of drift ratio in Storey 1, (e) Storey 1 BRB (virtual twin) response for DMHS vs. reference, (f) Storey 1 BRB (virtual twin) response for DMHS without RMU vs. reference.

Figure C.8: Virtual hybrid simulation of the BRBF using 2DLFM under the 2011 Miyagi, Japan-IWTH24 earthquake, (a) history of drift ratio in Storey 2, (b) Storey 2 BRB (digital twin) response for DMHS vs. reference, (c) Storey 2 BRB (digital twin) response for DMHS without RMU vs. reference, (d) history of drift ratio in Storey 1, (e) Storey 1 BRB (virtual twin) response for DMHS vs. reference, (f) Storey 1 BRB (virtual twin) response for DMHS without RMU vs. reference.
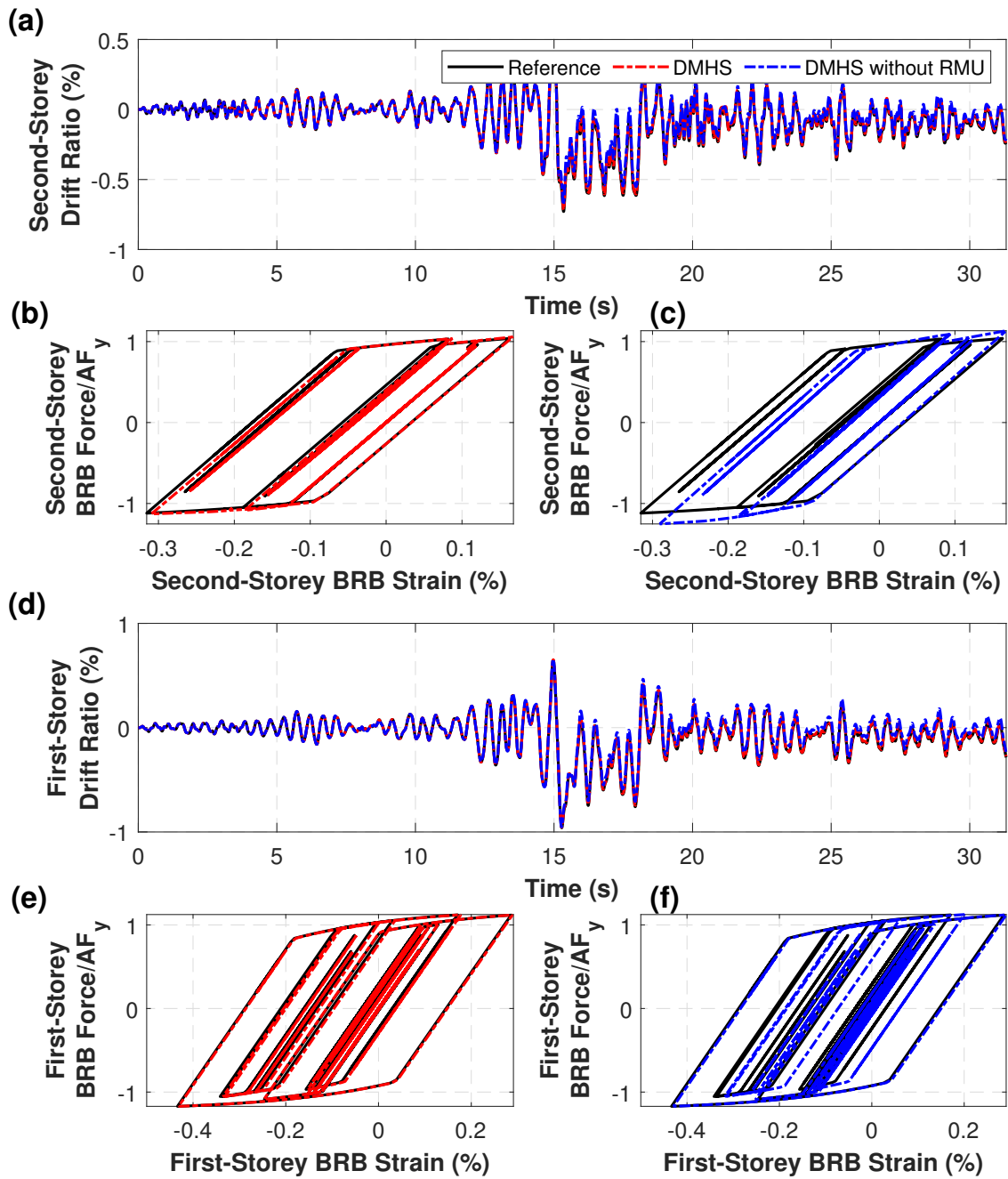
Figure C.9: Virtual hybrid simulation of the BRBF using 2DLFM under the 2001 Southern Peru-POCO earthquake, (a) history of drift ratio in Storey 2, (b) Storey 2 BRB (digital twin) response for DMHS vs. reference, (c) Storey 2 BRB (digital twin) response for DMHS without RMU vs. reference, (d) history of drift ratio in Storey 1, (e) Storey 1 BRB (virtual twin) response for DMHS vs. reference, (f) Storey 1 BRB (virtual twin) response for DMHS without RMU vs. reference.
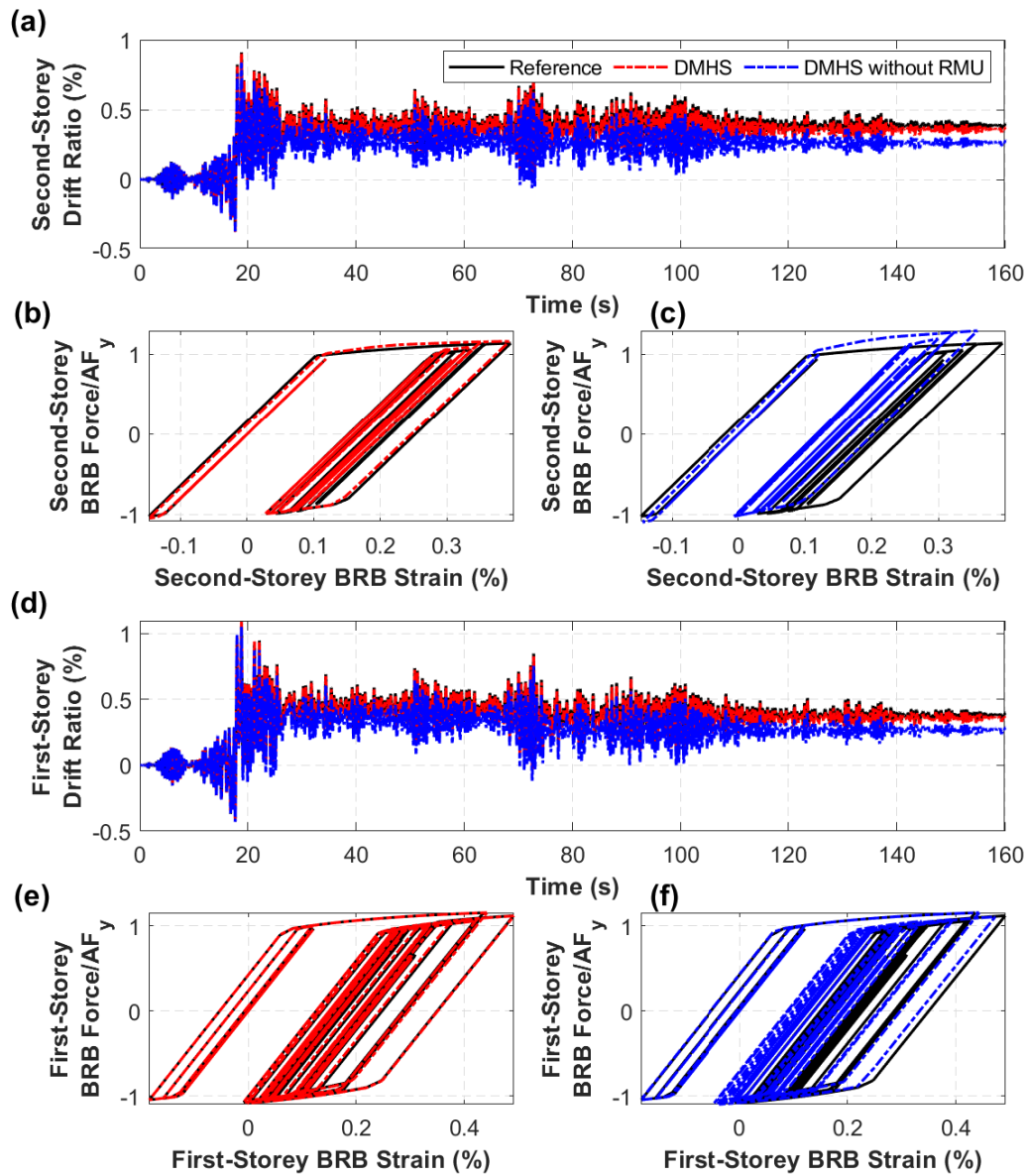
163

Figure C.10: Virtual hybrid simulation of the BRBF using 2DLFM under the 2007 Pisco, Peru-UNICA earthquake, (a) history of drift ratio in Storey 2, (b) Storey 2 BRB (digital twin) response for DMHS vs. reference, (c) Storey 2 BRB (digital twin) response for DMHS without RMU vs. reference, (d) history of drift ratio in Storey 1, (e) Storey 1 BRB (virtual twin) response for DMHS vs. reference, (f) Storey 1 BRB (virtual twin) response for DMHS without RMU vs. reference.
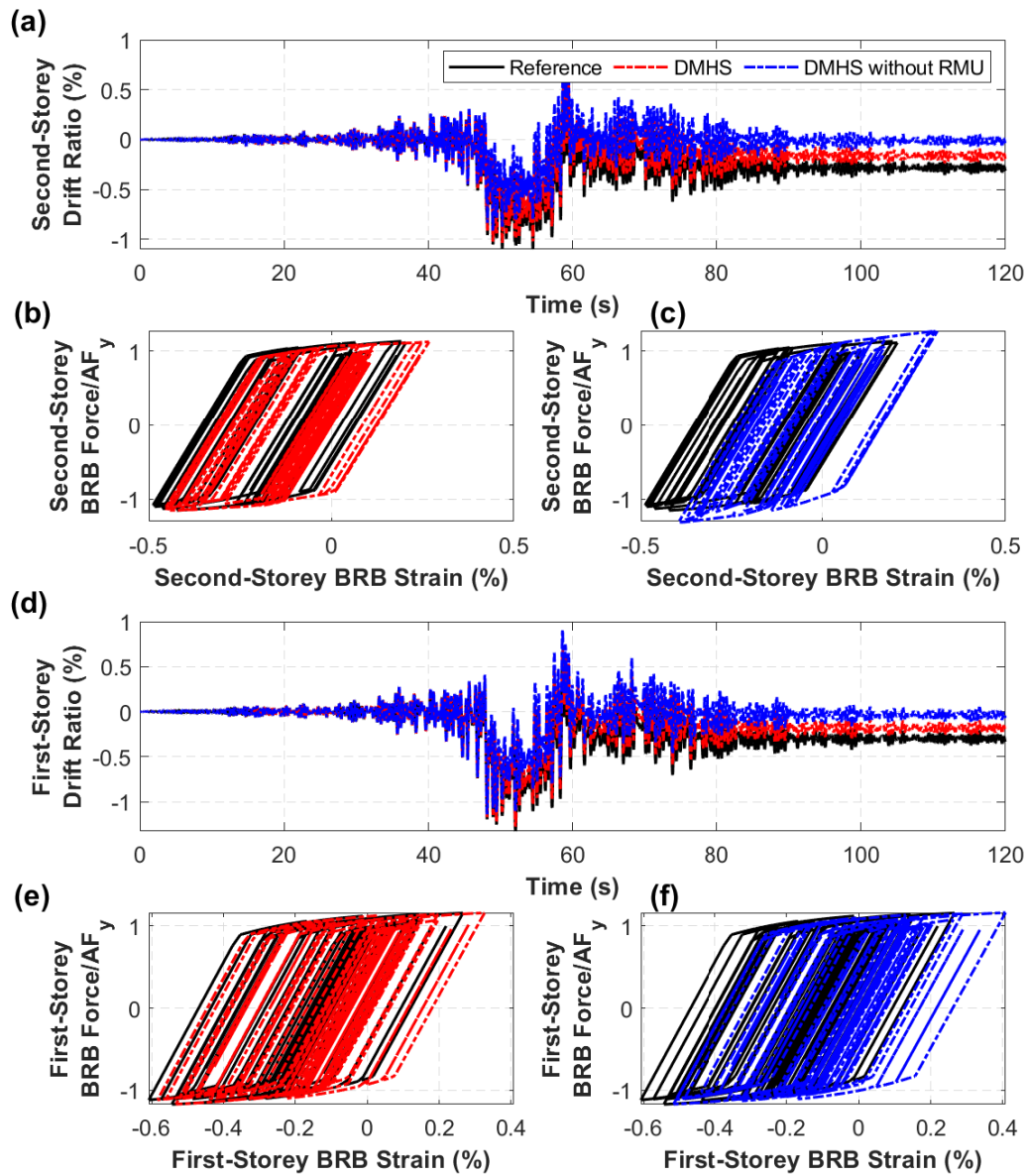
Figure C.11: Virtual hybrid simulation of the BRBF using 2DLFM under the 2010 Maule, Chile-LACHb earthquake, (a) history of drift ratio in Storey 2, (b) Storey 2 BRB (digital twin) response for DMHS vs. reference, (c) Storey 2 BRB (digital twin) response for DMHS without RMU vs. reference, (d) history of drift ratio in Storey 1, (e) Storey 1 BRB (virtual twin) response for DMHS vs. reference, (f) Storey 1 BRB (virtual twin) response for DMHS without RMU vs. reference.
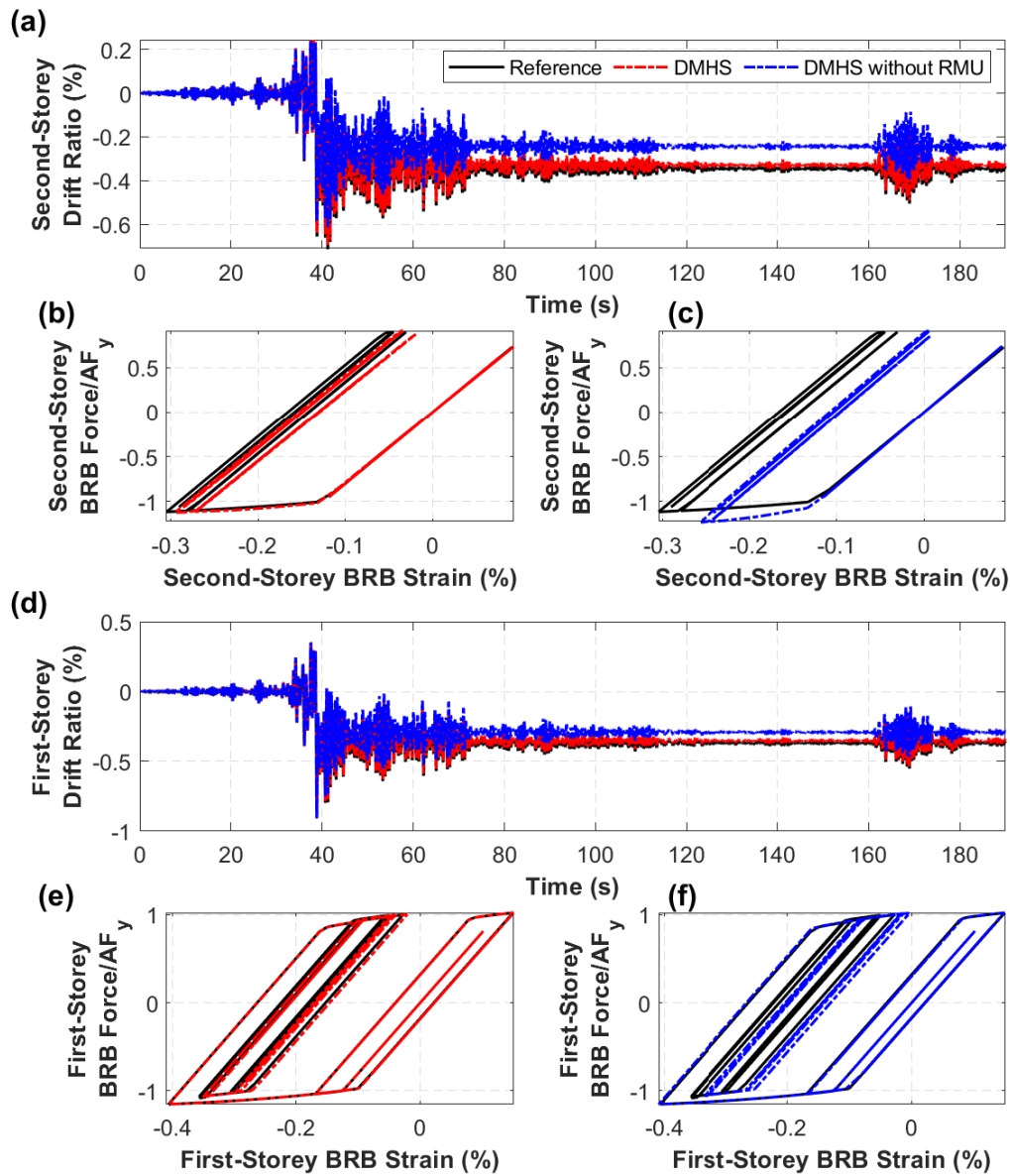
Figure C.12: Virtual hybrid simulation of the BRBF using 2DLFM under the 2014 Iquique, Chile-PB09 earthquake, (a) history of drift ratio in Storey 2, (b) Storey 2 BRB (digital twin) response for DMHS vs. reference, (c) Storey 2 BRB (digital twin) response for DMHS without RMU vs. reference, (d) history of drift ratio in Storey 1, (e) Storey 1 BRB (virtual twin) response for DMHS vs. reference, (f) Storey 1 BRB (virtual twin) response for DMHS without RMU vs. reference.